CONTRACTOR REPORT

SAND96–2538
Unlimited Release
UC–721

Hydrogen Generation by Metal Corrosion in Simulated Waste Isolation Pilot Plant Environments

M.R. Telander,
R.E. Westerman (Retired)
Battelle Pacific Northwest Laboratory
Battelle Blvd.
Richland, WA 99352

Prepared by
Sandia National Laboratories
Albuquerque, New Mexico 87185 and Livermore, California 94550
for the United States Department of Energy
under Contract DE-AC04-94AL85000

Printed March 1997

Issued by Sandia National Laboratories, operated for the United States Department of Energy by Sandia Corporation.

Available to DOE and DOE contractors from
Office of Scientific and Technical Information
P.O. Box 62
Oak Ridge, TN 37831

Prices available from (615) 576-8401, FTS 626-8401

Available to the public from
National Technical Information Service
U.S. Department of Commerce
5285 Port Royal Rd
Springfield, VA 22161

NTIS price codes
Printed copy: A10
Microfiche copy: A01

SAND96-2538
Unlimited Release
Printed March 1997

Distribution
Category UC-721

Hydrogen Generation by Metal Corrosion in Simulated Waste Isolation Pilot Plant Environments

FINAL REPORT

M. R. Telander and R. E. Westerman

Prepared for
Sandia National Laboratories
Waste Isolation Pilot Plant Gas Generation Program
Albuquerque, New Mexico under
US Department of Energy Contract DE-AC06-76RLO 1830
by the Pacific Northwest Laboratory
Operated for the US Department of Energy
by Battelle Memorial Institute

ABSTRACT

The corrosion and gas-generation characteristics of four material types: low-carbon steel (the current waste packaging material for the Waste Isolation Pilot Plant), Cu-base and Ti-base (alternative packaging) materials, and Al-base (simulated waste) materials were determined in both the liquid and vapor phase of Brine A, a brine representative of an intergranular Salado Formation brine. Test environments consisted primarily of anoxic brine with overpressures of N_2, CO_2, H_2S, and H_2. Limited tests of low-carbon steel were also performed in simulated-backfill environments and in brine environments with pH values ranging from 3 to 11. Low-carbon steel reacted at a slow, measurable rate with anoxic brine, liberating H_2 on an equimolar basis with Fe reacted. Presence of CO_2 caused the initial reaction to proceed more rapidly, but CO_2-induced passivation stopped the reaction if the CO_2 were present in sufficient quantities. Addition of H_2S to a CO_2-passivated system caused reversal of the passivation. Low-carbon steel immersed in brine with H_2S showed no reaction, apparently because of passivation of the steel by formation of FeS. Addition of CO_2 to an H_2S-passivated system did not reverse the passivation. Cu- and Ti-base materials showed essentially no corrosion when exposed to brine and overpressures of N_2, CO_2, and H_2S except for the rapid and complete reaction between Cu-base materials and H_2S. The Al-base materials reacted at approximately the same rate as low-carbon steel when immersed in anoxic Brine A; considerably more rapidly in the presence of CO_2 or H_2S; and much more rapidly when iron was present in the system as a brine contaminant. High-purity Al was much more susceptible to corrosion than the 6061 alloy. No significant reaction took place on any material in any environment in the vapor-phase exposures.

ACKNOWLEDGMENTS

The authors acknowledge the excellent programmatic guidance of the present work provided by Drs. L. H. Brush and M. A. Molecke, Sandia National Laboratories; the technical assistance of D. J. Criswell, S. M. Faber, R. F. Klein, S. P. Pednekar, N. D. Stice, and R. B. Watson, PNL, in the performance of the experimental work; the contributions of K. H. Pool, PNL, and his analytical laboratory staff, for makeup and analysis of the test brines as well as valuable insights into the chemistry of the test environments; D. E. McCready, PNL, for his skill and dedication in performing XRD analyses; R. E. Brinson and M. W. Goheen, PNL, for their cooperation in performing the many gas analyses required; B. L. Hopkins, Westinghouse Hanford Corporation, for performing the He leak checks of the test containers; and B. O. Barnes, for his assistance with the Quality Assurance (QA) aspects of the program.

CONTENTS

CONTENTS (Continued)

CONTENTS (Continued)

CONTENTS (Continued)

Figures

CONTENTS (Continued)

Tables

CONTENTS (Continued)

CONTENTS (Continued)

EXECUTIVE SUMMARY

A mined geologic repository site for demonstrating the safe management and disposal of defense-related transuranic (TRU) waste is being developed by the US Department of Energy near Carlsbad, New Mexico. The site, designated the Waste Isolation Pilot Plant (WIPP), is located in the bedded salt of the Salado Formation, at a depth of 655 m (2150 ft) below the land surface.

If brine should enter the repository and contact the low-carbon steel waste containers (and metallic items in the waste), the possibility exists that corrosion product H_2 could pressurize the facility. The rate of H_2 formation and the ultimate H_2 pressure attained would be dependent on the amount of brine available, the corrosion products formed, and the kinetics of the specific corrosion reactions involved.

Sandia National Laboratories (SNL), WIPP Gas Generation Program, issued a subcontract to Pacific Northwest Laboratory (PNL)[a] authorizing the performance of laboratory experiments to assist in resolving the gas generation and performance assessment-related questions. The present report summarizes the laboratory corrosion results obtained through the program conclusion.

The experimental work focused on the corrosion/gas generation characteristics of four material types: low-carbon steel (the current packaging material), Cu-base materials, Ti-base materials, and Al-base materials. The Cu- and Ti-base materials are considered to be alternative packaging materials should low-carbon steels prove unusable. The Al-base materials were intended to represent metallic Al and Al alloys present in the waste. Four basic test environments were used in the tests: Brine A (a Na, Mg, K chloride-sulfate brine simulating a WIPP intergranular Salado Formation brine) with an N_2 overpressure; Brine A with a CO_2 overpressure; Brine A with an H_2S overpressure; and Brine A with an H_2 overpressure. Test specimens were exposed to the test environments in the entirely immersed condition as well as the vapor-phase-only condition.

Limited testing was done with steel specimens embedded in nearly pure particulate halite (NaCl) obtained from the WIPP site, and in a simulated backfill material consisting of a mixture of 70% halite and 30% bentonite. In addition, tests of low-carbon steel were performed in simulated modified ERDA-6 brine environments with pH values ranging from pH 3 to pH 11. All testing was done at 30°C. The experimental work involved a determination of the rate at which pressure (H_2 gas) builds in test containers; the gravimetric determination of the metal lost from the test specimens because of the corrosion reaction; correlation between H_2 formed and metal reacted, where possible; identification of the corrosion products formed; and post-test determination of the compositions of gases and brines in the test containers.

It was shown that the long-term (last 12 months of 24-month corrosion tests) corrosion rate of steel in anoxic Brine A with a 10-atm overpressure of N_2 is 0.71 μm/yr,[b] producing 0.10 mol H_2/m^2-

---

[a] Pacific Northwest Laboratory is operated by Battelle Memorial Institute for the US Department of Energy under Contract DE-AC06-76RLO 1830.

[b] A corrosion rate (or "penetration rate") expressed in μm/yr may be converted to mil/yr (mpy) by dividing by 25.4.

steel-yr. The corrosion product was not adherent and was not identifiable by x-ray diffraction analysis (XRD); its principal metallic constituents were Fe and Mg. The long-term corrosion rate was approximately linear, but the rate is expected to continually decrease with time.

The effect of gas pressure on reaction kinetics of low-carbon steel in Brine A was determined for H_2, N_2, and CO_2 over the range 2 to 127 atm for H_2, 10 to 131 atm for N_2, and 10 to 62 atm for CO_2. Increasing the pressure of H_2 from 2 to 127 atm had little effect on the corrosion rate observed. Increasing the pressure of N_2 from 10 to 131 atm increased the corrosion rate, but by less than a factor of 2. A dichotomy existed in the case of CO_2 overpressures, in that increasing the gas overpressure increased the initial corrosion rate and also increased the probability of passivation due to the formation of an impermeable corrosion product film ($FeCO_3$ or a close crystallographic relative).

In the low-carbon steel corrosion studies, the molar equivalency between Fe reacted and H_2 formed was satisfactory in both the N_2/immersed and the CO_2/immersed tests. Steel exposed to the vapor phase over Brine A only, with either N_2 or CO_2 present, showed essentially no evidence of corrosion.

Steel specimens exposed to an H_2S pressure of 5 atm, either immersed in Brine A or suspended in Brine A vapor, showed essentially no reaction. The lack of reaction of the immersed specimens was attributed to the passivating effect of a layer of mackinawite (FeS) on the specimen surfaces.

Tests were conducted to determine the effect of pH on the corrosion/gas generation behavior of low-carbon steel in a saturated anoxic brine. A modified ERDA-6 brine (a Na, K chloride-sulfate brine) was used in the tests. The pH was controlled at levels of (approximately) 3, 5, 7, 9 and 11 by means of pH-stats. The corrosion rates were lowest at the highest pH levels. At pH 3 the average rate was 7900 μm/yr; at pH 5, 89 μm/yr; at pH 7, 51 μm/yr; at pH 9, 2 μm/yr; at pH 11, 3.6 μm/yr. In separate seal-welded container tests with no pH adjustment, the corrosiveness of ERDA-6 brine and Brine A were observed to be comparable.

Limited anoxic corrosion studies were performed in which steel specimens were embedded in particulate salt (halite) that had been obtained from the Salado Formation in the WIPP underground workings. The particulate salt was either (a) contacting a pool of Brine A in a test autoclave (a "wicking" test) or (b) suspended above the Brine A (an attempt to form a "vapor transport" test). The corrosion rates observed in the former test were similar to those observed in tests in which steel specimens were immersed in Brine A with a N_2 overpressure. In the latter test, the intended vapor-transport process was compromised by an unexpected condensation-drip process from the underside of the autoclave head. The corrosion rates were relatively low, because of (a) lack of reactant H_2O, or (b) the low-Mg test environment resulting from the condensed-H_2O drip.

In two autoclave experiments similar to those just described, steel specimens were embedded in a simulated backfill medium consisting of 70% halite and 30% bentonite. Precautions were taken in these tests to prevent condensation from dripping on the mass of simulated backfill. Specimens embedded in backfill contacting the brine (a "wicking" test) showed corrosion rates higher by a factor of ~2 than specimens exposed to anoxic brine alone. Specimens embedded in simulated backfill exposed to the vapor phase only showed an average corrosion rate ~1/3 that expected from immersion in anoxic brine.

Alternative packaging materials (Cu-base and Ti-base alloys) showed essentially no corrosion when exposed to environments of Brine A and overpressures of N_2, CO_2, and H_2S, except for the rapid and complete reaction between immersed specimens of Cu-base materials and H_2S. The alternative packaging materials showed essentially no evidence of reaction when exposed to the overpressure gas and Brine A vapor. Cu-base materials would appear to be a poor choice for use in the WIPP repository if H_2S is expected to be present in the environment, for example, through generation by microbial sulfate-reduction processes. It appears as though Ti-base materials could be used without concern for significant gas production.

There is a concern that Al-base-material scrap contained in the TRU waste could react with brine and generate H_2. The corrosion/gas-generation rates of two Al-base materials, high-purity (99.99%) Al and 6061 alloy, were therefore investigated in Brine A with N_2, CO_2, and H_2S overpressures for time periods up to 24 months. In anoxic brine (brine/N_2 test), the corrosion rates of the Al-base materials approximated the corrosion rate of low-carbon steel. The corrosion rate of 99.99% Al was estimated to be twice that of the 6061 alloy. With CO_2 or H_2S present, the corrosion rates of the Al-base materials increased to approximately 10 times that observed in the brine/N_2 test, with the corrosion rate of 99.99% Al material ranging from about equal to that of the 6061 alloy (CO_2) to about four times that of the 6061 alloy (H_2S). With Fe present in solution, the corrosion rate in all tests escalated dramatically, to about 30 times that of the brine/N_2 test. The relatively high corrosion rates with CO_2 and H_2S present are ascribed to a lower system pH. The high rates with Fe present are ascribed to the deposition of Fe on the Al-base-material surface, where it can function as a cathode in electrolytic corrosion cells. Corrosion was, in general, highly nonuniform, and evidence was present of crevice-corrosion tendencies.

Steel specimens included in the Al-base-material corrosion tests (to serve as a source of Fe^{++}) were examined to determine their corrosion rates in the corroding Al environments. Their corrosion rates were relatively high for the first 13 months of exposure, suggesting strong Fe^{++} ion scavenging by the corroding Al-base materials, but essentially nil in all cases for the final 11 months of exposure. The precise reason for this is not known, but a relatively corrosion-resistant film could either form on (through corrosion reactions), or be deposited on, the steel specimen surfaces, effectively halting further reaction.

This page intentionally left blank.

1.0 INTRODUCTION

A mined geologic repository for demonstrating the safe management and disposal of defense-related transuranic (TRU) waste is being developed by the US Department of Energy near Carlsbad, New Mexico. The site, designated the Waste Isolation Pilot Plant (WIPP), is located in the bedded salt of the Salado Formation, at a depth of 655 m (2150 ft) below the land surface. Eight storage panels of seven rooms each will be mined. The panels, access ways, and shafts will be sealed before the site is decommissioned.

At the present time, a large quantity of transuranic (TRU) wastes are being temporarily stored in steel drums and steel waste boxes at waste generator sites. Under current plans, these wastes would be transported to and emplaced within the WIPP site without additional modification of the original packaging. Additional metal pieces (Fe- and Al-base alloys, for example) are contained within the waste containers as contaminated waste materials.

A number of scenarios have been advanced whereby brine could intrude into the repository (Guzowski, 1990). Should brine contact the metallic waste containers (and certain of the metallic wastes within the containers), anoxic corrosion product H_2 would be expected to form (Lappin et al., 1989, Brush et al., 1991, Brush et al., 1992, Brush, 1990). The amount of H_2 and the ultimate H_2 pressure attained would be dependent on the amount of brine available for reaction, the corrosion products formed, and the kinetics of the corrosion reactions involved. The effect of microbes in the brine/waste repository environment and the possible formation of CO_2 and/or H_2S by microbial activity have also been cited as being potentially important gas-generation processes.

Butcher (1990) has discussed the potential negative effects of gas pressure on the WIPP site. This pressure will tend to retard room closure; it can contribute to fractures within the disturbed rock zone; it has the potential of leaking from the site, possibly causing perceptual, technical, or regulatory concerns; it can contribute to two-phase gas-driven flow from the repository; and it could possibly degrade the repository sealing system.

The site-pressurization concerns led to a selection of alternative container materials; that is, materials that would not be expected to generate significant quantities of gas in the WIPP repository environment. A Waste Container Materials Panel was convened by the WIPP Project in 1990 (EATF, 1991) to make a preliminary selection of alternative packaging materials. Of the metallic

container materials considered, copper-base and titanium-base alloys were judged to offer the best combination of properties when fabricability, availability, technology status, cost, and gas-generation potential were taken into account. Though no programmatic decision has yet been made regarding the use of these alternative materials, verification of their corrosion and gas-generating characteristics has been considered to be an important task in support of the WIPP Project so that their use could be invoked if deemed necessary.

Past studies have not permitted an unambiguous resolution of the WIPP gas generation and repository pressurization question, because of 1) use of test temperatures different from those expected in WIPP disposal rooms, 2) inadequate test durations, 3) inadequate backpressure of corrosion product gases, and 4) an inadequate simulation of the brine chemistry specific to the WIPP site. For these reasons, the Sandia National Laboratories (SNL) WIPP Gas Generation Program, on behalf of the WIPP Project, issued a subcontract to Pacific Northwest Laboratory (PNL) authorizing the performance of laboratory experiments to assist in resolving the gas-generation question as it relates to corrosion of low-carbon steel, alternative packaging materials, and Al-base materials.

This final project report summarizes all available results obtained since the receipt of work authorization at PNL in November 1989 through the end of the experimental and data analysis portions of the project (September 30, 1995). The initial results, obtained from the project inception through December 1992, were reported in the progress report Telander and Westerman (1993). The present final report does not duplicate all of the data and all of the data analyses reported in the earlier progress report. However, data obtained from experimental work that is considered to be closely related to experiments concluded since December 1992, as well as all of the technical conclusions drawn from the earlier work, are reported herein for completeness. Because of the many references required to the earlier progress report in the present work, the earlier report will be simply referred to as "SAND92-7347," rather than the relatively indirect "Telander and Westerman 1993."

2.0 OBJECTIVE

The objective of the present WIPP-PNL project is to determine the rate of hydrogen generation and the hydrogen pressurization potential associated with the reaction of steel drum and waste box materials, alternative packaging materials, and metal wastes contained in drums and waste boxes with simulated, repository-relevant WIPP environments.

This page intentionally left blank.

3.0 SCOPE OF WORK

The initial (and major) effort in the present project was directed toward characterizing the behavior of low-carbon steels in simulated WIPP environments: namely, environments consisting of liquid Brine A or water vapor in equilibrium with Brine A, with overpressures of N_2, CO_2, H_2, or H_2S gas. Four lots (heats) of steel were included in the tests: two lots of ASTM A366, representative of 55-gallon steel waste drums, and two lots of ASTM A570, representative of steel waste boxes and steel waste components. The N_2 overpressure was used in the anoxic test environments in which only the brine constituents were to react with the metal specimens. Because microbial degradation activity on organic-matrix waste materials isolated in the WIPP repository may produce significant quantities of CO_2 and H_2S, these species were included in selected tests. The test matrices describing the gas-generation studies performed involving low-carbon steels are presented in Tables 3-1, 3-2, and 3-3. As shown in Table 3-2, the original studies were extended to include tests with environments of halite obtained from the WIPP site, and environments of simulated backfill material (70% halite, 30% bentonite). Also, as shown in Table 3-3, the low-carbon steel tests were extended to include the effects of pH on the corrosion and gas generation rate. Discussions of specific low-carbon-steel tests and test results in the present report will be keyed to these matrices by test environment and container (test) identification.

The scope of work of the present study was extended beyond low-carbon-steel studies in 1991 to include an assessment of the anoxic corrosion and gas-generation behavior of four alternative WIPP metal packaging materials. These materials are unalloyed copper, cupronickel 90-10, Ti Grade 2 (a grade of commercial-purity Ti), and Ti Grade 12 (a crevice-corrosion-resistant Ti-base alloy containing 0.7-0.9% Ni and 0.2-0.4% Mo). As in the case of the low-carbon-steel studies, the corrosion rates of these materials was investigated in brine environments with overpressures of N_2, CO_2, and H_2S. The test matrix describing the gas-generation studies performed on alternative materials is presented in Table 3-4.

Concern regarding the possible generation of H_2 gas by Al-base materials contained in the packaged waste led to the initiation in 1993 of a study of the corrosion and gas-generating characteristics of Al-base materials. Specimens of both high-purity Al and 6061 Al alloy were

exposed to Brine A with overpressures of N_2, CO_2, and H_2S. In selected tests specimens of steel were present in the brine, for purposeful introduction of Fe^{++} ion contamination. The test matrix for these tests is shown in Table 3-5.

Throughout this report, "psig" refers to psi gauge and "psia" refers to psi absolute, where psig + 14.7 is equivalent to psia. The term "atm" always refers to atmospheres pressure absolute. In describing pressure differences "psi" is used.

The "Brine A" environment referred to in the test matrices refers to a saturated Na-Mg-K chloride-sulfate brine intended to simulate intergranular Salado Formation brines at or near the stratigraphic horizon of the WIPP repository. The "ERDA-6" environment referred to in Tables 3.1 and 3.2 is a modification of a brine originally found in a brine pocket within the boundaries of the WIPP site (Molecke, 1983). The chemistry of the original brine was modified by eliminating its Ca^{++}, Mg^{++}, and HCO_3^- constituents, making it essentially a saturated Na-K chloride-sulfate brine. Throughout this document, the terms "Brine A" or "ERDA-6 brine" refer to laboratory-simulated brines, not brines obtained from the WIPP site. The brines are discussed in detail in Section 5.2.4 of this report.

Table 3-1. Test Matrix, Low-Carbon Steel Tests Using Seal-Welded Test Containers. Pressures given in table are approximate. Test temperature = 30 ±5°C.

Test Type	Overpressure Gas	Container (or Test) Identification	Test Time, Months Aim	Test Time, Months Actual	Initial Gas Overpressure or Amount	Steel Lots[a] in Test	Remarks
Specimens immersed in Brine A	N_2	1, 2	3	3	10 atm	J, K, L, M	Results described in SAND92-7347
		9, 10	6	6			
		17, 18	12	12			
		25, 26	24	24			
		46, 47	6	6			Purpose of test was to produce corrosion product for analysis/identification
	CO_2	3,[b]4[b]	3	3	12 atm		Results described in SAND92-7347
		11,[b] 12[b]	6	6			
		19,[b] 20[b]	12	12			
		27,[b] 28[b]	24	24			
		33	—	38.5	0.32 mol/m² steel		All tests except Test 36 had H_2S addition at 19.2 months
		34			0.16 mol/m² steel		
		35			0.063 mol/m² steel		
		36			0.032 mol/m² steel		
		37			0.016 mol/m² steel		
		38[c]			0.00 mol/m² steel		
	H_2S	40[b]	—	14	5 atm		No CO_2 addition made
		41[b]		35.3			CO_2 addition was made at 16.2 months
Specimens in vapor phase, Brine A	N_2	5, 6	3	3	10 atm		Results described in SAND92-7347
		13, 14	6	6			
		21, 22	12	12			
		29, 30	24	24			
	CO_2	7, 8	3	3			
		15, 16	6	6			
		23, 24	12	12			
		31, 32	24	24			
	H_2S	42	—	14	5 atm		No CO_2 addition made
		43		35.3			CO_2 addition was made at 16.2 months
Specimens immersed in ERDA-6 brine	N_2	44	—	10	10 atm		Purpose of test was to compare corrosion rates between Brine A and ERDA-6 brine environments
		45					

[a] J = ASTM A366; K = ASTM A366; L = ASTM A570; M = ASTM A570.
[b] Containers equipped with 300-psig full-range gauges. All other SWC tests equipped with 200-psig full-range gauges.
[c] Part of test series directed toward determining the effect of CO_2, but contains only N_2 as a control.

Table 3-2. Test Matrix, Low-Carbon Steel Tests Using High-Pressure Autoclave Systems. Brine A was used in all tests. Pressures given in table are approximate. Test temperature = 30 ±5°C.

Test Type	Overpressure Gas	Container (or Test) Identification	Test Time, Months Aim	Test Time, Months Actual	Initial Gas Overpressure	Steel Lots[a] in Test	Remarks
Specimens immersed in brine	H_2	AUT-1	3	6	70 atm	J, K	Results described in SAND92-7347
		AUT-3	6	12	36 atm		
		AUT-4			70 atm		
		AUT-9	6	6	127 atm	J, K, L, M	High-pressure test, to determine effect of pressure on corrosion rate
	N_2	AUT-2	3	6	73 atm	J, K	Results described in SAND92-7347
		AUT-10	6	6	127 atm	J, K, L, M	High-pressure test
	CO_2	AUT-7	6	6	36 atm		Results described in SAND92-7347
		AUT-8	12	12			
		AUT-11	6	6	62 atm		High-pressure test
Specimens embedded in particulate salt	N_2	AUT-5	3	3	10 atm	J	Salt mass contacting brine Results described in SAND92-7347
		AUT-6					Salt mass above brine Results described in SAND92-7347
Specimens embedded in simulated salt and bentonite backfill		AUT-12	6	6			Simulated backfill contacting brine
		AUT-13					Simulated backfill above brine

[a] J = ASTM A366; K = ASTM A366; L = ASTM A570; M = ASTM A570.

Table 3-3. Test Matrix, Tests of Low-Carbon Steel in Anoxic ERDA-6 Brine Under Constant pH Conditions. Tests were conducted in glass vessels. Specimens were completely immersed. Test temperature = 30 ±5°C.

Material[a]	Overpressure Gas	pH	Test Time, Months (Days) Aim	Test Time, Months (Days) Actual	Remarks
Low-carbon steel lots J, K, L, M	N_2, 1 atm	3	6	(5.6)	Test terminated prematurely because of high corrosion rate
		5	6	6	Tests attained aim test duration
		7	6	6	
		9	6	6	
		11	6	6	

[a] J = ASTM A366; K = ASTM A366; L = ASTM A570; M = ASTM A570.

Table 3-4. Test Matrix, Alternative Packaging Materials Tests. Specimens immersed in Brine A in seal-welded test containers. Pressures given in table are approximate. Temperature = 30 ±5°C.

Material	Overpressure Gas	Container (or Test) Identification	Test Time, Months Aim	Actual	Remarks
Copper and cupronickel 90-10	N_2, 10 atm	1A	6	10	Results described in SAND92-7347
		7A	12	15	
		13A	24	24	Long-term test concluded
	CO_2, 10 atm	2A	6	10	Results described in SAND92-7347
		8A[a]	12	15	
		14A[a]	24	24	Long-term test concluded
	H_2S, 5 atm	3A	6	9	Results described in SAND92-7347
		9A[a]	12	15	H_2 vented, container re-pressurized with H_2S at 9 months. Described in SAND92-7347
		15A[a]	24	24	H_2 vented, container re-pressurized with H_2S at 9 months. Long-term test concluded
Ti Grade 2 and Ti Grade 12	N_2, 10 atm	4A	6	10	Results described in SAND92-7347
		10A	12	15	
		16A	24	24	Long-term test concluded
	CO_2, 10 atm	5A	6	10	Results described in SAND92-7347
		11A	12	15	
		17A[a]	24	24	Long-term test concluded
	H_2S, 5 atm	6A	6	9	Results described in SAND92-7347
		12A	12	15	
		18A[a]	24	24	Long-term test concluded
None	H_2S, 5 atm	19A	Open	24	"Control" container

[a] Tests equipped with 300-psig full-range gauges. All others equipped with 200-psig full-range gauges.

Table 3-5. Test Matrix, Tests of Al-Base Materials Using Seal-Welded Containers. Brine A was used in all tests. Pressures given in table are approximate. Temperature = 30 ±5°C.

Material	Test Type	Overpressure Gas	Container (or Test) Identification	Test Time, Months Aim	Test Time, Months Actual	Remarks
99.99% Al 6061 Alloy	Specimens immersed in brine	N_2, 10 atm	1B	6	13	A decision was made to extend all Al-base material tests to 13 and 24 months after the tests had been initiated
			10B[a]	12	24	
		CO_2, 10 atm	2B	6	13	
			11B[a]	12	24	
		H_2S, 5 atm	3B	6	13	
			12B[a]	12	24	
99.99% Al 6061 Alloy Low-carbon steel (Lot J)		N_2, 10 atm	4B	6	13	Steel specimens were included in these tests to determine the effect of Fe contamination on the corrosion rate of the Al-base materials
			13B[a]	12	24	
		CO_2, 10 atm	5B	6	13	
			14B[a]	12	24	
		H_2S, 5 atm	6B	6	13	
			15B[a]	12	24	
99.99% Al 6061 Alloy	Specimens in vapor phase over brine	N_2, 10 atm	7B	6	13	
			16B[a]	12	24	
		CO_2, 10 atm	8B	6	13	
			17B[a]	12	24	
		H_2S, 5 atm	9B	6	13	
			18B[a]	12	24	

[a] Containers equipped with 300-psig full-range gauges. All other SWC tests were equipped with 200-psig full-range gauges.

4.0 TECHNICAL BACKGROUND

The present study focused on the corrosion and gas-generation characteristics of low-carbon steel, Cu-base materials, Ti-base materials, and Al-base materials in simulated WIPP environments consisting of brine with overpressures of N_2, CO_2, H_2, and H_2S. If it is assumed that a significant amount of a given metal is present in a WIPP-relevant environment, gas generation is considered to be of no consequence if 1) thermodynamic considerations preclude the formation of gas pressures higher than the lithostatic pressure at the WIPP repository horizon, or 2) the reaction rate of the metal is so slow that insufficient gas is produced over the life of the repository to cause a concern. A review of the technical literature was made to obtain preliminary insights into the thermodynamics and kinetics of the reactions of low-carbon steels, Cu-base materials, Ti-base materials, and Al-base materials with anoxic chloride brines and brines with CO_2 and H_2S present. The results of the review of low-carbon steels, Cu-base materials, and Ti-base materials were presented in the prior report, SAND92-7347, and will not be repeated here. However, the Al-base-material corrosion work had not been initiated at the time that report was issued, so a discussion of the behavior of Al-base materials in brine environments was not included in that report. Because of their strong relevance to gas generation within the WIPP repository, the mechanistic considerations, thermodynamic characteristics, and kinetic behavior of Al-base materials in brine environments will be described in the following three subsections of this report.

4.1 Al-Base Materials: Mechanistic Considerations

Aluminum is a reactive metal that has a high affinity for oxygen. The metal demonstrates a high degree of corrosion resistance in a wide variety of environments because of the protective character of the oxide film that forms on the metal surface. In this manner aluminum is similar to stainless steels and titanium alloys (Shreir, 1963, Hatch, 1984). Aluminum oxide dissolves in strong acids and alkalis. Such environments cause a loss of protective film and a general dissolution of the metal. Generally, the oxide film is stable over a pH range of 4 to 9 (Hatch, 1984).

Aluminum alloys have a reasonably high degree of corrosion resistance to chloride brines. This resistance permits their use (for example) in a wide range of seawater applications. When corrosion occurs, it is a pitting-type attack, initiating at weak spots in the oxide film. The localized corrosion resulting is caused by a local electrochemical cell, usually because of the presence of cathodic microconstituents in the metal surface, such as $CuAl_2$, $FeAl_3$, and Si. The presence of O_2 as an electron acceptor at the cathode greatly facilitates pitting corrosion (Hatch, 1984).

It is reported that very high purity Al is far superior to commercial alloys in regard to resistance to pitting corrosion. Of the commercial alloys, the 5XXX Series (Al-Mg family) has the best resistance to pitting. In the 6XXX Series (Al-Mg-Si family) pitting is often observed in conjunction with intergranular corrosion (Hatch, 1984).

A well-known phenomenon frequently contributing to the poor corrosion performance of Al alloys in a variety of environments (especially environments containing Cl^-) involves the deposition of reducible metals onto the surface of the Al alloy by a replacement reaction, with the subsequent functioning of the deposit as a relatively efficient cathode in a localized electrochemical cell. Ions of the "heavy metals," Cu, Co, Pb, Ni, Sn, and Hg are the ones most often cited as being harmful to Al-base alloys (Schweitzer, 1989).

Especially relevant in this regard is the work described by Cook and McGeary (1964). They showed that Fe is also able to deposit on an Al-alloy substrate from a concentrated chloride brine solution and increase the corrosion rate of the underlying alloy if the solution is anoxic and if the iron present in the solution is in the form of ferrous ion. Ferric ion will not enhance the corrosion rate, even in deaerated neutral brine, because it is present only at extremely low activities as a hydrated ferric oxide. Cook and McGeary suggest that only the most electronegative Al alloys, notably those with a significant Zn concentration, are able to bring about the deposition of metallic Fe and the increase in the Al alloy corrosion rate.

All of the "heavy metals" noted, including Fe, are apt to be found in the waste material in the WIPP site, so the corrosion of Al-base materials might be routinely accelerated in the WIPP site relative to corrosion occurring in brine uncontaminated by Fe. Unfortunately, the corrosion results found in the literature are strictly qualitative in nature, as none of the referenced work attempted to quantify the corrosion enhancement associated with deposition of a heavy metal. However, the iron-induced service failure cited by Cook and McGeary suggests a corrosion rate of an Al-2.5% Zn alloy

of approximately 1.5 mm/year (0.060 in./year) in a 10 wt% chloride brine solution. This corrosion rate is estimated to be at least a factor of 100 higher than that which would be expected in the absence of ferrous ion, based on the corrosion of similar alloys in seawater without ferrous ion present (ASM, 1987).

4.2 Al-Base Materials: Thermodynamic Considerations

When Al alloys react with water over a pH range of approximately 4 to 9, alumina trihydrate, $Al_2O_3 \cdot 3H_2O$, is commonly found to be the reaction product (Shreir, 1963, Hatch, 1984). This reaction product, which tends to passivate the Al alloy surface, forms according to the reaction

$$2Al + 6H_2O = Al_2O_3 \cdot 3H_2O + 3H_2 \quad (1)$$

Because of the extremely high reactivity of Al metal, the reaction strongly tends to the right, with the potential for producing a high equilibrium H_2 pressure. If thermodynamic values for the Gibbs free energy formation at 25°C are assigned to H_2O and $Al_2O_3 \cdot 3H_2O$ (Garrels and Christ, 1965), the following equilibrium constant results:

$$\frac{f_{H_2}^3}{f_{H_2O}^6} = 3.7 \times 10^{153} \quad (2)$$

If the fugacity of H_2O is assigned the value 0.03 atm (Brush, 1990), then

$$f_{H_2} = 1 \times 10^{48} \text{atm} \quad (3)$$

This equilibrium pressure is obviously much greater than that required to overcome the lithostatic forces operative at the WIPP repository horizon.

The preceding discussion assumed that the corrosion product was $Al_2O_3 \cdot 3H_2O$. Initial laboratory studies at PNL involving the exposure of Al-base materials to Brine A with overpressures of N_2,

CO_2, and H_2S have shown that the situation is much more complex, and that a wide range of corrosion products are formed when Al-base materials contact anoxic chloride brines. Some, but not all, of the corrosion products in the PNL studies were identifiable by XRD (x-ray diffraction analysis). In no case was alumina trihydrate the corrosion product observed in these studies. Complex hydrated oxide/hydroxide combinations containing Cl were the compounds commonly observed. The thermodynamic characteristics of these complex compounds are not known. In order to obtain some insights into the H_2 pressure possible from reactions other than that described in Equation (1), the equilibrium H_2 pressures resulting from the formation of aluminum hydroxide [$Al(OH)_3$] and aluminum chloride oxide (AlClO) were calculated:

$$2Al + 6H_2O = 2Al(OH)_3 + 3H_2 \tag{4}$$

$$2Al + 4H_2O + 2NaCl = 2AlClO + 2NaOH + 3H_2 \tag{5}$$

The values of the Gibbs free energy of formation for H_2O and NaOH at 25°C were obtained from Garrels and Christ (1965), and the values for NaCl and AlClO at 30°C were taken from JANAF (1985). Assigning these values, and the value $f_{H2O} = 0.03$ atm, results in the following equilibrium constants and H_2 pressures:

- For Equation (4) [$Al(OH)_3$ product]:

$$\frac{f_{H_2}^3}{f_{H_2O}^6} = 1.6 \times 10^{147} \tag{6}$$

$$f_{H_2} = 8 \times 10^{45} \text{atm} \tag{7}$$

- For Equation (5) [AlClO product]:

$$\frac{f_{H_2}^3 \cdot a_{NaOH}^2}{f_{H_2O}^4 \cdot a_{NaCl}^2} = 2 \times 10^{88} \quad (8)$$

$$f_{H_2} = 2 \times 10^{27} \text{ atm} \quad (9)$$

For the calculation of f_{H_2} associated with the formation of AlClO [Equation (9)], it was assumed that the activity of NaCl and NaOH were both unity. For NaCl, it is a reasonable assumption, as the brine approximates a saturated brine with respect to NaCl. For NaOH, the assumption of unit activity makes the calculated value of the fugacity of H_2 [Equation (9)] less than it actually would be (i.e., conservatively low), as the solution is not expected to become saturated with respect to NaOH and the a_{NaOH} is therefore expected to be < 1 in Equation (8).

All of the foregoing results lead to the conclusion that, on a thermodynamic basis, the reaction of Al-base materials with the water constituent of a repository brine will produce H_2 pressures that are far in excess of that which can be contained by the repository.

4.3 Al-Base Materials: Kinetic Considerations

It is difficult to estimate, or even gain a reasonable insight into, the corrosion resistance of Al-base materials in anoxic chloride brines under WIPP repository conditions from the available technical literature. This is primarily because the combination of anoxic repository conditions and unique repository brine composition precludes in-depth, detailed comparisons with available data. The behavior of Al alloys in seawater is of some interest, however, and will be reviewed here briefly.

The behavior of Al alloys in seawater has received very extensive investigation, and many tables of corrosion rates of Al alloys in seawater exist. It is reported (ASM, 1987) that the corrosion rate of Al alloys in seawater increases with oxygen content, decreasing pH, and decreasing

temperature. The corrosion rate at great ocean depths is not dissimilar from corrosion near the ocean surface, as the lower pH and lower temperatures in deep water compensate for the oxygen concentration difference.

The tabulated seawater corrosion data suggest that Al-base materials will demonstrate significant corrosion rates under WIPP repository conditions. For example, specimens of 6061 alloy were reported to corrode to the extent of 26 g Al/m^2-year when immersed in seawater near Harbor Island, North Carolina, during a 2-year corrosion test (ASM, 1987). If Al_2O_3 is assumed to be the corrosion product, and if it is further assumed that O_2 does not take part in the cathodic reduction reaction (or, equivalently, that the corrosion rate does not vary with O_2 fugacity), this corrosion rate is equivalent to the production of 1.5 mol H_2/m^2-year, a rate which is a factor of 15 higher than the production of H_2 observed in tests of low-carbon steel exposed to anoxic Brine A, when equivalent metal areas are compared (SAND92-7347). While it must be acknowledged that the comparison made between seawater corrosion and repository corrosion is extremely simplistic, the comparison does suggest that the generally "good" corrosion resistance of Al alloys in seawater may not be "good," in a relative sense, under repository conditions.

As a final note on the kinetics of corrosion of Al-base materials, it is well known that the corrosion rate escalates rapidly outside the pH range of approximately 4 to 9. While it is improbable that the pH of a repository brine could attain a value <4 through purposeful adjustment of the composition of the backfill material, it would be possible to exceed a pH of 9 through the use of an alkaline grout. The impact of such a pH change might have to be assessed in terms of its impact on the corrosion of Al-base materials in the repository waste.

o

5.0 APPROACH

All of the H_2-generation studies were performed using laboratory test equipment and laboratory facilities. Each test followed one of three basic testing methods, dictating the type of reaction vessel employed. The test methods, the metallic test materials, and the brines used in the testing program are described in this section of the report.

5.1 Testing Methods

Three test methods were used in the program: the seal-welded-container test method, the autoclave test method, and the constant-pH test method.

5.1.1 Seal-Welded-Container Test Method

Tests performed in the presence of brine and low-to-intermediate gas pressures (e.g., 0 to 20 atm) made use of seal-welded containers made of Hastelloy C-22®, a corrosion-resistant Ni-Cr-Mo alloy (Figures 5-1 and 5-2). The specimen rack shown in Figure 5-1 was used for low-carbon-steel tests. The alternative packaging material tests and the Al-base material tests used somewhat different specimen arrangements; these are described in Section 6.2. In all tests the same basic specimen support rack was used. The rack shown in Figure 5-1 is in the position used for immersed-specimen testing. For vapor-phase testing the rack would be inverted.

Because the course of the reaction was monitored by the pressure of H_2 retained within the container by means of the pressure gauge, and because atmospheric gases must be rigorously excluded from the test environment, it was imperative that the containers be leak-free. To that end, the containers were of all-welded construction (with the exception of the gauge's pipe-thread joint with

® Hastelloy C-22 is a registered trademark of Haynes International, Kokomo, Indiana.

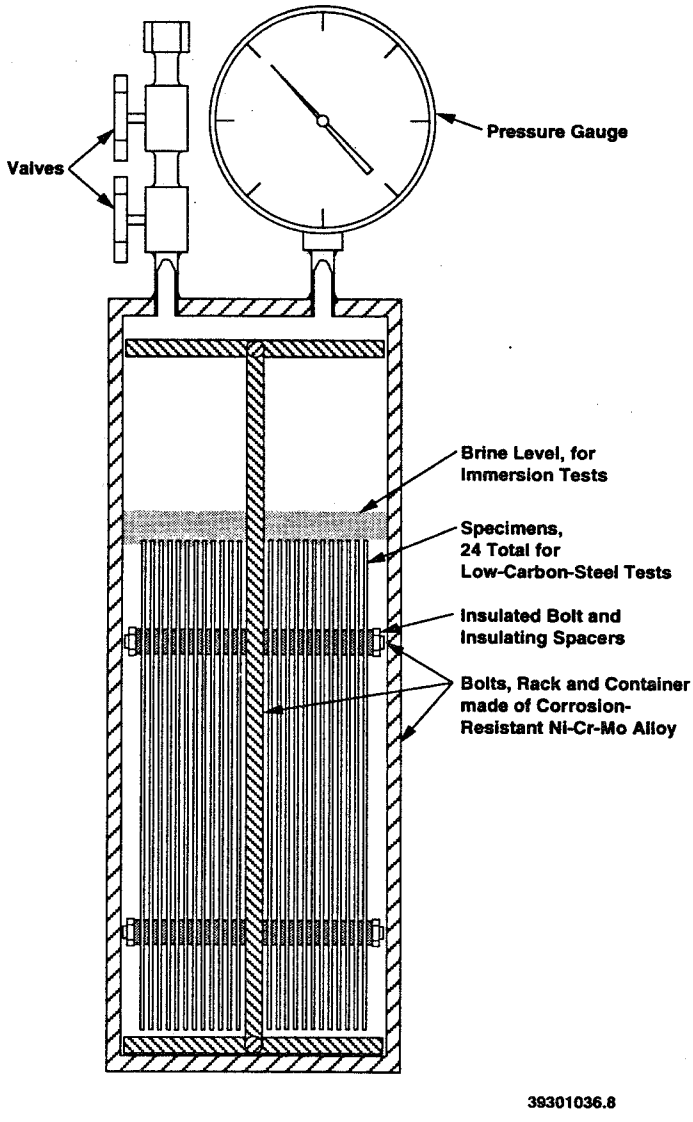

Figure 5-1. Seal-welded test container with specimen rack in place. Inside dimensions (typical): 28.9 cm (11.4 in.) high, 10.2 cm (4.0 in.) diameter.

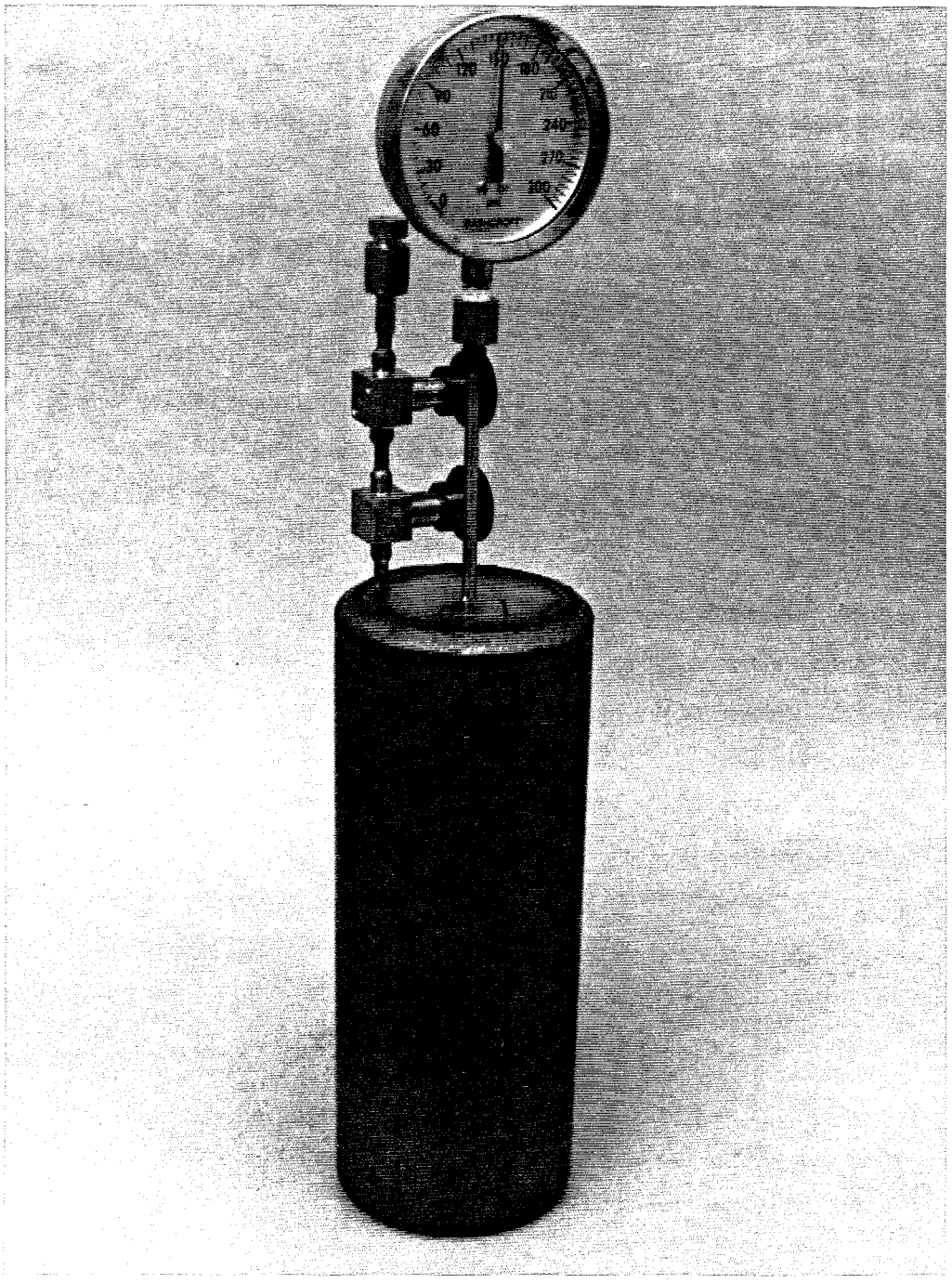

Figure 5-2. Seal-welded test container, fully charged, ready for placement in oven.

the body of the container, which was made up very tightly, with Teflon® tape applied to the threads). The pre-weighed test specimens (of large area, to expedite rapid quantification of gas generation) and the brine were placed in the container before welding the top on the container. The sealed containers were then pressurized with He gas to 4.4 atm (50 psig). Two additional He fills with intermediate evacuations were made to ensure minimization of contamination with residual air. After the third He fill, the containers were given a standard He leak-check test capable of sensing a He leak rate of 1.2×10^{-10} atm-cc/s. A container that did not pass the leak test was not used. If the leak test was successfully passed, the He was evacuated from the container and the appropriate overpressure gas was added. The containers were then placed in forced-convection (incubator) ovens maintained at 30 ± 5°C, and the course of the gas-generating reaction monitored by observing the pressure changes on the pressure gauges. Gas samples could be obtained from the containers at any time for gas analysis, though taking such a sample perturbed the container gas inventory and gas pressure. For this reason, gas sampling was generally performed at the conclusion of a test, after the final pressure readings had been obtained.

In the seal-welded-container tests, two methods were used to determine the rates of the corrosion and gas-generation reactions: 1) determination of the container gas pressure as a function of time and 2) determination of the amount of metal lost from each specimen at the conclusion of a test by gravimetric methods. The former method had the advantage of yielding real-time information on the course of the gas-generating reaction. Confidence in the results obtained in any given test environment was dependent on accurate pressure gauge information and accurate estimations of specimen area and the plenum volume (vapor space) of the test container. The result obtained represents the gross integrated reaction of the specimen assembly, without quantifying the contribution of each specimen, hence each lot of material, to the H_2 being generated. The latter method had the advantage of being capable of specifying the contribution of each specimen to the H_2 generated during the test.

A detailed analysis of the accuracy of the pressure gauges and sources of variability in the gravimetric data are presented in SAND92-7347.

® Registered trademark, E. I. Du Pont de Nemours, Wilmington, Delaware.

At the conclusion of a test, the container was opened by means of a milling operation that removed the top closure weld. The specimens were quickly lifted from the container, removed from the specimen rack, rinsed, and placed in desiccators. X-ray diffraction (XRD) analyses of the corrosion products were typically performed on selected specimens, usually within 24 h if there was judged to be a possibility of oxidation of the corrosion product by contact with air. The brine from the test container was retained for chemical analysis. The corrosion product was stripped from the specimens by means of an inhibited acid solution, and the amount of metal lost from each specimen was determined. The gravimetric analysis permitted an estimate to be made of the metal loss from (or penetration of) each specimen. The metal-loss data were compared with the quantity of H_2 generated and the corrosion product formed, for determination and corroboration of the overall corrosion/gas generation processes.

5.1.2 Autoclave Test Method

Tests performed at high gas overpressures, e.g., pressures greater than ~20 atm, utilized heavy-wall autoclave systems. The autoclaves were typically of 3.8-L capacity. Because the autoclaves had high-pressure gasket seals, they could not be expected to be as gas tight as the seal-welded containers. However, pressure-time data could be obtained from an autoclave pressure gauge when the autoclave was extremely well sealed. Otherwise, the data from an autoclave system consisted of the gravimetric results and the analysis of the corrosion product film by XRD or other methods.

While autoclave systems were often employed for high-pressure studies, they had additional uses associated with their relatively large volume. For example, if it were considered necessary to keep major components of a test separate, as in the case of a mass of salt containing test specimens suspended in the vapor phase over a pool of brine, an autoclave was able to provide the flexibility and volume required.

5.1.3 Constant-pH Test Method

The constant-pH tests were performed in glass resin kettles, each of 3 L capacity. A plexiglass cover was clamped over each vessel, with a neoprene O-ring placed between the vessel and the cover. Polyethylene tube fittings screwed into the cover were used for insertion of thermocouples and tubing

for N_2 sparge gas and delivery of acid and basic solutions for maintenance of constant pH. A ring-shaped specimen holder for supporting the corrosion specimens, a rectangular specimen for E_{corr} measurements, a glass electrode, and a chloride SIE (Specific Ion Electrode) were also placed within each vessel. (The specific functions of the electrodes in measuring brine pH are described in detail in Section 6.1.2.1.)

Each test vessel was placed on a magnetic stirrer plate, and the brine (ERDA-6) was stirred with a Teflon-coated magnet placed within the vessel. Heating was done by means of a heating tape wound around the vessel. All tubing and metal components contacted by brine were made of alloy 600 (76% Ni, 16% Cr, 8% Fe) to avoid brine contamination. The N_2 sparge gas was high purity (>99.93% N_2). The test coupons were suspended from the support ring by lengths of Teflon tape.

Each vessel was filled with 2.36 L of brine at the beginning of the test exposure. With this quantity of brine there was a vapor-phase plenum region ~50 mm deep within which the specimen support ring could reside without contacting the brine. Eight corrosion specimens, two each of lots J, K, L, and M were included (fully immersed) in each test. The specimens measured 25 mm × 51 mm (1.0 in. × 2.0 in.) and each specimen had two 4.8 mm (3/16 in.) holes for suspension.

The pH of the brine was maintained by automatic or manual additions of acid (1 M HCl) or base (1 M NaOH). Automatic addition, required, for example, in the low-pH tests, was done automatically by pH-stats.[1] The N_2-sparged solution was delivered directly to the test vessel by the pH-stat pumps through polytetraflouroethylene (PTFE) tubing.

The glass electrode and the chloride SIE were left inside the test vessel, partially immersed in brine, for the entire 6-month test duration. The electrode leads were passed through gas-tight seals in the vessel lid. Neither electrode required a leaking liquid junction. The calibration of the internal electrodes was checked on a weekly basis by drawing out small (10 mL) samples and checking the pHCl on a pair of freshly calibrated electrodes. As a rule, the potential measured *in situ* and the externally measured potential did not differ by more than 10mV.

[1] Model 1488, FMS, Inc., Watertown, MA.

5.2 Materials

The H_2-generation study focused on three major material classes: low-carbon steel, intended to closely represent the drum steel and the waste-box steel materials while approximately representing the steel wastes within the containers; alternative packaging materials, consisting of unalloyed Cu and Ti and selected Cu- and Ti-base alloys; and Al-base materials, representing Al-base scrap material present in the waste.

5.2.1 Low-Carbon Steels[2]

The drums and waste boxes containing the TRU waste will make by far the greatest contribution of metallic Fe to the WIPP repository (Brush, 1990). This Fe will be in the form of low-carbon steel, ranging in composition from the low-C, low-Mn material used in the fabrication of the Department of Transportation (DOT) 17-C drums (0.04 to 0.1% C, 0.25 to 0.5% Mn) to the somewhat more highly alloyed material used in the waste boxes (for example, ASTM A36 steel, with 0.25% C maximum and 0.8 to 1.2% Mn; and ASTM A569 steel, with 0.15% C and 0.60% Mn maximum). The steel waste contained within the waste boxes can be expected to range widely in composition, from low-carbon steel (for example, nails, wire, structural steel) to highly alloyed material (for example, tools, high-strength fasteners, machine components).

Ideally, a corrosion or a gas-generation study would utilize test specimens and a test environment that exactly duplicate the field conditions. In the present case, this was not possible, as a wide range of steel compositions will exist in the repository, and the compositions cannot ever be known with a high degree of certainty. It was therefore necessary to simulate the WIPP site conditions by using a range of steel compositions approximating the range of material compositions expected in the WIPP site. To this end, four lots (heats) of steel were obtained for test specimens, two lots each of ASTM A366 (standard specification for cold-rolled sheet), representative of steel waste drums, and ASTM A570 (standard specification for hot-rolled carbon steel sheet and strip), representative of steel

[2] The term "low-carbon steels" is a broad material classification, generally considered to include steels having less than 0.25% C, 1.65% Mn, and 0.60% Cu, along with small amounts of other elements (ASM, 1978). According to this definition, the drum materials and the waste box materials are "low-carbon steels."

waste boxes and other steel waste materials. The two lots of ASTM A366 steel were designated "J" and "K," and the two lots of ASTM A570 steel were designated "L" and "M." The thickness of the as-received material is given below:

Lot	Thickness, mm (in.)
J	0.70 (0.028)
K	0.86 (0.034)
L	1.5 (0.059)
M	1.6 (0.063)

The compositions of the four lots of steel are presented in Table 5-1. Two values are presented for the C content of each lot of steel, representing analyses provided by 1) the steel vendor and 2) an independent testing laboratory.[3] The discrepancies in C concentration noted for the J and K lots between the two analyses are not considered important to the results of the study.

Table 5-1. Compositions of Low-Carbon Steels, Weight Percent

	ASTM A366		ASTM A570	
Specie	Lot J	Lot K	Lot L	Lot M
C	0.06/0.10	0.05/0.09	0.13/0.14	0.13/0.13
Mn	0.30	0.30	0.77	0.75
Si	0.08	0.07	0.11	0.10
P	0.015	0.015	0.017	0.020
S	0.012	0.009	0.015	0.015
Cu	0.015	0.020	0.015	0.040
Fe	bal	bal	bal	bal

[3] Koon-Hall Testing Corporation, 5687 S.E. International Way #A, Portland, OR 97222.

In all of the calculations conducted in the present work equating molar equivalencies of corrosion reactants and corrosion products, and in all calculations equating corrosion (penetration) rates with metal lost, the steels were treated as though they were pure Fe, with a molecular weight of 55.85 and a density of 7.86 g/cm^3.

Additional information on the low-carbon steels employed in the tests, and justification for their use, is presented in SAND92-7347.

5.2.2 Alternative Packaging Materials

The potential for gas pressurization of the WIPP underground facility due to corrosion of packaging materials and metal waste has necessitated consideration of several different options for waste form modification. One possible option involves repackaging the waste in containers that do not have the gas-generation characteristics of mild steel. To identify suitable alternative materials for waste packaging, an expert panel referred to as the Waste Container Materials Panel (WCMP) was convened in 1990 by the DOE WIPP Project Office, as a part of the Engineered Alternatives Task Force (EATF) activities. The panel evaluated a wide range of metallic, ceramic, cementitious, polymeric, and coating materials for their applicability to WIPP containers (EATF, 1991).

An important criterion for the selection of suitable metallic materials was absence or significant minimization of gas-generation tendency. Additional criteria were fabricability, availability, fabrication capacity (industrial production capacity), status of technology development, cost, and mechanical properties. The overall ranking of materials indicated that the Cu-base and Ti-base material classes offered the best combination of material properties and overall economic incentive for replacing carbon steel as a metallic container material at the WIPP site. Cu-base materials, though obviously susceptible to attack by and reaction with certain chemical species such as nitrates and sulfides, offer a high degree of thermodynamic stability in near-neutral aqueous solutions; and Ti-base materials are extremely corrosion resistant in a wide variety of low- and intermediate-temperature brines because of the protection afforded by their oxide film (SAND92-7347). Unalloyed Cu (oxygen-free, electronic) and unalloyed Ti (Ti Grade 2) were accordingly selected from the candidate material list for an investigation of their corrosion/gas-generation characteristics in simulated WIPP environments. In addition, cupronickel 90-10 was chosen for study, as its mechanical properties are far superior to

unalloyed Cu due to the presence of 10% Ni. Ti Grade 12, a Ti-Ni-Mo alloy, was also selected because of its well known resistance to crevice corrosion. The chemical compositions of the specific materials procured for study are presented in Table 5-2.

Table 5-2. Composition of Alternative Packaging Materials Used in Corrosion/Gas-Generation Study

Material[a]	Weight Percent, or (ppm)										
	Cu	Ti	Ni	Zn	Mn	Mo	Fe	Pb	O	S	C
Unalloyed Cu (C10100)	99.99	–	–	–	–	–	–	(3)	(2)	(10)	–
Cupronickel 90-10 (C70600)	87.58	–	10.4	0.2	0.5	–	1.3	0.01	–	0.005	0.01
Ti Grade 2 (R50400)	–	Bal	–	–	–	–	0.16	–	0.13	–	0.01
Ti Grade 12 (R53400)	–	Bal	0.80	–	–	0.30	0.14	–	0.12	–	0.01

a Unified Numbering System (UNS) designations are in parentheses.

5.2.3 Al-Base Materials

Al and Al alloys contained within TRU waste drums emplaced within the WIPP repository would be capable of reacting with a brine environment to form H_2. The corrosion and gas-generation rates will depend to some extent on the specific Al-base material(s) present in the waste. In order to cover the range of anticipated Al-base materials, it was decided by the Sandia National Laboratories technical staff that the waste would be represented by two specimen materials, viz., unalloyed Al of 99.99% purity, expected to simulate relatively pure Al-base materials, and 6061 alloy, a Si-Mn-Mg-Cu-Cr alloy representative of structural Al alloys present in the waste. The compositions of the materials are presented in Table 5-3.

The 99.99% pure Al was supplied in sheet stock, approximately 1.2 mm (0.047 in.) thick. The 6061 alloy was supplied in the form of sheet stock approximately 1.4 mm (0.055 in.) thick. The material had been solution annealed and artificially aged (T6 temper) prior to its receipt at PNL.

Table 5-3. Composition of Al-Base Materials Used in Corrosion/Gas Generation Study

Material	Weight Percent, or (ppm)										
	Si	Fe	Cu	Mn	Mg	Cr	Zn	Ti	B	Ca	Al
99.99% pure Al	(15)	(7)	(3)	(0.2)	(0.5)	(0.3)	—	—	(5)	(0.3)	bal
6061 Alloy (A96061)[a]	0.64	0.46	0.32	0.036	0.96	0.19	0.023	0.012	—	—	bal

a Unified Numbering System (UNS) designation is in parentheses.

5.2.4 Brines

Two brines were used in the present study. One brine, designated "Brine A," was based on the WIPP Brine A composition described by Molecke (1983). Brine A is a high Mg, K, and Na chloride-sulfate brine and is used as a simulant for intergranular Salado Formation brine that might intrude into the WIPP repository horizon. The composition of Brine A, as well as the average value and range of compositions of the three lots of brine made up for usage at PNL in the present study, are given in Table 5-4.

Only the major constituents of Brine A as described by Molecke (1983) were used to make up the PNL simulant version. Omitted minor constituents, deemed to have little or no effect on the corrosiveness of the brine, were Fe, Cs, Rb, Li, Sr, and I. These minor elements totaled only 58 mg/L in the composition described by Molecke.

The second brine used in the study was chosen because of the peculiar requirements of the constant-pH tests. In these tests, the brine reactant was to be maintained at pH values ranging from 3 to 11. Because of the tendency for precipitation of $Mg(OH)_2$ from solution at pHs >8.6, it was judged best to eliminate the Mg^{++} constituent from the brine altogether, so that the presence or absence of Mg^{++} in solution would not constitute an additional test variable. Accordingly, a WIPP-relevant brine was sought having a relatively low Mg^{++} concentration.

Table 5-4. Composition of Brine A Used in Tests

Chemical Specie	Concentration, mg/L	
	Brine A (target)	PNL Brines
Na	42,000	$39,400^{+1200}_{-1100}$
Mg	30,000	$34,700^{+1000}_{-1500}$
K	35,000	$29,900^{+600}_{-400}$
Ca	600	560^{+40}_{-60}
B	220	220^{+1}_{-4}
Cl	190,000	$188,300^{+2700}_{-4300}$
SO_4	3,500	$4,130^{+50}_{-60}$
HCO_3	700	680^{+30}_{-60}
pH	6.5	$7.4^{+0.5}_{-0.7}$

The second brine used in the study was designated "ERDA-6" brine, as it is a modification of a brine of the same name described by Molecke (1983). The brine described by Molecke was from a drill hole designated "ERDA-6" on the original WIPP Site. The hole lies approximately 8.6 km (5.3 mi) north-northeast of the present WIPP Site. The "ERDA-6" brine issued from a brine pocket encountered at a depth of about 826 m (2711 ft) in the Anhydrite II unit of the Castile formation.

The compositions of the ERDA-6 brine, as reported by Molecke, and the PNL modification of the brine (involving elimination of Mg^{++}, Ca^{++}, Sr^{++}, Fe^{3+}, HCO_3^-, and F^-) are shown in Table 5-5.

The Mg^{++}, Ca^{++}, and HCO^-_3 activities were considered to be sensitive to pH, and were eliminated for that reason; and the Sr^{++}, Fe^{3+}, and F^- were considered to be unimportant constituents. Only one batch of ERDA-6 brine was made at PNL.

Table 5-5. Composition of ERDA-6 Brine

Chemical Specie	Concentration, mg/L		
	Flow ERDA-6[a]	Downhole ERDA-6[a]	PNL ERDA-6 Simulation
Na	112,000	140,000	113,000
K	3,800	4,800	3,770
Mg	450	270	--
Ca	490	360	--
Sr	18	--	--
Fe	3.6	5.7	--
Cl	170,000	180,000	164,000
SO_4	16,000	14,000	16,100
B	680	740	830
HCO_3	2,600	1,800	--
Br	880	720	830
F	--	1.7	--
pH	6.42	7.02	6.15[b]

a Taken from Molecke (1983).
b Not corrected to take into account activities of brine constituents.

5.2.5 Salt (Halite)

Four corrosion and gas-generation tests were conducted in which the specimens were packed in either particulate salt (halite) (tests AUT-5 and AUT-6) or in a mixture of salt (halite) and bentonite (tests AUT-12 and AUT-13). The salt used in the tests was shipped to PNL from SNL in two 1-gallon containers, identified as "WIPP Salt E140-N635." The salt was originally gathered from the floor of "E 140 drift, 194 m (635 ft) north of the salt shaft." It was assumed to be essentially pure (>95%) NaCl, and was not analyzed.

5.2.6 Bentonite

The bentonite used in tests AUT-12 and AUT- 13 was obtained from SNL. The material is a product of the American Colloid Company, Arlington Heights, Illinois, and is designated "Volclay GPG 30 bentonite." (American Colloid Company, 1995). Data sheet on file in the SWCF as WPO# 39636. It is a hydrous aluminum silicate consisting primarily (>90%) of the mineral montmorillonite. The material supplied had a particle size between 20 and 70 mesh.

A typical analysis (supplied by the vendor) is given below in weight percent:

SiO_2	63.02
Al_2O_3	21.08
Fe_2O_3	3.25
FeO	0.35
MgO	2.67
Na_2O	2.57
CaO	0.65
H_2O	5.64
Trace elements	0.72

6.0 RESULTS

Three major efforts were undertaken in the present corrosion and gas-generation laboratory study: experiments directed toward determining the behavior of current packaging materials (low-carbon steels in simulated WIPP environments); experiments directed toward determining the behavior of alternative packaging (Cu- and Ti-base) materials in simulated WIPP environments; and experiments directed toward determining the behavior of Al-base (simulated scrap) materials in simulated WIPP environments. The experimental results associated with each major materials group will be discussed separately in this section of the report. The basic division in the experimental work is reflected in the summary test matrices for the project, presented in Tables 3-1 through 3-5. Reference may be made to these tables for information of a summary nature on any of the individual tests described in this section of the report.

Where possible, each test was designed to provide 1) time-dependent container pressure, from which H_2 pressure data could be determined; 2) gas composition data, for quantification of corrosion-product gas generation rates in conjunction with item 1; 3) corrosion rate (metal penetration) data, obtained gravimetrically after corrosion-product film stripping; and 4) corrosion product identification. Post-test brine analyses were also obtained. Items 1 and 2 have the most value and are most defensible when obtained from a demonstrably leak-tight container, such as the seal-welded containers used in the present tests. Information from items 1, 2, and 3 permit a comparison of the moles of H_2 formed versus moles of metal reacted, to verify the legitimacy of the conclusions drawn. Item 4 provides insights into the potential protectiveness of the corrosion product film and also ensures that the appropriate reaction is being considered when the molar equivalency of metal and H_2 are being compared.

In general, "stand-alone" work completed prior to the publication of SAND92-7347 is not duplicated in the present report. However, work completed prior to the publication of SAND92-7347 that is considered important to the understanding of work presented in the present report, or which is closely related to work presented in the present report, is included herein for completeness.

The raw data describing container pressure as a function of time for those seal-welded container tests for which such data are considered meaningful are contained in Appendix A to this report.

The individual specimen data for all tests may be found in Appendix B. These data details are presented to permit additional, independent evaluation and corroboration of the results presented and conclusions drawn in the present report and to facilitate statistical treatment of the data according to the specific future needs of the WIPP Project modelers. Such treatments were not attempted in the present report because of the many different approaches to the data that could be taken in such statistical analyses.

6.1 Low-Carbon Steel Tests

The corrosion and gas-generation behavior of low-carbon steels was evaluated in three environments: anoxic brine (brine/N_2)[4], brine/CO_2, and brine/H_2S. In each environment specimens were exposed either fully immersed in the brine (Brine A or ERDA-6 brine) or in the vapor phase over the brine. All tests were performed at 30 $\pm$5°C. The test conditions are summarized in Table 3-1.

All steel specimens were surface ground using 60-grit emery cloth to remove mill scale or other surface deposits. After grinding, they were dimensionally measured, degreased (using trisodium phosphate followed by a water rinse, and an absolute alcohol rinse), and weighed. The specimen dimensions were obtained to a minimum accuracy of $\pm$0.01 mm ($\pm$0.0004 in.); the specimen weights (pre- and post-test) were obtained to $\pm$0.0001 g. After the final degreasing and weighing operations, the specimens were stored in a desiccator until needed. At that time, the steel specimens exhibited a bright, clean, as-ground appearance.

Upon conclusion of a test, the specimens were removed from the test container, rinsed in deionized water and alcohol, and placed in a desiccator to minimize the possibility of further reactions. Selected specimens were held in reserve for analysis of corrosion products, usually accomplished by x-ray diffraction (XRD). The corrosion product layer was removed from the remainder of the specimens by immersing the specimens in an inhibited HCl corrosion-product stripping solution per

[4] Strictly speaking, each of the environments investigated consisted of anoxic brine, as O_2 was excluded from the test containers. The term "anoxic brine" as used here to describe the environment having no reactive gas (CO_2, H_2S) overpressure signifies that the reactant is anoxic brine alone, without an added reactive constituent.

National Association of Corrosion Engineers (NACE) standard TM-01-69, 1976 revision.[5] The stripping solution is made by adding 12 ml formaldehyde to 1 L of 50% HCl solution. A final weighing was then performed so that the mass of metal lost from each specimen by corrosion could be calculated.

6.1.1 Seal-Welded-Container Tests

Each seal-welded container test described in this section of the report contained a rack of 24 test specimens, comprising six replicate test specimens of each of the four lots of low-carbon steel previously described in Section 5.2. The six test specimens of each lot of steel consisted of three wide specimens, 86 mm (3.4 in.) × 190 mm (7.5 in.), and three narrow specimens, 51 mm (2.0 in.) × 190 mm (7.5 in.). Each specimen had two holes, 8 mm (0.31 in.) in diameter, to accommodate the insulated rack supports. The narrow specimens were placed on the outer part of the rack to optimize material loading in the container. The total specimen area in each container lay in the range 0.60 to 0.64 m^2. In the immersed-specimen tests, sufficient brine (1.34 to 1.40 L) was added to the container to cover the tops of the specimens to a depth of ~6.4 mm (~0.25 in.). In the vapor-phase exposure tests, 0.25 L of brine was placed in the bottom of the test container. The level of the brine was below the racked specimens, though the brine unintentionally splashed on the bottoms of the specimens during container handling. The immersed-specimen containers had a calculated vapor-space plenum volume of 0.634 L. The plenum volume in the vapor-phase exposure tests was 1.74 L. The specimen area-to-plenum volume ratio was made large to promote a rapid response on the test container pressure gauge to the H_2 generated by corrosion reactions.

6.1.1.1 ANOXIC BRINE (BRINE/N_2) TESTS

The anoxic brine tests were intended to provide basic information on the corrosion/gas-generation proclivity of low-carbon steel in the absence of reactants other than low-carbon steel and Brine A or ERDA-6 brine. The anoxic brine immersed-specimen testing regimen using Brine A as the test

---

[5] *Laboratory Corrosion Testing of Metals for the Process Industries*, National Association of Corrosion Engineers, Houston, Texas 77084. The stripping solution was made by adding 12 ml formaldehyde to 1 L of 50% HCl solution.

environment included test containers 1, 2; 9, 10; 17, 18; 25, 26; and 46, 47; the vapor-phase-specimen testing regimen using Brine A included test containers 5, 6; 13, 14; 21, 22; and 29, 30. The immersed-specimen tests using ERDA-6 brine were test containers 44 and 45. Proximate identification numbers (e.g., 1, 2) signify duplicate tests. These test container identification data are also contained in Table 3-1.

All of the pressure-time plots from the Brine A/N_2 test series, exclusive of tests 46 and 47, are presented in Figure 6-1. The figure, and the corresponding raw data, were previously presented in SAND92-7347. The figure is presented here as well because the pressure-time results derived from the data, i.e., the last 12 months of the 24-month tests, were used to arrive at the basic long-term steel H_2 generation rate of 0.10 mol H_2/m^2 steel-yr, equivalent to a steel corrosion (penetration) rate of 0.71 μm/year (SAND92-7347). A detailed assessment of the test results, including gas analysis results, specimen appearance, agreement between test containers and between gas generation and metal lost, brine analyses, the attempts to identify corrosion products by XRD, and the lack of corrosion/gas generation exhibited by vapor-phase specimens may be found in SAND92-7347.

The initial (unsuccessful) attempts to identify the corrosion product formed in the 12- and 24-month brine/N_2 tests were described in detail in SAND92-7347. An additional attempt, using both an XRD and a chemical analysis approach, was undertaken using corrosion products derived from anoxic brine tests of six months duration (tests 46 and 47, Table 3-1). The pressure-time histories of these tests closely matched those of equivalent earlier tests, supporting the assumption of equivalent corrosion products.

It is known that low-carbon-steel corrosion products derived from anoxic brine tests rapidly oxidize in the presence of air. The blue-green corrosion product obtained from the test container begins to convert to the red-orange corrosion product in a matter of minutes unless special care is taken to prevent O_2 contact with the material. For the present corrosion product examination, container 46 was removed from its incubator oven after $\sim$6 months test duration, shaken vigorously for several minutes, then inverted over a vacuum filtration device covered with a N_2-filled plastic bag. The valve assembly was opened, allowing brine and particulate corrosion product to enter the filter. After about 30 seconds a substantial amount of corrosion product had collected on the filter paper.

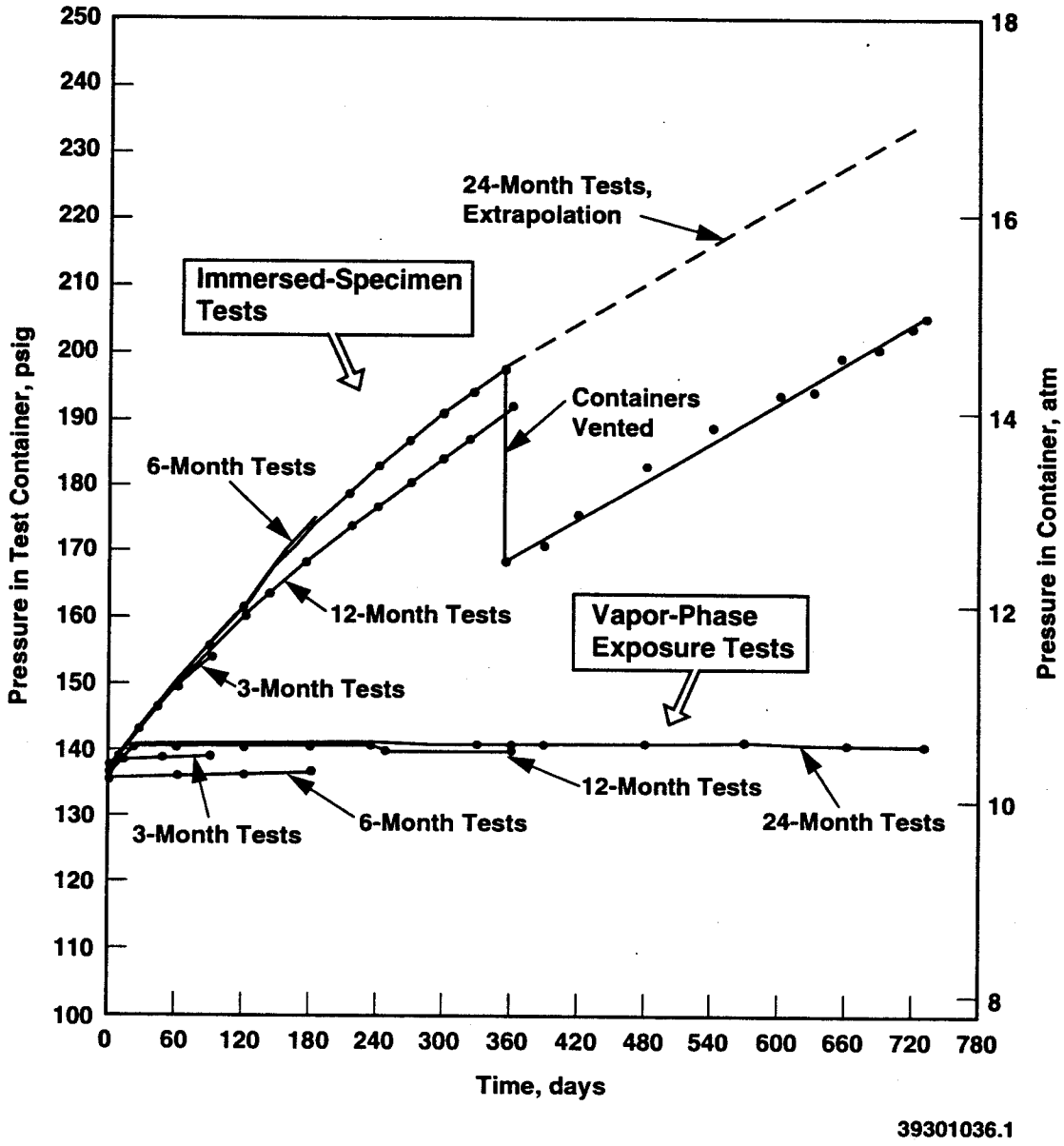

Figure 6-1. Pressure-time curves, low-carbon steel anoxic brine tests. Each curve represents two (duplicate) tests.

The corrosion product was then washed thoroughly with deionized water from a N_2-sparged wash bottle. When the washing was complete, the filter paper and corrosion product residue was transferred to an evacuatable desiccator, where it was stored under vacuum (for ~2 h) prior to obtaining the XRD pattern. The procedure was then repeated to obtain a corrosion product sample for chemical analysis.

XRD Results[6]

The diffraction pattern obtained from the corrosion product from test 46 was a very close match to that obtained from the 24-month brine/N_2 test (test 25), except that several additional peaks were present in the test 25 pattern. This finding implies the presence of an additional compound in the test 25 corrosion product.

The corrosion product from test 46 was not identifiable using XRD, as no matching database entries were found (through Set 44, 1994). As previously reported (SAND92-7347), the corrosion product from test 25 was also not identifiable.

Chemical Analysis Results

Chemical analyses of samples of corrosion product taken from tests 46 and 47 were performed by inductively coupled argon plasma optical emission spectroscopy (ICAP) and ion chromatography (IC). The corrosion product specimen was dissolved in 2% HNO_3 solution prior to analysis.

The results of the chemical analyses are presented below (wt %):

---

[6] The x-ray diffractogram of the test 46 filter sample was compared to the Powder Diffraction File database, Sets 1-44 (PDF-2, International Centre for Diffraction Data, 1994). Comparison of the experimental pattern with this database was effected using the full-pattern, analog search/match algorithm resident in Jade+, Ver. 2.1 (Materials Data, Inc., Livermore, CA). Additional Comparison was made using the traditional D-I search/match algorithm of Micro-ID+, Ver. 2.0 (MDI).

Specie	Test 46	Test 47
Fe	38	37
Mg	6.7	7.7
Mn	0.18	0.11
K	<0.2	~0.03
Na	<0.1	0.05
Ca	<0.022	0.02
S	<0.07	0.24

The high Mg content of the corrosion product is reminiscent of the compound amakinite, an Fe, Mg hydroxide, commonly found in the testing of ferritic materials in anoxic brines in past studies (Westerman et al., 1988). The amakinite found at 150°C, for example, when an ASTM type A216 steel was exposed to an anoxic high Mg salt/brine environment for 12 months, contained 25 wt% Fe and 6 wt% Mg, for a compound of the composition $Fe_{0.64}$ $Mg_{0.36}$ $(OH)_2$, or, approximately, $Fe_{2/3}Mg_{1/3}(OH)_2$ (Westerman et al., 1988). Though the corrosion product chemical composition in the present test suggests amakinite, the XRD results do not show a match with amakinite, or any other related compound.

Although the corrosion product cannot be identified exactly, it will continue to be considered a close relative of, or some form of, $Fe,Mg(OH)_2$, because of its chemical similarity to amakinite and because amakinite has been found under similar steel-reaction circumstances.

6.1.1.2 BRINE/CO_2 TESTS

The brine/CO_2 tests were intended to provide information on the corrosion and gas-generation proclivity of low-carbon steel in the presence of Brine A and CO_2. The presence of CO_2 in the WIPP at significant fugacities is considered to be a distinct possibility because it is an expected byproduct of the microbially mediated degradation of cellulosic materials and other organic materials that will presumably be disposed of in the WIPP in large quantities.

Two types of brine/CO_2 experiments were performed: experiments in which CO_2 was present in the test containers in quantities so large that its complete consumption was not possible (the "excess-CO_2" tests); and tests in which the quantities of CO_2 added to the test containers were controlled so as to permit the essentially complete consumption of the CO_2 in some of the tests, but not

in others (the "controlled-CO_2-addition" tests). These tests will be discussed separately in the following subsections.

Excess-CO_2 Tests

The excess-CO_2 tests were intended to provide information on the corrosion and gas-generation characteristics of low-carbon steel in the presence of Brine A and excess CO_2. The brine/CO_2 immersed-specimen testing regimen included test containers 3, 4; 11, 12; 19, 20; and 27, 28. The brine/CO_2 vapor-phase-specimen testing regimen included containers 7, 8; 15, 16; 23, 24; and 31, 32. Proximate identification numbers (e.g., 3, 4) signify duplicate tests.

In the immersed-specimen tests the CO_2 was added to the test containers at an initial hypothetical starting pressure of ~155 psig (~170 psia, or ~12 atm). This starting pressure is termed "hypothetical" because, in general, equilibration between the CO_2 present in the plenum of the test container and CO_2 present in the brine was not achieved for several days after test initiation, in spite of the fact that each container was agitated (by hand-shaking) for a period of 10 to 15 min after addition of the final CO_2 charge. The average quantity of CO_2 added to each of the immersed-specimen test containers was 19.3 g, or 0.44 mol. As the average steel area in each test container in this series of tests was 0.604 m^2, the initial CO_2 charge in each test container was equivalent to 0.73 mol per square meter of steel in an $FeCO_3$-forming reaction.

The Henry's Law coefficient, S, for CO_2 in equilibrium with Brine A

$$S = \frac{\text{moles } CO_2 \text{ per liter of brine}}{\text{pressure } CO_2, \text{ atm}} \tag{10}$$

was experimentally determined to be equal to 0.012 at 20°C, and 0.010 at 30°C. During a 30°C test, assuming equilibrium conditions, the major portion of the CO_2 (~65%) would be expected to be present in the gas phase with the remainder (~35%) dissolved in the brine. The H_2 generated by the corrosion reaction, on the other hand, would collect in the plenum region of the test container only, as it is essentially insoluble in the brine phase. As the CO_2 is consumed by the corrosion reaction to form $FeCO_3$, the pressure will tend to decrease in the plenum, but not to the extent that the pressure increases due to H_2 formation because the brine phase will continually supply a fraction of the CO_2

involved in the corrosion reaction. Thus, a pressure buildup in the plenum (caused by H_2 generation) will be observed on the pressure gauge as the reaction proceeds, even though a mole of CO_2 is consumed for each mole of H_2 formed.

The pressure-time curves for the excess-CO_2 tests are presented in Figure 6-2. This figure, along with the raw data, were originally published in SAND92-7347. The figure is duplicated here because of its relevance to associated steel-Brine A-CO_2 tests that will be discussed in the next section of the report. For additional details of the study that led to the pressure-time relationships shown in Figure 6-2, including gas and brine analyses, specimen appearance, XRD results, agreement between H_2 formed and metal reacted, determination of amount of CO_2 required to passivate the steel specimens, and the lot-to-lot differences in steel corrosion rates and the lack of corrosive attack of vapor-phase specimens, the report SAND92-7347 may be consulted.

Controlled-CO_2-Addition Tests (With Eventual H_2S Addition)

The initiation of these tests, and a description of their progress for ~300 days, was described in SAND92-7347. The tests have been completed since the publication of that document, so they will receive a relatively complete and detailed treatment here.

When the activity of CO_2 dissolved in Brine A is increased, two opposing effects are manifested: 1) the brine becomes a more aggressive corrodant toward steel due to effects already discussed [Equations (1) through (7), (SAND92-7347)]; and 2) the presence of CO_2 tends to stop the reaction through the formation of a stable $FeCO_3$ layer. The controlled-CO_2-addition tests were intended to provide information on the amount of CO_2 required/unit area of steel to attain a passivated state, such as was attained in the excess-CO_2 tests after CO_2 (initially at ~12 atm pressure) had reacted with the steel to the extent of ~0.42 mol CO_2/m^2 steel (SAND92-7347).

Once CO_2-induced passivation was attained, the tests were to provide information as to whether or not CO_2-passivated specimens could become depassivated by addition of H_2S to the system. This is considered likely on thermodynamic grounds because of the extreme stability of FeS (or FeS_2) relative to $FeCO_3$ (SAND92-7347).

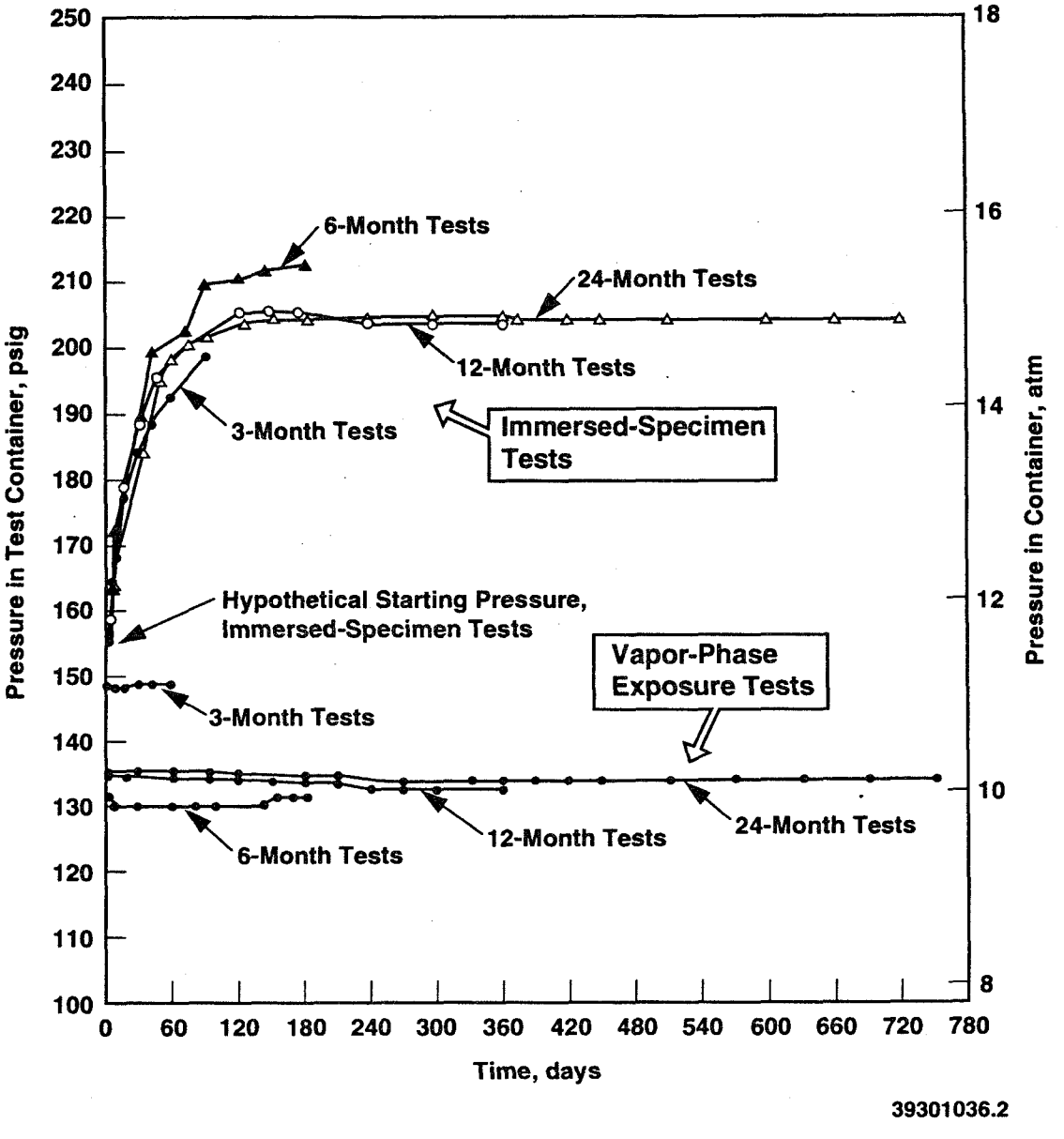

Figure 6-2. Pressure-time curves, low-carbon steel/brine-CO_2 tests. Each curve represents two (duplicate) tests.

The subject investigation comprised test containers 33 through 38. The initial test conditions are summarized in Table 6-1. An N_2 addition was made to test containers 36 through 38 so that the pressure gauges would provide a positive initial reading.

Table 6-1. Summary of Initial Test Conditions, Controlled-CO_2-Addition Tests

Test Container	Initial CO_2 Charge Pressure, atm (psia)[a]	N_2 Pressure, atm (psia)	Mol CO_2/m^2 steel[b]
33	7.8 (115)	no N_2	0.32
34	3.8 (56)	no N_2	0.16
35	1.5 (22)	no N_2	0.063
36	0.75 (11)	2.0 (30)	0.032
37	0.39 (5.7)	2.0 (30)	0.016
38	0 (0)	3.1 (45)	0.0

[a] Assumes plenum = 0.634 L, T = 30°C, insignificant CO_2 dissolution in brine at the time of CO_2 charging.

[b] Total area of steel specimens in each test container = 0.629 m^2.

The highest ratio of mol CO_2/m^2 steel (0.32) employed in the test series was intended to approximate the 0.42 mol/m^2 value causing passivation in the excess-CO_2 tests described in the preceding section of this report. Lesser quantities of CO_2 were also used to determine if passivation, or temporary passivation, would develop under conditions of relatively low concentrations of CO_2.

The pressure-time curves for the controlled-CO_2-addition tests are shown in Figure 6-3. Prior to the H_2S addition made at 575 days, the CO_2 and the Brine A were the only reactants present in the test containers. During this initial test period, it is apparent that at least some degree of passivity has been attained in the two test containers with the maximum amount of CO_2 added (containers 33 and 34). Though the pressure-time curves for these two containers appear to attain a near-zero slope after a time period of ~150 days, the curve for container 34 indicates some degree of reaction to the end of the CO_2-only (575-day) test duration shown in the figure. Thus, it appears as though a completely

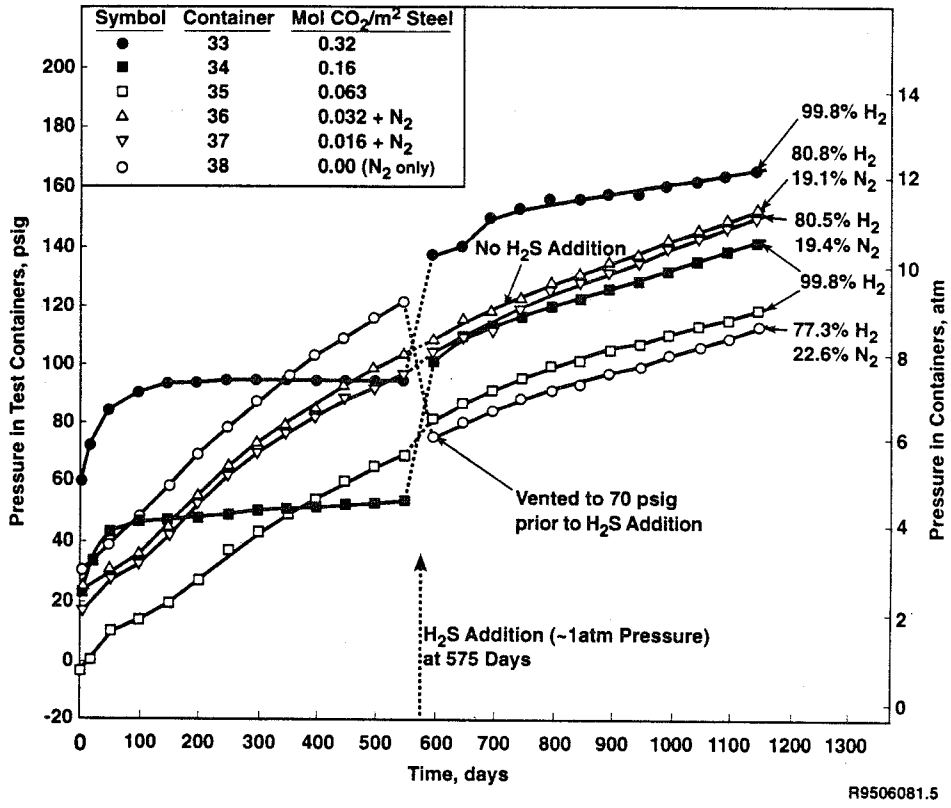

Figure 6-3. Pressure-time curves, controlled-CO_2-addition tests. The final plenum gas analyses are given next to the last data points on the curves. Note the complete absence of CO_2 or H_2S in the gas phase. The data in the vicinity of the H_2S addition at 575 days are not included in the figure because of the complications that would be introduced, which would make the figure difficult to interpret. These data may be found in Appendix A.[7]

[7] The raw pressure-time data for the test containers 33 through 38 corresponding to the curves of Figure 6-3 are presented in Appendix A-1. The individual-specimen descriptions are presented in Appendix B-1.

passive state was not ultimately achieved by the specimens in this test. A continual pressure increase was not observed in the excess-CO_2 tests after passivation of the specimens was achieved (see Figure 6-2).

Assuming that all of the H_2 resulting from the corrosion reaction collects in the plenum of the test container, that all of the H_2 resulting from the corrosion reaction is accounted for, that passivation of the steel does not stop the corrosion reaction, and that the reaction

$$Fe + CO_2 + H_2O = FeCO_3 + H_2 \qquad (11)$$

is the only H_2-producing reaction, then the reaction will stop when the H_2 pressure in the plenum equals the original starting CO_2 charge pressure (i.e., the CO_2 pressure in the container plenum before its dissolution in the brine).[8] The initial charge pressures are given in Table 6-1. From these data and associated assumptions it can be calculated that the reaction in container 33 has consumed 95% of the original CO_2 charge at 250 days, that the reaction in container 34 has consumed the equivalent of 110% of the original CO_2 charge at 250 days, and that the reaction in container 35 has consumed the equivalent of 220% of the original CO_2 charge at 250 days. Obviously, an Fe-H_2O reaction is proceeding and producing H_2 in the latter two cases cited. The containers with less CO_2 than container 35 essentially behaved as though no CO_2 had been added at all, as their pressure-time curves closely simulate that of the CO_2-free control, container 38.

The pressure-time curve of container 35 appeared to temporarily passivate in the time period 30-50 days. If it is assumed as before that H_2 generated is equivalent to CO_2 consumed, at 50 days the initial CO_2 charge has been 110% consumed. This good agreement between apparent passivation and CO_2 consumption suggests that a state of imperfect passivation was produced by the available CO_2, perhaps produced by a siderite ($FeCO_3$) layer containing defects that could not remain "healed" due to the absence of a continuing supply of CO_2. The defective film then eventually lost its

[8] Strictly speaking, there will always be some CO_2 remaining unreacted, as equilibrium conditions require a residual CO_2 fugacity equal to $\sim 2 \times 10^{-4} f_{H2}$ (SAND92-7347). In the practical terms of the present test, this CO_2 fugacity will not be sensed by the pressure gauges employed, nor will it affect the conclusions drawn in the subsequent discussion.

protectiveness entirely, and permitted the competing Fe-H_2O reaction to proceed at a normal rate, as in the case of the Fe-anoxic brine (brine/N_2) tests or the case of container 38.

If it is assumed 1) that container 33 represents truly passivated conditions, and 2) that container 34 represents almost-passivated conditions, then the conclusion can be drawn that the minimum amount of CO_2 required to passivate steel under the test conditions employed (Brine A at 30°C) is an amount lying between 0.32 and 0.16 mol CO_2/m^2 steel.

An addition of H_2S was made to the controlled-CO_2-addition tests to determine 1) if the passivating effect of CO_2 would persist if H_2S were added to a CO_2-passivated system (container 33 and, to a lesser extent, container 34), and 2) if the H_2S would have the same passivating effect on the steel in the controlled-CO_2-addition tests as it exhibited in the case of a 5-atm H_2S addition test in which no other reactant was present except Brine A. (This study is described in the next section of this report.)

The amount of H_2S to be added to the test containers was arbitrarily selected to be that quantity that would result in an equilibrium H_2S partial pressure of 1 atm in the plenum of the test container. The amount added to each container is presented in Table 6-2. Container 36 was designated a control test, so no H_2S was added to that container.

Table 6-2. Summary of H_2S Additions to Test Containers

Test Container	Pressure Increase (Quasi-Equilibrated) Due to H_2S Addition, atm (psi)
33	1.2 (17)
34	1.4 (21)
35	1.2 (18)
36	0.0 (0.0)
37	0.9 (13)
38	0.8 (11)

Because of the simultaneous reaction of the H_2S with the contents of the containers (specimens plus existing reaction products), and because of H_2S does not dissolve immediately in the brine, the exact amount of H_2S added to each test container cannot be known with certainty. For this reason, Table 6-2 presents the pressure increase as an estimate associated with a state of quasi equilibrium.

The amount of H_2S added can be estimated quantitatively from knowledge of the pressure increase seen in the plenum of the container upon adding the H_2S to the individual containers. The average amount added was 0.11 mols H_2/container, or 0.18 mols H_2S/m^2 steel. This quantity of H_2 is a factor of ~ 3 greater than that required to passivate steel in the Brine A/H_2S studies previously reported (SAND92-7347), based on the amount of H_2S that had actually reacted with the steel to form the passive FeS layer. However, the H_2S partial pressure used in that study was 5 atm, a factor of ~ 5 higher than the H_2S partial pressure present in the tests described here.

Immediately after the H_2S addition was made, the pressure began to drop in the containers initially having relatively small quantities of CO_2 (containers 37 and 38 — see Appendix A for the detailed pressure-time data). This is ascribed to an on-going reaction, expected to be thermodynamically favored, between the H_2S addition and the ferrous-hydroxide-type corrosion products already present in the containers that would have formed in these tests in the absence of sufficient CO_2 to passivate the steel specimens. This reaction will proceed without gas formation:

$$Fe(OH)_2 + H_2S = FeS + 2H_2O \qquad (12)$$

The post-H_2S-addition pressure immediately began to increase in the two canisters in which sufficient CO_2 had initially been added to passivate the systems (containers 33 and 34). This pressure increase can be explained in at least two different ways:

- The H_2S could have damaged the passivating film of $FeCO_3$ present on the steel specimens, allowing the H_2S to initiate a H_2-producing reaction with the steel surfaces of the specimens producing H_2 gas; and/or
- The H_2S could be reacting with the $FeCO_3$ on the steel surfaces to form FeS, CO_2, and H_2O, according to the following thermodynamically favored reaction:

$$H_2S + FeCO_3 = FeS + CO_2 + H_2O \quad (13)$$

Because the solubility of CO_2 in the brine is significantly less than that of H_2S,[9] the result would be a positive pressure change in the container even though there is no net increase in the moles of gas present in the system. The CO_2 so released would be expected to eventually re-react with the steel surface, ending up either as adherent or loose (particulate) corrosion product.

The "control" container having no H_2S addition (container 36) behaved as expected, i.e., it slowly increased in pressure as would be expected from a test essentially consisting of steel specimens immersed in anoxic Brine A.

The addition of ~ 1 atm pressure of H_2S to the limited-CO_2 tests clearly disrupted the passive state of the previously CO_2-passivated specimens; and it did not bring about an H_2S-induced passivity, as might be expected from the tests previously described (tests 40-43) which passivated in the presence of 5 atm pressure of H_2S in Brine A (SAND92-7347 and the next section of this report).

The XRD analyses of the reaction products formed on the surfaces of specimens (all lot J steel) taken from each test container, as well as a specimen of particulate material taken from the (common) brine-dump vessel, which represented an averaged specimen of the non-adherent reaction products formed during the test exposures, are presented in Table 6-3.

From the table, it can be seen that specimens from containers 33 and 34 show both $FeCO_3$ (siderite) and FeS (mackinawite) reaction products on their surfaces, suggesting the not-unexpected reaction with the steel by both CO_2 and H_2S. Neither the CO_2 nor the H_2S addition ultimately resulted in a passivated condition, and it is not known from the available information what gas fugacities, if any, would have been capable of causing a passivated state to exist *once active corrosion had been initiated.*

---

[9] In the course of the present study, the Henry's law coefficient (expressed as mol gas/atm-L) for CO_2 in Brine A was determined to be 0.010 at 30°C; the corresponding value for H_2S was determined to be 0.050. In a typical seal-welded container test, CO_2 under equilibrium conditions will be distributed so that the major portion ($\sim 65\%$) will be in the plenum, with 35% in the brine. Because of its greater solubility in brine, H_2S will be distributed so that $\sim 73\%$ resides in the brine, with only $\sim 27\%$ in the container plenum.

Table 6-3. Identification by XRD of Reaction Products Formed During "Limited-CO_2-Addition with H_2S Addition" Tests. Lot J specimens were selected for analysis.

Source of Specimen	Gas Added, mol/m² steel		Principal Reaction Products
	CO_2	H_2S	
Container 33	0.32	~0.18	$FeCO_3$ FeS
Container 34	0.16	~0.18	$FeCO_3$ FeS
Container 35	0.063	~0.18	$Fe_2(OH)_3Cl$ $Fe_8(O,OH)_{16}Cl_{1.3}$ $FeCO_3$
Container 36	0.032	0.00	$Fe_2(OH)_3Cl$ $Fe_8(O,OH)_{16}Cl_{1.3}$
Container 37	0.016	~0.18	$Fe_2(OH)_3Cl$ $Fe_8(O,OH)_{16}Cl_{1.3}$
Container 38	0.00	~0.18	$Fe_2(OH)_3Cl$ $Fe_8(O,OH)_{16}Cl_{1.3}$
Particulate material (mixed)			FeO(OH) $FeCO_3$

Containers 36, 37, and 38 show no $FeCO_3$, which is not surprising, given the small amount of CO_2 added to these tests. An unexplainable result of the analyses, however, relates to the lack of FeS corrosion product observed on the surfaces of specimens from containers 35, 37, and 38, as well as the lack of a sulfide in the particulate corrosion product.

Container 36 is of additional interest. This container, nominally treated as an anoxic brine/N_2 container (as, for example, test containers 25 and 26, Table 3-1) except for the initial addition of a small amount of CO_2, yielded an identifiable corrosion product, unlike past experience with anoxic brine/N_2 tests, whose corrosion products resisted identification (SAND92-7347). The corrosion product identified (container 36, Table 6-3) was Mg-free, unlike the corrosion products found in past studies (see Section 6.1.1.1 of this report). It must be noted that the XRD procedure that identified a corrosion product was not a procedure that utilized minimization of oxygen contact with the corrosion

product prior to its analysis. Two additional tests (tests 46 and 47, Table 3-1) were initiated specifically to obtain further insights into the nature of the corrosion product from this kind of a test. The results of this investigation are also presented in Section 6.1.1.1.

If the initial addition of CO_2 is ignored, and if the pressure buildup in the plenum of container 36 is equated (as has been done in the past) to H_2 buildup and equivalent metal reacted, then this test provides an excellent check on the previous long-term measurement of gas generation by steel under anoxic brine conditions (Figure 6-1). If the slope of the container 36 curve between 1 and 2 years is determined, excellent agreement is found with the 12-to-24 month reaction rate of Figure 6-1. If the final year of the 3.2-year container 36 test is examined similarly, it is found that the reaction rate is ~70% that of the 1-to-2 year reaction rate. Thus, as was earlier suggested, the rate under the test conditions will continue to decrease with increasing test time, at least until some limiting rate is achieved.

6.1.1.3 BRINE/H_2S TESTS (WITH EVENTUAL CO_2 ADDITION)

The brine/H_2S tests (with eventual CO_2 addition) were intended to provide information on 1) the corrosion and gas generation proclivity of low-carbon steel in the presence of Brine A and H_2S, and 2) the effect of CO_2 additions on specimens pre-passivated by H_2S. Like CO_2, H_2S is a potential byproduct of microbial activity through sulfate reduction in the WIPP, so its presence in the site environment is considered to be a credible possibility. As has been shown [Equations (17) and (18), SAND92-7347], the thermodynamic tendency for reaction of Fe with H_2S is strong. There is a possibility, however, of passivating steel in the presence of H_2S at sufficient activity to form stable, relatively unreactive sulfide layers (SAND92-7347, Section 4.3).

The brine/H_2S tests of low-carbon steel were performed in test containers 40, 41, 42, and 43. In replicate test containers 40 and 41, the specimens were exposed under immersed conditions; in test containers 42 and 43 the specimens were suspended in the vapor phase over Brine A. The method of racking the specimens in test containers was similar to that used in the anoxic brine (brine/N_2) and the CO_2-brine tests previously described, and the amount of brine used in each test container was essentially the same as that used in the previous tests: 1.4 L in the immersed-specimen tests, 250 mL in the vapor-phase tests. The area of steel specimens present in each test container was 0.497 m^2.

The partial pressure of H_2S in these initial Fe/H_2S tests was purposefully chosen to be a high value relative to H_2S concentrations expected in the WIPP. An arbitrary (equilibrium) partial pressure of 5 atm was selected for these tests. For H_2S, the gas-charging method employed was similar to that used for N_2 and CO_2 in tests previously described, in that the H_2S gas was charged into the plenum of a previously evacuated test container with both steel specimens and Brine A already in place.

The H_2S gas dissolved much more rapidly into the brine than did the CO_2. The Henry's Law coefficient, S, for H_2S was determined to be 0.050 mols/atm-L at the gas-charging temperature of ~25°C. As a consequence of the high solubility of the H_2S in Brine A, the major amount of the H_2S charged into the immersed-specimen test containers is dissolved in the brine phase. Because H_2S shows significant non-ideal behavior, even at pressures as low as 5 atm, a van der Waals relationship was used to determine the relationship between moles H_2S and pressure of H_2S throughout all of the H_2S investigations (Lange's Handbook, 1985), unless noted otherwise.

The pressure-time curves for tests 40 through 43 are shown in Figure 6-4. Specimens in containers 40 and 42 were exposed to Brine A and H_2S only. Specimens in containers 41 and 43 were exposed to Brine A and H_2S only for 487 days. At that time CO_2 was admitted into the test containers.

The raw data associated with the pressure-time curves of Figure 6-4 are presented in Appendix A-2; the individual specimen data are presented in Appendix B-2.

From the time of test initiation the H_2S appeared to have a strong passivating effect on the coupons in the immersed-specimen tests (40 and 41), and appeared to be essentially unreactive in the vapor-phase tests (42 and 43). After an initial period of activity lasting about 6 days, the specimens appeared to be essentially inert in all of the test environments. During the initial period of activity the immersed specimens appeared to generate some corrosion-product H_2, as expected. The vapor-phase tests appeared to simply show the effect of continued H_2S dissolution in the brine phase present (the vapor-phase test containers were not shaken after gas addition to expedite equilibration of gas between vapor space and brine, as this procedure would have caused the brine to contaminate the surfaces of the specimens).

The lack of continued reaction after a time period of about 6 days in the immersed-specimen test condition suggested that a sulfide phase had rapidly formed on the specimen surfaces and stopped further reaction from taking place. An examination of the specimens removed from container 40 after

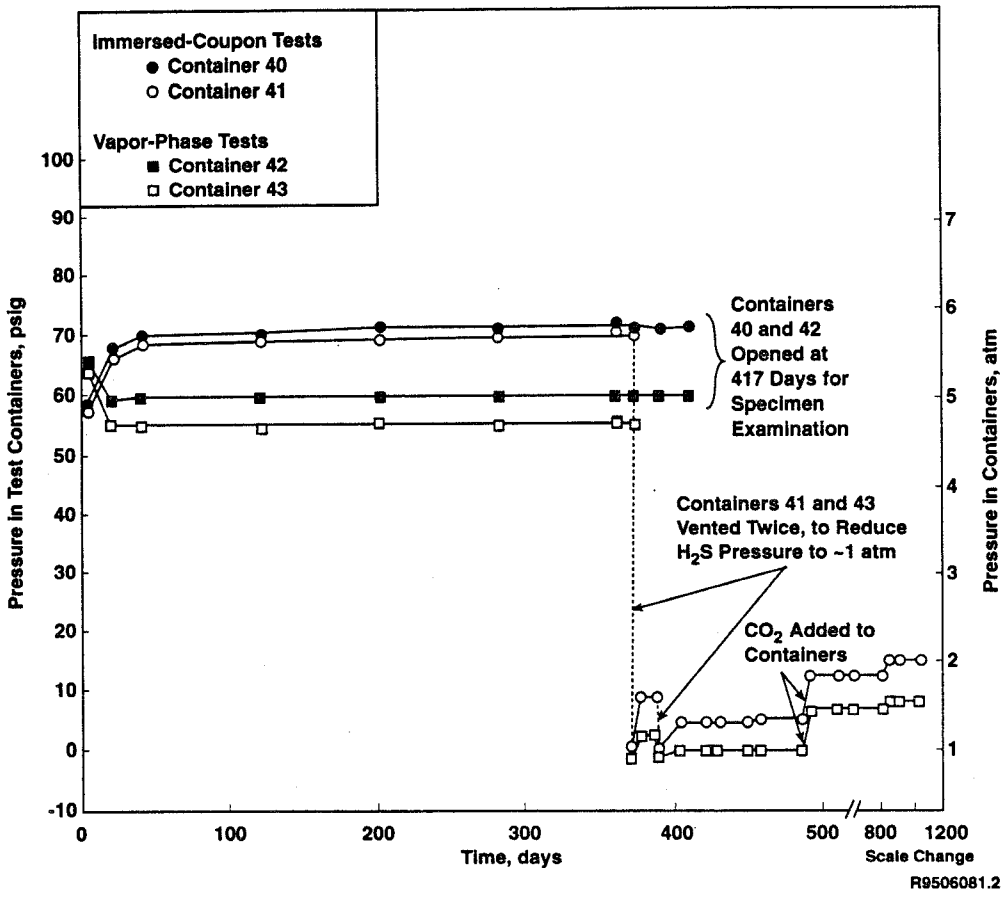

Figure 6-4. Pressure-time curves, low-carbon steel/H_2S tests

417 days revealed that the specimens were coated with a thin, adherent reaction product. The specimens from container 40 were black; the reaction product film on specimens from container 42 was extremely thin, giving the specimen a grey tarnished appearance. In both cases, the reaction product was identified as FeS (mackinawite) by XRD analyses. The finding of a passive film consisting of the "low" sulfide FeS is not in agreement with the findings of other investigations, who attribute passivity primarily to the higher sulfides, viz. pyrrhotite, $Fe_{1-x}S$, and pyrite, FeS_2 (SAND92-7347, Section 4.3).

A CO_2 addition was made to containers 41 and 43, to determine whether the passive nature of the reaction product layer would be retained in the presence of this gas. After venting the containers

to ~1 atm total equilibrium pressure, CO_2 was added until an equilibrium CO_2 partial pressure of ~1/2 atm was attained. The test was allowed to continue for an additional period of 592 days.

It is evident from the curves of Figure 6-4 that the passive nature of the systems was not compromised by the CO_2 addition, as the corrosion process, as evidenced by pressure buildup in the system, did not occur to any substantial extent for the duration of the test. A small pressure increase of 1 to 2 psi was observed in the test containers at 820 days; this was coincidental with the movement of the containers from one laboratory to another, and is attributed, at least in part, to jostling the mechanical pressure gauges to a new "equilibrium" reading (needle position).

The specimens from containers 41 and 43 exhibited the same visual appearance as those from containers 40 and 42. Once again, XRD analysis showed FeS, mackinawite, to be the most significant reaction product on the specimen surfaces.

The composition of the gas in the plenum of the test containers at the conclusion of the tests is shown in Table 6-4. The immersed-specimen containers show, as expected, the greatest amount of reaction-product H_2 present.

Table 6-4. Composition of Gas in Plenum of Containers 40, 41, 42, and 43 at Conclusion of Test. Only the principal constituents are listed.

	Concentration, mole percent			
Specie	Container 40	Container 41	Container 42	Container 43
CO_2	3.7	17.3	0.50	34.1
H_2	9.7	8.2	1.0	2.4
H_2S	86.0	74.5	98.1	63.3

The specimens from container 40 were stripped of their corrosion product, and the overall metal loss during the test was determined gravimetrically. It was determined that the amount of metal lost during the test was a total of 1.6 g, or 0.056 moles of Fe were lost per m^2 of steel exposed. The mackinawite-forming reaction

$$Fe + H_2S = FeS + H_2 \quad (14)$$

consumes a mole of H_2S per mole Fe reacted. Therefore, in the present test passivation occurred with the consumption of 0.056 moles H_2S/m^2 steel exposed. As in the case of CO_2-brine tests, the amount of reactant required to passivate the steel surface is very likely to be a function of the fugacity of the H_2S present in the test environment, and this fugacity-passivity dependence may be a major reason for the lack of agreement between investigators as to what constitutes a passive film, and the test environments that do or do not produce passive steel surfaces (SAND92-7347, and Section 6.1.1.2 of this report).

The thermodynamic stability of iron sulfides relative to $FeCO_3$ is consistent with the lack of disruption of the FeS film by CO_2 shown in the present tests, and the disruption of the $FeCO_3$ film by H_2S described in the previous section (Section 6.1.1.2) of this report.

6.1.1.4 ANOXIC ERDA-6 BRINE (ERDA-6 BRINE/N_2) TESTS

Anoxic tests using low-carbon steel specimens immersed in ERDA-6 brine were performed as adjunct tests to the constant-pH tests, described in the next subsection of this report. The constant-pH tests were to be done using constant-pH brine environments having pH values controlled at 3, 5, 7, 9, and 11. Because Mg was known to precipitate from solution at pH values greater than ~8.6, ERDA-6 brine (Molecke, 1983), a low-magnesium WIPP-relevant brine, was substituted for Brine A as a candidate brine for the constant-pH tests. It was further found in a PNL investigation that both the Mg and Ca constituents of ERDA-6 brine essentially completely precipitated from solution at a pH value of 11. To avoid having a brine of variable composition (other than H^+ concentration) in the constant-pH tests, it was decided to use an ERDA-6 brine modified to eliminate the Mg, Ca, and HCO_3 constituents. The base composition of the modified ERDA-6 brine used in the PNL studies is given in Table 5-5.

In order to interpret the results of the constant-pH tests, and apply the results of those tests broadly to the extensive tests using Brine A test environments, it was necessary to obtain an

information base relating the corrosion rates of low-carbon steels in anoxic modified ERDA-6 brine to the corrosion rates of low-carbon steel in anoxic Brine A environments. This requirement gave rise to the tests described here.

The seal-welded container tests using anoxic modified ERDA-6 brine (tests 44 and 45) were essentially identical in specimen type, specimen racking, brine quantity, and experimental procedure to the equivalent tests using Brine A (e.g., tests 1, 2, 9, 10, 17, 18, 25 and 26) described in Sections 5.1 and 6.1.1.1 of this report. A significant difference exists between the two tests in total specimen area: 0.604 m^2 for the Brine A tests vs. 0.638 m^2 for the ERDA-6 brine tests.

The pressure-time plots of tests 44 and 45 are presented in Figure 6-5. Also included in the figure for comparison are curve segments taken from Figure 6-1, depicting pressure-time data from almost equivalent tests using a Brine A environment.

The raw pressure-time data for the ERDA-6 brine curves of Figure 6-5 are presented in Appendix A-3; the individual-specimen data may be found in Appendix B-3.

If it is assumed 1) that pressure buildup in the test containers is directly proportional to metal loss through steel reaction and H_2 generation, and 2) that the steel reaction rate is proportional to sample area, the curves of Figure 6-5 can, in theory, be used to draw conclusions concerning the reaction rates in the two different brine environments. In fact, the validity of the assumptions has been repeatedly shown in past related work (SAND92-7347).

If the 150- to 300-day period only is examined, the slopes of the curves of Figure 6-5 yield the data tabulated below:

Curve	Rate, psi/year	Average, psi/year
24-month, Brine A	54.8	50.7
12-month, Brine A	46.6	
Container 44	44.7	42.8
Container 45	40.9	

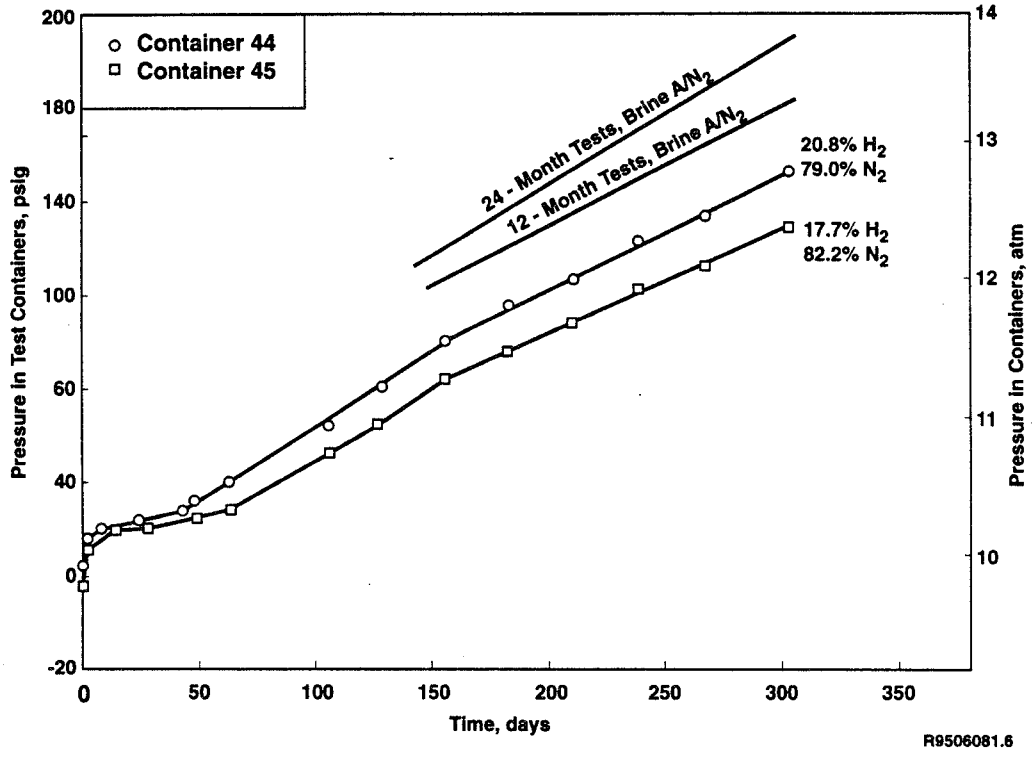

Figure 6-5. Pressure-time curves, containers 44 and 45, compared with segments of pressure-time curves taken from Figure 6-1

Because the specimen area in containers 44 and 45 is greater than that of the Brine A tests, a downward adjustment has to be made in the average pressurization rate of containers 44 and 45, if it is to be compared with the Brine A data, i.e., the pressurization rate in the Brine A containers (50.7 psi/year) must be compared with 42.8 psi/year × 0.606/0.638, or 40.5 psi/year. This container-pressurization data comparison appears to make Brine A significantly more reactive than

ERDA-6 brine. However, it appears in the present case that such a conclusion is not warranted, because the gravimetric (weight-change data) present a different picture.

Though past correlations between H_2 generation data and Fe metal reacted have shown very good agreement, especially in the case of tests of 6 months duration or longer (SAND92-7347), the present ERDA-6 brine tests have proved to be exceptions. If the metal lost to reaction (determined gravimetrically) is compared to H_2 generated, the moles H_2/moles Fe reacted ratio for container 44 is only 0.55; for container 45 the ratio is 0.77. These ratios are considerably lower than the ratio of 0.90 for the 12-month anoxic Brine A tests (SAND92-7347). The reason for the apparent lack of accountability of corrosion-product H_2 in tests 44 and 45 is not known. Possible reasons for lack of H_2 accountability, and a discussion of the possible errors associated with both gas-pressure and gravimetric data, are presented in SAND92-7347. It is not obvious that a significant error-inducing factor is operative in the present case. However, the lack of agreement between H_2 formed and Fe reacted plainly renders the foregoing analysis of the reactivity of Brine A relative to ERDA-6 brine based on pressure data alone highly questionable.

If the total Fe lost to reaction in containers 44 and 45 (11.50 g) is corrected assuming linear reaction kinetics, for the short test duration (10 months vs. the 12-month Brine A tests) and the relatively large total specimen area (0.638 m^2 vs. 0.604 m^2 for the Brine A tests), the following adjusted weight loss is obtained:

$$11.50\text{g} \times \frac{12}{10} \times \frac{0.604}{0.638} = 13.1\text{g Fe} \qquad (15)$$

The result of the computation of Equation 15 must then be compared with the total of 12.1 g of Fe reacted in the 12-month Brine A tests (containers 17 and 18, SAND92-7347). From this gravimetric-based analysis, ERDA-6 brine would be judged to be actually slightly *more* reactive than Brine A.

The ERDA-6 brine seal-welded container test has obviously not yielded conclusive quantitative results regarding the reactivity of ERDA-6 brine, relative to Brine A, toward low-carbon steel. It is apparent, however, that the basic reactivity difference between the two brines is slight, relative to

other factors known to be important in affecting corrosion rates. The effects of pH on the corrosion/gas-generation of low-carbon steel in ERDA-6 brine are therefore assumed to be equally applicable to Brine A environments.

6.1.2 Constant-pH Tests

The constant-pH tests were designed to yield information on the corrosion/gas generation rates of low-carbon steel that would be expected under a variety of pH-altering conditions in the WIPP repository, e.g., the effects of microbe metabolites, or the effects of purposeful pH-altering additions to the backfill material. A range of pH values from 3 to 11 was selected for the investigation, as it was considered highly unlikely that a brine pH would be encountered in the WIPP lying outside of this range.

Some background information is presented here on the relationship between pH and corrosion product solubility. The information will aid in the interpretation of the constant-pH test results.

The anodic reaction in the corrosion of Fe in aqueous solutions is

$$Fe = Fe^{++} + 2e^{-} \tag{16}$$

In acidic solution, the reduction reaction is

$$2H^{+} + 2e^{-} = H_2 \tag{17}$$

In an alkaline solution, the reduction reaction is

$$2H_2O + 2e^{-} = 2(OH)^{-} + H_2 \tag{18}$$

Whether the cathodic reaction is given by Equation 17 or 18, the result is the same — as more Fe dissolves into the solution, the solution becomes more concentrated in OH^- ions, resulting in an increased pH. On reaching saturation, Fe will precipitate out of solution as $Fe(OH)_2$. The concentration of iron in solution is determined by the equilibrium for the dissociation of $Fe(OH)_2$:

$$Fe(OH)_2 = Fe^{++} + 2OH^- \tag{19}$$

for which the solubility product, K, may be written

$$K = [Fe^{++}] \cdot [OH^-]^2 \tag{20}$$

At 25°C, log K has the value -14.71 (Pourbaix, 1974), for concentrations expressed in mol/L. As $\log (OH)^- = -14 + pH$, we obtain

$$\log[Fe^{++}] = 13.29 - 2pH \tag{21}$$

At pH values > 10.53, the dissolution reaction for $Fe(OH)_2$ is not the reaction given by Equation 19, but

$$Fe(OH)_2 = HFeO_2^- + H^+ \tag{22}$$

For Equation 22, the dependence of the concentration of the dihypoferrite ion, $HFeO_2^-$, on pH (Pourbaix, 1974) is given by

$$\log\left[HFeO_2^-\right] = -18.3 + pH \tag{23}$$

It may be seen, from Equation 23, that, as the solution pH increases, larger amounts of Fe can remain in solution without precipitation of $Fe(OH)_2$. Further, because the formation of each $HFeO_2^-$ ion consumes one $(OH)^-$ anion, the pH of the solution decreases as more and more Fe dissolves into the solution. Thus, left to itself, the corrosion of Fe in an aqueous anoxic solution will lead to an equilibrium pH. This situation is more readily visualized by means of the construction presented in Figure 6-6, which plots the log concentration (in mol/L) of Fe in solution in equilibrium with solid $Fe(OH)_2$ at 25°C.

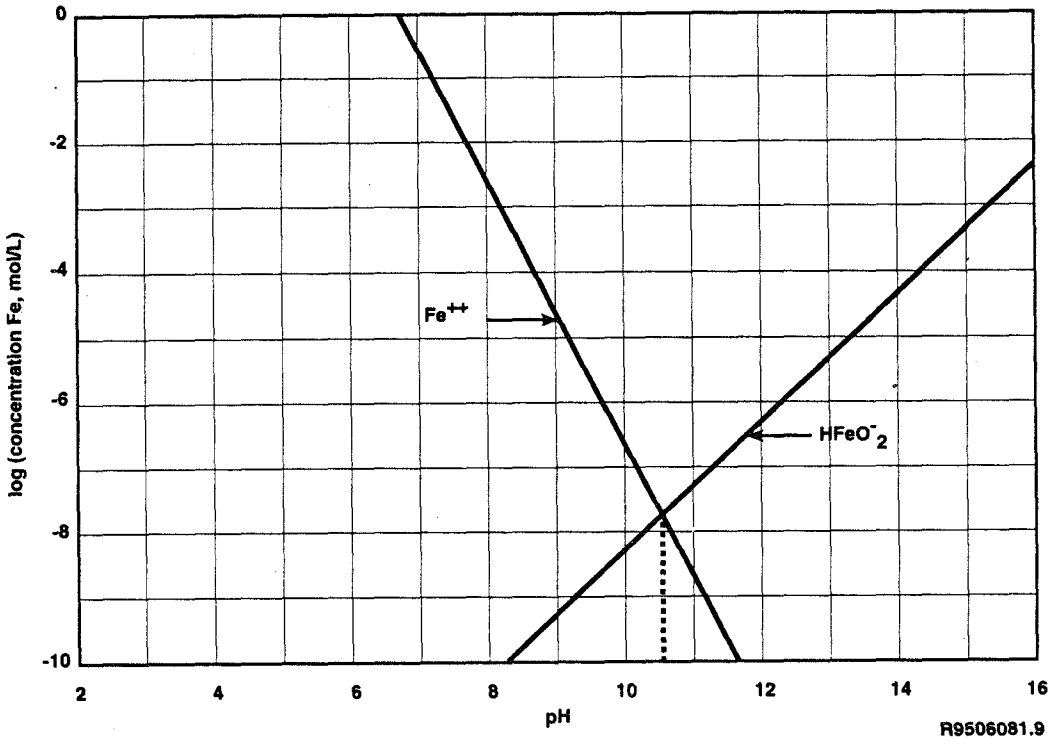

Figure 6-6. Influence of pH on the solubility of $Fe(OH)_2$ at 25°C

The figure shows that, at pH values < 10.53, if the pH is not controlled by external means, the corrosion process will continue until the numerical value of the ion product $[Fe^{++}] \cdot [OH^-]^2$ reaches the solubility product value, given by the Fe^{++} curve. Similarly, at pH values > 10.53, the corrosion process will continue and the pH will decrease until the equilibrium associated with Equation 22 (the $HFeO_2^-$ curve) is established. At pH = 10.53, Fe^{++} and $HFeO_2^-$ represent equal Fe concentrations in the solution.

If, on the other hand, the solution is maintained at a constant pH, either by addition of an acid at pH values < 10.53 or by addition of a base at pH values > 10.53, Fe will continue to go into solution until the solution becomes saturated in Fe. Once this saturation level has been reached, further additions of acid or base are not required to keep the pH constant.

The numerical values used in the previous discussions are true only for dilute solutions. For concentrated solutions, such as Brine A and ERDA-6 brine, concentrations of all dissolved substances must be replaced by their respective activities. Despite this reservation, the foregoing discussion and the representation of Figure 6-6 are expected to be at least qualitatively applicable to the present brine studies.

6.1.2.1 MEASUREMENT OF pH IN BRINES

Because the brines used in the present study are relatively complex solutions of high ionic strength ($\sim 6\underline{M}$) and the solutions in reference electrodes are simple solutions of significantly different composition, the liquid-junction potential between the two solutions is expected to be high, and therefore needs to be known or eliminated if the brine pH is to be known with a satisfactory degree of accuracy. The measurement of pH in the brine can be accomplished by utilizing a chloride selective ion electrode (SIE), through the reasoning presented below.

As the name implies, the chloride SIE may be used to measure the chloride ion activity of a solution. It consists of a thin solid electrolyte disk of a composite of silver chloride dispersed in silver sulfide, Ag_2S, matrix attached to one end of a chemically inert plastic tube. The inside of the tube is filled with an internal filling solution (e.g., Ag-saturated KCl solution). An AgCl-coated silver wire is immersed in the filling solution and serves as one terminal of the measuring cell. The SIE is immersed in the test solution along with a reference electrode for chloride activity

measurement. Knauss, Wolery, and Jackson employed the chloride SIE for pH measurement in brines using a glass electrode immersed in the test brine as the other half of the measurement (Knauss, Wolery, and Jackson, 1990).

When used for pH measurement at the internal surface of the membrane of the SIE, the potential is fixed by the equilibrium between the silver in the internal solution and in the membrane. At the external surface, a similar equilibrium is established between the membrane and the test solution. The portion of the total potential of the measuring cell that is due to the membrane/test solution interface is:

$$\delta E = 2.303 \frac{RT}{F} \log a_{Ag+} \tag{24}$$

Where a_{Ag+} is the silver ion activity in test solution. Since $a_{Ag+} = K_{sp}/a_{Cl^-}$, where K_{sp} is the solubility product of AgCl, the above equation becomes:

$$\delta E = 2.303 \left[\log K_{sp} - \frac{RT}{F} \log a_{Cl^-} \right] \tag{25}$$

The solubility of Ag in most common aqueous solutions is negligible (e.g., at 25°C, the solubility product for AgCl, with concentrations expressed in mole/L, is $1.56 \cdot 10^{-10}$), so the danger of changing the activities of other dissolved species in the test solution is minimal. There is still the problem of relating log a_{Cl^-} to pH. Knauss, Wolery, and Jackson solve it in the following manner:

Using the liquid-junction free cell:

$$\text{glass } H^+ \text{ electrode} \mid H^+, Cl^- \mid \text{solid state } Cl^- \text{ SIE} \tag{26}$$

one can directly measure a_{HCl}. According to the Nernst equation, the potential across the cell is:

$$E_{HCl} = E^{0}_{HCl} + 2.303(RT/F) \cdot pHCl \quad (27)$$

where E_{HCl} = potential difference between the glass electrode, which really is a H^+ SIE, and the Cl^- SIE, where E^0_{HCl} = standard potential of the cell, and

$$pHCl = pH + pCl = -\log a_{H^+} - \log a_{Cl^-} \quad (28)$$

Operatively, the potential differences between a glass pH-sensitive electrode and a Cl^- SIE measured in two or more solutions of known pHCl are used to construct an E vs. pHCl calibration curve. [Known pHCl solutions which bracket the expected pHCl of unknowns can be prepared using solution compositions given by Knauss, Wolery, and Jackson (1990)]. The potential difference measured between the glass electrode and Cl^- SIE immersed in an unknown solution is compared to the calibration curve, from which a $pHCl_x$ value for the unknown solution is obtained. The pH of the unknown solution, pH_x, is then calculated from the measured $pHCl_x$ value from the relation

$$pH_x = pHCl_x - pCl_x = pHCl_x + \log(y_{Cl^-} \cdot M_{Cl^-}) \quad (29)$$

where y_{Cl^-} is the chloride activity coefficient and M_{Cl^-} is the molal concentration of Cl^- in the unknown solution.

To calculate y_{Cl}, Knauss, Wolery, and Jackson used methods that were developed by Pitzer and coworkers (Pitzer, 1979) to calculate mean molal activity coefficients of dissolved salts. Because these hand calculations are tedious, Pitzer's procedure was incorporated by Jackson (Jackson, 1988) into a computer code, named EQ3/6 Brine Model, that would make the calculations from compositions entered, using equilibrium data included in the code. His experimental results, obtained with solutions of ionic strengths from 0.001 to 4.0 M, showed that commercially available chloride SIE in combination with a glass electrode in solutions of a wide range of ionic strengths and pHs showed a Nernstian behavior, i.e., the relationship between potential and calculated -pHCl was linear

with a slope equal to 2.303 (RT/F), and that K^+, Ca^{2+}, Mg^{2+}, SO_4^{2-}, HCO_3^-, and BO_3^{3-} ions, commonly present in brines, do not interfere. Instead of EQ3/6, we used GMIN, a model developed by Felmy (Felmy, 1990) using the same approach and same Pitzer equations as Jackson. Felmy's model was used here because it employs more recent data and also because its author was immediately accessible for discussions. The two codes give nearly identical results.

Using the activities of Brine A constituents as defined by GMIN, and assuming that the overall activity coefficient for H^+ ions is unity, we obtain for Brine A

$$pH = pHCl - pCl = pHCl + 1.894 \tag{32}$$

Using a specific electrode pair (Orion 910100 glass electrode and Orion 941700 chloride SIE, Orion Research, Cambridge, Massachusetts 02139), and solutions described by Knauss, Jackson, and Wolery, the pHCl of Brine A was determined to be 6.71. Thus, the pH of Brine A is 6.71 + 1.894, or 8.60.

The constant-pH tests were performed at nominal pH values of 3, 5, 7, 9, and 11. These pHs are termed "nominal" because, at the start of the program, it was thought that the modified ERDA-6 brine would have approximately the same pCl value (1.57) as that initially calculated for a certain Brine A composition. As the glass electrode-chloride SIE combination measures pHCl, which equals (pH+ pCl), in our tests we aimed at pHCl values of 1.43, 3.43, 5.43, 7.43, and 9.43, respectively. However, since the pCl value is calculated rather than measured, the pCl value and the pH value are subject to change as the assumptions and empirical data underlying its calculation are modified in the future. Because of this uncertainty in correlating measured pHCl values with calculated pH values, in these tests particular pHCl values that were regularly spread apart and which covered the pH range from $\sim$3 to $\sim$11 were used. The value of pCl was finally calculated to be 1.20 for the modified ERDA-6 brine used in the present program, rather than the value of 1.57 initially obtained.

6.1.2.2 TEST RESULTS

The corrosion rates obtained in the constant-pH tests are presented in Table 6-5. The column titled "Actual pH" takes into account the discrepancy cited in the foregoing paragraph between the

pCl values calculated for Brine A and ERDA-6 brine, and also takes into account the averaged value of pH so calculated maintained over the course of the experiment. The raw corrosion-rate data are presented in Appendix B-4.

As expected, the data of Table 6-5 show the corrosion rate to decrease with pH, consistent with the findings of Simpson and Schenk (1989). It is not known whether the apparent increase in corrosion rate between pH 9 and pH 11 in the present work is real, or a manifestation of experimental

Table 6-5. Summary of Corrosion-Rate Results, Constant-pH Tests, Based on Weight Change Data

Actual pH	Test Duration, mo.	Mat'l	Corrosion Rate, μm/yr (mpy)[a]	Average Corrosion Rate, μm/yr (mpy)[b]
2.8	0.19	J	7900 (310)	7900 (310)
		K	7100 (280)	
		L	8900 (350)	
		M	8100 (320)	
4.8	6	J	89 (3.5)	89 (3.5)
		K	110 (4.4)	
		L	81 (3.2)	
		M	71 (2.8)	
7.0	6	J	36 (1.4)	51 (2.0)
		K	36 (1.4)	
		L	64 (2.5)	
		M	66 (2.6)	
8.6	6	J	1.5 (0.06)	2.0 (0.08)
		K	1.8 (0.07)	
		L	2.3 (0.09)	
		M	2.5 (0.10)	
10.6	6	J	1.8 (0.07)	3.6 (0.14)
		K	1.8 (0.07)	
		L	5.6 (0.22)	
		M	4.3 (0.17)	

[a] Average of 2 specimens.
[b] Average of 8 specimens.

error. As an example, such error could be introduced into the results because of the fact that the tests were not conducted under truly anoxic conditions, and the pH 11 test could have been exposed to higher concentrations of O_2 than the pH 9 test.

For comparison with the data of Table 6-5, the average corrosion rate for the same steels in anoxic Brine A for a 6-month test was 1.72 μm/yr (0.068 mpy). Because Brine A exhibited a post-test pH of $\sim$8.3 under the N_2-overpressure test conditions, the results of the Brine A tests and the current ERDA-6 brine tests are judged to be in excellent agreement. This comparison supports the earlier observation (Section 6.1.1.4) regarding the approximately equivalent corrosiveness of Brine A and ERDA-6 brine toward low-carbon steels under anoxic conditions.

The pH 3 experiment (Table 6-5) was terminated early, because the specimens were reacting so vigorously with the acidified brine that there was concern that they would disintegrate.

The pH 5 experiment proceeded in a well-behaved fashion throughout the entire test duration. The specimens appeared to be film-free throughout the exposure.

In the pH 7 experiment, the brine reached saturation with Fe after 38 days exposure, as no acid additions were called for after that time to maintain the pH. The specimens appeared clean upon removal from test.

In the pH 9 experiment, the brine became buffered during the first day of exposure and no acid additions were required after that time. A gray, gelatinous-appearing film formed on the specimens in the first few days and remained for the entire test exposure. A post-test XRD analysis of a specimen showed the corrosion product to be close to akaganeite, β-FeOOH.

In the pH 11 experiment no acid additions were required to maintain the pH at 11. When the specimens were removed from test, they were covered with a gelatinous film, similar to that observed on the pH 9 specimens. When the specimens were rinsed to remove the gelatinous film, their surfaces were observed to be covered with a thin, whitish film and numerous shallow ($<$2.5 μm) pits. An XRD analysis showed the residual corrosion product to have a crystal structure similar to that on the surface of the specimens from the pH 9 tests.

6.1.3 High-Pressure Autoclave Tests

The seal-welded container tests previously described were charged with overpressure gas to equilibrium pressures in the range of 5 to 12 atm. These pressures are, of course, low by comparison with the pressure expected when the contents of the WIPP equilibrate with lithostatic pressure. High-pressure autoclave tests were conducted to gain insights into the effect of high CO_2, H_2, and N_2 pressures on the reaction kinetics, with equilibrium pressures in the range 36 to 127 atm. The high-pressure testing regimen comprised tests AUT-1, -2, -3, -4, -7, -8, -9, -10, and -11 (Table 3-2). In general, the steel specimens were prepared pre-test and examined post-test in the same manner as for the seal-welded-container tests. The specimen area per test was much smaller in the autoclave tests, however, because emphasis was placed on gravimetric analysis of the specimens rather than following the pressure as a function of time. This basic difference in test approach is based on the fact that autoclave systems cannot be relied upon to be (essentially) leak free for very long periods of time, even though this is sometimes observed to be the case in practice.

The specimens were completely immersed in a Brine A test environment in all of the high-pressure autoclave tests.

6.1.3.1 HIGH H_2 PRESSURE TESTS

Tests AUT-1, -3, -4, and -9 were initiated to determine to what extent, if any, high H_2 pressures inhibit the progress of the Fe-H_2O (Brine A) reaction. Tests AUT-1, -3, and -4 each used ten low-carbon-steel specimens, five of lot J and five of lot K. (A summary of these tests was presented in SAND92-7347.) Test AUT-9, which extended the testing pressure to 127 atm, used a total of 20 corrosion specimens, five each of lots J, K, L, and M steel. The specimens measured 38 × 76 mm (1.5 × 3.0 in.). The detailed specimen data are given in Appendix B-5. The specimens were exposed with the different lots interspersed on the same insulated wire support rack. The test proceeded without incident, maintaining a stable H_2 pressure of 1850 psig (127 atm) throughout the 6-month test duration.

At the conclusion of test AUT-9 the specimens were clean and shiny. The brine had a bluish-green color, as did the small amount of corrosion product lying in the bottom of the autoclave. The

specimens obviously reacted with the brine forming a non-adherent corrosion product. The results of the gravimetric analysis are shown in Table 6-6.

Table 6-6. Corrosion of Low-Carbon Steels with H_2 Overpressure. Test durations 6 and 12 months. Test temperature 30 ±5°C. Tabulated corrosion rates are given in μm/yr with standard deviation.

Steel Lot	6-Month Tests, H_2 Pressure, atm				12-Month Tests, H_2 Pressure, atm			
	2[a]	36	70	127	2[a]	36	70	127
J	1.61 ± 0.07	b	0.32 ± 0.12	1.16 ± 0.12	1.05 ± 0.05	0.20 ± 0.01	0.20 ± 0.01	b
K	1.65 ± 0.04	b	0.40 ± 0.04	1.26 ± 0.06	1.26 ± 0.04	0.25 ± 0.02	0.27 ± 0.03	b
L	1.91 ± 0.04	b	b	0.86 ± 0.03	1.31 ± 0.04	b	b	b
M	1.71 ± 0.08	b	b	0.78 ± 0.05	1.29 ± 0.03	b	b	b

[a] Approximate mean H_2 pressure in seal-welded container test with N_2 overpressure. Approximate mean total pressure in container = ~12 atm.
[b] Not determined.

An analysis of low-carbon-steel corrosion rate as a function of H_2 overpressure is somewhat hampered by the fact that the 36-atm tests were only carried out for 12 months, and the 127-atm tests were only carried out for 6 months. However, if it is assumed that the test results are not strongly time-dependent, because of the intrinsic non-protective nature of the corrosion product formed, then one can draw the conclusion that, over the range or pressures studied, the corrosion rate of low-carbon steel in Brine A goes through a minimum at intermediate H_2 pressures (36-70 atm), and is at a maximum at low pressures (~2 atm) and high pressures (127 atm). Presumably, intermediate pressures of H_2 retard the steel corrosion, due to a reaction-inhibiting effect associated with the presence of reaction product, whereas the higher pressures of H_2 enhance the reaction, possibly because of pressure effects on the activated complex associated with the electron-accepting reaction product at the cathodic site. This latter reaction-enhancing pressure effect is seen when the system is pressurized with an inert gas, and was discussed in detail in SAND92-7347. (The foregoing analysis disregards system-associated variables, such as the difference in specimen surface/brine volume ratio between the

seal-welded container tests and the autoclave tests. The potential importance of this variable to the conclusions drawn in the study is not currently known.)

The foregoing results show phenomenologically that the corrosion rates of steel expected at the pressure of the repository will not deviate substantially from those determined in the (essential) absence of H_2, regardless of the pressure of H_2 in the repository.

6.1.3.2 HIGH N_2 PRESSURE TESTS

Tests AUT-2 (described in SAND92-7347) and AUT-10 (Table 3-2) were initiated to determine the effect of high inert-gas pressures on the corrosion rate of low-carbon steels in Brine A. The specimen number and specimen dimensions in test AUT-10 match those of AUT-9, previously described. (Specimen details are given in Appendix B-6.)

Specimens removed from test AUT-10 were reasonably clean. A small amount of gray corrosion product was found on the specimens, the specimen rack, and the bottom of the autoclave.

Table 6-7. Corrosion of Low-Carbon Steels with N_2 Overpressure. Test duration 6 months. Test temperature 30 ±5°C. Tabulated corrosion rates are given in μm/yr with standard deviation.

Steel Lot	N_2 Pressure, atm		
	10[a]	73	127
J	1.61 ± 0.07	2.76 ± 0.24	2.51 ± 0.13
K	1.65 ± 0.37	3.17 ± 0.04	2.19 ± 0.03
L	1.91 ± 0.04	b	2.91 ± 0.11
M	1.71 ± 0.08	b	3.29 ± 0.06

[a] Seal-welded-container test data. Also present is H_2 at ~2 atm partial pressure, as noted in Table 6-6.
[b] Not determined.

The results of the gravimetric analysis are shown in Table 6-7, and, as before, the assumption is made that the difference in gravimetric results tabulated is due to overpressure gas only, and has no dependence on test type. The corrosion rate found at 127 atm is clearly higher than that found at 10 atm, but it appears that the effect of pressure on the corrosion rates between 73 and 127 atm would have to be considered statistically insignificant. On average, it appears that a rate enhancement between the 10 atm data and the 127 atm (repository pressure) data would amount to approximately 60%. This degree of rate enhancement would probably be considered inconsequential in the production of a repository pressurization model when other factors (pH, presence of reactive gases, presence of microbe metabolites) could have much more profound effects on gas generation rates.

6.1.3.3 HIGH CO_2 PRESSURE TESTS

Tests AUT-7 and AUT-8 (described in SAND92-7347) and AUT-11 (Table 3-2) were initiated to determine the effect of high CO_2 pressure on the corrosion rate and passivation of low-carbon steels in Brine A. The specimen number and specimen dimensions in test AUT-11 match those of AUT-9, previously described (specimen details are given in Appendix B-7). The specimens removed from the high-pressure CO_2 test were coated with the expected tenacious black $FeCO_3$ (siderite) reaction product layer. The results of the gravimetric analysis are presented in Table 6-8.

As expected from past investigations (SAND92-7347), the higher-pressure tests result in a greater degree of attack, i.e., more Fe is consumed before a stable passive corrosion product layer forms. And, as in past autoclave studies, the specimens in the present test passivated after a time period of approximately 60 days. This time-to-passivation was estimated from the pressure readings on the autoclave pressure gauge, which reflected the overpressure of H_2 formed during the course of the test. As the initial, or starting, fugacity of CO_2 in a steel/Brine A system is increased, as in going from 10 atm CO_2 to 62 atm CO_2, the amount of steel reacting prior to its passivation increases, but at a rapidly diminishing rate.

6.1.4 Simulated-Backfill Autoclave Tests

When a WIPP disposal room has received its full complement of waste receptacles, the void space between the room walls and the waste receptacles will be filled with a particulate "backfill"

Table 6-8. Corrosion of Low-Carbon Steels with CO_2 Overpressure. Test duration 6 months. Test temperature 30 ±5°C. Tabulated corrosion rates are given in μm/yr with standard deviation.

Steel Lot	CO_2 Pressure, atm		
	10[a]	36	62
J	8.5 ± 1.9	22.1 ± 1.8	27.2 ± 0.8
K	7.9 ± 2.5	24.9 ± 1.0	26.3 ± 0.4
L	3.8 ± 0.7	36.0 ± 1.3	38.6 ± 0.6
M	5.0 ± 0.9	35.8 ± 1.7	42.1 ± 1.9

[a] Seal-welded-container test.

material. A candidate backfill that has received consideration has the composition 30 wt% bentonite clay and 70 wt% WIPP-derived salt (halite). The bentonite would be expected to 1) reduce the permeability of the backfill, and 2) aid in sealing the repository, because of its tendency to expand when it absorbs water. Sandia staff recognized that, should the decision be made to use such a backfill, the effect of bentonite on the corrosion of steel would constitute an unknown that would have to be resolved before such a backfill could be used. The present tests were designed to provide the required corrosion/gas generation information.

Two experiments, designated tests AUT-12 and AUT-13, closely paralleling the earlier particulate salt tests AUT-5 and AUT-6 (SAND92-7347), were initiated using high-pressure, 3.8L autoclave systems. The test arrangements are shown schematically in Figure 6-7.

Test AUT-12 was designed to investigate the effect of brine "wicking" to the surface of the specimens. In this test the bottom of the backfill mass was below the level of the brine but the bottom of the specimens in the lowest tier was above the brine liquid level. Test AUT-13 was designed to investigate the effect of vapor transport, so the bottom of the backfill mass was above the liquid level of the brine. In both tests the mass of backfill, with embedded specimens, was held in a stainless steel mesh basket. The low-carbon steel specimens were separated from the basket to avoid

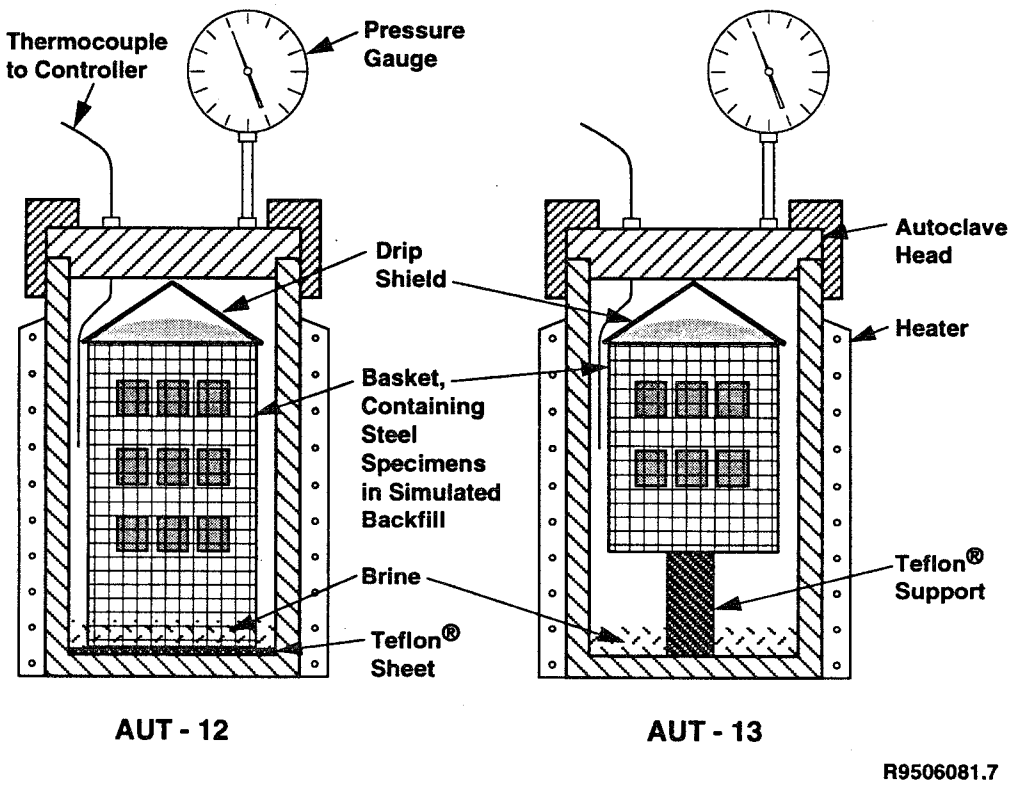

Figure 6-7. Test arrangements, tests AUT-12 and AUT-13

galvanic effects. A "drip shield" prevented condensate from dripping on the top of the backfill mass. The backfill was made up of 30 wt% bentonite and 70 wt% salt (nearly pure halite, from the WIPP site). The particle size of the salt used in the backfill blend was between 2.0 and 3.4 mm. In both tests the overpressure gas was N_2 at 10 atm pressure, the test temperature was 30 $\pm$5°C, and the test duration was 6 months.

The specific test parameters associated with each test, and the test results, are presented in the following two report subsections.

6.1.4.1 TEST AUT-12

In test AUT-12, 18 specimens of lot J low-carbon steel were embedded in 2000 g (dry weight) of simulated backfill. A total of 530 ml of Brine A was placed in the bottom of the autoclave. [A "dry run" had shown that this quantity of brine would rapidly (within hours) reach the top of the backfill by "wicking", while leaving a liquid brine residue having a liquid level well below (~25 mm) the bottom of the bottom tier of specimens.] The specimens were arranged in three tiers of six specimens each. The specimen dimensions were 25 mm × 25 mm (0.98 in. × 0.98 in.). The specimen tiers were separated by a distance of ~15 mm.

When the specimens were removed from the mass of simulated backfill at the conclusion of the test, no sign of a gray, green, or blue reaction product was observed in the vicinity of the specimens. (Corrosion products from anoxic brine tests commonly exhibit the hues noted.) The reaction product observed on the surfaces of the specimens was a uniform dark brown color. Because the specimens were "dredged" from the backfill very soon after autoclave disassembly, it is believed that the reaction products did not oxidize to the dark brown color observed upon air exposure, but that the reaction products formed were inherently of that color. The specimen weight change data are summarized in Table 6-9. It can be seen that the corrosion rate decreased with distance from the brine phase, and that the maximum corrosion rate observed (bottom specimen tier) is approximately twice the average corrosion rate observed in the six-month immersion test with N_2 overpressure (1.72 μm/yr). The backfill was noticeably more moist in the vicinity of the bottom tier than the top, and visually there was more corrosion product associated with the bottom-tier than the top-tier coupons. Individual specimen data are presented in Appendix B-8.

Table 6-9. Average Corrosion Rates of Specimens from Test AUT-12, μm/yr. Six specimens per tier, with standard deviation.

Top Tier	2.18±0.54
Middle Tier	3.86±0.58
Bottom Tier	4.58±0.61

The amount of H_2 in the gas phase at test completion (0.27 mol%) did not agree well with the amount of metal reacted (equivalent to 0.57 mol% in the gas phase, assuming divalent-Fe reaction product); this may be due to consumption of corrosion product H_2 through redox reactions, or direct participation in the corrosion reaction by reactive oxidants present in the system (e.g., Fe^{+3}).

6.1.4.2 TEST AUT-13

In test AUT-13, ten 25 mm × 25 mm (0.98 in. × 0.98 in.) specimens of Lot J material were embedded in a mass of simulated backfill, and arranged in two tiers of five specimens each. The backfill weighed 1672 g; the brine pool consisted of 250 ml of Brine A; and the distance from the surface of the brine to the bottom of the basket was ~25 mm. The distance from the bottom of the basket to the bottom of the lowest tier of specimens was ~25 mm.

The pressure in the autoclave stayed essentially constant at 140 psig during the run, indicating negligible gas loss from the autoclave. Gas samples were taken from the autoclave for analysis prior to dismantling the system for specimen recovery. The (duplicate) gas analyses showed only N_2. The H_2 present was below the detection level, i.e., <0.001 mol %. This low H_2 level is indicative of a very low corrosion rate.

Upon removal from the autoclave, the mass of simulated backfill did not appear to be moist. The salt crystals had maintained their original appearance. The specimens of low-carbon steel did not show any unusual characteristic that could be associated with position in the backfill. All specimens appeared basically uncorroded, except for many small splotches of dark brown corrosion product which covered perhaps 10 to 20% of the area of each specimen. The corrosion product was not raised, but had more of the appearance of a tarnish film. Compared to specimens removed from the "wicking" test, the extent of corrosion on the present specimens appeared to be negligible. A gravimetric analysis was performed to determine the amount of metal lost to corrosion. The results of the analysis are given in Table 6-10. Individual-specimen corrosion rate data are presented in Appendix B-9.

The corrosion rates observed in the test are very low for 6-month-duration tests. The average rate of all the specimens (0.48 μm/y) is about 30% of the rate that would be expected in a 6-month Brine A immersion test with an N_2 overpressure and no backfill present. The corrosion rates

Table 6-10. Corrosion Rates of Specimens from Test AUT-13

Position	Specimen I.D.	Specimen Corrosion Rate, μm/y (mpy)	Average Corrosion Rate, μm/y, with Std. Deviation
Bottom Tier	13-1	0.72	
	13-2	0.43	
	13-3	0.38	0.50±0.13
	13-4	0.52	
	13-5	0.47	
Top Tier	13-6	0.58	
	13-7	NA[a]	
	13-8	0.36	0.45±0.11
	13-9	0.41	
	13-10	NA[a]	

[a] Not available. Specimen archived.

observed in the present autoclave test match closely the corrosion rates observed in the seal-welded-container vapor-phase tests, without backfill, which produced basically "shiny" specimens with very little corrosion evident.

Because the backfill used in the present test was approximately 70% salt (halite), the test results appear to show that the results produced by the salt-only backfill test, test AUT-6 (SAND92-7347) in which condensate from the autoclave head dripped onto the salt mass during the course of the test, produced corrosion rates considerably higher than would have been produced if no water had dripped onto the salt. Test AUT-6 produced an average corrosion rate ~50% higher than test AUT-13.

6.2 Alternative Packaging Material Tests

The corrosion and gas-generation behavior of the four candidate alternative packaging materials [high-purity Cu, cupronickel 90-10, commercial-purity Ti (Ti Grade 2), and Ti Grade 12] was investigated in three environments—anoxic brine (Brine A with N_2); Brine A with CO_2; and Brine A with H_2S. Only the seal-welded-container method of testing was used, as reliance was placed on gas-pressure measurements as well as gravimetric analyses of the test specimens to establish the behavior of the materials in the test environments. The test matrix summarizing these tests is shown in Table 3-4.

The manner of racking the specimens in the alternative material tests was different from the method of racking used in the low-carbon steel tests. In the latter tests, the specimens were held on a specimen rack with no effort made to produce well-defined metal-to-metal crevices between the test specimens. In the alternative materials tests, two specimen geometries were used: rectangular specimens 64 mm × 190 mm (2.5 in. × 7.5 in.), and circular specimens 38 mm (1.5 in.) in diameter. The rectangular specimens were provided with two holes, each 0.79 cm (0.31 in.) in diameter for rack mounting; the circular specimens had one centrally located hole of the same size. The manner of racking the specimens is shown in Figure 6-8.

Each test contained 16 rectangular specimens and 16 circular specimens. The 16 circular specimens were tightly compressed between adjacent rectangular specimens, as shown in Figure 6-8, to provide regions for crevice corrosion if the tendency for that degradation mode existed in a given test system.

During alternative material testing, Cu-base and Ti-base materials were always tested in separate containers. In tests of Cu-base materials, all of the high-purity-Cu specimens (8 rectangular, 8 circular) were placed on one side of a specimen rack, and 16 equivalent specimens of cupronickel were situated on the other side of the rack. In a similar manner, in a test of Ti-base materials, specimens of Ti Grade 2 were placed on one side of a rack, and specimens of Ti Grade 12 on the other. The specimens were always completely immersed in Brine A during a test. All tests were conducted at 30 ±5°C.

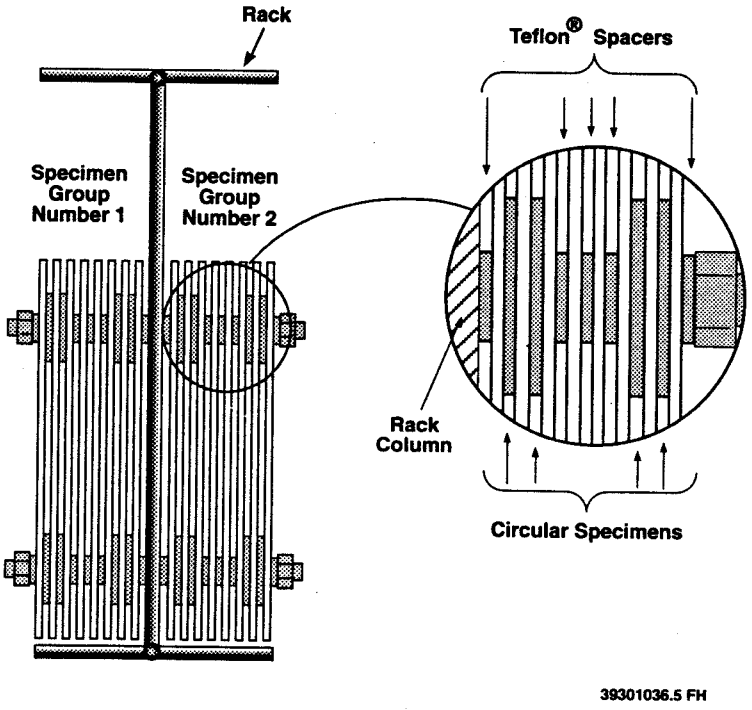

Figure 6-8. Method of mounting specimens on specimen rack for alternative packaging materials tests.

The alternative packaging materials investigation comprised tests 1A through 19A. Details of the tests, expanding on the information presented in Table 3-4, are presented in Table 6-11. Individual-specimen data for the 24-month tests are presented in Appendix B-10.

No gravimetric investigations were performed on any of the specimens from the 24-month tests. A visual assessment of the condition of the specimens was made at the conclusion of these tests, and a gas sample from each container was taken for analysis.

Table 6-11. Initial Conditions, Alternative Packaging Material Tests 1A through 19A

Test Identification	Material Base	Initial Overpressure Gas/atm[a]	Total Specimen Area, m^2	Brine Volume, L	Actual Test Duration, Months
1A	Cu	N_2/10.6	0.43	1.415	10
2A	Cu	CO_2/11.5	0.43	1.375	10
3A	Cu	H_2S/4.9	0.43	1.390	9
4A	Ti	N_2/10.7	0.44	1.435	10
5A	Ti	CO_2/11.6	0.44	1.360	10
6A	Ti	H_2S/4.7	0.44	1.415	9
7A	Cu	N_2/10.4	0.43	1.420	15
8A	Cu	CO_2/11.0	0.43	1.405	15
9A	Cu	H_2S/5.1	0.43	1.405	15
10A	Ti	N_2/10.5	0.44	1.420	15
11A	Ti	CO_2/10.9	0.44	1.400	15
12A	Ti	H_2S/5.1	0.44	1.360	15
13A	Cu	N_2/10.2	0.43	1.380	24
14A	Cu	CO_2/10.9	0.43	1.410	24
15A	Cu	H_2S/4.9	0.43	1.420	24
16A	Ti	N_2/10.2	0.44	1.365	24
17A	Ti	CO_2/10.8	0.44	1.360	24
18A	Ti	H_2S/5.1	0.44	1.360	24
19A	Control	H_2S/4.5	--	1.740	24

[a] At attainment of 30°C test temperature.

6.2.1 Cu in Brine A with N_2

Cu and cupronickel 90-10 specimens exposed to anoxic Brine A showed no significant reaction, as indicated by either pressure increase within the test container or by consumption of metal by a corrosion reaction. This is consistent with thermodynamic expectations (SAND92-7347).

Specimens removed from test containers 1A, 7A, and 13A after test periods of 10, 15, and 24 months, respectively, exhibited freshly ground, as-received surface conditions reminiscent of the pre-test specimen conditions. A gravimetric analysis of specimens from test 7A (see SAND92-7347 for individual specimen weight-change data) showed that the weight changes undergone by the circular specimens were within the accuracy limits of the four-place balance used for the analysis. The rectangular specimens showed weight gains up to 0.0117 g. The pressure changes in the three test containers over the entire period of the tests was within ± 1 psi. A gas analysis performed at the conclusion of the 24-month test (test 13A) showed the gas to consist of 99.8% N_2 and 0.009% H_2. Thus, it can be concluded, on the basis of the evidence currently available, that Cu and cupronickel 90-10 will not react with Brine A to form significant H_2 under the anoxic test conditions employed.

6.2.2 Cu in Brine A with CO_2

Cu and cupronickel 90-10 specimens exposed to Brine A with CO_2 showed no significant reaction, as indicated by either pressure increase within the test container or by consumption of metal by a corrosion reaction. This is consistent with thermodynamic expectations (SAND92-7347).

Specimens removed from test containers 2A, 8A, and 14A after test durations of 10, 15, and 24 months, respectively, appeared clean and uncorroded. The pressure in these containers dropped during the test periods by approximately 2 psi. The test specimens from test 8A lost a small amount of weight during the test, possibly due to Cu dissolution or Cu-complex dissolution effects. (See SAND92-7347 for individual specimen weight-change data.) A gas analysis performed at the conclusion of the 24-month test (test 14A) showed the gas to consist of 98.8% CO_2 and 0.015% H_2. It can be concluded, on the basis of the available evidence, that Cu and cupronickel 90-10 will not react with Brine A to form significant H_2 under the test conditions used.

6.2.3 Cu in Brine A with H_2S

Cu and cupronickel 90-10 specimens exposed to Brine A with H_2S show a rapid H_2-generating reaction. These observations can be said to be consistent with thermodynamic predictions (SAND92-7347), though the upper limits of H_2 pressure suggested by the thermodynamic calculations have not been nearly approached in the present tests.

The pressure-time curves showing the reaction between the Cu-base materials and H_2S were presented in SAND92-7347, through a time period of ~16 months. A gas analysis performed at the conclusion of the 24-month test (test 15A) showed the remaining gas to be 99.8% H_2. The specimens from this test were covered with a black Cu_2S corrosion product layer.

At this time it can be concluded that Cu and cupronickel 90-10 react rapidly and essentially completely with H_2S under the test conditions imposed to form Cu_2S and H_2 in the expected quantities, with little if any inhibition of reaction rate ascribable to the corrosion product film forming on the specimen surface. Because the reaction proceeds at a rapid rate (on a WIPP-relevant time scale) to very low activities of H_2S, it is difficult to conceive of a useful Cu-alloy container if H_2S has a significant probability of being present in the environment.

6.2.4 Ti in Brine A with N_2, CO_2, and H_2S

All alternative-material tests of Ti Grade 2 and Ti Grade 12 have shown essentially complete stability of the Ti-base materials in the test environments. The pressure changes observed in the Ti with N_2 and Ti with CO_2 tests were within 4 psi of the starting pressure over the entire period of the tests; the pressure changes observed were pressure drops. The Ti with H_2S tests, on the other hand, all showed a pressure increase of 9 to 10 psi within the first 30 h of gas addition, after which time the pressure stabilized, within ± 2 psi, for the remainder of the test. Gas taken from the 15-month-exposure test (test 12A) before test termination showed a trace of H_2 (0.5 mol%), consistent with a limited corrosion reaction at the beginning of the test. Gas taken from the 24-month Ti-base material tests had the compositions given in Table 6.12.

All of the Ti-base specimens appeared clean, shiny, and unreacted upon removal from the containers of terminated tests. A gravimetric analysis of a random sample of specimens from the 15-month tests (tests 10A, 11A, and 12A) showed that the majority of specimens from the N_2/brine tests gained weight, up to 0.0024 g; whereas all of the specimens from the other two environments (brine/CO_2 and brine/H_2S) lost weight, as much as 0.0014 g (see SAND92-7347 for individual-specimen weight change data). As in the case of the Cu-base alloys, weight changes to the extent observed in the present tests have little significance in an assessment of gas-generation potential.

Table 6-12. Compositions of Gas in Test Containers at Conclusion of 24-Month Ti-Base Material Tests

Test	Gas/Initial Pressure	Final Gas Analysis (mol %)
16A	N_2/10 atm	99.8% N_2, 0.005% H_2
17A	CO_2/10 atm	98.8% CO_2, 0.03% H_2
18A	H_2S/5 atm	94.5% H_2S, 0.36% H_2
19A[a]	H_2S/5 atm	93.4% H_2S, 0.35% H_2

[a] A control test, duplicating 18A but containing no test specimens.

It appears, on the basis of the information obtained to date, that Ti Grade 2 and Ti Grade 12 could be used as alternative packaging materials in the WIPP without concern about gas generation.

The gas analyses from the 24-month tests support the observation previously made (SAND92-7347) concerning the lack of reactivity of Ti-base materials in WIPP-relevant environments.

6.3 Al-Base Material Tests

The corrosion and gas-generation behavior of the two Al-base materials selected for study (99.99% Al and 6061 alloy) was investigated in three environments—anoxic brine (Brine A with N_2); Brine A with CO_2; and Brine A with H_2S. In addition, certain tests included low-carbon steel test coupons, in order to purposefully contaminate the brine with Fe^{++} ions, thereby promoting Fe deposition on the Al-base materials and concomitant corrosion enhancement. Because of the ubiquitous presence of steel in the repository, these Fe-containing tests are considered the most important and meaningful tests in the Al-base materials investigation.

Only the seal-welded-container method of testing was used, as major reliance was placed on gas-pressure measurement to establish the corrosion/gas-generation behavior of the specimen materials in the test environments. The test matrix summarizing the test parameters is presented in Table 3-5.

The method used to rack the specimens in the Al-base materials tests was similar to that used in the alternative material tests described in the preceding section of this report, in that two specimen geometries of each material type was used, and an effort was made to produce crevices for the promotion of crevice corrosion, should such a mode of attack be feasible in the test environments employed. The method of racking the specimens, with and without steel coupons present, is shown in Figure 6-9. The racking shown is for immersed specimens. For vapor-phase specimens, the rack would be inverted. Steel coupons were not included in the vapor-phase tests. The circular specimens, 38 mm (1.5 in.) in diameter, were compressed between rectangular coupons 64 mm × 190 mm (2.5 in. × 7.5 in.) of like material. Each test comprised 12 coupons of each Al-base material, or 24 coupons (0.33 m^2) total. On any one rack, the 6061 alloy was always on one side, and the 99.99% pure Al was on the other.

Each test with low-carbon steel coupons (tests 4B, 5B, 6B, 13B, 14B, and 15B) contained four coupons of lot J steel. Each steel coupon was 64 mm × 190 mm (2.5 in. × 7.5 in.), the same size as the rectangular Al-base material coupons. The steel coupons were electrically insulated from the rack and the Al-base material coupons.

The corrosion rates of the steel coupons were determined gravimetrically, so that some insight could be obtained regarding the influence of corroding Al on the corrosion rate of low-carbon steel in the test environments employed. The H_2 produced by steel corrosion was inconsequential in the Fe-containing tests compared with the amount of H_2 generated by the Al-base materials.

The raw presure-time data for the Al-base materials tests are presented in Appendix A-4. The individual specimen data are given in Appendix B-11.

6.3.1 Anoxic Brine (Brine/N_2) Tests

The anoxic brine (brine/N_2) tests included immersed-specimen tests (tests 1B and 10B); immersed-specimen tests with steel present (tests 4B and 13B); and vapor-phase-exposure tests (tests

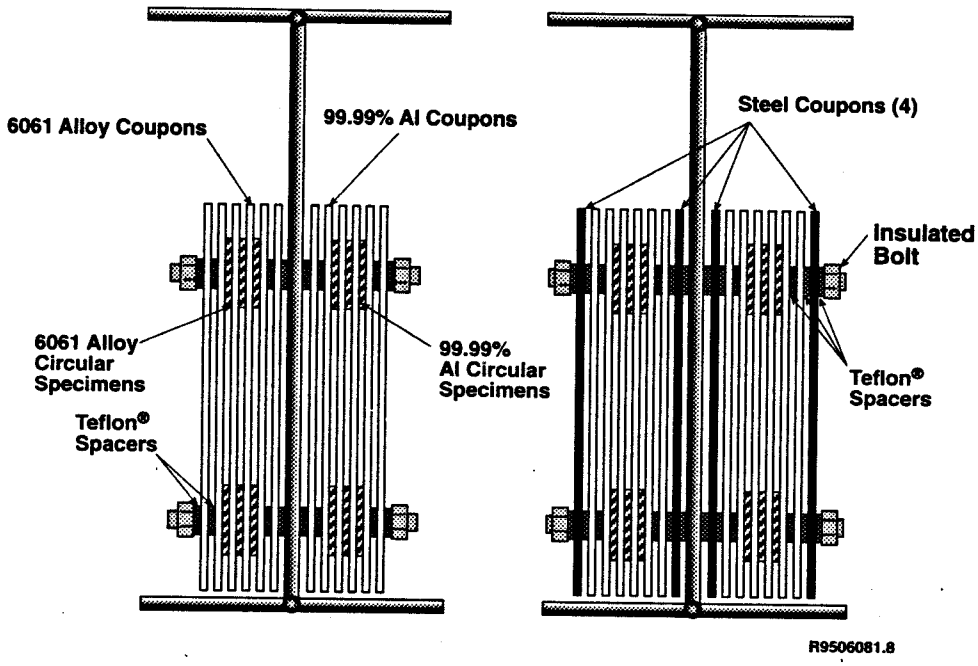

Figure 6-9. Method of racking Al-base material specimens for immersed-specimen tests. Method for including steel specimens is shown in the right-hand diagram.

7B and 16B). Duplicate tests were run for test durations of 13 months and 24 months. The pressure-time histories and gas analysis results for these tests are presented in Figure 6-10. (The raw pressure-time data for each test are presented in Appendix A; the individual-specimen data may be found in Appendix B.)

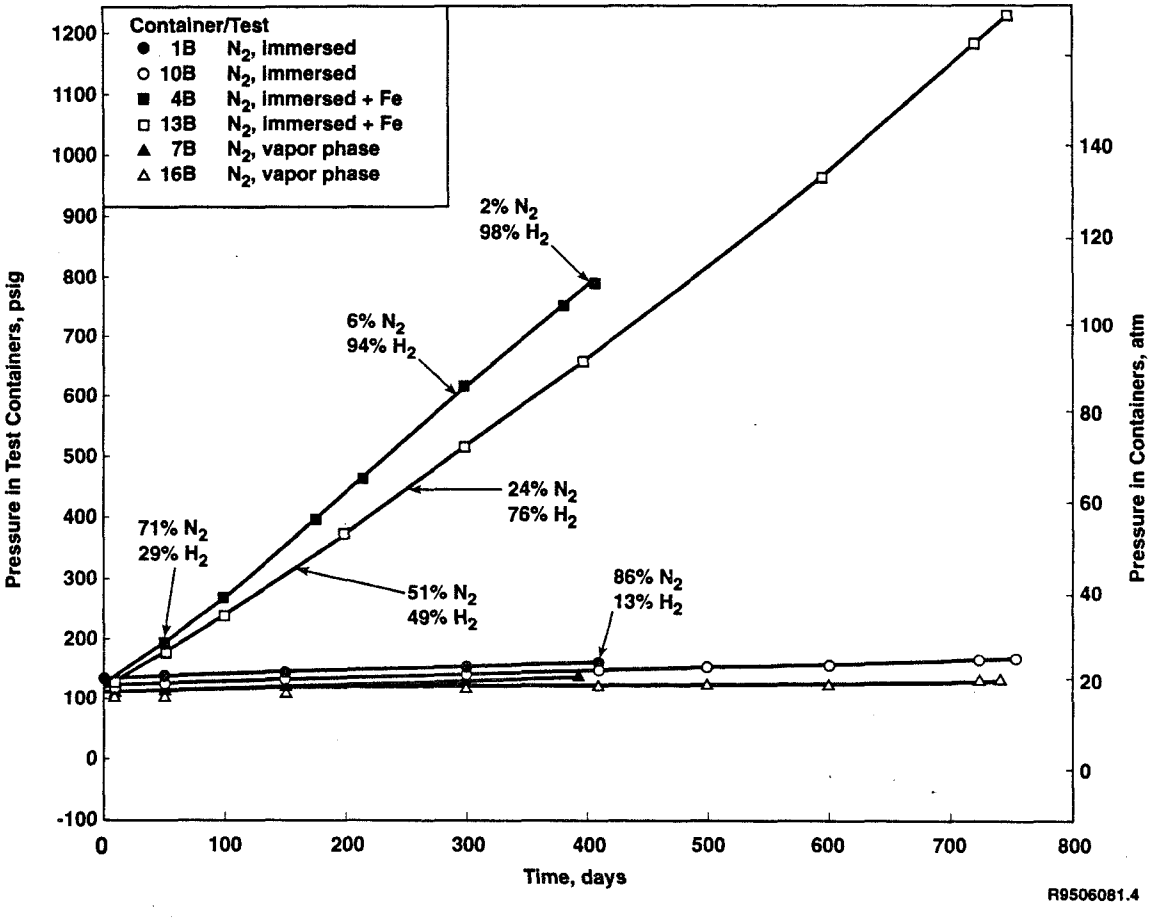

Figure 6-10. Pressure-time curves, Al-base materials in anoxic brine (Brine A/N_2), 30 $\pm$5°C. Gas analysis results (in mole %) are given for each test at the time the analyses were made.

The seal-welded test containers were limited to either 200 psig or to 300 psig because of the pressure gauge range restrictions. Test container gas ventings were therefore required in the case of tests exceeding the limit of the gauge used. (The ventings are tabulated in the data of Appendix A.) Where ventings were required, the amount of gas vented was determined by before-and-after pressure readings. The vented gas was then included in the gas pressure "inventory" as though it had not been lost. Thus, the container pressures noted on the ordinate of Figure 6-10 for tests 4B and 13B are in

reality "virtual pressures," the pressures that would have been attained if 1) a pressure gauge with an unlimited upper range had been used, and 2) if the reaction rate were independent of pressure over the range indicated on the ordinate. The assumption associated with item 1) is resolvable by simple computation; the assumption associated with item 2) is not believed to be significant over the pressure ranges involved.

The curves of Figure 6-10 show the profound effect of Fe in the environment on the corrosion rate of the Al-base materials. Presumably, the Fe^{++} ion resulting from the corrosion of the low-carbon steel is reduced by the oxidizing Al, deposits on the Al surface as metallic Fe, and participates as the cathode in the resulting electrochemical cell. Water would be reduced at the Fe cathode, liberating H_2 as the final cathode reaction product.

As containers 4B and 13B underwent repeated ventings the H_2/N_2 ratio increased until essentially all of the N_2 had been eliminated from the systems.

As would be expected from the pressure-time curves of Figure 6-10, the vapor-phase exposure specimens (tests 7B and 16B) showed essentially no corrosion attack when they were removed from their test containers, except where brine had splashed on the bottoms of the specimens during test container handling.

The specimens removed from the tests containing immersed specimens with no steel, tests 1B and 10B, showed evidence of some corrosion attack. The attack was nonuniform, and in the case of both the 99.99% Al and the 6061 alloy specimens, was frequently associated with the metal-to-metal crevices. The attack was either found within the prior crevices or in the vicinity of, and bordering on, the crevices. The 99.99% Al specimens in this test showed approximately two times the corrosion attack of the 6061 alloy specimens.

The specimens removed from the tests containing immersed specimens with Fe (tests 4B and 13B) were severely corroded, especially the specimens of 99.99% Al. The corrosion product was white, primarily paste-like (when wet), but was, in many regions, hard and adherent to the (dry) specimen surfaces. Because the attack was highly nonuniform on all of the samples, quantification of the degree of attack between the 99.99% Al and the 6061 specimens was difficult. However, specimen-thickness measurements, coupled with visual observation and estimation of metal lost to corrosion, indicated that the 99.99% Al specimens had undergone >90% of the total corrosion that had taken place.

A common finding on the 99.99% Al specimens was an hourglass-shaped region, encompassing both metal-coupon crevices, of a relatively high degree of corrosion attack. Because a thick encrustation of corrosion product filled the gaps between the coupons, it is likely that the equivalent of a large crevice region, of chemistry different from the bulk brine, formed in these central zones. Because of the amphoteric nature of aluminum, either acid or basic conditions, resulting in a pH outside the Al-compatible range of 4 to 9, could have enhanced the corrosion rate in these "virtual-crevice" regions. The chemistry of the solution existing in these regions is not known with certainty. However, if the reactions are similar to those occurring, for example, within pits on stainless steel surfaces, with hydrolysis of the chloride salts formed from the corrosion reactions, one would expect low-pH (acid) conditions to prevail in the crevice regions. This conclusion is consistent with the aluminum-hydroxide type of corrosion products found on the specimen surfaces (see Section 6.3.4).

No attempt was made to obtain gravimetric corrosion-rate information from the individual coupons because of 1) the difficulty that would be entailed in cleaning all of the corrosion products from the specimens; 2) the nonuniformity of the attack; and 3) the generally clear message of the pressure-time curves of Figure 6-10 regarding the ready corrodibility of Al-base materials.

The post-test appearance of the specimens, as cleaned with deionized water and a soft bristle brush, is shown in Figure 6-11 (99.99% Al) and Figure 6-12 (6061 alloy). The photographs do not accurately portray the disparity in corrosion between the two Al-base materials in the tests containing steel specimens.

Corrosion product samples were taken from the immersed-specimen tests for XRD analysis. Results of these investigations are presented in Section 6.3.5 of the report. The corrosion rates of the Al-base materials were estimated from the pressure-time curves of Figure 6-10. Because the 13-month and the 24-month curves are in generally good agreement, only the 24-month curves were used in the calculations. *For the initial calculations reported here, all of the specimens were assumed to corrode at the same rate in each test container.* This assumption "spreads" the corrosion uniformly between the 99.99% Al and the 6061 alloy. The implications of this assumption are discussed in more detail in Section 6.3.4 of this report.

The procedure used to calculate the H_2 generation rates in the Brine/N_2 studies is presented in Appendix C.

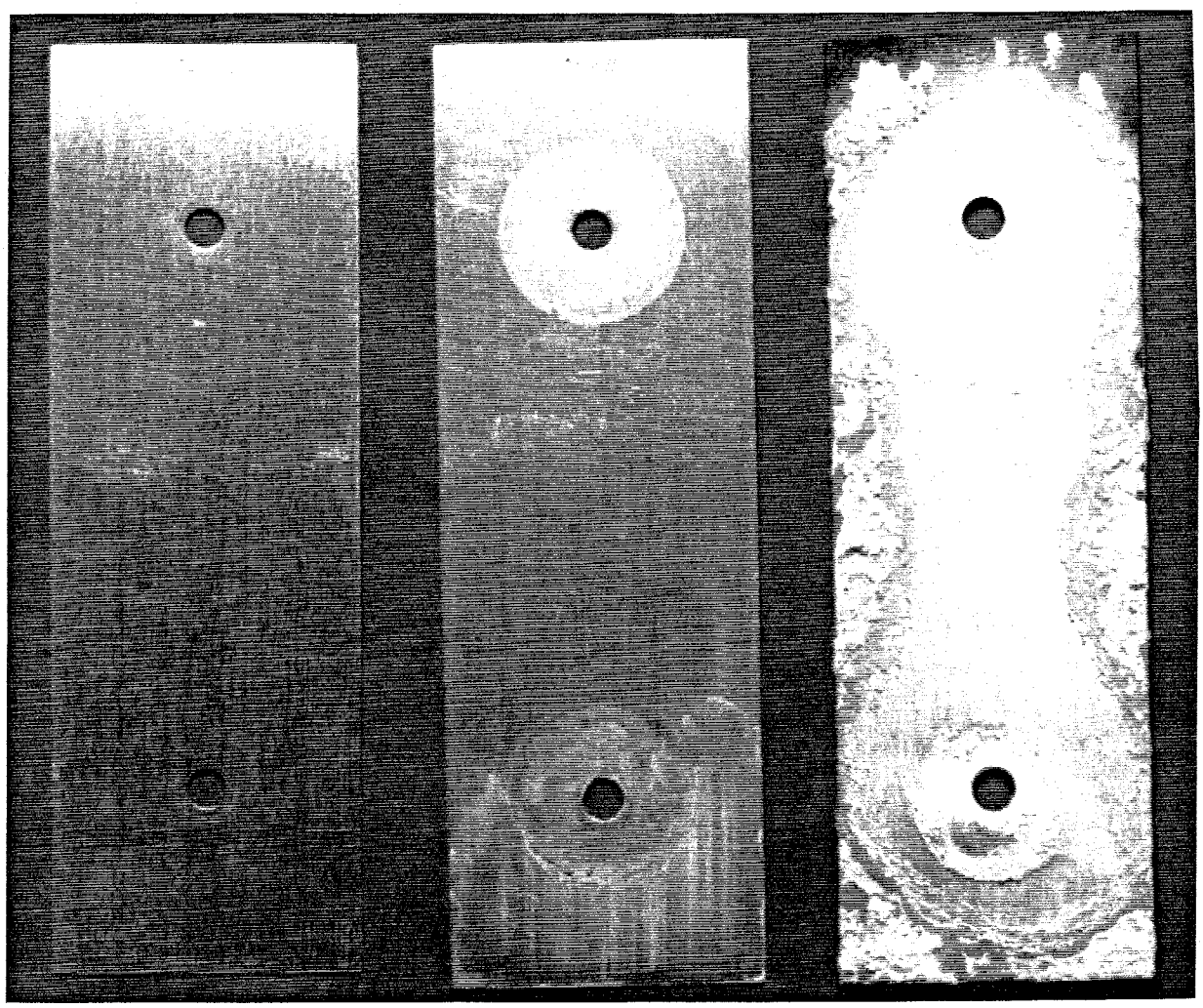

Specimen 1-292	Specimen 1-257	Specimen 1-275
Vapor-phase exposure	Immersed, no Fe	Immersed, with Fe
Test 16B	Test 10B	Test 13B

Figure 6-11. Post-test appearance of 99.99% Al specimens from Brine A/N_2 tests. Test temperature: 30 ±5°C. Test duration: 24 months. Shown approximately one-half actual size.

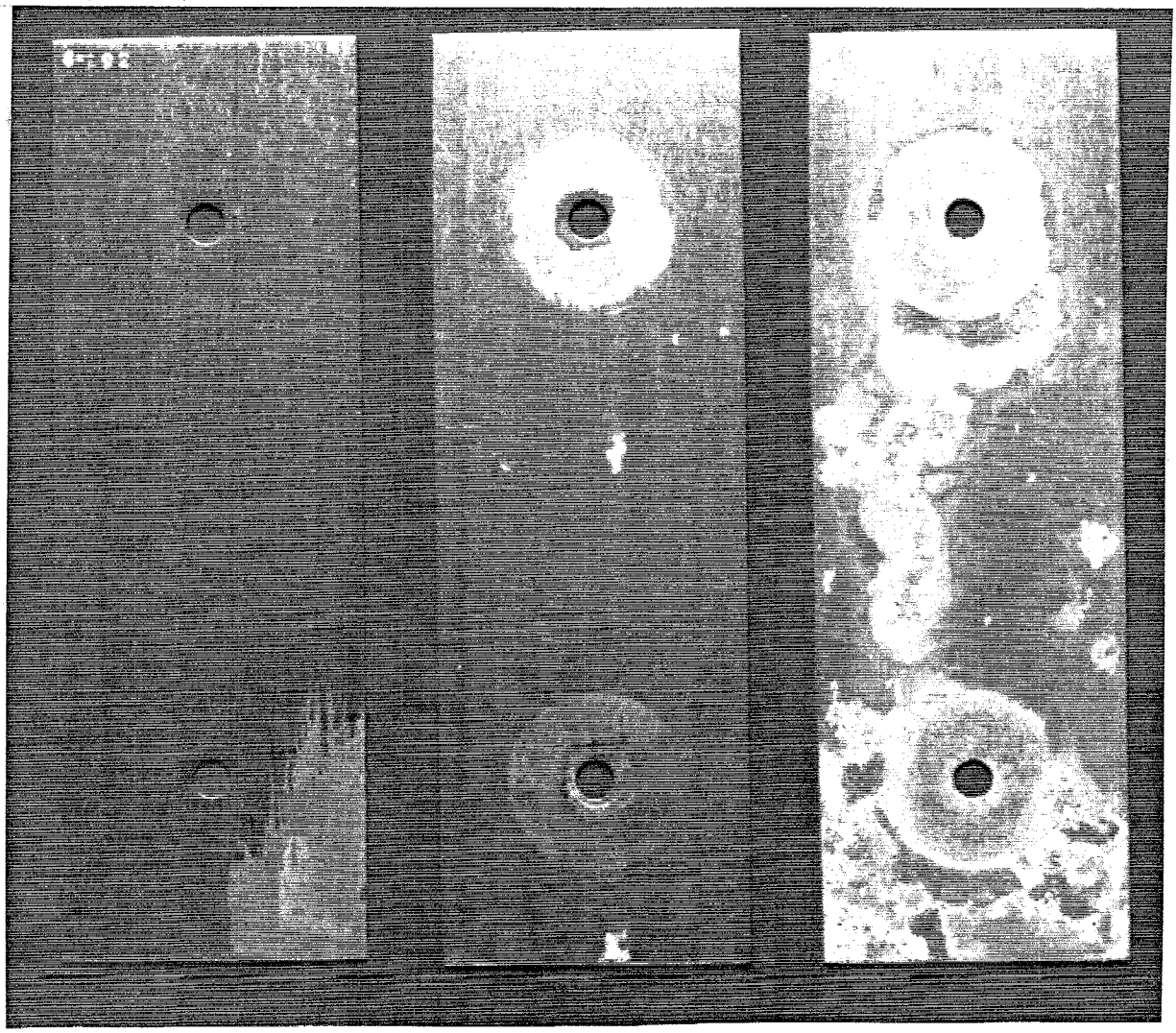

Specimen 6-292
Vapor-phase exposure
Test 16B

Specimen 6-257
Immersed, no Fe
Test 10B

Specimen 6-275
Immersed, with Fe
Test 13B

Figure 6-12. Post-test appearance of 6061 alloy specimens from Brine A/N_2 tests. Test temperature: 30 $\pm$5°C. Test duration: 24 months. Shown approximately one-half actual size.

For the 24-month Fe-containing tests, the H_2 production rate was calculated to be 2.9 mol H_2/m^2 Al-base material-year. For the tests without steel, the H_2 production rate was calculated to be 0.097 mol H_2/m^2 Al-base material-yr. When these H_2 production rates are compared with the H_2 production rate of low-carbon steel in anoxic Brine A, viz., 0.10 mol H_2/m^2 steel-year, it can be seen that the Fe-containing Al-base-material tests yield H_2 production rates far higher than the steel tests; and that, without Fe present, the corrosion/H_2 production rate of the Al-base materials in anoxic brine is approximately equal to the corrosion/H_2 production rate of steel.

Further analysis of the H_2 generation by Al-base materials is presented in Section 6.3.4 of this report.

6.3.2 Brine/CO_2 Tests

The brine/CO_2 tests included immersed-specimen tests (tests 2B and 11B), immersed-specimen tests with steel present (tests 5B and 14B), and vapor-phase-exposure tests (tests 8B and 17B). Duplicate tests were run for test durations of 13 months and 24 months. The pressure-time histories and gas analysis results for these tests are presented in Figure 6-13.

Several of the tests whose pressure-time curves are shown in Figure 6-13 would have exceeded the containers' pressure-gauge limits if gas were not vented prior to test termination. The procedure followed in those cases for determining the total pressure is the same as that described in Section 6.3.1 of this report. The timing and magnitude of the ventings are noted in the pressure-time tabulations of Appendix A-4.

The curves of Figure 6-13 show, as in the case of the anoxic brine tests, a profound effect of the presence of Fe^{++} in the brine, essentially a total lack of reaction in the case of the vapor-phase-exposure tests, and intermediate corrosion rates in the case of immersed specimens with no Fe. It is not surprising that the corrosion rates of the immersed-specimen tests are significantly higher than those exhibited by the specimens in the equivalent brine/N_2 tests, because of the known pH-lowering ability of dissolved CO_2 (SAND92-7347, Section 4.2.1). Crolet and Bonis (1984) have estimated that CO_2 at 10 atm can lower the pH of a 0.5 M NaCl solution at 25°C to ~3.4. This is well below the

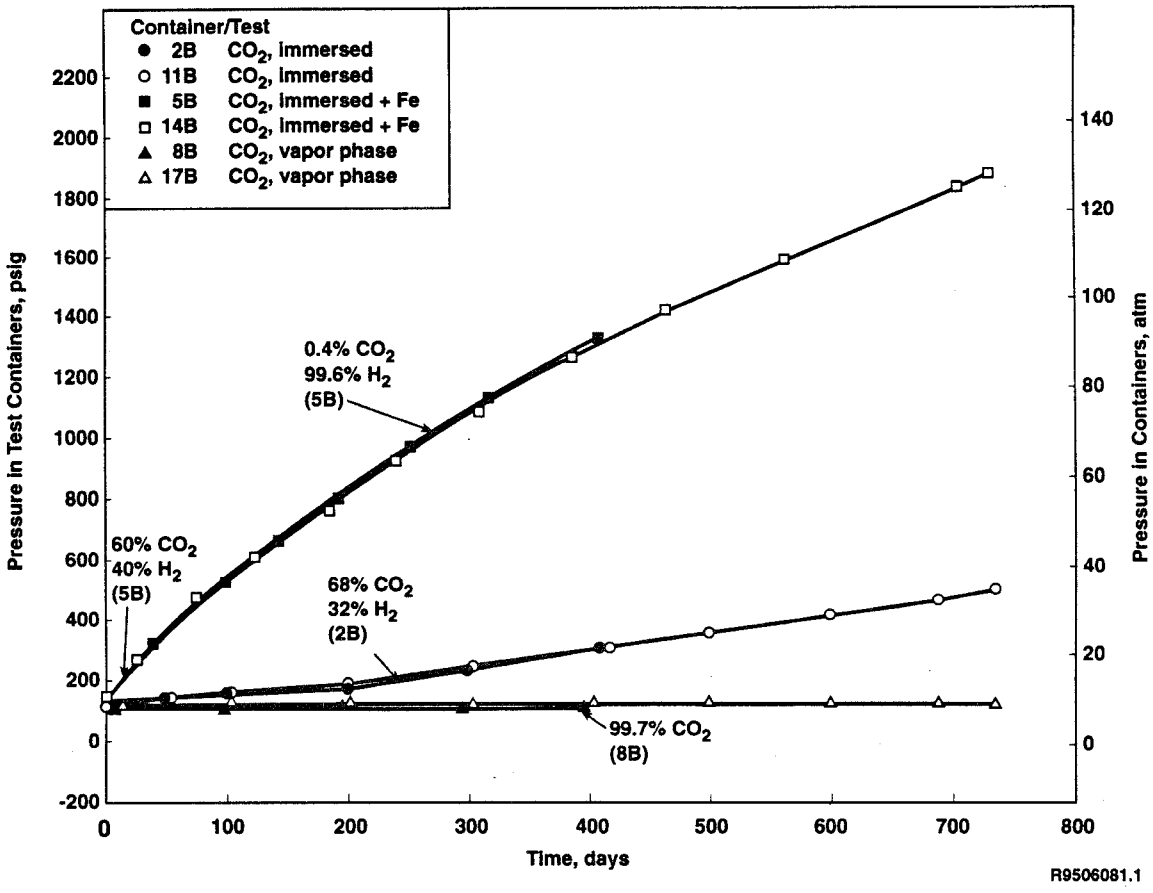

Figure 6-13. Pressure-time curves, Al-base materials in Brine A with CO_2, 30 $\pm$5°C. Gas analysis results (in mole %) are given for each tests at the time the analyses were made.

pH value of 4 which roughly defines the lower pH boundary for Al alloy corrosion resistance. As H_2 is generated and gas is vented from the test containers, the CO_2 content of the vented containers steadily diminishes and solution pH rises.

The decrease of CO_2 concentration in the container gas of the Fe-containing tests with time due to multiple gas ventings from the test containers, is evident from the gas analysis notations on the curve corresponding to test 5B in Figure 6-13. After about 300 days the CO_2 has been essentially eliminated from the Fe-containing systems, and the gas generation rate has decreased significantly.

After the CO_2 has been expelled, the slopes of the curves corresponding to tests 5B and 14B, Figure 6-13, approximate the slopes of the brine/N_2 curves of tests 4B and 13B, Figure 6-12.

The post-test appearance of the specimens from the brine/CO_2 tests was similar to that of the specimens from the brine/N_2 tests, described in the previous section of this report. The degree of attack ranged from essentially no attack for the vapor-phase exposure specimens to extremely severe attack for the immersed specimens in systems containing Fe.

The corrosion of specimens from the immersed-specimen test without Fe showed a strong dependence on the material composition. While the two materials appeared to corrode at similar rates in a gross sense, the 99.99% Al material appeared to corrode nonuniformly over fairly large planar areas, with a definite acceleration of corrosion in the vicinity of the metal-to-metal crevices, both internal and external to the crevices. The 6061 alloy, on the other hand, corroded by way of formation of pits and pit clusters, with no evidence of crevice involvement in the corrosion processes.

The specimens of 99.99% Al from the immersed-specimen tests with Fe showed extreme corrosion attack, whereas the 6061 alloy showed very little, even less than that observed in the anoxic brine tests discussed in the previous section of this report. The 99.99% Al specimens showed large areas of specimen thinning with pitting attack superimposed on the thinned substrate. Also evident was the hourglass-shaped areas of pronounced corrosion attack, encompassing the crevice regions. A definite enhancement of corrosion was found in the vicinity of the crevices. The 6061 alloy showed only a small amount of corrosion at the crevices, proximate to the crevice opening, and some small, isolated pitted regions on certain specimens. As in the case of the anoxic brine tests, it can be confidently stated that the corrosion of the 99.99% Al material was responsible for $>90\%$ of the corrosion and gas generation in the tests containing Fe.

The post-test appearance of the specimens is shown in Figures 6-14 and 6-15. The specimens were cleaned with deionized water and a soft bristle brush prior to being photographed.

The procedure used to calculate the H_2-generation rates for the brine/CO_2 tests is presented in Appendix C. It was arbitrarily decided to use a "mean" H_2 generation rate corresponding to the linear rate resulting from passing a straight line from the origin of each curve through its 24-month end point. Using this method to arrive at the container pressurization rate, and assuming that all of the Al-base-material specimens in each container corrodes at the same rate, a gas-generation rate of

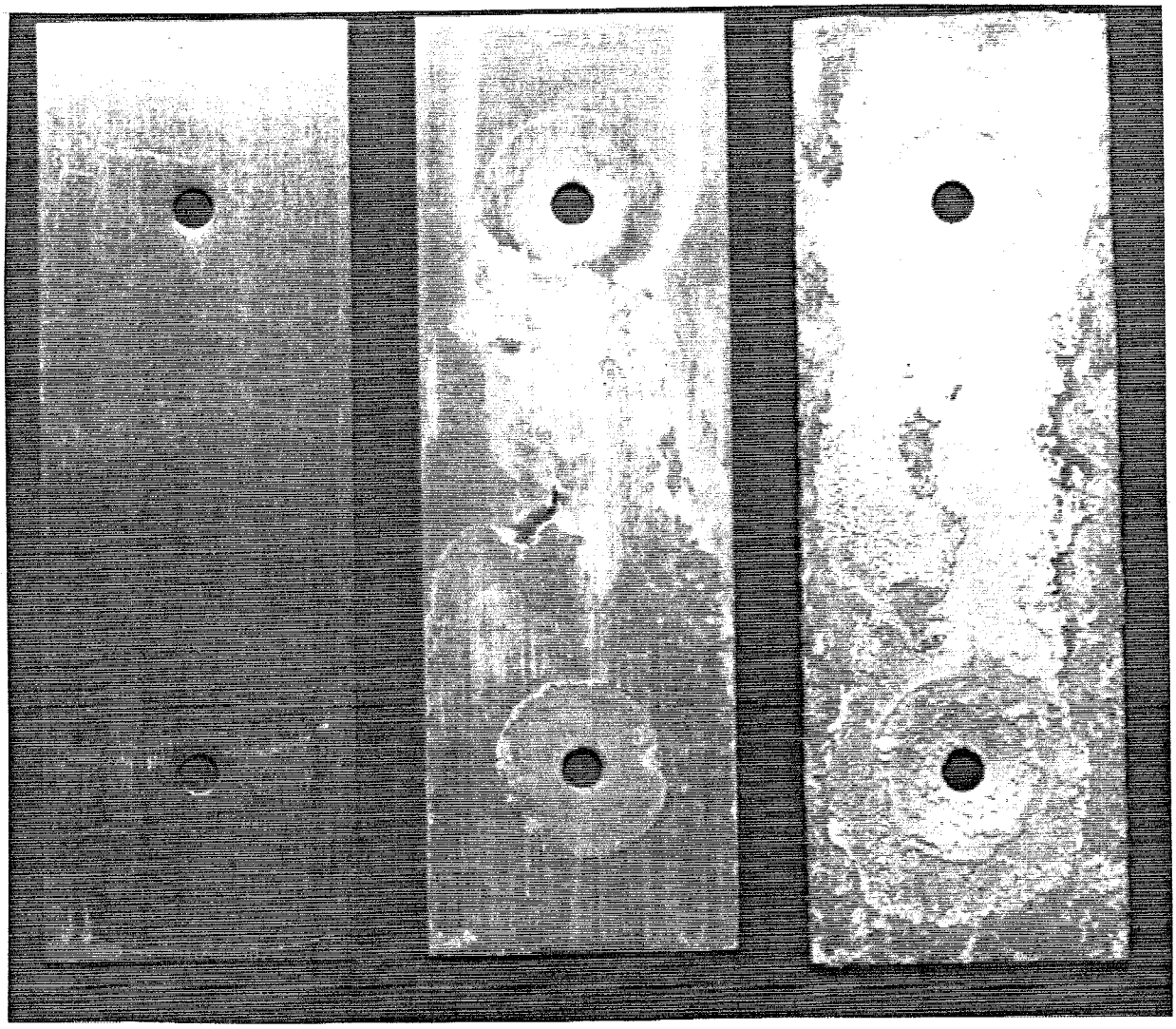

Specimen 1-301	Specimen 1-264	Specimen 1-282
Vapor-phase exposure	Immersed, no Fe	Immersed, with Fe
Test 17B	Test 11B	Test 14B

Figure 6-14. Post-test appearance of 99.99% Al specimens from Brine A/CO_2 tests. Test temperature: 30 $\pm$5°C. Test duration: 24 months. Shown approximately one-half actual size.

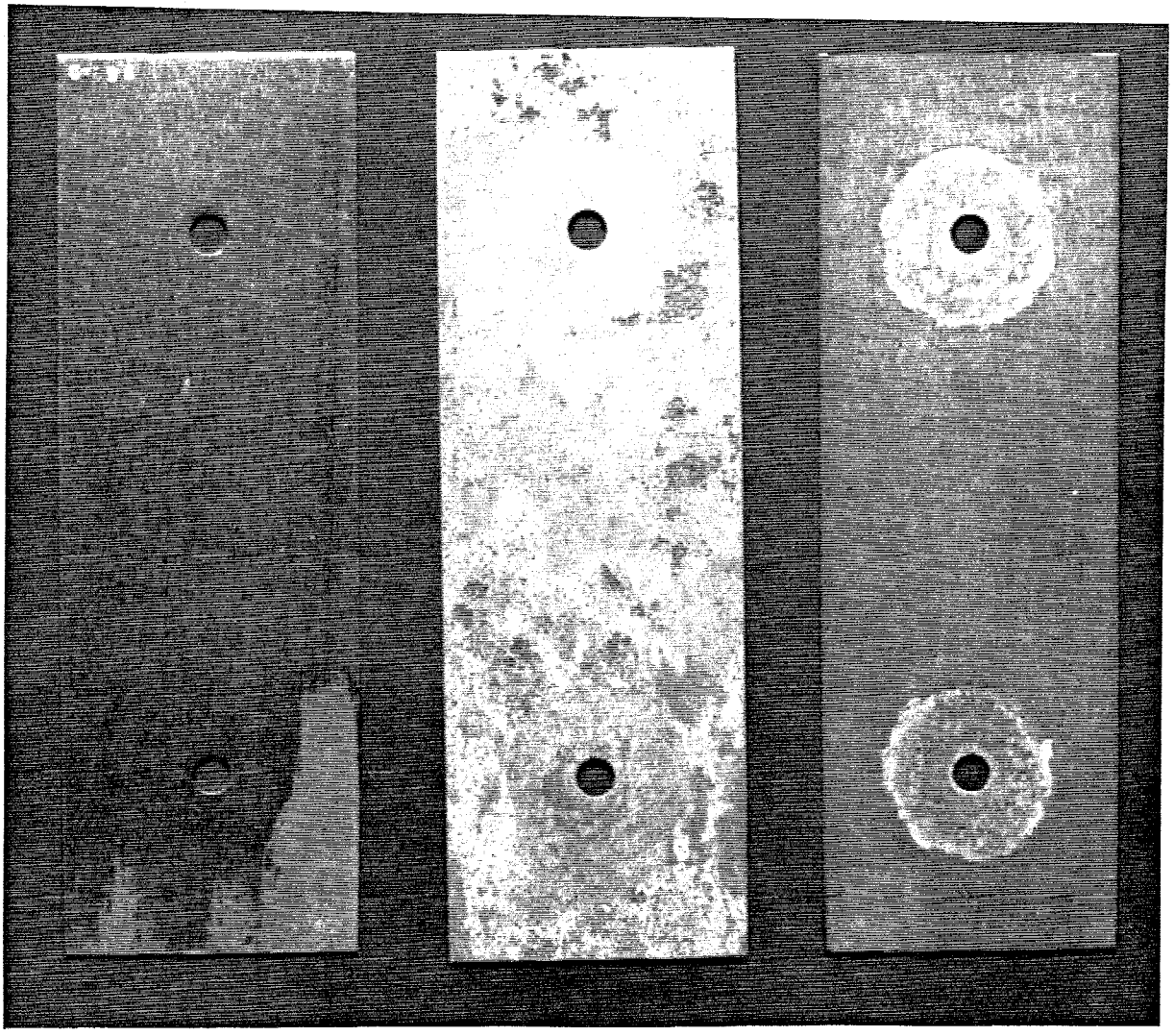

Specimen 6-298	Specimen 6-262	Specimen 6-280
Vapor-phase exposure	Immersed, no Fe	Immersed, with Fe
Test 17B	Test 11B	Test 14B

Figure 6-15. Post-test appearance of 6061 alloy specimens from Brine A/CO_2 tests. Test temperature: 30 $\pm$5°C. Test duration: 24 months. Shown approximately one-half actual size.

4.4 mol H_2/m^2 Al-base material-year was calculated for the immersed-specimen tests with Fe present, and a value of 0.90 mol H_2/m^2 Al-base material-yr was determined for the immersed-specimen tests with no Fe.

Further analysis of the H_2 generation rate of Al-base materials in brine environments is presented in Section 6.3.4 of this report; the results of XRD examination of the corrosion products is presented in Section 6.3.5.

6.3.3 Brine/H_2S Tests

The brine/H_2S tests included immersed-specimen tests (tests 3B and 12B), immersed-specimen tests with steel present (tests 6B and 15B); and vapor-phase-exposure tests (tests 9B and 18B). Duplicate tests were run for test durations of 13 months and 24 months. The pressure-time histories and gas analysis results for these tests are presented in Figure 6-16.

The gas-generation rates of the Brine A/H_2S tests presented in Figure 6-16 show some similarity to the Brine A/N_2 tests (the immersed-specimen tests with Fe) and to the Brine A/CO_2 tests (the immersed-specimen tests without Fe). No H_2 generation was observed in the case of the vapor-phase exposure. It is likely that the activity of Fe in the system was reduced by the passivation of the steel specimens through the formation of an FeS film. This diminution of the activity of Fe^{++} could inhibit its reduction into metallic Fe on the surface of the Al-base-material specimens, making the steel-containing tests behave much like the tests containing no steel. The immersed-specimen tests containing no steel exhibited gas-generation rates similar to equivalent tests with CO_2, consistent with the lowering of pH by both H_2S and CO_2 [Crolet and Bonis (1984) give a pH value of $\sim$3.8 for a 0.5 M NaCl solution in equilibrium with H_2S at 5 atm pressure.]

The usual post-test analysis of the specimens provided the following information:

- The vapor-phase exposure specimens appeared essentially clean, as in the brine/N_2 and the brine/CO_2 tests.

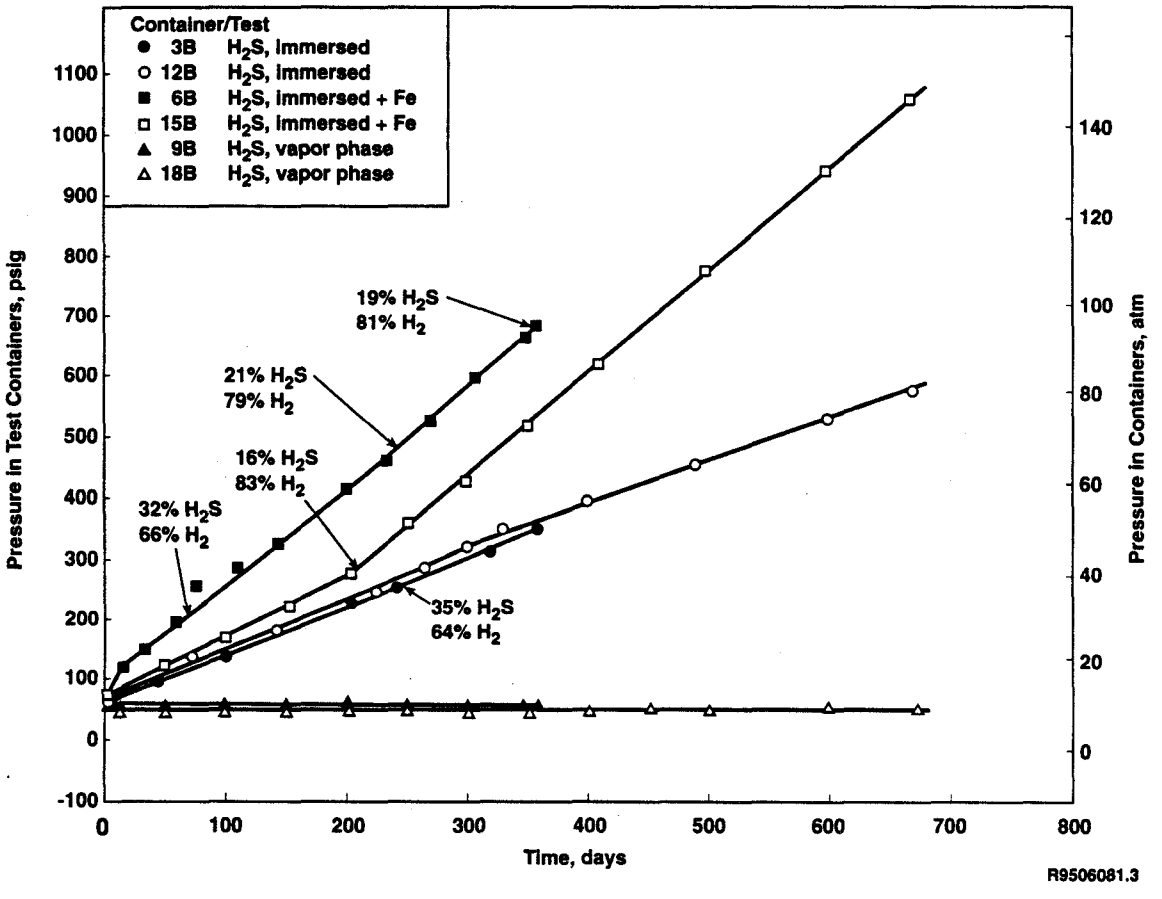

Figure 6-16. Pressure-time curves, Al-base materials in Brine A with H_2S, 30 ± 5°C. Gas analysis results (in mole %) are given for each test at the time the analyses were made.

- The 99.99% Al specimens appeared to corrode significantly more in the brine/H_2S tests without Fe than in the brine/CO_2 tests without Fe, whereas the 6061 alloy specimens corroded significantly less. It was (visually) estimated that the 99.99% Al alloy corroded approximately four times as much as the 6061 alloy in these tests. Once again the 99.99% Al specimens showed a strong tendency toward crevice corrosion, whereas the 6061 alloy did not.

- In the immersed tests with Fe, once again the 99.99% Al specimens suffered >90% of the corrosion attack. The mode of attack of the two materials was similar to that presented for the brine/CO_2 tests in the previous section of this report.

The post-test appearance of the specimens is shown in Figures 6-17 and 6-18. The specimens were cleaned with deionized water and a soft bristle brush prior to being photographed.

The 24-month curves of Figure 6-16 were linearized to obtain "mean" H_2 generation rates (as they were for the brine/CO_2 tests), and the rate of gas generation by the corrosion specimens computed as it was for the brine/N_2 and the brine/CO_2 tests (Appendix C). Assuming that the specimens corroded uniformly throughout the sample arrays, a gas-generation rate of 2.4 mol H_2/m^2 Al-base material-year was arrived at for the immersed-specimen tests with Fe, and a value of 1.3 mol H_2/m^2 Al-base material-year was determined for the immersed-specimen tests with no Fe.

Additional information on the H_2 generation rate of Al-base materials in brine environments is presented in Section 6.3.4 of this report; the results of XRD examination of the corrosion products is presented in Section 6.3.5.

6.3.4 Summary of Corrosion Rates of Al-Base Materials

A summary of the corrosion rate data presented in the preceding three subsections of the report, are presented in Table 6-13. For the tabulated values, the assumption is made that all of the specimens in each test corrode at the same rate. The vapor-phase tests are not included in the table.

In the brine/N_2 test without Fe present, the 99.99% Al material was estimated to corrode at about twice the rate of the 6061 alloy. In the brine/CO_2 test without Fe, the two materials corroded approximately equally. In the brine/H_2S test without Fe, the 99.99% Al material was estimated to corrode at about 4 times the rate of the 6061 alloy.

It was noted in each of the preceding report subsections that the corrosion rate of the 99.99% Al material in the Fe-containing tests was far higher than the corrosion rate of the 6061 alloy, the disparity in corrosion being so great that it could be assumed that the 99.99% Al material was responsible for >90% of the corrosion observed. These results point to a sensitive dependence of Al-base material corrosion rate on alloy composition. Because only two Al-base material compositions were present in the tests, there is no way to correlate corrosion rate with alloy composition, or even alloy class. And, even if such detailed data were available, it would be necessary to know the composition of the Al-base materials in the waste in order to make proper use of the data. Because neither specific-alloy corrosion rates nor detailed waste composition is known, it is suggested that the Al-base

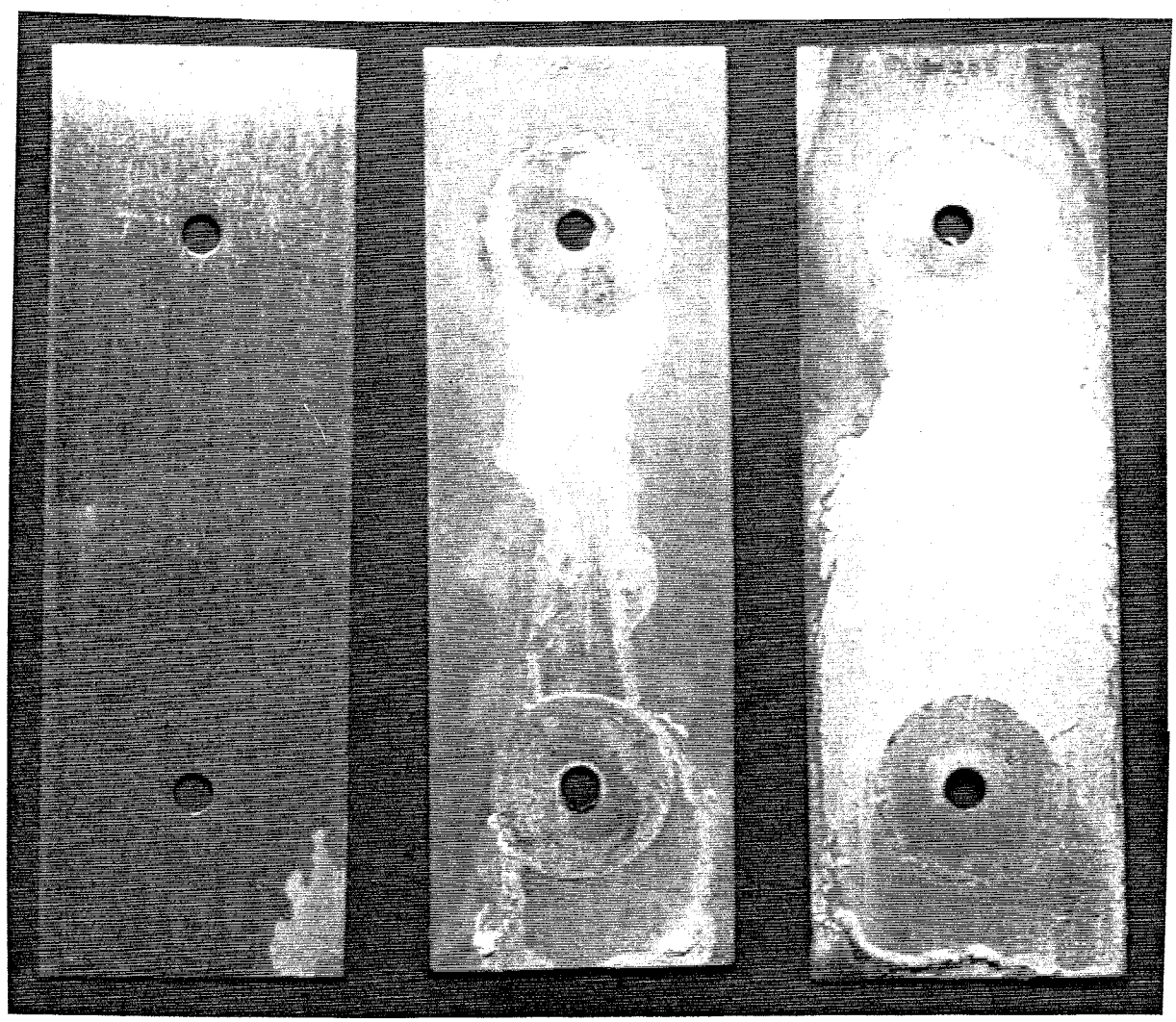

Specimen 1-305	Specimen 1-270	Specimen 1-286
Vapor-phase exposure	Immersed, no Fe	Immersed, with Fe
Test 18B	Test 12B	Test 15B

Figure 6-17. Post-test appearance of 99.99% Al specimens from Brine A/H_2S tests. Test temperature: 30 $\pm$5°C. Test duration: 24 months. Shown approximately one-half actual size.

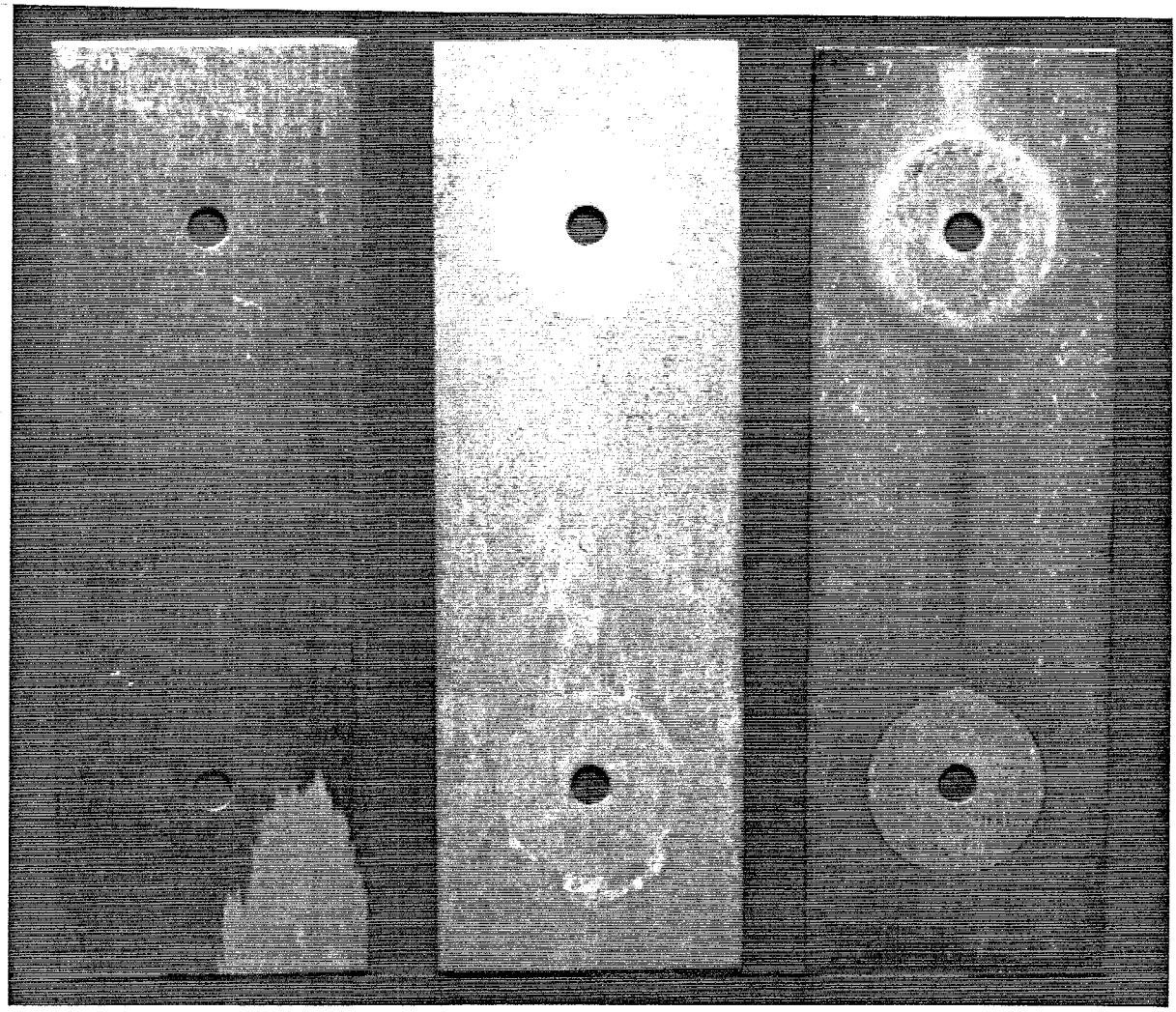

Specimen 6-305	Specimen 6-270	Specimen 6-287
Vapor-phase exposure	Immersed, no Fe	Immersed, with Fe
Test 18B	Test 12B	Test 15B

Figure 6-18. Post-test appearance of 6061 alloy specimens from Brine A/H_2S tests. Test temperature: 30 $\pm$5°C. Test duration: 24 months. Shown approximately one-half actual size.

Table 6-13. Summary of H_2 Generation Rates, Al-Base Material Tests, 24-Month Test Duration

Test	Environment, Initial Gas Pressure	H_2 Generation Rate, mol H_2/m^2 Al-base material-year
10B	Brine/N_2 (10 atm)	0.097
13B	Brine/N_2 (10 atm) with Fe	2.9[a]
11B	Brine/CO_2 (10 atm)	0.90
14B	Brine/CO_2 (10 atm) with Fe	4.4[a]
12B	Brine/H_2S (5 atm)	1.3
15B	Brine/H_2S (5 atm) with Fe	2.4[a]

[a] A conservative approach would double these values, for reasons given in the text.

material corrosion rate data obtained in the present tests be used in the most conservative fashion possible, which in turn would depend on the corrosion model being developed. If, for example, a rapid corrosion gas-generation rate would be considered inimical to repository integrity, a conservative approach would assume 1) that the brine is anoxic and contains a substantial amount of Fe^{++} ions, and 2) that all of the Al-base material present corrodes at the rate of the 99.99% Al material. The assumptions both appear to be intrinsically realistic. The first assumption is basic to the general view of the post-closure repository. The second assumes that the Al-base material present in the waste will demonstrate a corrosion behavior that is much closer to high-purity Al than 6061 alloy. This is consistent with the waste primarily containing Al-base materials having a very low concentration of alloying elements that import resistance to brine corrosion, such as Mg or Mn. It is expected that Al foil, for example, would corrode in a manner similar to 99.99% Al. This rationale does not imply an understanding of the reasons for the sensitivity of high-purity aluminum to anoxic brine containing Fe^{++} and the lack of sensitivity of the 6061 alloy. It could be related to the ability to reduce Fe^{++} to metallic Fe on the Al-base material surface [Cook and McGeary (1964) suggest that only the most electronegative Al alloys could accomplish this]; the rapidity of the post-deposition cell reactions; or other reasons not yet identified. At the present time, the Al-base material corrosion must be

considered largely phenomenological in nature. The assumptions would lead to a corrosion rate twice as high as the rate arrived at in the initial calculations, when it was assumed that all of the corrosion coupons corroded at the same rate. Thus, for the brine/N_2 tests, 2×2.9 mol H_2/m^2 Al-base material-year equals the conservative result of 5.8 mol H_2/m^2 Al-base material-year.

The highest corrosion rates observed in the Al-base material tests were associated with a test environment containing an overpressure of CO_2 gas and steel specimens. This combination resulted in a long-term corrosion rate (Table 6-13) 50% greater than that associated with N_2 gas and steel specimens. It is believed that availability of Fe has a strong influence on the corrosion rate observed. It is shown in Section 6.3.6 of this report that the steel specimens included in the brine/CO_2/Fe tests exhibited far more penetration (corrosion attack) than did steel specimens in the brine/N_2/Fe or the brine/H_2S/Fe tests, indicating more Fe was available in the CO_2-containing system to "plate out" on the Al-base material specimens. The solubility product of $FeCO_3$ is considerably greater than that of FeS (Blaedel and Meloche, 1963), further suggesting a greater Fe^{++} availability in the test with a CO_2 overpressure. Additionally, the CO_2 overpressure tests will have a lower pH than the other tests, at least until the CO_2 is dissipated by repeated container venting.

6.3.5 Analysis of Corrosion Products of Al-Base Materials

Corrosion products adhering to the surfaces of specimens of Al-base materials taken from tests 1B through 9B after 13 months exposure to a variety of brine environments were examined by means of XRD in an attempt to identify the principal compounds present. The analysis of the corrosion product specimens was not straightforward, as the corrosion products produced only weakly resolved patterns. In a few cases, the corrosion products were entirely amorphous. In those cases where the corrosion products were crystalline, only very tentative phase identification was considered to be possible by the analyst, who stated that "the information provided was in lieu of none at all regarding the possible compositions of the crystalline corrosion products."

The summary of corrosion product specimens analyzed, designated according to specimen serving as source of corrosion product, is given in Table 6-14. In addition, specimens of solids removed from the bottom of each test container were also analyzed.

Table 6-14. Al-Base Material Corrosion Products Analyzed for Crystalline Constituents by XRD

Test Container	Overpressure Gas	Specimen ID, High-Purity Al	Specimen ID, 6061 Alloy
1B	N_2	1-006	6-205D
2B	CO_2	1-012	6-211D
3B	H_2S	1-018	6-213D
4B	N_2 (with Fe)	1-022	6-224D
5B	CO_2 (with Fe)	1-028	6-230D
6B	H_2S (with Fe)	1-031	6-235D

A summary of the results of the XRD analyses follows:

Specimens 1-006, 1-018, and 1-031

- $Al_{10}Cl_3(OH)_{27}\cdot 13H_2O$ (aluminum chloride hydroxide hydrate)

and/or

- $Al_{10}Cl_4(OH)_{26}\cdot xH_2O$ (aluminum chloride hydroxide hydrate)

plus

- $Ca_4Al_2O_6(CN)_2\cdot 10H_2O$ (calcium aluminum oxide cyanide hydrate)

and/or

- $C_2H_2CaO_4\cdot Al_2O_3\cdot 3CaO\cdot 11H_2O$ (calcium aluminum oxide formate hydrate)

plus

- $CCa_{0.5}O_2\cdot 3CaO\cdot Al_2O_3\cdot 0.5Ca(OH)_2\cdot 9H_2O$ (calcium aluminum oxide oxalate hydroxide hydrate)

Specimens 1-022 and 1-028

- $Al_{10}Cl_3(OH)_{27}\cdot 13H_2O$ (aluminum chloride hydroxide hydrate)

and/or

- $Al_{10}Cl_4(OH)_{26}\cdot xH_2O$ (aluminum chloride hydroxide hydrate)

plus

- $CCa_{0.5}O_2\cdot 3CaO\cdot Al_2O_3\cdot 0.5Ca(OH)_2\cdot 9H_2O$ (calcium aluminum oxide oxalate hydroxide hydrate)

Specimen 1-012

- Specimen apparently entirely amorphous, as it yielded no crystalline peaks.

Specimens 6-205D, 6-213D, 6-230D, 6-235D, and 6-224D

- $CCa_{0.5}O_2\cdot 3CaO\cdot Al_2O_3\cdot 0.5Ca(OH)_2\cdot 9H_2O$ (calcium aluminum oxide oxalate hydroxide hydrate)

Specimen 6-211D

- Specimen apparently entirely amorphous, as it yielded no crystalline peaks.

Specimens of Solids from Bottoms of Containers 1B through 6B

- No compounds of Al were identified in the solids from the bottoms of the containers. The identifiable solids primarily consisted of some combination of the following compounds: NaCl, $KMgCl_3\cdot 6H_2O$ (potassium magnesium chloride hydrate), $MgCl_2\cdot 6H_2O$, KCl, $CaCO_3$, and $(NH_4)_3Fe(SO_4)_3$ (ammonium iron sulfate).

The complexity of the corrosion products was alluded to earlier in this report (Section 4.2), when it was pointed out that a thermodynamic analysis of the Al-base material corrosion reactions could not be simply based on the supposition of an Al_2O_3 reaction product, even though that is the product commonly cited in the literature [for example, Hatch (1984)]. A survey of the corrosion products formed shows some possible Al_2O_3 corrosion product constituents, especially on the 6061 alloy, but aluminum chloride hydroxide hydrate compounds are also commonly found, especially on the 99.99% Al material. The data presented strongly imply a basic difference in corrosion product formed between the 99.99% Al material and the 6061 alloy. If the differences implied are indeed real, it appears that the Ca constituent of the brine (Ca is a minor constituent, present at ~560 mg/L)

could be important in the formation of the corrosion product on the 6061 alloy, but not necessarily on the 99.99% Al alloy.

6.3.6 Corrosion of Steel in the Presence of Al-Base Materials

A third of the seal-welded containers dedicated to corrosion testing of Al-base materials had coupons of low-carbon steel (Lot J) included in them, to provide Fe^{++} ions to the environment. Presence of Fe^{++} generally accelerates the corrosion of Al-base materials via the replacement reaction that deposits metallic Fe on the surface of the Al-base material, and such corrosion acceleration was indeed found in all of the Fe^{++} containing tests.

The low-carbon steel specimens that had been included in both the 13-month and the 24-month tests were analyzed to determine the effect of Al-base materials on the corrosion behavior of steel in the Brine A environments. Four steel coupons were available from each test container. As the initial weight of the coupons was known, the metal penetration could be determined by stripping the corrosion product from the coupons, weighing them, and determining the weight change. Because the H_2 produced by the rapid corrosion of the Al-base-material coupons masked the H_2 formed by the relatively inconsequential steel corrosion in the test containers, the kinetics of the steel corrosion could not be determined by pressure-gauge readout. The agreement in metal-penetration values between the four specimens in each environment was very good. The average metal penetration in each test environment after 13 and 24 months exposure is given in Table 6-15.

By comparison with the above-tabulated values of steel corrosion in Brine A with aluminum, at a one-year exposure time, the corrosion rate of the same steel immersed in Brine A with an N_2 overpressure is 1.1 μm/y; with a CO_2 overpressure is 3.7 μm/y (passivated); and with an H_2S overpressure is 0.35 μm/y (passivated). Thus, at a test duration of about 1 year, the presence of Al had accelerated the corrosion of steel under N_2-overpressure conditions by a factor of 7, under CO_2-overpressure conditions by a factor of 4, and under H_2S-overpressure conditions by a factor of 2.

It is likely that this acceleration of corrosion is due to the continual scavenging of Fe^{++} ion from the solution by the Al-base-material specimens, keeping the solution from saturating (at least in the near vicinity of the specimen surfaces) with that specie and thereby maintaining the corrosion rate

Table 6-15. Penetration of Low-Carbon-Steel Specimens in Al-Base Material Corrosion Tests

Initial Test Environment[a]	Test Identification	Average Metal Penetration, μm/y[b]
Brine A, N_2 at 10 atm	4B	8.0±1.3
	13B	3.9±0.27
Brine A, CO_2 at 10 atm	5B	15.0±1.7
	14B	5.8±0.58
Brine A, H_2S at 5 atm	6B	0.71±0.17
	15B	0.46±0.11

[a] The initial test environment does not maintain under the test conditions, most importantly in the case of the CO_2 and the H_2S test environments. This is because the rapid corrosion of the Al-base materials required frequent gas ventings from the plenums of the test containers to avoid overpressurization of the gauges. The venting effectively dissipated the original overpressure gas. For example, after 10 months and 13 prior ventings, the gas in the plenum of test 5B was 99.6% H_2, 0.4% CO_2; after 13 months and 8 prior ventings, the gas in the plenum of test 6B was 81% H_2, 19% H_2S. This subject is treated in more detail in Appendix C.

[b] Average of four coupons in each test. The standard deviation of the corrosion rate values is shown for each set of four coupons.

of steel at a higher rate than was observed in the tests without Al. The 24-month data, however, reveal a corrosion rate in all test environments approximately half that shown in the 13-month tests. This conclusion is consistent with essentially no corrosion occurring in the 13- to 24-month time period. This is understandable in the case of the environments containing CO_2 and H_2S, as passivation could possibly occur early in the exposure that could inhibit further corrosion.

In the case of the brine/N_2 environments, the reason for the cessation of corrosion is not clear. It is possible that a film, either corrosion-product or brine-derived, eventually formed on the steel specimens, effectively slowing the rate of corrosion. Regardless of the reason for the observed corrosion inhibition, it appears that the corrosion enhancement observed after 13 months is not an obvious reason for re-evaluation of the corrosion rates obtained from anoxic brine tests with no Al present, because the corrosion enhancement does not appear, on the basis of the limited tests performed, to be a long-lived effect.

7.0 CONCLUSIONS

The present report constitutes the final deliverable to Sandia National Laboratories from the PNL WIPP-support gas-generation program. All of the conclusions developed during the course of the program, including those either wholly or partially alluded to in the previous report (SAND92-7347), are presented here.

7.1 Steel with N_2 Overpressure

- The corrosion rate of low-carbon steel immersed in anoxic Brine A at 30°C for test durations of 24 months decreased slowly with time. The corrosion rate of the steel during the final 12-month period of the 24-month test was 0.71 μm/yr, equivalent to the generation of 0.10 mol H_2/m^2-steel-yr. It is expected that this rate would continue to decrease with time beyond 24 months. In support of this expectation, a test similar to the anoxic brine tests described, except for the initial presence of a small, nonpassivating amount of CO_2, showed a corrosion rate in the final 12 months of a 38-month test that was only 70% of the 12-to-24 month rate cited for the anoxic brine tests. At intermediate times the pressure-time data curves for the tests noted were in excellent agreement.

- In the long-term tests (12 and 24 months) of steel immersed in anoxic Brine A there was good agreement between moles of Fe reacted and moles of H_2 produced, assuming the Fe in the corrosion product is in the divalent state. The nonadherent, green-blue gray corrosion product could not be identified by x-ray diffraction (XRD) methods. Chemical analyses established the presence of a significant amount of Mg in the corrosion product. It is believed that the corrosion product is, or is a close relative to, an iron magnesium hydroxide [$Fe,Mg(OH)_2$].

- Steel specimens exposed at 30°C to the vapor phase of Brine A with an N_2 overpressure of 10 atm showed no discernible corrosion reaction. The corrosion product adhering to the bottoms of these specimens where they were contacted by the brine during handling of the containers was $\beta Fe_2(OH)_3Cl$ in all cases investigated.

- Steel specimens immersed for 6 months in Brine A at 30°C showed a gas-generation/corrosion rate enhancement of about a factor of two when the N_2 overpressure was increased from 10 to 73 atm. No further increase was observed when the pressure was increased to 127 atm. Imposition of full WIPP lithostatic pressure is not expected to have a profound effect on the corrosion/gas generation reaction of steel in Brine A, or brines similar to Brine A.

- The corrosion rate of low-carbon steel specimens immersed in modified ERDA-6 brine (a Na, K chloride-sulfate brine) was strongly dependent on the pH of the brine. At pH 3 the average penetration rate was 7900 μm/yr; at pH 5, 89 μm/yr; at pH 7, 51 μm/yr; at pH 9, 2 μm/yr; and at pH 11, 3.6 μm/yr.

- The corrosiveness of modified (Ca, Mg, and HCO_3^- constituents eliminated) ERDA-6 brine toward low-carbon steel specimens under N_2 overpressure conditions, and without pH adjustment, was determined to be similar to that of Brine A, as determined by 6-month tests at 30°C.

- Steel specimens embedded in simulated backfill (30% bentonite, 70% salt) wicking brine from a pool of Brine A under anoxic (N_2 overpressure) test conditions at 30°C over a period of 6 months showed corrosion rates approximately twice those observed in 6-month immersion tests with no backfill present. A similar 6-month test was run in which the backfill/specimen array was suspended in the vapor phase over the Brine A pool. The steel corrosion rate under these circumstances was low, about 30% of that observed in a Brine A immersion test under N_2 with no backfill present.

- Steel specimens immersed in Brine A with an N_2 overpressure and with Al-base materials present in the environment revealed an initially rapid rate of reaction, as determined by a 13-month test exposure. The penetration rate was approximately a factor of 7 higher than expected from anoxic brine tests without Al present. However, the specimens appeared to be passive for the next 11 months (as determined by 24-month tests), suggesting that either a corrosion-derived or a deposition-derived passive film had formed on the specimen surfaces.

- The brine in the test containers did not, in general, undergo an appreciable change in composition during the N_2/immersed-specimen tests.

- Steel specimens embedded in a mass of simulated particulate salt (halite) backfill, with the salt mass "wicking" Brine A from a brine source, under an N_2 overpressure at 30°C for a 3-month test duration, showed corrosion rates similar to those expected under Brine A/immersed test conditions.

7.2 Steel with CO_2 Overpressure

- CO_2 in Brine A causes an initial increase in the reaction rate of steel, relative to anoxic (brine/N_2) conditions. The initial reaction rate increases with the CO_2 pressure imposed. Additions of CO_2 beyond a certain threshold amount cause the reaction to essentially stop, however, typically in < 100 days, due to the formation of an adherent carbonate reaction product [$FeCO_3$, siderite, or $Fe,Mn,Zn(CO_3)$, oligonite]. The amount of steel reacted (metal penetration) prior to passivation increases from $\sim$ 6 μm at 10 atm initial CO_2 pressure to $\sim$ 34 μm at 62 atm.

- The immersed-specimen tests in Brine A with CO_2 showed fairly good agreement between moles of Fe reacted and moles of H_2 produced, assuming that Fe is only in the divalent state in the corrosion product.

- The minimum amount of CO_2 required to passivate low-carbon steel under the seal-welded container test conditions used in the present study (Brine A, 30°C) lay in the range between 0.32 and 0.16 mol CO_2/m^2 steel.

- Addition of H_2S to an equilibrium pressure of ~1 atm to seal-welded test containers containing Brine A and CO_2-passivated low-carbon steel specimens at 30°C resulted in activation of the previously passivated specimens. The de-passivated specimens exhibited gas generation characteristics approximately characteristic of low-carbon steel exposed to anoxic brine. The H_2S added did not cause repassivation of the steel specimens.

- Steel specimens exposed to a 10 atm CO_2 pressure and vapor of Brine A at 30°C showed insignificant corrosion. Corrosion product in the splash zone of the test specimens was siderite, $FeCO_3$.

- The brine in the test containers underwent an appreciable change in composition during the CO_2/immersed tests. The post-test brines showed a relatively high Fe concentration, a relatively low Ca concentration, and a low pH.

7.3 Steel with H_2S Overpressure

- Steel specimens exposed in the immersed and vapor-phase test conditions to Brine A at 30°C with a 5-atm equilibrium pressure of H_2S showed no significant reaction. The immersed specimens became passivated by a thin layer of FeS, mackinawite, which formed on the specimen surfaces and prevented further reaction. Approximately 0.056 mol Fe/m^2 steel reacted to form the passive film.

- Addition of H_2S to ~1 atm equilibrium partial pressure in a related study (CO_2 with eventual H_2S addition) did not result in passivation of the steel specimens, and the H_2S destroyed the passive state of steel specimens previously passivated with CO_2.

- Addition of CO_2 to an equilibrium pressure of ~0.5 atm to the test containers containing H_2S-passivated steel specimens did not alter the specimens' passive state.

7.4 Steel with H_2 Overpressure

- The corrosion rate of low-carbon steel immersed in Brine A at 30°C goes through a minimum at intermediate H_2 pressures (36 to 70 atm) and is at a maximum at low

pressures (~2 atm) and high pressures (127 atm) in tests of 6-month duration. The overall effect of H_2 pressure on corrosion of low-carbon steel is not believed to be significant at long times, even at H_2 pressures equivalent to lithostatic pressure at the WIPP horizon.

7.5 Alternative Packaging Materials

- Cu-base alternative packaging materials (Cu and cupronickel 90-10) showed insignificant reaction when immersed in Brine A at 30°C with overpressures of N_2 or CO_2 for time periods to 24 months. The Cu-base materials reacted rapidly with H_2S, however, and produced H_2 equivalent on a molar basis to the H_2S added. The reaction product was Cu_2S, chalcocite. Cu-based packaging materials could not be recommended for use in the WIPP if there were any possibility of H_2S being present in the repository environment.

- Ti-base alternative packaging materials (Ti Grade 2 and Ti Grade 12) showed insignificant reaction in all test environments, i.e., in N_2/immersed, CO_2/immersed, and H_2S/immersed environments, for test durations to 24 months. It appears at the present time that Ti-base packaging materials could be used in the WIPP site without concern for corrosion or gas generation.

7.6 Al-Base Materials

- Al-base materials (99.99% Al and 6061 alloy) showed no reaction when exposed to the vapor phase of Brine A with N_2, CO_2, or H_2S at 30°C for time periods to 24 months.

- Al-base materials exhibited significant corrosion and gas generation when immersed in Brine A at 30°C. With an N_2 overpressure the material-averaged, linearized 24-month gas generation rate was 0.097 mol H_2/m^2 Al-base material-year, approximately equivalent to that of low-carbon steel under the same test conditions. The 99.99% Al material corroded at about twice the rate of 6061 alloy in these tests. With a CO_2 overpressure the material-averaged, linearized rate was 0.85 mol H_2/m^2 Al-base material-yr. In these tests the 99.99% Al and the 6061 alloy specimens appeared to corrode at approximately the same rate. With an H_2S overpressure the material-averaged, linearized rate was 1.3 mol H_2/m^2 Al-base material-yr, with the 99.99% Al material corroding approximately four times as fast as the 6061 alloy.

- Al-base materials exhibited their highest corrosion rates when Fe, derived from steel coupons, was included in the environment as a brine contaminant. In all of these tests the 99.99% Al material was responsible for >90% of the corrosion taking place. Making the assumption that the rates were linear over the 24-month, 30°C tests, and assuming that all materials corroded at the same rate, the following H_2 generation rates

(given in mol H_2/m^2 Al-base material-yr) were found: with an N_2 overpressure, 2.9; with a CO_2 overpressure, 4.4; and with an H_2S overpressure, 2.4.

- The corrosion products from the brine/Al-base material tests were not easy to identify by XRD, because of their complexity and/or their ill-defined crystallinity. In no case did a single, simple corrosion product [e.g., Al_2O_3, $Al(OH)_3$] predominate.

- The greater corrosion attack of the Al-base materials in the CO_2-overpressure tests containing Fe relative to the H_2S overpressure tests was ascribed to (a) a much greater corrosive attack of the steel specimens in the CO_2-containing tests, and (b) a significantly greater solubility product of $FeCO_3$ relative to FeS. The corrosion observed in the Al-base material tests was, in general, highly nonuniform. The 99.99% Al alloy specimens commonly exhibited irregular regions of varying degrees of specimen thinning, whereas the 6061 alloy exhibited some variable thinning but a great deal of pitting attack. Crevice corrosion was commonly observed in the metal-to-metal crevice regions; it was not, however, generally observed in the vicinity of the crevice formed by the insulating washer.

This page intentionally left blank.

8.0 REFERENCES

American Colloid Company. 1995. "Technical Data Sheet, Volclay GPG 30." Arlington Heights, IL: American Colloid Company, Industrial Chemical Division. (Copy on file in the Sandia WIPP Central Files, Sandia National Laboratories, Albuquerque, NM as WPO#39636.)

ASM (American Society for Metals). 1978. *Metals Handbook. Volume 1 Properties and Selection: Irons and Steels.* 9th ed. Metals Park, OH: American Society for Metals. 161.

ASM (American Society for Metals). 1987. *Metals Handbook. Volume 13 Corrosion.* 9th ed. Metals Park, OH: American Society for Metals. 598-607.

Bates, R.G. 1973. *Determination of pH: Theory and Practice.* New York, NY: John Wiley & Sons. 31-39.

Blaedel, W.J., and V.W. Meloche. 1963. *Elementary Quantitative Analysis: Theory and Practice.* 2nd ed. New York, NY: Harper & Row. Appendix V.

Brush, L.H. 1990. *Test Plan for Laboratory and Modeling Studies of Repository and Radionuclide Chemistry for the Waste Isolation Pilot Plant.* SAND90-0266. Albuquerque, NM: Sandia National Laboratories. (Available from the National Technical Information Service (NTIS), Springfield, VA as DE90013595/XAB.)

Brush, L.H., D. Grbic-Galic, D.T. Reed, X. Tong, R.H. Vreeland, and R.E. Westerman. 1991. "Preliminary Results of Laboratory Studies of Repository Chemistry for the Waste Isolation Pilot Plant," *Scientific Basis for Nuclear Waste Management XIV, Materials Research Society Symposium Proceedings, Boston, MA, November 26-29, 1990.* Eds. T.A. Abrajano, Jr. and L.H. Johnson. SAND90-1031C. Pittsburgh, PA: Materials Research Society. Vol. 212, 893-900. (SAND90-1031C is available from the National Technical Information Service (NTIS), Springfield, VA as DE90016219/XAB.)

Brush, L.H., M.A. Molecke, A.R. Lappin, R.E. Westerman, X. Tong, J.N.P. Black, D. Grbic-Galic, R.H. Vreeland, and D.T. Reed. 1992. "Laboratory and Bin-Scale Tests of Gas Generation for the Waste Isolation Pilot Plant," *Gas Generation and Release from Radioactive Waste Repositories, 3rd OECD/NEA Workshop: Near-Field Effects of Gas Release, Aix-en-Provence, France, September 23-26, 1991.* SAND91-0675C. Paris, France: Organisation for Economic Co-Operation and Development. 142-154. (SAND91-0675C is available from the National Technical Information Service (NTIS), Springfield, VA as DE91019052/XAB.)

Butcher, B.M. 1990. *Preliminary Evaluation of Potential Engineered Modifications for the Waste Isolation Pilot Plant (WIPP).* SAND89-3095. Albuquerque, NM: Sandia National Laboratories. (Available from the National Technical Information Service (NTIS), Springfield, VA as DE90010165/XAB.)

Cook, E.H., and F.L. McGeary. 1964. "Electrodeposition of Iron from Aqueous Solutions Onto an Aluminum Alloy," *Corrosion*. Vol. 20, no. 4, 111t-114t.

Crolet, J.L., and M.R. Bonis. 1984. "pH Measurements Under High Pressures of CO_2 and H_2S," *Corrosion/84, International Corrosion Forum Devoted Exclusively to the Protection and Performance of Materials, New Orleans, LA, April 2-6, 1984*. Paper No. 294. Houston, TX: National Association of Corrosion Engineers.

EATF (Engineered Alternatives Task Force). 1991. "Appendix H Report of the Waste Container Materials Panel," *Evaluation of the Effectiveness and Feasibility of the Waste Isolation Pilot Plant Engineered Alternatives: Final Report of the Engineered Alternatives Task Force*. DOE/WIPP-91-007. [Carlsbad, NM]: Waste Isolation Pilot Plant. Vol. 1.

Felmy, A.R. 1990. *GMIN: A Computerized Chemical Equilibrium Model Using a Constrained Minimization of Gibbs Free Energy*. PNL-7281. Richland, WA: Pacific Northwest Laboratory. (Available from the National Technical Information Service (NTIS), Springfield, VA as DE90010250/XAB.)

Garrels, R.M., and C.L. Christ. 1965. *Solutions, Minerals, and Equilibria*. San Francisco, CA: Freeman, Cooper, and Company. 403.

Guzowski, R.V. 1990. *Preliminary Identification of Scenarios That May Affect the Escape and Transport of Radionuclides From the Waste Isolation Pilot Plant, Southeastern New Mexico*. SAND89-7149. Albuquerque, NM: Sandia National Laboratories. (Available from the National Technical Information Service (NTIS), Springfield, VA as DE90011787/XAB.)

Hatch, J.E., ed. 1984. "Chapter 7 Corrosion Behavior," *Aluminum: Properties and Physical Metallurgy*. Metals Park, OH: American Society for Metals. 242-254.

Jackson, K.J. 1988. *Verification and Validation Studies of the Addition of Pitzer=s Equations to the EQ3/6 Brine Model*. UCRL-53841. Livermore, CA: Lawrence Livermore National Laboratory. (Available from the National Technical Information Service (NTIS), Springfield, VA as DE89003708/XAB.)

JANAF. 1985. *JANAF Thermochemical Tables*. 3rd ed. Eds. M.W. Chase, Jr., C.A. Davies, J.R. Downey, Jr., D.J. Frurip, R.A. MacDonald, and A.N. Syverud. Journal of Physical and Chemical Reference Data Volume 14, Part 1. Washington, DC: American Chemical Society; New York, NY: American Institute of Physics. (Data for AlClO are found on page 79; data for NaCl are found on page 770.)

Knauss, K.G., T.J. Wolery, and K.J. Jackson. 1990. "A New Approach to Measuring pH in Brines and Other Concentrated Electrolytes," *Geochimica et Cosmochimica Acta*. Vol. 54, no. 5, 1519-1523.

Lange's Handbook. 1985. *Lange's Handbook of Chemistry*. 13th ed. Ed. J.A. Dean. New York, NY: McGraw-Hill. 11-21.

Lappin, A.R., R.L. Hunter, D.P. Garber, and P.B. Davies, eds. 1989. *Systems Analysis, Long-Term Radionuclide Transport, and Dose Assessments, Waste Isolation Pilot Plant (WIPP), Southeastern New Mexico; March 1989*. SAND89-0462. Albuquerque, NM: Sandia National Laboratories. (Available from the National Technical Information Service (NTIS), Springfield, VA as DE89014586/XAB.)

Molecke, M.A. 1983. *A Comparison of Brines Relevant to Nuclear Waste Experimentation*. SAND83-0516. Albuquerque, NM: Sandia National Laboratories. (Available from the National Technical Information Service (NTIS), Springfield, VA as DE83012968/XAB.)

Pitzer, K.S. 1979. "Theory: Ion Interaction Approach," *Activity Coefficients in Electrolyte Solutions*. Ed. R.M. Pytkowicz. Boca Raton, FL: CRC Press, Inc. Vol. I, 157-208.

Pourbaix, M. 1974. *Atlas of Electrochemical Equilibria in Aqueous Solutions*. 2nd ed. Houston, TX: National Association of Corrosion Engineers. 307-321.

SAND92-7347. See Telander and Westerman (1993).

Schweitzer, P.A. 1989. *Corrosion and Corrosion Protection Handbook*. 2nd ed. New York, NY: Marcel Dekker. 168.

Shreir, L.L., ed. 1963. *Corrosion. Volume 1: Corrosion of Metals and Alloys*. New York, NY: John Wiley & Sons. 4.9-4.25.

Simpson, J.P., and R. Schenk. 1989. "Corrosion Induced Hydrogen Evolution on High Level Waste Overpack Materials in Synthetic Groundwaters and Chloride Solutions," *Scientific Basis for Nuclear Waste Management XII, Materials Research Society Symposium Proceedings, Berlin, Germany, October 10-13, 1988*. Eds. W. Lutze and R.C. Ewing. Pittsburgh, PA: Materials Research Society. Vol. 127, 389-396.

Telander, M.R., and R.E. Westerman. 1993. *Hydrogen Generation by Metal Corrosion in Simulated Waste Isolation Pilot Plant Environments: Progress Report for the Period November 1989 Through December 1992*. SAND92-7347. Albuquerque, NM: Sandia National Laboratories. (Available from the National Technical Information Service (NTIS), Springfield, VA as DE94001556/XAB.)

Westerman, R.E., J.H. Haberman, S.G. Pitman, K.H. Pool, K.C. Rhoads, and M.R. Telander. 1988. *Corrosion Behavior of A216 Grade WCA Mild Steel and Ti Grade 12 Alloy in Hydrothermal Brines: Salt Repository Project. Annual Report FY 1986*. PNL/SRP-6221. Richland, WA: Pacific Northwest Laboratory. (Available from the National Technical Information Service (NTIS), Springfield, VA as DE89000284/XAB.)

This page intentionally left blank.

APPENDIX A-1: PRESSURE HISTORIES, TESTS OF LOW-CARBON STEEL IN BRINE A WITH CONTROLLED CO_2 (AND EVENTUAL H_2S) ADDITIONS, SEAL-WELDED CONTAINER TEST METHOD

APPENDIX A-1: PRESSURE HISTORIES, TESTS OF LOW-CARBON STEEL IN BRINE A WITH CONTROLLED CO_2 (AND EVENTUAL H_2S) ADDITIONS, SEAL-WELDED CONTAINER TEST METHOD

Summary of Initial Container Environments:
All specimens were completely immersed in Brine A in each container (containers 33 through 38)

Container 33: 0.32 mol CO2/m2 steel
Container 34: 0.16 mol CO2/m2 steel
Container 35: 0.063 mol CO2/m2 steel
Container 36: 0.032 mol CO2/m2 steel + N2
Container 37: 0.016 mol CO2/m2 steel + N2
Container 38: 0.00 mol CO2/m2 Steel (N2 only)
Test Temperature: 30±5°C

	Pressure in Container, psig				Pressure in Container, psig		
Time, days	Cont. 33	Cont. 34	Cont. 35	Time, days	Cont. 36	Cont. 37	Cont. 38
0	59	21	-2 (est.)	0	22	19	31
8	69	30	0	6	25	20	34
14	73	33	4	12	27	21	34
22	77	37	6	20	28	23	35
29	80	38	8	27	30	24	36
36	82	40	10	34	31	25	37
43	84	42	10	41	31	26	38
50	85	43	10	48	32	27	39
71	88	44	12	69	34	30	42
85	89	45	13	83	34	31	44
99	90	46	14	97	36	34	46
113	92	46	15	111	38	35	49
127	93	46	17	125	41	39	52
141	94	47	19	139	44	41	56
155	94	47	21	153	46	43	58
162	94	47	22	160	48	44	60
176	94	48	24	174	51	47	63
190	94	48	26	188	53	50	65
212	95	48	30	210	57	53	70
225	95	49	32	223	60	56	72

APPENDIX A-1 (CONT'D)

	Pressure in Container, psig				Pressure in Container, psig		
Time, days	Cont. 33	Cont. 34	Cont. 35	Time, days	Cont. 36	Cont. 37	Cont. 38
239	95	49	34	237	62	58	75
253	96	49	36	251	64	61	79
267	95	50	38	265	67	63	81
281	95	50	40	279	69	65	83
295	95	50	42	293	72	67	86
350	95	51	48	350	79	76	95
400	95	51	52	400	85	81	101
450	95	52	60	450	92	87	109
500	95	52	65	500	98	92	116
570	95	53	69	570	105	100	125
575[a]	(11)	(13)	(18)	575[a]	(0)	(21)	(17)
578	112	75	88	578	106	113	81
582	129	94	81	582	106	103	80
589	137	102	81	589	107	103	75
596	140	100	81	596	107	105	75
600	139	101	82	600	107	104	76
650	141	112	86	650	113	112	81
700	149	115	91	700	118	117	84
750	152	117	95	750	123	120	87
800	155	120	99	800	128	124	91
850	156	123	102	850	131	127	93
900	157	127	105	900	133	132	98
950	158	130	107	950	138	135	101
1000	159	133	109	1000	142	138	104
1050	161	135	113	1050	145	143	107
1100	163	138	115	1100	148	147	109
1128	164	140	117	1128	150	149	111

- Tests Completed -

[a] H_2S was added to all test containers except Container 36 at 575 days. Sufficient H_2S was added to each test container to result in an equilibrium pressure increase of ~1 atm. The number in parentheses on the 575-day line represents the approximate quasi-equilibrium pressure of H_2S added to each test container (in psi). Because of simultaneous reaction of H_2S with the specimens in the container and the dissolution of the H_2S in the brine over a finite period of time, the exact amount of H_2S added to each test container cannot be known with certainty. Container 38 was vented to 70 psig before the H_2S was added.

APPENDIX A-2: PRESSURE HISTORIES, TESTS OF LOW-CARBON STEEL IN BRINE A WITH H_2S (AND EVENTUAL CO_2) ADDITIONS, SEAL-WELDED CONTAINER TEST METHOD

APPENDIX A-2: PRESSURE HISTORIES, TESTS OF LOW-CARBON STEEL IN BRINE A WITH H_2S (AND EVENTUAL CO_2) ADDITIONS, SEAL-WELDED CONTAINER TEST METHOD

Summary of Initial Container Environments:
Containers with specimens immersed in Brine A - containers 40 and 41
Containers with specimens suspended over Brine A - containers 42 and 43
All containers initially charged with ~5 atm H_2S (equilibrated)
Test Temperature: 30±5°C

	Pressure in Container, psig			
Time, days	Cont. 40	Cont. 41	Cont. 42	Cont. 43
0	59	58	64	64
4	67	66	60	57
12	67	66	59	55
18	67	67	59	55
25	68	68	59	55
32	69	69	60	55
54	69	69	60	55
67	70	69	60	55
102	70	70	59	55
151	70	70	60	55
193	71	71	59	55
305	71	71	59	55
372	71	0[a]	59	0[a]
376	71	8	59	3
385	71	0[a]	59	0[a]
417	-[b]	5	-[b]	0
457	-	6	-	0
487	-	13[c]	-	7[c]
596	-	13	-	7
659	-	13	-	7
813	-	13	-	7
820	-	15	-	8
896	-	15	-	8
1015	-	15	-	8
1068	-	15	-	8

- Tests Completed-

[a] Containers vented preparatory to H_2S charging
[b] Test completed, containers opened for specimen retrieval and analysis
[c] CO_2 added to containers, to produce pressure shown

APPENDIX A-3: PRESSURE HISTORIES, TESTS OF LOW-CARBON STEEL IN MODIFIED ERDA-6 BRINE WITH N_2, SEAL-WELDED CONTAINER TEST METHOD

APPENDIX A-3: PRESSURE HISTORIES, TESTS OF LOW-CARBON STEEL IN MODIFIED ERDA-6 BRINE WITH N_2, SEAL-WELDED CONTAINER TEST METHOD

Summary of Test Parameters:
Specimens completely immersed in both tests (containers 44 and 45)
Brine Environment: modified ERDA-6 brine
Overpressure Gas: N_2 at 10 atm
Test Temperature: 30±5°C

	Pressure in Container, psig	
Time, days	Cont. 44	Cont. 45
0	131	129
7	135	134
14	136	135
28	136	135
49	138	136
70	140	139
98	145	142
119	148	145
140	152	148
168	157	152
196	160	156
224	164	159
252	168	161
280	171	165
302	173	167

- Tests Completed -

APPENDIX A-4: PRESSURE HISTORIES, TESTS OF Al-BASE MATERIALS (99.99% Al AND 6061 ALLOY) IMMERSED IN BRINE A AND IN VAPOR PHASE OF BRINE A, WITH N_2, CO_2, AND H_2S, SEAL-WELDED CONTAINER TEST METHOD

TABLE A-4-1

Pressure Histories, Al-Base Materials
Seal-Welded Container Tests
Brine A with N_2 Overpressure

Summary of Container Environments:
Container 1B: Immersed, 13-month exposure
Container 10B: Immersed, 24-month exposure
Container 4B: Immersed with steel specimens, 13-month exposure
Container 13B: Immersed with steel specimens, 24-month exposure
Container 7B: Vapor phase, 13-month exposure
Container 16B: Vapor phase, 24-month exposure
Test Temperature: 30±5°C

	Pressure in Container, psig					
Time, days	1B	10B	4B	13B	7B	16B
0	133	129	131	131	134	133
18	137	133	155	149	137	136
47	-	-	-	-	136	135
50	139	134	199	182	-	-
75	140	135	237v[a]	211	137	136
106	143	136	283v	247	137	136
156	146	139	365v	312v	137	136
205	148	140	447v	383	137	136
240	151	142	513v	433	137	136
289	153	144	598v	501v	137	136
354	156	146	702v	589v	137	136
410	160	148	791v	671v	137	136
	T[b]	-	T	-	T	-
462	-	150	-	747v	-	136
565	-	154	-	907v	-	136
656	-	160	-	1057v	-	137
705	-	163	-	1144v	-	137
739	-	-	-	-	-	137
754	-	166	-	1232	-	T
	-	T	-	T	-	-

[a] Gas was vented during time period, typically to a container pressure of ~130 psig. Frequency of venting depends on gas generation rate as well as maximum pressure rating of pressure gauge.
[b] Test terminated.

TABLE A-4-2

Pressure Histories, Al-Base Materials
Seal-Welded Container Tests
Brine A with CO_2 Overpressure

Summary of Container Environments:
Container 2B: Immersed, 13-month exposure
Container 11B: Immersed, 24-month exposure
Container 5B: Immersed with steel specimens, 13-month exposure
Container 14B: Immersed with steel specimens, 24-month exposure
Container 8B: Vapor phase, 13-month exposure
Container 17B: Vapor phase, 24-month exposure
Test Temperature: 30±5°C

	Pressure in Container, psig					
Time, days	2B	11B	5B	14B	8B	17B
0	131	128	130	133	131	132
18	138	139	197v[a]	234	128	130
47	-	146	-	378v	128	130
50	141	-	377v	-	-	-
75	144	153	461v	476v	128	130
106	150	-	553v	-	-	-
110	-	164	-	569v	129	131
156	160	-	699v	-	-	-
159	-	180	-	696v	128	131
205	169	-	832v	-	-	-
208	-	197	-	833v	129	131
254	186	-	972v	-	-	-
257	-	219	-	968v	129	131
354	234v	-	1208v	-	-	-
355	-	259	-	1189v	129	131
401	-	283	-	1279v	129	131
410	256v	-	1322v	-	T[b]	-
	T	-	T	-	-	-
467	-	341v	-	1421v	-	132
563	-	393	-	1587v	-	131

[a] Gas was vented during time period, typically to a container pressure of ~130 psig. Frequency of venting depends on gas generation rate as well as maximum pressure rating of pressure gauge.
[b] Test terminated.

TABLE A-4-2 (CONT'D)

Pressure in Container, psig

Time, days	2B	11B	5B	14B	8B	17B
661	-	450	-	1752v	-	132
710	-	487v	-	1834v	-	133
738	-	501	-	1878	-	-
	-	T	-	T	-	-
739		-	-	-	-	133
	-	-	-	-	-	T

TABLE A-4-3

Pressure Histories, Al-Base Materials
Seal-Welded Container Tests
Brine A with H_2S Overpressure

Summary of Container Environments:
Container 3B: Immersed, 13-month exposure
Container 12B: Immersed, 24-month exposure
Container 6B: Immersed with steel specimens, 13-month exposure
Container 15B: Immersed with steel specimens, 24-month exposure
Container 9B: Vapor phase, 13-month exposure
Container 18B: Vapor phase, 24-month exposure
Test Temperature: 30±5°C

	Pressure in Container, psig					
Time, days	3B	12B	6B	15B	9B	18B
0	52	54	53	56	63	63
14	74	86	122	81	56	56
28	87	103	152	101	57	56
56	109	126	196	131	57	55
75	138	153	261v[a]	165	57	55
154	173	188	348v	223	57	56
203	226v	225	420v	280	57	56
252	275v	265	501v	364v	57	57
301	307	329v	587v	428	57	57
351	348v	366	667v	518v	57	57
357	352	371	685v	527	57	57
	T[b]	-	T	-	T	
417	-	411	-	618v	-	57
510	-	488v	-	706v	-	56
608	-	545	-	968v	-	56
671	-	579	-	1061	-	56
	-	T	-	T	-	T

[a] Gas was vented during time period, typically to a container pressure of ~130 psig. Frequency of venting depends on gas generation rate as well as maximum pressure rating of pressure gauge
[b] Test terminated.

APPENDIX B-1: INDIVIDUAL SPECIMEN DATA, TESTS OF LOW-CARBON STEEL IN BRINE A WITH CONTROLLED CO_2 (AND EVENTUAL H_2S) ADDITIONS, SEAL-WELDED CONTAINER TEST METHOD

TABLE B-1-1
Specimen Data, Test No. 33

Test Type: Immersion
Test Environment: Simulated WIPP Brine A, initial charge 111 psia CO2 overpressure.
Addition of 1.2 atm of H2S was made after 19 months exposure.
Test Temperature: 30±5°C
Test Exposure: 38½ months

Specimen	Material Type	Length, mm	Width, mm	Thickness, mm	Top Hole ID, mm	Bottom Hole ID, mm	Area, dm2	Initial Wt., g
JW1	Low-C Steel, Lot J	190.33	85.74	0.720	8.15	8.17	3.286	88.1212
JW2	Low-C Steel, Lot J	190.59	85.42	0.697	8.15	8.32	3.277	86.3021
JW3	Low-C Steel, Lot J	190.75	85.40	0.696	8.19	8.41	3.278	85.8410
KW1	Low-C Steel, Lot K	189.91	84.93	0.868	7.97	8.01	3.258	107.2175
KW2	Low-C Steel, Lot K	189.97	85.28	0.854	7.98	8.00	3.271	104.9561
KW3	Low-C Steel, Lot K	189.86	84.90	0.828	7.96	7.99	3.253	103.4531
LW1	Low-C Steel, Lot L	190.40	85.09	1.516	7.93	7.94	3.312	190.3307
LW2	Low-C Steel, Lot L	190.30	84.99	1.538	7.95	7.94	3.307	190.9461
LW3	Low-C Steel, Lot L	189.99	85.04	1.507	7.93	7.94	3.302	186.9180
MW1	Low-C Steel, Lot M	190.54	84.81	1.602	7.96	7.95	3.308	197.7654
MW2	Low-C Steel, Lot M	190.34	85.01	1.590	7.94	7.97	3.312	198.1445
MW3	Low-C Steel, Lot M	190.24	85.06	1.590	7.97	7.94	3.312	194.4153
JN1	Low-C Steel, Lot J	190.62	50.57	0.693	7.96	7.92	1.945	51.0151
JN2	Low-C Steel, Lot J	190.57	50.47	0.700	8.14	8.12	1.940	50.6745
JN3	Low-C Steel, Lot J	190.47	50.52	0.687	7.98	8.12	1.941	49.8880
KN1	Low-C Steel, Lot K	190.24	50.08	0.857	7.97	7.97	1.931	62.7980
KN2	Low-C Steel, Lot K	190.02	50.07	0.863	7.98	7.98	1.929	62.8816
KN3	Low-C Steel, Lot K	189.94	50.11	0.870	7.99	8.00	1.930	63.9791
LN1	Low-C Steel, Lot L	190.30	50.19	1.551	7.93	7.93	1.973	111.6290
LN2	Low-C Steel, Lot L	190.18	50.31	1.522	7.92	7.92	1.975	111.1045
LN3	Low-C Steel, Lot L	190.12	51.03	1.519	7.95	7.91	2.001	112.8156
MN1	Low-C Steel, Lot M	190.64	50.15	1.573	7.88	7.92	1.976	116.3996
MN2	Low-C Steel, Lot M	190.72	50.10	1.594	7.92	7.92	1.976	116.7978
MN3	Low-C Steel, Lot M	190.52	50.26	1.587	7.93	7.91	1.980	116.2153

TABLE B-1-2

Specimen Data, Test No. 34

Test Type: Immersion

Test Environment: Simulated WIPP Brine A, initial charge 56 psia CO_2 overpressure.
Addition of 1.4 atm of H_2S was made after 19 months exposure.

Test Temperature: 30±5°C

Test Exposure: 38½ months

Specimen	Material Type	Length, mm	Width, mm	Thickness, mm	Top Hole ID, mm	Bottom Hole ID, mm	Area, dm2	Initial Wt., g
JW4	Low-C Steel, Lot J	190.49	85.36	0.703	8.18	8.14	3.274	84.9027
JW5	Low-C Steel, Lot J	190.88	85.35	0.720	8.23	8.20	3.281	87.3236
JW6	Low-C Steel, Lot J	190.24	85.97	0.703	8.37	8.28	3.292	88.0031
KW4	Low-C Steel, Lot K	189.91	85.08	0.848	7.99	8.00	3.262	106.7222
KW5	Low-C Steel, Lot K	189.87	84.92	0.837	7.98	7.99	3.255	103.9743
KW6	Low-C Steel, Lot K	190.04	84.81	0.833	7.97	8.02	3.253	103.7588
LW4	Low-C Steel, Lot L	190.09	85.23	1.524	7.95	7.94	3.312	191.1092
LW5	Low-C Steel, Lot L	190.22	85.03	1.541	7.95	7.93	3.308	190.7076
LW6	Low-C Steel, Lot L	190.38	85.34	1.528	7.95	7.95	3.321	190.4544
MW4	Low-C Steel, Lot M	190.38	84.96	1.581	7.92	7.94	3.310	196.3483
MW5	Low-C Steel, Lot M	190.52	84.89	1.577	7.96	7.96	3.310	194.7741
MW6	Low-C Steel, Lot M	190.52	85.00	1.586	7.96	7.94	3.314	194.8852
JN4	Low-C Steel, Lot J	190.60	50.56	0.677	8.06	8.02	1.943	49.7823
JN5	Low-C Steel, Lot J	191.20	50.37	0.659	8.02	8.02	1.941	49.0095
JN6	Low-C Steel, Lot J	190.60	50.46	0.678	8.05	8.09	1.939	49.8886
KN4	Low-C Steel, Lot K	189.92	49.99	0.871	7.93	7.97	1.925	63.5955
KN5	Low-C Steel, Lot K	189.95	50.28	0.862	8.00	7.98	1.936	63.1999
KN6	Low-C Steel, Lot K	190.09	50.01	0.859	7.99	8.00	1.927	62.3230
LN4	Low-C Steel, Lot L	189.96	49.95	1.515	7.93	7.93	1.958	110.0661
LN5	Low-C Steel, Lot L	190.26	50.26	1.526	7.93	7.94	1.974	111.6656
LN6	Low-C Steel, Lot L	189.55	50.07	1.536	7.94	7.93	1.960	110.9448
MN4	Low-C Steel, Lot M	190.59	50.07	1.588	7.91	7.87	1.973	115.8499
MN5	Low-C Steel, Lot M	190.70	50.19	1.592	7.92	7.91	1.979	116.2775
MN6	Low-C Steel, Lot M	190.68	50.12	1.568	7.92	7.90	1.975	114.8387

TABLE B-1-3
Specimen Data, Test No. 35

Test Type: Immersion
Test Environment: Simulated WIPP Brine A, initial charge 22 psia CO2 overpressure.
Addition of 1.2 atm of H2S was made after 19 months exposure.
Test Temperature: 30±5°C
Test Exposure: 38½ months

Specimen	Material Type	Length, mm	Width, mm	Thickness, mm	Top Hole ID, mm	Bottom Hole ID, mm	Area, dm2	Initial Wt., g
JW7	Low-C Steel, Lot J	190.25	85.34	0.715	8.27	8.26	3.269	87.0807
JW8	Low-C Steel, Lot J	190.00	85.17	0.695	8.08	8.16	3.258	85.3121
JW9	Low-C Steel, Lot J	190.37	85.07	0.704	8.10	8.43	3.260	85.3889
KW7	Low-C Steel, Lot K	189.90	84.87	0.836	7.97	7.98	3.254	104.0760
KW8	Low-C Steel, Lot K	189.56	84.59	0.821	7.96	8.05	3.236	103.6197
KW9	Low-C Steel, Lot K	189.92	84.92	0.835	8.05	7.99	3.256	103.5790
LW7	Low-C Steel, Lot L	190.33	85.11	1.511	7.95	7.94	3.311	187.1416
LW8	Low-C Steel, Lot L	190.35	85.18	1.521	7.95	7.95	3.314	188.6702
LW9	Low-C Steel, Lot L	190.34	85.16	1.502	7.95	7.94	3.312	186.2714
MW7	Low-C Steel, Lot M	190.97	85.09	1.607	7.97	7.96	3.327	196.8036
MW8	Low-C Steel, Lot M	190.40	85.05	1.599	7.96	7.98	3.315	199.0834
MW9	Low-C Steel, Lot M	190.29	85.24	1.585	7.96	7.95	3.319	199.1392
JN7	Low-C Steel, Lot J	190.51	50.21	0.699	8.11	8.06	1.930	49.6171
JN8	Low-C Steel, Lot J	190.52	50.51	0.684	8.05	8.13	1.941	49.9949
JN9	Low-C Steel, Lot J	191.36	50.42	0.653	8.25	8.07	1.944	48.4476
KN7	Low-C Steel, Lot K	190.10	50.00	0.862	7.94	7.94	1.927	62.7686
KN8	Low-C Steel, Lot K	190.17	50.10	0.862	7.92	8.00	1.931	62.5218
KN9	Low-C Steel, Lot K	190.18	50.15	0.872	7.97	7.95	1.934	63.2507
LN7	Low-C Steel, Lot L	190.19	50.27	1.551	7.94	7.95	1.975	112.5286
LN8	Low-C Steel, Lot L	190.01	50.30	1.541	7.93	7.95	1.973	112.0774
LN9	Low-C Steel, Lot L	190.08	50.26	1.548	7.95	7.93	1.973	111.9558
MN7	Low-C Steel, Lot M	190.86	50.13	1.570	7.92	7.93	1.977	114.8986
MN8	Low-C Steel, Lot M	190.57	50.42	1.563	7.94	7.92	1.985	115.0848
MN9	Low-C Steel, Lot M	190.48	50.66	1.524	7.92	7.91	1.991	113.7382

TABLE B-1-4

Specimen Data, Test No. 36

Test Type: Immersion

Test Environment: Simulated WIPP Brine A, initial charge 11psia of CO2 + 30 psia of N2. No H_2S addition made.

Test Temperature: 30±5°C

Test Exposure: 38½ months

Specimen	Material Type	Length, mm	Width, mm	Thickness, mm	Top Hole ID, mm	Bottom Hole ID, mm	Area, dm2	Initial Wt., g
JW10	Low-C Steel, Lot J	190.01	85.22	0.718	8.26	8.15	3.261	86.2623
JW11	Low-C Steel, Lot J	190.80	86.10	0.692	8.09	8.39	3.306	86.4216
JW12	Low-C Steel, Lot J	190.51	85.49	0.701	8.11	8.18	3.279	85.2159
KW10	Low-C Steel, Lot K	189.73	84.95	0.827	7.96	7.99	3.253	104.9050
KW11	Low-C Steel, Lot K	189.71	84.77	0.862	7.99	7.98	3.248	107.4346
KW12	Low-C Steel, Lot K	189.72	84.78	0.845	7.99	7.98	3.247	105.3387
LW10	Low-C Steel, Lot L	190.33	84.95	1.512	7.95	7.95	3.305	187.2511
LW11	Low-C Steel, Lot L	190.25	84.99	1.494	7.95	7.94	3.304	187.0021
LW12	Low-C Steel, Lot L	190.64	85.56	1.465	7.95	7.94	3.331	183.3987
MW10	Low-C Steel, Lot M	190.30	84.69	1.580	7.96	7.95	3.298	196.2899
MW11	Low-C Steel, Lot M	190.38	85.08	1.576	7.96	7.95	3.314	196.7680
MW12	Low-C Steel, Lot M	190.74	84.94	1.584	7.95	7.95	3.316	196.9510
JN10	Low-C Steel, Lot J	191.16	50.42	0.654	8.08	8.05	1.942	48.0890
JN11	Low-C Steel, Lot J	191.13	50.48	0.652	8.18	8.14	1.944	48.8352
JN12	Low-C Steel, Lot J	190.57	49.35	0.666	8.11	8.15	1.896	47.9686
KN10	Low-C Steel, Lot K	189.98	50.00	0.866	7.94	7.98	1.926	63.0152
KN11	Low-C Steel, Lot K	190.18	50.12	0.866	7.96	7.99	1.932	63.7764
KN12	Low-C Steel, Lot K	189.93	50.04	0.858	8.00	7.96	1.926	63.0786
LN10	Low-C Steel, Lot L	190.16	50.24	1.541	7.92	7.91	1.973	111.4649
LN11	Low-C Steel, Lot L	190.44	50.24	1.537	7.94	7.94	1.975	111.7071
LN12	Low-C Steel, Lot L	189.89	50.16	1.538	7.88	7.89	1.967	111.4004
MN10	Low-C Steel, Lot M	190.47	50.26	1.533	7.93	7.94	1.976	113.4046
MN11	Low-C Steel, Lot M	190.46	50.17	1.549	7.92	7.94	1.974	112.1868
MN12	Low-C Steel, Lot M	190.35	50.14	1.576	7.90	7.94	1.973	113.9416

TABLE B-1-5

Specimen Data, Test No. 37

Test Type: Immersion

Test Environment: Simulated WIPP Brine A, initial charge 5.7 psia of CO_2 + 30 psia of N_2 overpressure. Addition of 0.9 atm of H_2S was made after 19 months exposure.

Test Temperature: 30±5°C

Test Exposure: 38½ months

Specimen	Material Type	Length, mm	Width, mm	Thickness, mm	Top Hole ID, mm	Bottom Hole ID, mm	Area, dm2	Initial Wt., g
JW13	Low-C Steel, Lot J	190.30	85.24	0.701	8.37	8.26	3.265	84.9404
JW14	Low-C Steel, Lot J	190.08	85.41	0.695	8.16	8.14	3.268	84.4024
JW15	Low-C Steel, Lot J	190.53	85.31	0.697	8.20	8.20	3.272	85.8943
KW13	Low-C Steel, Lot K	189.64	84.81	0.841	7.97	8.03	3.247	106.3402
KW14	Low-C Steel, Lot K	189.64	84.68	0.866	8.05	7.98	3.243	106.3181
KW15	Low-C Steel, Lot K	189.84	84.82	0.832	8.00	8.06	3.250	104.6479
LW13	Low-C Steel, Lot L	190.72	85.71	1.493	7.94	7.95	3.339	185.2357
LW14	Low-C Steel, Lot L	190.66	85.73	1.465	7.96	7.96	3.337	184.9999
LW15	Low-C Steel, Lot L	190.77	85.63	1.500	7.96	7.94	3.338	186.7577
MW13	Low-C Steel, Lot M	190.48	84.93	1.554	7.92	7.96	3.309	194.2971
MW14	Low-C Steel, Lot M	190.85	84.90	1.590	7.94	7.95	3.316	196.8647
MW15	Low-C Steel, Lot M	190.81	84.95	1.590	7.95	7.94	3.318	197.5009
JN13	Low-C Steel, Lot J	190.91	50.67	0.663	7.96	7.89	1.950	48.1501
JN14	Low-C Steel, Lot J	191.09	50.69	0.641	8.12	8.06	1.951	48.8142
JN15	Low-C Steel, Lot J	191.23	50.78	0.658	8.04	8.17	1.957	48.4822
KN13	Low-C Steel, Lot K	190.00	50.00	0.876	7.96	7.97	1.927	63.5386
KN14	Low-C Steel, Lot K	189.98	50.17	0.868	7.99	7.97	1.932	63.5974
KN15	Low-C Steel, Lot K	190.02	50.11	0.867	7.94	8.00	1.930	63.6225
LN13	Low-C Steel, Lot L	190.37	50.11	1.531	7.95	7.93	1.969	110.6430
LN14	Low-C Steel, Lot L	190.44	50.05	1.517	7.93	7.93	1.967	110.6268
LN15	Low-C Steel, Lot L	190.62	50.09	1.542	7.93	7.92	1.972	110.7552
MN13	Low-C Steel, Lot M	190.43	49.95	1.553	7.94	7.92	1.965	111.5338
MN14	Low-C Steel, Lot M	190.52	50.35	1.548	7.95	7.95	1.981	112.6598
MN15	Low-C Steel, Lot M	189.81	50.07	1.523	7.94	7.90	1.962	110.7545

TABLE B-1-6

Specimen Data, Test No. 38

Test Type: Immersion

Test Environment: Simulated WIPP Brine A, initial charge 45 psia N_2 overpressure.
Addition of 0.8 atm of H2S was made after 19 months exposure.

Test Temperature: 30±5°C

Test Exposure: 38½ months

Specimen	Material Type	Length, mm	Width, mm	Thickness, mm	Top Hole ID, mm	Bottom Hole ID, mm	Area, dm2	Initial Wt., g
JW16	Low-C Steel, Lot J	190.27	85.96	0.668	8.08	8.10	3.291	84.2522
JW17	Low-C Steel, Lot J	190.22	85.14	0.684	8.22	8.33	3.259	82.7062
JW18	Low-C Steel, Lot J	190.42	85.39	0.690	8.16	8.28	3.272	83.8789
KW16	Low-C Steel, Lot K	189.60	85.07	0.838	7.96	7.98	3.256	104.7348
KW17	Low-C Steel, Lot K	189.44	84.81	0.842	7.99	7.99	3.244	104.5493
KW18	Low-C Steel, Lot K	189.60	84.83	0.839	7.99	8.01	3.247	103.9338
LW16	Low-C Steel, Lot L	190.74	85.00	1.476	7.96	7.94	3.312	183.8760
LW17	Low-C Steel, Lot L	190.34	84.52	1.533	7.94	7.94	3.290	189.6979
LW18	Low-C Steel, Lot L	190.27	84.36	1.547	7.95	7.94	3.283	190.9421
MW16	Low-C Steel, Lot M	191.08	85.00	1.573	7.93	7.95	3.323	196.5668
MW17	Low-C Steel, Lot M	190.86	85.06	1.569	7.98	7.94	3.321	196.3437
MW18	Low-C Steel, Lot M	190.78	85.01	1.608	7.93	7.98	3.320	199.7132
JN16	Low-C Steel, Lot J	190.34	50.65	0.680	8.05	8.03	1.944	49.9990
JN17	Low-C Steel, Lot J	190.75	50.63	0.665	8.15	8.08	1.946	50.3541
JN18	Low-C Steel, Lot J	190.58	50.61	0.676	8.18	8.12	1.944	50.9490
KN16	Low-C Steel, Lot K	190.00	50.10	0.865	8.00	7.94	1.930	63.2493
KN17	Low-C Steel, Lot K	190.01	50.09	0.858	8.01	8.00	1.929	62.6792
KN18	Low-C Steel, Lot K	189.70	49.98	0.864	7.98	7.95	1.922	62.6678
LN16	Low-C Steel, Lot L	190.10	50.98	1.541	7.90	7.94	2.001	113.7395
LN17	Low-C Steel, Lot L	190.21	49.14	1.538	7.95	7.92	1.931	110.5290
LN18	Low-C Steel, Lot L	190.33	50.75	1.538	7.97	8.49	1.993	113.7133
MN16	Low-C Steel, Lot M	190.63	50.08	1.561	7.95	7.88	1.973	113.9053
MN17	Low-C Steel, Lot M	189.90	50.14	1.538	7.94	7.94	1.966	111.2087
MN18	Low-C Steel, Lot M	190.62	50.11	1.564	7.94	7.94	1.974	113.6006

APPENDIX B-2: INDIVIDUAL SPECIMEN CORROSION-RATE DATA, TESTS OF LOW-CARBON STEEL IN BRINE A WITH H_2S (AND EVENTUAL CO_2) ADDITIONS, SEAL-WELDED CONTAINER TEST METHOD

TABLE B-2-1
Specimen Data, Test No. 40

Test Type: Immersion
Test Environment: Simulated WIPP Brine A, H2S overpressure (5 atm)
Test Temperature: 30±5°C
Test Exposure: 14 months

Specimen	Material Type	Length, mm	Width, mm	Thickness, mm	Top Hole ID, mm	Bottom Hole ID, mm	Area, dm2	Initial Wt., g	Final Wt., g	Corrosion Rate, mpy	Corrosion Rate, µm/yr
JW19	Low-C Steel, Lot J	190.52	85.03	0.689	8.23	8.12	3.261	84.5695	84.4762	0.012	0.32
JW20	Low-C Steel, Lot J	190.65	85.37	0.677	8.26	8.19	3.275	84.3452	84.2352	0.015	0.37
JN19	Low-C Steel, Lot J	190.42	50.10	0.684	8.15	8.14	1.924	50.3294	SA*	SA	SA
JN20	Low-C Steel, Lot J	190.59	50.59	0.684	8.00	7.92	1.945	51.0877	51.0271	0.014	0.34
JN21	Low-C Steel, Lot J	190.51	50.50	0.683	8.12	8.07	1.940	50.4830	50.4209	0.014	0.35
KW19	Low-C Steel, Lot K	189.75	84.89	0.839	8.00	8.03	3.252	104.5542	104.4649	0.012	0.30
KW20	Low-C Steel, Lot K	189.63	85.07	0.833	7.99	8.02	3.256	104.4951	104.3828	0.015	0.38
KN19	Low-C Steel, Lot K	189.68	50.05	0.845	8.00	7.96	1.923	62.1595	62.1061	0.012	0.31
KN20	Low-C Steel, Lot K	189.78	50.12	0.850	7.98	8.00	1.927	62.2217	62.1594	0.014	0.36
KN21	Low-C Steel, Lot K	189.82	50.11	0.853	7.96	7.98	1.928	62.5327	62.4725	0.014	0.34
LW19	Low-C Steel, Lot L	190.26	84.89	1.535	7.94	7.94	3.303	191.5376	191.4350	0.013	0.34
LW20	Low-C Steel, Lot L	190.30	85.20	1.509	7.94	7.94	3.314	189.5056	189.3899	0.015	0.38
LN19	Low-C Steel, Lot L	190.58	50.15	1.530	7.91	7.94	1.973	111.3457	111.2829	0.014	0.35
LN20	Low-C Steel, Lot L	190.55	50.13	1.534	7.95	7.92	1.972	112.0986	112.0375	0.013	0.34
LN21	Low-C Steel, Lot L	190.36	50.14	1.529	7.95	7.92	1.970	111.8573	111.7876	0.015	0.39
MW19	Low-C Steel, Lot M	190.94	84.92	1.589	7.97	7.94	3.319	198.7928	198.6814	0.015	0.37
MW20	Low-C Steel, Lot M	190.41	84.97	1.561	7.97	7.95	3.310	196.7772	196.6699	0.014	0.36
MN19	Low-C Steel, Lot M	189.84	49.94	1.511	7.92	7.95	1.956	109.4529	109.3910	0.014	0.35
MN20	Low-C Steel, Lot M	190.46	50.08	1.567	7.92	7.94	1.971	114.2826	114.2146	0.015	0.38
MN21	Low-C Steel, Lot M	190.65	50.22	1.557	7.95	7.92	1.978	114.6117	114.5427	0.015	0.38

*SA = Specimen was retained for surface analysis.

TABLE B-2-2
Specimen Data, Test No. 41

Test Type: Immersion
Test Environment: Simulated WIPP Brine A, H2S Overpressure (5 atm); 7 psi CO2 was added after 16 months exposure
Test Temperature: 30±5°C
Test Exposure: 35 months

Specimen	Material Type	Length, mm	Width, mm	Thickness, mm	Top Hole ID, mm	Bottom Hole ID, mm	Area, dm2	Initial Wt., g
JW21	Low-C Steel, Lot J	190.58	85.33	0.664	8.06	8.35	3.271	83.4695
JW22	Low-C Steel, Lot J	189.94	85.70	0.685	8.10	8.02	3.276	85.1118
JN22	Low-C Steel, Lot J	190.61	50.47	0.676	8.04	8.10	1.940	50.0161
JN23	Low-C Steel, Lot J	190.64	50.52	0.675	8.09	8.11	1.942	49.9827
JN24	Low-C Steel, Lot J	190.66	50.48	0.676	8.07	8.13	1.940	50.4879
KW21	Low-C Steel, Lot K	189.68	85.00	0.845	8.00	7.99	3.255	104.8541
KW22	Low-C Steel, Lot K	189.63	85.04	0.848	7.98	8.02	3.256	104.4074
KN22	Low-C Steel, Lot K	189.83	49.99	0.848	8.00	7.97	1.923	62.2011
KN23	Low-C Steel, Lot K	189.97	50.18	0.850	7.98	7.96	1.932	62.2877
KN24	Low-C Steel, Lot K	189.60	50.16	0.848	7.99	8.01	1.927	61.8963
LW21	Low-C Steel, Lot L	190.15	84.92	1.506	7.96	7.94	3.300	189.4176
LW22	Low-C Steel, Lot L	190.15	84.97	1.492	7.94	7.94	3.301	186.6393
LN22	Low-C Steel, Lot L	190.06	50.24	1.536	7.93	7.92	1.971	112.5519
LN23	Low-C Steel, Lot L	190.56	50.11	1.530	7.95	7.92	1.971	111.7724
LN24	Low-C Steel, Lot L	190.72	50.91	1.545	7.94	7.91	2.005	114.2352
MW21	Low-C Steel, Lot M	190.88	84.85	1.584	7.96	7.96	3.315	198.2044
MW22	Low-C Steel, Lot M	190.66	84.87	1.593	7.97	7.95	3.312	198.2775
MN22	Low-C Steel, Lot M	189.90	50.32	1.527	7.96	7.93	1.972	111.0662
MN23	Low-C Steel, Lot M	190.79	50.08	1.583	7.90	7.91	1.975	114.1351
MN24	Low-C Steel, Lot M	190.48	50.11	1.589	7.96	7.95	1.974	113.8557

TABLE B-2-3
Specimen Data, Test No. 42

Test Type: Vapor Phase Exposure
Test Environment: Simulated WIPP Brine A vapor + H2S (5 atm)
Test Temperature: 30±5°C
Test Exposure: 14 months

Specimen	Material Type	Length, mm	Width, mm	Thickness, mm	Top Hole ID, mm	Bottom Hole ID, mm	Area, dm2	Initial Wt., g	Final Wt., g	Corrosion Rate, mpy	Corrosion Rate, µm/yr
JW23	Low-C Steel, Lot J	189.94	85.10	0.670	8.17	8.23	3.252	81.9993	81.9615	0.0050	0.128
JW24	Low-C Steel, Lot J	190.09	85.27	0.672	8.00	8.01	3.262	83.5107	83.4660	0.0059	0.151
JN25	Low-C Steel, Lot J	190.61	50.59	0.665	8.04	8.15	1.943	49.5121	SA*	SA	SA
JN26	Low-C Steel, Lot J	190.45	50.47	0.668	8.02	8.01	1.938	49.7380	49.7139	0.0054	0.137
JN27	Low-C Steel, Lot J	190.40	50.52	0.670	8.03	8.07	1.939	49.8737	49.8498	0.0053	0.136
KW23	Low-C Steel, Lot K	189.79	84.93	0.845	7.96	7.98	3.254	105.3014	105.2678	0.0045	0.114
KW24	Low-C Steel, Lot K	189.78	85.04	0.848	7.95	8.00	3.259	105.1483	105.1173	0.0041	0.105
KN25	Low-C Steel, Lot K	189.61	49.88	0.867	7.98	8.00	1.917	62.6298	62.6076	0.0050	0.128
KN26	Low-C Steel, Lot K	189.69	50.19	0.862	8.00	7.98	1.930	62.8897	62.8676	0.0050	0.126
KN27	Low-C Steel, Lot K	189.95	50.06	0.860	7.99	7.97	1.927	61.9578	61.9365	0.0048	0.122
LW23	Low-C Steel, Lot L	189.44	84.86	1.475	7.96	7.94	3.284	183.9554	183.9181	0.0049	0.125
LW24	Low-C Steel, Lot L	190.35	84.80	1.491	7.91	7.94	3.298	186.2220	186.1859	0.0047	0.121
LN25	Low-C Steel, Lot L	190.57	50.02	1.523	7.95	7.93	1.968	111.3891	111.3667	0.0049	0.125
LN26	Low-C Steel, Lot L	190.71	50.22	1.531	7.94	7.94	1.977	111.0253	111.0006	0.0054	0.138
LN27	Low-C Steel, Lot L	190.65	50.12	1.518	7.93	7.92	1.972	111.1057	111.0857	0.0044	0.112
MW23	Low-C Steel, Lot M	190.93	85.11	1.591	7.98	7.94	3.326	199.9350	199.8933	0.0054	0.138
MW24	Low-C Steel, Lot M	191.07	84.86	1.605	7.95	7.94	3.320	198.9818	198.9471	0.0045	0.115
MN25	Low-C Steel, Lot M	190.56	50.19	1.586	7.93	7.94	1.977	114.7991	114.7800	0.0042	0.106
MN26	Low-C Steel, Lot M	190.38	50.25	1.590	7.92	7.92	1.978	115.5028	115.4814	0.0047	0.119
MN27	Low-C Steel, Lot M	189.84	50.12	1.524	7.96	7.92	1.964	110.8930	110.8742	0.0042	0.105

*SA = Specimen was retained for surface analysis.

TABLE B-2-4
Specimen Data, Test No. 43

Test Type: Vapor Phase Exposure
Test Environment: Simulated WIPP Brine A vapor + H2S (5 atm);
7 psi CO2 was added after 16 months exposure
Test Temperature: 30±5°C
Test Exposure: 35 months

Specimen	Material Type	Length, mm	Width, mm	Thickness, mm	Top Hole ID, mm	Bottom Hole ID, mm	Area, dm2	Initial Wt., g
JW25	Low-C Steel, Lot J	190.89	86.10	0.691	7.95	7.94	3.309	87.7441
JW26	Low-C Steel, Lot J	190.78	86.13	0.687	7.96	7.94	3.308	87.2817
JN28	Low-C Steel, Lot J	190.39	50.55	0.666	8.04	8.05	1.940	49.9632
JN29	Low-C Steel, Lot J	190.44	50.50	0.668	8.00	7.96	1.939	49.9180
JN30	Low-C Steel, Lot J	191.18	51.84	0.682	7.94	7.93	1.999	52.6037
KW25	Low-C Steel, Lot K	189.73	84.96	0.837	7.98	7.94	3.254	104.2601
KW26	Low-C Steel, Lot K	189.65	84.93	0.840	7.99	7.96	3.252	104.4880
KN28	Low-C Steel, Lot K	190.00	50.02	0.862	7.95	7.99	1.927	62.9746
KN29	Low-C Steel, Lot K	190.13	50.17	0.869	7.94	7.98	1.934	63.9695
KN30	Low-C Steel, Lot K	189.82	49.88	0.867	7.93	7.98	1.920	62.5357
LW25	Low-C Steel, Lot L	190.39	85.05	1.480	7.95	7.95	3.308	183.6378
LW26	Low-C Steel, Lot L	190.48	85.38	1.475	7.94	7.95	3.322	184.6739
LN28	Low-C Steel, Lot L	190.31	50.24	1.524	7.94	7.94	1.973	112.1188
LN29	Low-C Steel, Lot L	190.18	49.35	1.529	7.93	7.95	1.938	111.0874
LN30	Low-C Steel, Lot L	189.94	49.92	1.518	7.95	7.96	1.957	111.6168
MW25	Low-C Steel, Lot M	191.26	85.22	1.578	7.95	7.98	3.335	198.2962
MW26	Low-C Steel, Lot M	190.35	85.18	1.589	7.94	7.98	3.318	197.3339
MN28	Low-C Steel, Lot M	189.77	50.11	1.533	7.95	7.93	1.963	110.9017
MN29	Low-C Steel, Lot M	190.52	50.02	1.530	7.93	7.92	1.967	111.9782
MN30	Low-C Steel, Lot M	190.48	50.17	1.553	7.94	7.93	1.974	112.4285

APPENDIX B-3: INDIVIDUAL SPECIMEN CORROSION-RATE DATA, TESTS OF LOW-CARBON STEEL IN MODIFIED ERDA-6 BRINE WITH N_2, SEAL-WELDED CONTAINER TEST METHOD

TABLE B-3-1
Specimen Data, Test No. 44

Test Type: Immersion
Test Environment: Simulated ERDA 6 Brine, N2 overpressure (10 atm)
Test Temperature: 30±5°C
Test Exposure: 10 months

Specimen	Material Type	Length, mm	Width, mm	Thickness, mm	Top Hole ID, mm	Bottom Hole ID, mm	Area, dm2	Initial Wt., g	Final Wt., g	Corrosion Rate, mpy	Corrosion Rate, µm/yr
JE1	Low-C Steel, Lot J	190.52	86.32	0.684	8.01	7.99	3.310	86.8435	86.3777	0.084	2.14
JE2	Low-C Steel, Lot J	190.62	85.97	0.691	8.00	8.01	3.299	87.7161	87.3552	0.066	1.67
JE3	Low-C Steel, Lot J	190.38	85.52	0.671	7.99	8.00	3.277	83.8027	83.1783	0.114	2.90
JE7	Low-C Steel, Lot J	190.17	50.56	0.677	7.97	7.96	1.939	49.6954	49.5178	0.055	1.39
JE8	Low-C Steel, Lot J	190.21	50.93	0.686	7.97	7.98	1.954	50.8109	50.6256	0.057	1.44
JE9	Low-C Steel, Lot J	190.54	50.95	0.692	7.99	7.99	1.958	51.4767	51.3124	0.050	1.28
KE1	Low-C Steel, Lot K	190.51	85.91	0.841	7.95	7.96	3.304	105.5749	105.2366	0.061	1.56
KE2	Low-C Steel, Lot K	190.48	85.68	0.837	7.92	7.80	3.295	105.9284	105.5609	0.067	1.70
KE3	Low-C Steel, Lot K	190.53	85.78	0.844	7.93	7.98	3.300	106.5590	106.2406	0.058	1.47
KE7	Low-C Steel, Lot K	190.41	50.94	0.861	8.01	7.96	1.966	63.6745	63.2625	0.126	3.19
KE8	Low-C Steel, Lot K	190.47	50.77	0.849	8.00	7.96	1.959	63.2525	63.0406	0.065	1.65
KE9	Low-C Steel, Lot K	190.64	50.91	0.846	7.95	7.98	1.966	63.4930	63.2601	0.071	1.80
LE1	Low-C Steel, Lot L	190.55	86.03	1.488	7.99	7.98	3.348	191.1520	190.8120	0.061	1.55
LE2	Low-C Steel, Lot L	190.62	85.95	1.521	7.99	8.00	3,348	194.6676	194.3416	0.058	1.48
LE3	Low-C Steel, Lot L	190.56	85.82	1.539	8.01	8.00	3.343	194.6512	194.3730	0.050	1.27
LE7	Low-C Steel, Lot L	190.51	51.08	1.543	7.97	7.99	2.009	115.4239	115.2229	0.060	1.52
LE8	Low-C Steel, Lot L	190.51	51.05	1.531	7.95	7.98	2.007	114.6376	114.4426	0.058	1.48
LE9	Low-C Steel, Lot L	190.51	51.08	1.517	7.98	7.99	2.007	113.1265	112.9628	0.049	1.24
ME1	Low-C Steel, Lot M	190.55	85.94	1.605	7.94	7.96	3.352	200.9110	200.5917	0.057	1.45
ME2	Low-C Steel, Lot M	190.49	85.95	1.586	7.95	7.96	3.350	199.1208	198.8266	0.053	1.34
ME3	Low-C Steel, Lot M	190.39	85.92	1.515	7.97	8.00	3.343	191.2219	190.8956	0.059	1.49
ME7	Low-C Steel, Lot M	190.68	50.85	1.626	7.93	7.97	2.006	119.3610	119.1557	0.061	1.56
ME8	Low-C Steel, Lot M	190.64	50.97	1.619	7.90	7.96	2.010	119.5325	119.1877	0.103	2.61
ME9	Low-C Steel, Lot M	190.59	50.96	1.614	7.90	7.93	2.009	119.3898	119.1508	0.071	1.81

TABLE B-3-2
Specimen Data, Test No. 45

Test Type: Immersion
Test Environment: Simulated ERDA 6 Brine, N2 overpressure (10 atm)
Test Temperature: 30±5°C
Test Exposure: 10 months

Specimen	Material Type	Length, mm	Width, mm	Thickness, mm	Top Hole ID, mm	Bottom Hole ID, mm	Area, dm2	Initial Wt., g	Final Wt., g	Corrosion Rate, mpy	Corrosion Rate, µm/yr
JE4	Low-C Steel, Lot J	190.65	85.82	0.693	8.00	7.97	3.294	86.6943	86.4600	0.043	1.08
JE5	Low-C Steel, Lot J	190.68	85.64	0.688	7.97	7.98	3.287	87.0600	86.7956	0.048	1.22
JE6	Low-C Steel, Lot J	190.93	85.94	0.689	7.99	7.95	3.303	87.2583	87.0382	0.040	1.01
JE10	Low-C Steel, Lot J	190.77	50.95	0.692	7.98	7.98	1.961	51.3587	51.2098	0.046	1.16
JE11	Low-C Steel, Lot J	190.76	50.93	0.692	7.99	7.99	1.960	51.3874	51.2764	0.034	0.86
JE12	Low-C Steel, Lot J	190.58	50.98	0.694	7.99	7.99	1.960	51.6283	51.5134	0.035	0.89
KE4	Low-C Steel, Lot K	190.75	85.97	0.869	7.91	7.96	3.312	107.2228	107.0175	0.037	0.94
KE5	Low-C Steel, Lot K	190.67	86.03	0.848	8.00	7.98	3.312	107.0463	106.8404	0.037	0.95
KE6	Low-C Steel, Lot K	190.58	86.00	0.848	7.97	7.98	3.309	106.8764	106.6686	0.038	0.96
KE10	Low-C Steel, Lot K	190.60	50.96	0.814	7.92	7.96	1.966	62.3019	62.1757	0.038	0.98
KE11	Low-C Steel, Lot K	190.59	50.93	0.812	7.97	7.98	1.965	61.5576	61.4421	0.035	0.90
KE12	Low-C Steel, Lot K	190.68	50.96	0.832	7.96	7.96	1.968	62.6512	62.5290	0.037	0.95
LE4	Low-C Steel, Lot L	190.75	86.02	1.553	7.94	7.95	3.356	194.8938	194.6510	0.043	1.10
LE5	Low-C Steel, Lot L	190.71	86.03	1.559	7.98	7.96	3.356	194.3756	194.1000	0.049	1.25
LE6	Low-C Steel, Lot L	190.82	86.09	1.556	7.97	7.99	3.360	193.3775	193.1689	0.037	0.95
LE10	Low-C Steel, Lot L	190.60	50.47	1.511	7.97	7.95	1.984	110.9276	110.8114	0.035	0.89
LE11	Low-C Steel, Lot L	190.61	51.16	1.551	7.98	7.99	2.013	115.4949	115.3593	0.040	1.03
LE12	Low-C Steel, Lot L	190.65	51.12	1.535	7.97	7.93	2.011	113.0493	112.9121	0.041	1.04
ME4	Low-C Steel, Lot M	190.69	85.57	1.603	7.95	7.97	3.340	200.8528	200.5791	0.049	1.25
ME5	Low-C Steel, Lot M	190.67	86.13	1.619	7.93	7.97	3.362	203.9628	203.7223	0.043	1.09
ME6	Low-C Steel, Lot M	190.72	86.00	1.610	7.94	7.95	3.358	201.4978	201.2192	0.050	1.26
ME10	Low-C Steel, Lot M	190.72	51.13	1.598	7.91	7.97	2.016	118.4738	118.3449	0.038	0.97
ME11	Low-C Steel, Lot M	190.76	51.18	1.591	7.95	7.98	2.018	118.6007	118.4396	0.048	1.22
ME12	Low-C Steel, Lot M	190.71	51.10	1.598	7.93	7.97	2.014	118.0882	117.9512	0.041	1.04

APPENDIX B-4: INDIVIDUAL SPECIMEN CORROSION-RATE DATA, TESTS OF LOW-CARBON STEEL IN MODIFIED ERDA-6 BRINE UNDER CONSTANT-pH CONDITIONS

APPENDIX B-4: INDIVIDUAL SPECIMEN CORROSION-RATE DATA, TESTS OF LOW-CARBON STEEL IN MODIFIED ERDA-6 BRINE UNDER CONSTANT-pH CONDITIONS

TABLE B-4-1: pH 3 TEST

Specimen	Initial Wt., g	Final Wt., g	Weight Change, g	Area, cm^2	Time, mo	Corrosion Rate, µm/yr	(mpy)[a]
3J1	6.9061	4.5478	2.3582	25.2	0.19	7800	(308)
3J2	6.8650	4.4430	2.4219	25.3	0.19	8000	(316)
3K1	8.5489	6.3004	2.2482	25.2	0.19	7400	(291)
3K2	8.5845	6.4496	2.1346	25.1	0.19	7000	(277)
3L1	14.5541	11.7820	2.7721	25.2	0.19	8800	(345)
3L2	14.6813	11.8413	2.8399	25.2	0.19	9000	(354)
3M1	15.9061	13.6239	2.2821	25.2	0.19	7200	(283)
3M2	15.9284	13.1112	2.8171	25.0	0.19	8800	(348)

TABLE B-4-2: pH 5 TEST

Specimen	Initial Wt., g	Final Wt., g	Weight Change, g	Area, cm^2	Time, mo	Corrosion Rate, µm/yr	(mpy)[a]
3J9	6.7458	5.9463	0.7995	25.2	6	82	(3.22)
3J10	6.7979	5.8672	0.9307	25.2	6	95	(3.76)
3K9	8.5741	7.3324	1.2417	25.2	6	130	(5.01)
3K10	8.5864	7.6724	0.9140	25.2	6	94	(3.69)
3L9	14.8138	14.1490	0.6648	25.2	6	68	(2.68)
3L10	14.6059	13.7074	0.8985	25.2	6	92	(3.62)
3M9	15.9673	15.1659	0.8014	25.2	6	82	(3.23)
3M10	15.8972	15.3407	0.5925	25.2	6	61	(2.39)

[a] Primary calculation, carried out to three significant figures. Only two significant figures are justifiable.

TABLE B-4-3: pH 7 TEST

Specimen	Initial Wt., g	Final Wt., g	Weight Change, g.	Area, cm^2	Time, mo	Corrosion Rate, µm/yr	(mpy)[a]
3J11	6.8999	6.5770	0.3429	25.3	6	35	(1.38)
3J12	6.8440	6.4995	0.3445	25.2	6	35	(1.39)
3K11	8.5722	8.2201	0.3521	25.1	6	36	(1.42)
3K12	8.5593	8.2024	0.3569	25.1	6	37	(1.45)
3L11	14.7188	14.0915	0.6273	25.2	6	64	(2.52)
3L12	14.3881	13.7533	0.6348	25.2	6	65	(2.55)
3M11	15.9061	15.2989	0.6075	25.2	6	62	(2.45)
3M12	15.9284	15.2673	0.6611	25.2	6	68	(2.67)

TABLE B-4-4: pH9 TEST

Specimen	Initial Wt., g	Final Wt., g	Weight Change, g	Area, cm^2	Time, mo	Corrosion Rate, µm/yr	(mpy)
3J5	6.8285	6.8146	0.0139	25.2	6	1.5	(0.06)
3J6	6.8173	6.8033	0.0140	25.2	6	1.5	(0.06)
3K5	8.5864	8.5683	0.0181	25.1	6	1.8	(0.07)
3K6	8.5662	8.5502	0.0160	25.1	6	1.5	(0.06)
3L5	14.7278	14.7074	0.0204	25.2	6	2.0	(0.08)
3L6	14.4894	14.4674	0.0220	25.2	6	2.3	(0.09)
3M5	15.8882	15.8648	0.0234	25.1	6	2.5	(0.10)
3M6	15.9431	15.9106	0.0235	25.1	6	2.5	(0.10)

TABLE B-4-5: pH11 TEST

Specimen	Initial Wt., g	Final Wt., g	Weight Change, g	Area, cm^2	Time, mo.	Corrosion Rate, µm/yr	(mpy)
3J7	6.8772	6.8571	0.0201	25.2	6	2.0	(0.08)
3J8	6.7332	6.7176	0.0156	25.2	6	1.5	(0.06)
3K7	8.5866	8.5695	0.0171	25.1	6	1.8	(0.07)
3K8	8.5430	8.5239	0.0191	25.0	6	2.0	(0.08)
3L7	14.6188	14.5962	0.0226	25.1	6	2.3	(0.09)
3L8	14.5547	14.4675	0.0872	25.2	6	8.9	(0.35)
3M7	15.8595	15.8348	0.0247	25.1	6	2.5	(0.10)
3M8	15.8950	15.8355	0.0595	25.1	6	6.1	(0.24)

[a] Primary calculation, carried out to three significant figures. Only two significant figures are justifiable.

APPENDIX B-5: INDIVIDUAL SPECIMEN CORROSION-RATE DATA, TESTS OF LOW-CARBON STEEL IN BRINE A UNDER HIGH H_2 PRESSURES, AUTOCLAVE TEST METHOD

APPENDIX B-5: INDIVIDUAL SPECIMEN CORROSION-RATE DATA, TESTS OF LOW-CARBON STEEL IN BRINE A UNDER HIGH H_2 PRESSURES, AUTOCLAVE TEST METHOD

Test No: AUT-9
Test Type: Immersion
Test Environment: Simulated WIPP Brine A,
H2 overpressure (127 atm)
Test Temperature: 30±5°C
Test Exposure: 6 months

Specimen	Material Type	Length, mm	Width, mm	Thickness, mm	Top Hole ID, mm	Bottom Hole ID, mm	Area, dm2	Initial Wt., g	Final Wt., g	Corrosion Rate, mpy	Corrosion Rate, µm/yr	Weight Loss, g
J9-1	Low-C Steel, Lot J	76.07	38.15	0.673	7.92	0.00	0.588	14.8989	14.8766	0.038	0.95	
J9-2	Low-C Steel, Lot J	75.91	38.09	0.654	7.94	0.00	0.585	14.5719	14.5430	0.049	1.24	
J9-3	Low-C Steel, Lot J	75.78	38.11	0.654	7.95	0.00	0.584	14.6162	14.5872	0.049	1.25	
J9-4	Low-C Steel, Lot J	75.69	37.87	0.654	7.97	0.00	0.580	14.3539	14.3265	0.047	1.19	
J9-5	Low-C Steel, Lot J	75.99	37.94	0.671	7.97	0.00	0.584	14.8225	SA*	SA	SA	
K9-1	Low-C Steel, Lot K	75.65	37.80	0.862	8.08	0.00	0.583	18.8199	18.7902	0.050	1.28	
K9-2	Low-C Steel, Lot K	75.56	38.03	0.865	8.07	0.00	0.586	18.9457	18.9185	0.046	1.17	
K9-3	Low-C Steel, Lot K	75.67	38.06	0.860	7.98	0.00	0.588	18.9511	18.9203	0.052	1.32	
K9-4	Low-C Steel, Lot K	75.52	38.00	0.864	8.07	0.00	0.586	18.9174	18.8878	0.050	1.27	
L9-1	Low-C Steel, Lot L	75.89	37.96	1.483	8.06	0.00	0.603	32.6740	32.6534	0.034	0.86	
L9-2	Low-C Steel, Lot L	75.86	38.01	1.487	8.08	0.00	0.604	32.6707	32.6503	0.033	0.85	
L9-3	Low-C Steel, Lot L	75.95	37.92	1.491	8.09	0.00	0.603	32.5126	32.4926	0.033	0.83	
L9-4	Low-C Steel, Lot L	76.01	37.96	1.506	8.05	0.00	0.605	32.8774	32.8556	0.036	0.91	
M9-1	Low-C Steel, Lot M	76.33	37.98	1.557	8.06	0.00	0.609	34.2958	34.2768	0.031	0.78	
M9-2	Low-C Steel, Lot M	74.48	37.97	1.575	8.07	0.00	0.595	33.8667	33.8493	0.029	0.74	
M9-3	Low-C Steel, Lot M	76.29	37.97	1.551	8.07	0.00	0.608	34.2358	34.2174	0.030	0.76	
M9-4	Low-C Steel, Lot M	75.49	37.96	1.595	8.08	0.00	0.603	34.7365	34.7160	0.034	0.86	

*SA= Specimen was retained for surface analysis.

APPENDIX B-6: INDIVIDUAL SPECIMEN CORROSION-RATE DATA, TESTS OF LOW-CARBON STEEL IN BRINE A UNDER HIGH N_2 PRESSURES, AUTOCLAVE TEST METHOD

APPENDIX B-6: INDIVIDUAL SPECIMEN CORROSION-RATE DATA, TESTS OF LOW-CARBON STEEL IN BRINE A UNDER HIGH N_2 PRESSURES, AUTOCLAVE TEST METHOD

Test No: AUT-10
Test Type: Immersion
Test Environment: Simulated WIPP Brine A,
N2 overpressure (127 atm)
Test Temperature: 30±5°C
Test Exposure: 6 months

Specimen	Material Type	Length, mm	Width, mm	Thickness, mm	Top Hole ID, mm	Bottom Hole ID, mm	Area, dm2	Initial Wt., g	Final Wt., g	Corrosion Rate, mpy	Corrosion Rate, µm/yr	Weight Loss, g
J10-1	Low-C Steel, Lot J	75.73	38.06	0.656	7.96	0.00	0.583	14.5830	14.5181	0.107	2.7	
J10-2	Low-C Steel, Lot J	75.93	37.89	0.662	7.94	0.00	0.582	14.7302	14.6729	0.095	2.4	
J10-3	Low-C Steel, Lot J	76.20	38.07	0.676	7.97	0.00	0.587	15.0554	14.9982	0.094	2.4	
J10-4	Low-C Steel, Lot J	75.62	38.43	0.651	7.96	0.00	0.588	14.6560	14.5959	0.099	2.5	
J10-5	Low-C Steel, Lot J	75.81	38.04	0.653	7.95	0.00	0.583	14.5415	SA*	SA	SA	
K10-1	Low-C Steel, Lot K	75.62	37.97	0.865	7.99	0.00	0.586	18.9339	18.8821	0.085	2.2	
K10-2	Low-C Steel, Lot K	75.43	38.01	0.863	7.99	0.00	0.585	18.9285	18.8748	0.088	2.2	
K10-3	Low-C Steel, Lot K	75.82	36.86	0.863	7.94	0.00	0.571	18.4164	18.3656	0.086	2.2	
K10-4	Low-C Steel, Lot K	75.71	38.02	0.860	7.98	0.00	0.587	18.9269	18.8746	0.086	2.2	
L10-1	Low-C Steel, Lot L	75.92	37.95	1.488	8.07	0.00	0.604	32.7516	32.6807	0.113	2.9	
L10-2	Low-C Steel, Lot L	75.89	37.99	1.483	8.08	0.00	0.604	32.7954	32.7269	0.109	2.8	
L10-3	Low-C Steel, Lot L	75.88	37.93	1.462	8.07	0.00	0.602	32.2653	32.1893	0.122	3.1	
L10-4	Low-C Steel, Lot L	75.94	37.96	1.493	8.04	0.00	0.604	32.5210	32.4496	0.114	2.9	
M10-1	Low-C Steel, Lot M	76.36	38.00	1.561	8.03	0.00	0.610	34.2332	34.1494	0.132	3.4	
M10-2	Low-C Steel, Lot M	75.77	37.96	1.609	8.04	0.00	0.606	35.0051	34.9237	0.130	3.3	
M10-3	Low-C Steel, Lot M	74.82	38.01	1.567	8.07	0.00	0.598	33.9798	33.9018	0.126	3.2	
M10-4	Low-C Steel, Lot M	76.09	37.96	1.568	8.04	0.00	0.607	34.6229	34.5413	0.130	3.3	

*SA= Specimen was retained for surface analysis.

APPENDIX B-7: INDIVIDUAL SPECIMEN CORROSION-RATE DATA, TESTS OF LOW-CARBON STEEL IN BRINE A UNDER HIGH CO_2 PRESSURES, AUTOCLAVE TEST METHOD

Table B-7-1: Test AUT-8, 36 atm CO_2
Table B-7-2: Test AUT-11, 62 atm CO_2

TABLE B-7-1

Specimen Data, Test AUT-8, 36 atm CO_2

Test Type: Immersion
Test Environment: Simulated WIPP Brine A,
CO2 overpressure (36 atm)
Test Temperature: 30±5°C
Test Exposure: 12 months

Specimen	Material Type	Length, mm	Width, mm	Thickness, mm	Top Hole ID, mm	Bottom Hole ID, mm	Area, dm2	Initial Wt., g	Final Wt., g	Corrosion Rate, mpy	Corrosion Rate, µm/yr	Weight Loss, g
J8 1	Low-C Steel, Lot J	75.86	37.31	0.701	7.97	0.00	0.574	14.8788	14.3960	0.42	11	0.4828
J8 2	Low-C Steel, Lot J	76.42	37.76	0.705	8.00	0.00	0.585	15.1086	14.5475	0.47	12	0.5611
J8 3	Low-C Steel, Lot J	74.89	37.76	0.696	8.00	0.00	0.573	14.9006	SA*	SA	SA	SA*
J8 4	Low-C Steel, Lot J	76.02	37.43	0.700	8.00	0.00	0.577	15.1812	14.6709	0.44	11	0.5103
K8 1	Low-C Steel, Lot K	76.64	37.17	0.857	8.00	0.00	0.581	18.4704	17.9017	0.48	12	0.5687
K8 2	Low-C Steel, Lot K	75.97	37.37	0.844	7.93	0.00	0.579	18.0844	17.5036	0.50	13	0.5808
K8 3	Low-C Steel, Lot K	75.98	37.68	0.846	7.96	0.00	0.584	18.0115	17.4310	0.49	12	0.5805
K8 4	Low-C Steel, Lot K	76.17	36.93	0.863	7.85	0.00	0.575	18.0118	17.4675	0.47	12	0.5443
L8 1	Low-C Steel, Lot L	76.00	37.59	1.475	7.96	0.00	0.599	31.9348	31.0279	0.75	19	0.9069
L8 2	Low-C Steel, Lot L	74.61	37.85	1.480	7.97	0.00	0.592	31.3200	30.4520	0.72	18	0.868
L8 3	Low-C Steel, Lot L	75.70	37.80	1.505	7.97	0.00	0.600	32.4604	31.5429	0.75	19	0.9175
L8 4	Low-C Steel, Lot L	75.27	37.61	1.473	7.95	0.00	0.593	31.4263	30.5748	0.71	18	0.8515
M8 1	Low-C Steel, Lot M	76.18	37.80	1.559	7.97	0.00	0.605	34.1104	33.2333	0.72	18	0.8771
M8 2	Low-C Steel, Lot M	76.27	37.91	1.559	7.95	0.00	0.608	34.4325	33.6245	0.66	17	0.808
M8 3	Low-C Steel, Lot M	76.40	37.01	1.567	7.97	0.00	0.595	33.9265	33.0796	0.70	18	0.8469
M8 4	Low-C Steel, Lot M	76.09	36.92	1.562	7.93	0.00	0.591	33.4735	32.7177	0.63	16	0.7558

*SA= Specimen was retained for surface analysis.

TABLE B-7-2

Specimen Data, Test AUT-11, 62 atm CO_2

Test Type: Immersion
Test Environment: Simulated WIPP Brine A,
CO2 overpressure (62 atm)
Test Temperature: 30±5°C
Test Exposure: 6 months

Specimen	Material Type	Length, mm	Width, mm	Thickness, mm	Top Hole ID, mm	Bottom Hole ID, mm	Area, dm2	Initial Wt., g	Final Wt., g	Corrosion Rate, mpy	Corrosion Rate, µm/yr	Weight Loss, g
J11-1	Low-C Steel, Lot J	75.78	38.15	0.650	7.96	0.00	0.585	14.5363	13.8617	1.12	29	
J11-2	Low-C Steel, Lot J	76.22	38.09	0.666	7.94	0.00	0.588	14.9788	14.3403	1.06	27	
J11-3	Low-C Steel, Lot J	75.68	38.09	0.653	7.96	0.00	0.583	14.6614	14.0359	1.04	27	
J11-4	Low-C Steel, Lot J	76.58	38.06	0.661	7.95	0.00	0.590	15.0194	14.3824	1.05	27	
J11-5	Low-C Steel, Lot J	76.37	38.07	0.668	7.93	0.00	0.589	14.9469	SA*	SA	SA	
K11-1	Low-C Steel, Lot K	75.30	38.06	0.865	7.96	0.00	0.585	18.8652	18.2270	1.06	27	
K11-2	Low-C Steel, Lot K	75.64	38.05	0.870	7.96	0.00	0.588	18.9482	18.3254	1.03	26	
K11-3	Low-C Steel, Lot K	75.75	37.98	0.864	7.97	0.00	0.587	18.9901	18.3653	1.04	26	
K11-4	Low-C Steel, Lot K	75.73	38.03	0.858	7.96	0.00	0.588	18.9506	18.3380	1.02	26	
L11-1	Low-C Steel, Lot L	76.10	38.03	1.510	8.05	0.00	0.607	33.1199	32.1731	1.52	39	
L11-2	Low-C Steel, Lot L	75.89	37.99	1.478	8.08	0.00	0.604	32.4090	31.4687	1.52	39	
L11-3	Low-C Steel, Lot L	75.85	38.00	1.484	8.11	0.00	0.604	32.7295	31.7658	1.55	39	
L11-4	Low-C Steel, Lot L	75.98	37.97	1.513	8.06	0.00	0.605	33.1989	32.2720	1.49	38	
M11-1	Low-C Steel, Lot M	74.19	37.96	1.571	8.05	0.00	0.592	33.6877	32.7099	1.61	41	
M11-2	Low-C Steel, Lot M	75.20	37.96	1.574	8.07	0.00	0.600	34.3169	33.2791	1.68	43	
M11-3	Low-C Steel, Lot M	76.29	38.03	1.537	8.08	0.00	0.609	34.2141	33.1083	1.77	45	
M11-4	Low-C Steel, Lot M	76.35	37.98	1.546	8.04	0.00	0.609	34.3062	33.3198	1.58	40	

*SA= Specimen was retained for surface analysis.

APPENDIX B-8: INDIVIDUAL SPECIMEN CORROSION-RATE DATA, TESTS OF LOW-CARBON STEEL EMBEDDED IN SIMULATED BENTONITE-SALT BACKFILL CONTACTING BRINE A

APPENDIX B-8: INDIVIDUAL SPECIMEN CORROSION-RATE DATA, TESTS OF LOW-CARBON STEEL EMBEDDED IN SIMULATED BENTONITE-SALT BACKFILL CONTACTING BRINE A

Test No: AUT-12
Test Type: Wicking
Test Environment: Specimens were embedded in simulated backfill (coarse particulate WIPP salt and bentonite). The backfill was held in a mesh basket contacting simulated WIPP Brine A, permitting wicking of the liquid. The autoclave had a N2 overpressure of 10 atm.
Test Temperature: 30±5°C
Test Exposure: 6 months

Specimen	Material Type	Length, mm	Width, mm	Thickness, mm	Top Hole ID*, mm	Bottom Hole ID*, mm	Area, dm2	Initial Wt., g	Final Wt., g	Corrosion Rate, mpy	Corrosion Rate, µm/yr	Weight Loss, g
12-1	Low-C Steel, Lot J	24.86	24.91	0.694	0.00	0.00	0.131	3.3570	3.3355	0.158	4.0	0.0215
12-2	Low-C Steel, Lot J	24.84	24.78	0.695	0.00	0.00	0.130	3.3630	3.3351	0.206	5.2	0.0279
12-3	Low-C Steel, Lot J	24.88	24.89	0.690	0.00	0.00	0.131	3.3657	3.3371	0.210	5.3	0.0286
12-4	Low-C Steel, Lot J	24.80	24.84	0.686	0.00	0.00	0.130	3.3335	3.3092	0.179	4.6	0.0243
12-5	Low-C Steel, Lot J	24.73	24.87	0.692	0.00	0.00	0.130	3.3646	3.3402	0.180	4.6	0.0244
12-6	Low-C Steel, Lot J	24.90	24.76	0.696	0.00	0.00	0.130	3.3527	3.3323	0.150	3.8	0.0204
12-7	Low-C Steel, Lot J	24.81	24.92	0.695	0.00	0.00	0.131	3.3471	3.3281	0.140	3.6	0.0190
12-8	Low-C Steel, Lot J	24.84	24.84	0.668	0.00	0.00	0.130	3.2339	3.2076	0.193	4.9	0.0263
12-9	Low-C Steel, Lot J	24.89	24.81	0.688	0.00	0.00	0.130	3.3392	3.3195	0.145	3.7	0.0197
12-10	Low-C Steel, Lot J	24.84	24.87	0.697	0.00	0.00	0.130	3.3748	3.3576	0.127	3.2	0.0172
12-11	Low-C Steel, Lot J	24.79	24.90	0.696	0.00	0.00	0.130	3.3572	3.3374	0.146	3.7	0.0198
12-12	Low-C Steel, Lot J	24.91	24.90	0.650	0.00	0.00	0.131	3.1178	3.0957	0.162	4.1	0.0221
12-13	Low-C Steel, Lot J	24.85	24.84	0.689	0.00	0.00	0.130	3.3311	3.3146	0.121	3.1	0.0165
12-14	Low-C Steel, Lot J	24.76	24.95	0.698	0.00	0.00	0.130	3.3455	3.3322	0.098	2.5	0.0133
12-15	Low-C Steel, Lot J	24.87	24.90	0.694	0.00	0.00	0.131	3.3362	3.3267	0.070	1.8	0.0095
12-16	Low-C Steel, Lot J	24.91	24.89	0.699	0.00	0.00	0.131	3.3502	3.3394	0.079	2.0	0.0108
12-17	Low-C Steel, Lot J	24.83	24.89	0.672	0.00	0.00	0.130	3.2318	3.2204	0.083	2.1	0.0114
12-18	Low-C Steel, Lot J	24.85	24.94	0.691	0.00	0.00	0.131	3.3435	3.3349	0.063	1.6	0.0086

* = Specimens were simple rectangular coupons without holes.

APPENDIX B-9: INDIVIDUAL SPECIMEN CORROSION-RATE DATA, TESTS OF LOW-CARBON STEEL EMBEDDED IN SIMULATED BENTONITE-SALT BACKFILL SUSPENDED IN VAPOR PHASE OF BRINE A

APPENDIX B-9: INDIVIDUAL SPECIMEN CORROSION-RATE DATA, TESTS OF LOW-CARBON STEEL EMBEDDED IN SIMULATED BENTONITE-SALT BACKFILL SUSPENDED IN VAPOR PHASE OF BRINE A

Test No: AUT-13
Test Type: Vapor
Test Environment: Specimens were embedded in simulated backfill (coarse particulate WIPP salt and bentonite).
The backfill was held in a mesh basket above the level of the simulated WIPP Brine A in the autoclave.
The autoclave had an N2 overpressure of 10 atm.
Test Temperature: 30±5°C
Test Exposure: 6 months

Specimen	Material Type	Length, mm	Width, mm	Thickness, mm	Top Hole ID*, mm	Bottom Hole ID*, mm	Area, dm2	Initial Wt., g	Final Wt., g	Corrosion Rate, mpy	Corrosion Rate, µm/yr	Weight Loss, g
13-1	Low-C Steel, Lot J	25.06	24.90	0.672	0.00	0.00	0.1315	3.2850	3.2812	0.028	0.72	0.0038
13-2	Low-C Steel, Lot J	25.01	25.03	0.679	0.00	0.00	0.132	3.2791	3.2768	0.017	0.43	0.0023
13-3	Low-C Steel, Lot J	24.72	25.46	0.656	0.00	0.00	0.1325	3.2145	3.2125	0.015	0.38	0.0020
13-4	Low-C Steel, Lot J	24.95	25.47	0.665	0.00	0.00	0.1338	3.2681	3.2653	0.020	0.52	0.0028
13-5	Low-C Steel, Lot J	24.96	25.25	0.670	0.00	0.00	0.1328	3.2860	3.2835	0.018	0.47	0.0025
13-6	Low-C Steel, Lot J	25.03	25.05	0.669	0.00	0.00	0.1321	3.1868	3.1837	0.023	0.58	0.0031
13-7	Low-C Steel, Lot J	24.95	24.93	0.680	0.00	0.00	0.1312	3.3028	SA**	SA	SA	NA
13-8	Low-C Steel, Lot J	24.77	25.08	0.667	0.00	0.00	0.1309	3.1737	3.1718	0.014	0.36	0.0019
13-9	Low-C Steel, Lot J	25.09	24.92	0.681	0.00	0.00	0.1319	3.3303	3.3281	0.016	0.41	0.0022
13-10	Low-C Steel, Lot J	24.68	24.95	0.676	0.00	0.00	0.1299	3.2178	SA	SA	SA	NA

* = Specimens were simple rectangular coupons without holes.
**SA = Specimen was retained for surface analysis.

APPENDIX B-10: INDIVIDUAL SPECIMEN DATA, TESTS OF ALTERNATIVE PACKAGING MATERIALS (Cu-AND Ti-BASE MATERIALS) IMMERSED IN BRINE A, SEAL-WELDED CONTAINER TEST METHOD

TABLE B-10-1
Specimen Data, Test No. 13A

Test Type: Immersion

Test Environment: Simulated WIPP Brine A, N2 overpressure (10 atm)

Test Temperature: 30±5°C

Test Exposure: 24 months

Specimen	Material Type	Outer Diameter, mm	Hole ID, mm	Thickness, mm	Area, dm2	Initial Wt., g
C49	Unalloyed Copper	38.02	7.83	1.516	0.239	14.3807
C50	Unalloyed Copper	38.02	7.83	1.508	0.239	14.3428
C51	Unalloyed Copper	38.02	7.8	1.511	0.239	14.3613
C52	Unalloyed Copper	38.01	7.86	1.515	0.239	14.3538
C53	Unalloyed Copper	38.00	7.84	1.525	0.239	14.4568
C54	Unalloyed Copper	38.00	7.86	1.530	0.239	14.5065
C55	Unalloyed Copper	38.03	7.83	1.550	0.240	14.7508
C56	Unalloyed Copper	38.01	7.82	1.544	0.239	14.7127
CN49	Cupronickel 90-10	38.12	7.88	1.537	0.241	14.7515
CN50	Cupronickel 90-10	38.11	7.88	1.536	0.240	14.7742
CN51	Cupronickel 90-10	38.11	7.87	1.551	0.241	14.8546
CN52	Cupronickel 90-10	37.78	7.87	1.525	0.236	14.3284
CN53	Cupronickel 90-10	38.05	7.87	1.519	0.239	14.5190
CN54	Cupronickel 90-10	37.98	7.87	1.522	0.239	14.5103
CN55	Cupronickel 90-10	38.18	7.87	1.519	0.241	14.6382
CN56	Cupronickel 90-10	38.15	7.86	1.526	0.241	14.6935

Specimen	Material Type	Length, mm	Width, mm	Thickness, mm	Top Hole ID, mm	Bottom Hole ID, mm	Area, dm2	Initial Wt., g
C249	Unalloyed Copper	190.23	63.28	1.499	7.97	7.94	2.471	159.0512
C250	Unalloyed Copper	190.27	63.21	1.569	7.95	7.95	2.473	165.9819
C251	Unalloyed Copper	190.20	63.21	1.568	7.88	7.98	2.472	165.6376
C252	Unalloyed Copper	190.31	63.25	1.572	7.90	7.88	2.475	166.1265
C253	Unalloyed Copper	190.29	63.22	1.571	7.93	7.93	2.474	166.0701
C254	Unalloyed Copper	190.28	63.33	1.569	7.99	7.91	2.478	166.0268
C255	Unalloyed Copper	190.30	63.24	1.570	7.83	7.91	2.475	165.9701
C256	Unalloyed Copper	190.19	63.18	1.553	7.89	7.84	2.470	163.9881
CN249	Cupronickel 90-10	190.29	63.27	1.540	7.98	7.93	2.474	161.2555
CN250	Cupronickel 90-10	190.31	63.14	1.504	7.89	7.92	2.467	153.2101
CN251	Cupronickel 90-10	190.39	63.26	1.543	7.91	7.94	2.475	161.2411
CN252	Cupronickel 90-10	190.24	63.25	1.491	7.97	7.98	2.470	157.3044
CN253	Cupronickel 90-10	190.46	63.26	1.557	7.95	7.98	2.477	162.7911
CN254	Cupronickel 90-10	190.21	63.15	1.540	7.94	7.97	2.468	161.6902
CN255	Cupronickel 90-10	190.18	63.21	1.571	7.93	7.96	2.472	163.0500
CN256	Cupronickel 90-10	190.15	63.19	1.574	7.96	7.96	2.471	164.2091

TABLE B-10-2

Specimen Data, Test No. 14A

Test Type: Immersion

Test Environment: Simulated WIPP Brine A, CO2 overpressure (10 atm)

Test Temperature: 30±5°C

Test Exposure: 24 months

Specimen	Material Type	Outer Diameter, mm	Hole ID, mm	Thickness, mm	Area, dm2	Initial Wt., g
C57	Unalloyed Copper	38.02	7.87	1.542	0.239	14.6754
C58	Unalloyed Copper	38.01	7.83	1.539	0.239	14.6894
C59	Unalloyed Copper	38.02	7.85	1.538	0.239	14.6469
C60	Unalloyed Copper	38.02	7.77	1.518	0.239	14.4693
C61	Unalloyed Copper	38.02	7.87	1.534	0.239	14.5895
C62	Unalloyed Copper	38.01	7.81	1.529	0.239	14.5983
C63	Unalloyed Copper	38.03	7.86	1.521	0.239	14.4193
C64	Unalloyed Copper	38.01	7.83	1.540	0.239	14.6461
CN57	Cupronickel 90-10	38.16	7.90	1.535	0.241	14.7260
CN58	Cupronickel 90-10	38.14	7.87	1.545	0.241	14.8214
CN59	Cupronickel 90-10	38.08	7.90	1.524	0.240	14.5815
CN60	Cupronickel 90-10	38.05	7.86	1.531	0.240	14.6264
CN61	Cupronickel 90-10	38.07	7.90	1.523	0.240	14.5286
CN62	Cupronickel 90-10	38.01	7.89	1.530	0.239	14.6020
CN63	Cupronickel 90-10	37.66	7.86	1.509	0.235	14.1152
CN64	Cupronickel 90-10	38.08	7.90	1.519	0.240	14.5219

Specimen	Material Type	Length, mm	Width, mm	Thickness, mm	Top Hole ID, mm	Bottom Hole ID, mm	Area, dm2	Initial Wt., g
C257	Unalloyed Copper	190.15	63.23	1.574	7.83	7.81	2.473	166.0554
C258	Unalloyed Copper	190.23	63.28	1.582	7.82	7.85	2.476	166.9782
C259	Unalloyed Copper	190.15	63.12	1.579	7.83	7.77	2.469	166.6322
C260	Unalloyed Copper	190.10	63.24	1.573	7.90	7.91	2.472	165.7625
C261	Unalloyed Copper	190.07	63.08	1.591	7.80	7.85	2.467	166.7534
C262	Unalloyed Copper	190.00	63.19	1.597	7.91	7.90	2.470	167.2345
C263	Unalloyed Copper	190.14	63.10	1.575	7.92	7.80	2.468	165.6515
C264	Unalloyed Copper	190.05	63.34	1.542	7.84	7.82	2.474	161.5678
CN257	Cupronickel 90-10	190.21	63.18	1.563	7.97	7.94	2.471	163.6655
CN258	Cupronickel 90-10	190.14	63.20	1.582	7.94	7.98	2.472	164.2870
CN259	Cupronickel 90-10	190.28	63.09	1.562	7.93	7.95	2.468	162.3155
CN260	Cupronickel 90-10	190.21	63.29	1.550	7.91	7.96	2.474	162.0227
CN261	Cupronickel 90-10	190.32	63.23	1.563	8.00	7.94	2.474	163.2696
CN262	Cupronickel 90-10	190.43	63.23	1.562	7.98	7.95	2.475	162.9196
CN263	Cupronickel 90-10	190.34	63.22	1.570	7.95	7.93	2.474	162.9507
CN264	Cupronickel 90-10	190.24	63.13	1.553	7.96	7.96	2.469	161.8247

TABLE B-10-3
Specimen Data, Test No. 15A

Test Type: Immersion

Test Environment: Simulated WIPP Brine A, H2S overpressure (5 atm)

Test Temperature: 30±5°C

Test Exposure: 24 months

Specimen	Material Type	Outer Diameter, mm	Hole ID, mm	Thickness, mm	Area, dm2	Initial Wt., g
C65	Unalloyed Copper	38.02	7.86	1.524	0.239	14.4727
C66	Unalloyed Copper	38.01	7.85	1.510	0.239	14.3891
C67	Unalloyed Copper	38.03	7.83	1.512	0.239	14.3526
C68	Unalloyed Copper	38.02	7.84	1.538	0.239	14.6810
C69	Unalloyed Copper	38.02	7.85	1.523	0.239	14.5617
C70	Unalloyed Copper	38.00	7.86	1.530	0.239	14.5673
C71	Unalloyed Copper	38.02	7.80	1.538	0.240	14.6572
C72	Unalloyed Copper	38.02	7.82	1.522	0.239	14.5249
CN65	Cupronickel 90-10	38.06	7.90	1.522	0.240	14.5151
CN66	Cupronickel 90-10	38.06	7.87	1.520	0.240	14.5940
CN67	Cupronickel 90-10	38.06	7.89	1.516	0.240	14.5300
CN68	Cupronickel 90-10	38.07	7.90	1.522	0.240	14.5383
CN69	Cupronickel 90-10	38.06	7.87	1.525	0.240	14.5186
CN70	Cupronickel 90-10	38.04	7.87	1.525	0.239	14.5638
CN71	Cupronickel 90-10	38.02	7.88	1.529	0.239	14.5693
CN72	Cupronickel 90-10	37.61	7.89	1.540	0.234	14.3708

Specimen	Material Type	Length, mm	Width, mm	Thickness, mm	Top Hole ID, mm	Bottom Hole ID, mm	Area, dm2	Initial Wt., g
C265	Unalloyed Copper	189.99	63.44	1.508	7.92	7.86	2.475	157.2453
C266	Unalloyed Copper	189.97	63.41	1.494	7.78	7.83	2.473	157.5416
C267	Unalloyed Copper	190.20	63.19	1.584	7.88	7.89	2.472	165.8740
C268	Unalloyed Copper	190.33	63.22	1.578	7.83	7.76	2.475	166.0372
C269	Unalloyed Copper	190.24	63.18	1.564	7.81	7.78	2.472	165.2174
C270	Unalloyed Copper	190.27	63.32	1.584	7.82	7.84	2.478	166.5285
C271	Unalloyed Copper	190.34	63.30	1.570	7.86	7.81	2.478	166.0302
C272	Unalloyed Copper	190.24	63.07	1.571	7.78	7.81	2.468	164.9797
CN265	Cupronickel 90-10	190.40	63.19	1.552	7.97	7.95	2.473	162.6055
CN266	Cupronickel 90-10	190.33	63.16	1.577	7.95	7.96	2.472	164.4899
CN267	Cupronickel 90-10	190.29	63.15	1.572	7.96	7.96	2.471	163.6594
CN268	Cupronickel 90-10	190.45	63.24	1.577	7.96	7.93	2.477	164.8258
CN269	Cupronickel 90-10	190.35	63.26	1.577	7.90	7.97	2.476	164.8795
CN270	Cupronickel 90-10	190.27	63.20	1.571	7.96	7.96	2.473	163.9865
CN271	Cupronickel 90-10	190.35	63.18	1.585	7.94	7.94	2.474	164.8628
CN272	Cupronickel 90-10	190.22	63.23	1.575	7.95	7.97	2.473	164.2231

TABLE B-10-4

Specimen Data, Test No. 16A

Test Type: Immersion

Test Environment: Simulated WIPP Brine A, N2 overpressure (10 atm)

Test Temperature: 30±5°C

Test Exposure: 24 months

Specimen	Material Type	Outer Diameter, mm	Hole ID, mm	Thickness, mm	Area, dm2	Initial Wt., g
T49	Titanium, Gr2	38.27	7.78	1.555	0.243	7.5706
T50	Titanium, Gr2	38.24	7.77	1.550	0.242	7.4934
T51	Titanium, Gr2	38.17	7.75	1.528	0.241	7.3737
T52	Titanium, Gr2	38.16	7.78	1.534	0.241	7.3694
T53	Titanium, Gr2	38.18	7.78	1.557	0.242	7.5377
T54	Titanium, Gr2	38.21	7.78	1.556	0.242	7.5610
T55	Titanium, Gr2	38.18	7.77	1.518	0.241	7.3351
T56	Titanium, Gr2	38.18	7.77	1.543	0.242	7.3993
TN49	Titanium, Gr12	38.13	7.82	1.560	0.241	7.5127
TN50	Titanium, Gr12	38.15	7.86	1.532	0.241	7.3810
TN51	Titanium, Gr12	38.18	7.83	1.500	0.241	7.2700
TN52	Titanium, Gr12	38.12	7.86	1.490	0.240	7.1963
TN53	Titanium, Gr12	38.10	7.84	1.507	0.240	7.2359
TN54	Titanium, Gr12	38.14	7.83	1.491	0.240	7.2053
TN55	Titanium, Gr12	38.14	7.88	1.517	0.241	7.3597
TN56	Titanium, Gr12	38.14	7.90	1.531	0.241	7.4162

Specimen	Material Type	Length, mm	Width, mm	Thickness, mm	Top Hole ID, mm	Bottom Hole ID, mm	Area, dm2	Initial Wt., g
T249	Titanium, Gr2	190.45	63.38	1.569	7.99	8.00	2.482	83.8036
T250	Titanium, Gr2	190.42	63.44	1.557	7.99	7.98	2.483	83.2117
T251	Titanium, Gr2	190.48	63.42	1.610	7.99	8.03	2.486	86.0366
T252	Titanium, Gr2	190.49	63.29	1.603	7.96	7.96	2.481	85.4095
T253	Titanium, Gr2	190.52	63.43	1.601	7.96	7.99	2.486	85.8162
T254	Titanium, Gr2	190.46	63.39	1.596	7.97	8.00	2.484	85.6188
T255	Titanium, Gr2	190.46	63.40	1.589	7.96	8.01	2.484	84.7301
T256	Titanium, Gr2	190.47	63.37	1.611	7.98	7.98	2.484	86.1996
TN249	Titanium, Gr12	190.55	63.41	1.533	7.86	7.86	2.483	82.8425
TN250	Titanium, Gr12	190.49	63.36	1.558	7.87	7.87	2.481	83.8907
TN251	Titanium, Gr12	190.47	63.52	1.548	7.87	7.88	2.487	83.7361
TN252	Titanium, Gr12	190.37	63.59	1.546	7.87	7.88	2.488	83.7410
TN253	Titanium, Gr12	190.56	63.42	1.558	7.86	7.86	2.484	84.0397
TN254	Titanium, Gr12	190.46	63.56	1.531	7.93	7.93	2.487	82.8461
TN255	Titanium, Gr12	190.53	63.63	1.524	7.91	7.91	2.490	83.6466
TN256	Titanium, Gr12	190.49	63.54	1.529	7.87	7.86	2.487	83.0086

TABLE B-10-5

Specimen Data, Test No. 17A

Test Type: Immersion

Test Environment: Simulated WIPP Brine A, CO2 overpressure (10 atm)

Test Temperature: 30±5°C

Test Exposure: 24 months

Specimen	Material Type	Outer Diameter, mm	Hole ID, mm	Thickness, mm	Area, dm2	Initial Wt., g
T57	Titanium, Gr2	38.20	7.79	1.537	0.242	7.4440
T58	Titanium, Gr2	38.21	7.78	1.550	0.242	7.4997
T59	Titanium, Gr2	38.22	7.77	1.550	0.242	7.5293
T60	Titanium, Gr2	38.17	7.78	1.548	0.242	7.3794
T61	Titanium, Gr2	38.22	7.79	1.548	0.242	7.4621
T62	Titanium, Gr2	38.23	7.78	1.508	0.242	7.3093
T63	Titanium, Gr2	38.23	7.79	1.547	0.242	7.4980
T64	Titanium, Gr2	38.18	7.77	1.485	0.241	7.1855
TN57	Titanium, Gr12	38.17	7.85	1.518	0.241	7.3367
TN58	Titanium, Gr12	38.17	7.87	1.548	0.241	7.4928
TN59	Titanium, Gr12	38.16	7.88	1.533	0.241	7.3558
TN60	Titanium, Gr12	38.11	7.89	1.476	0.240	7.1907
TN61	Titanium, Gr12	38.17	7.88	1.532	0.241	7.4107
TN62	Titanium, Gr12	38.16	7.82	1.523	0.241	7.3919
TN63	Titanium, Gr12	38.15	7.82	1.514	0.241	7.3466
TN64	Titanium, Gr12	38.17	7.87	1.473	0.240	7.1270

Specimen	Material Type	Length, mm	Width, mm	Thickness, mm	Top Hole ID, mm	Bottom Hole ID, mm	Area, dm2	Initial Wt., g
T257	Titanium, Gr2	190.50	63.42	1.600	7.97	7.98	2.486	85.8738
T258	Titanium, Gr2	190.49	63.40	1.602	8.00	7.97	2.485	85.8648
T259	Titanium, Gr2	190.49	63.51	1.592	7.97	7.95	2.489	85.6874
T260	Titanium, Gr2	190.47	63.39	1.589	7.97	7.98	2.483	85.0525
T261	Titanium, Gr2	190.45	63.34	1.606	7.96	7.96	2.482	85.6046
T262	Titanium, Gr2	190.43	63.46	1.599	7.98	8.00	2.486	85.5254
T263	Titanium, Gr2	190.35	63.51	1.593	7.99	7.98	2.487	84.9743
T264	Titanium, Gr2	190.37	63.51	1.598	7.99	7.98	2.487	85.6633
TN257	Titanium, Gr12	190.43	63.21	1.544	7.87	7.87	2.474	83.5436
TN258	Titanium, Gr12	190.34	63.27	1.550	7.86	7.87	2.475	83.7854
TN259	Titanium, Gr12	190.52	63.51	1.534	7.86	7.89	2.486	83.4271
TN260	Titanium, Gr12	190.45	63.59	1.553	7.88	7.88	2.489	83.9818
TN261	Titanium, Gr12	190.45	63.30	1.555	7.84	7.84	2.478	83.8515
TN262	Titanium, Gr12	190.60	63.62	1.492	7.84	7.85	2.489	80.7448
TN263	Titanium, Gr12	190.41	63.60	1.555	7.85	7.86	2.489	84.6839
TN264	Titanium, Gr12	190.55	63.59	1.521	7.86	7.86	2.489	82.7873

TABLE B-10-6
Specimen Data, Test No. 18A

Test Type: Immersion
Test Environment: Simulated WIPP Brine A, H2S overpressure (5 atm)
Test Temperature: 30±5°C
Test Exposure: 24 months

Specimen	Material Type	Outer Diameter, mm	Hole ID, mm	Thickness, mm	Area, dm2	Initial Wt., g
T65	Titanium, Gr2	38.23	7.77	1.539	0.242	7.4438
T66	Titanium, Gr2	38.22	7.77	1.542	0.242	7.5072
T67	Titanium, Gr2	38.22	7.79	1.549	0.242	7.5079
T68	Titanium, Gr2	38.19	7.78	1.504	0.241	7.3431
T69	Titanium, Gr2	38.19	7.79	1.540	0.242	7.4867
T70	Titanium, Gr2	38.21	7.80	1.548	0.242	7.4889
T71	Titanium, Gr2	38.24	7.78	1.577	0.243	7.5659
T72	Titanium, Gr2	38.20	7.79	1.592	0.243	7.7209
TN65	Titanium, Gr12	38.16	7.83	1.480	0.240	7.2012
TN66	Titanium, Gr12	38.10	7.79	1.554	0.241	7.5075
TN67	Titanium, Gr12	38.13	7.87	1.552	0.241	7.4566
TN68	Titanium, Gr12	38.19	7.86	1.483	0.241	7.1790
TN69	Titanium, Gr12	38.14	7.85	1.471	0.240	7.1208
TN70	Titanium, Gr12	38.16	7.84	1.498	0.241	7.2381
TN71	Titanium, Gr12	38.10	7.78	1.510	0.240	7.3490
TN72	Titanium, Gr12	38.17	7.89	1.553	0.241	7.5236

Specimen	Material Type	Length, mm	Width, mm	Thickness, mm	Top Hole ID, mm	Bottom Hole ID, mm	Area, dm2	Initial Wt., g
T265	Titanium, Gr2	190.44	63.37	1.587	7.96	7.97	2.482	84.8820
T266	Titanium, Gr2	190.45	63.39	1.601	7.99	7.95	2.484	85.5991
T267	Titanium, Gr2	190.42	63.52	1.607	7.98	7.95	2.489	86.2913
T268	Titanium, Gr2	190.48	63.43	1.599	7.96	7.97	2.486	85.8925
T269	Titanium, Gr2	190.46	63.36	1.592	7.96	7.96	2.482	85.5674
T270	Titanium, Gr2	190.47	63.42	1.604	7.97	8.00	2.485	85.9347
T271	Titanium, Gr2	190.48	63.43	1.589	7.94	7.94	2.485	85.4719
T272	Titanium, Gr2	190.49	63.35	1.596	7.98	8.01	2.482	85.5389
TN265	Titanium, Gr12	190.42	63.33	1.554	7.85	7.85	2.479	84.2182
TN266	Titanium, Gr12	190.53	63.57	1.547	7.88	7.87	2.489	84.7329
TN267	Titanium, Gr12	190.61	63.25	1.557	7.88	7.87	2.478	84.3890
TN268	Titanium, Gr12	190.68	63.44	1.484	7.88	7.87	2.483	81.5230
TN269	Titanium, Gr12	190.32	63.24	1.525	7.88	7.87	2.473	82.0805
TN270	Titanium, Gr12	190.38	63.29	1.517	7.88	7.89	2.475	81.8307
TN271	Titanium, Gr12	190.43	63.42	1.510	7.88	7.88	2.480	82.0905
TN272	Titanium, Gr12	190.51	63.21	1.535	7.87	7.88	2.474	83.7831

APPENDIX B-11: INDIVIDUAL SPECIMEN DATA, TESTS OF ALUMINUM-BASE MATERIALS (99.99% Al AND 6061 ALLOY) IMMERSED IN BRINE A AND IN VAPOR PHASE OF BRINE A, SEAL-WELDED CONTAINER TEST METHOD

TABLE B-11-1

Specimen Data, Test No. 1B

Test Type: Immersion

Test Environment: Simulated WIPP Brine A, N2 overpressure (10 atm)

Test Temperature: 30±5°C

Test Exposure: 13 months

Specimen	Material Type	Outer Diameter, mm	Hole ID, mm	Thickness, mm	Area, dm2	Initial Wt., g
1-001	99.99% Al	38.12	8.09	1.103	0.234	3.1393
1-002	99.99% Al	38.28	7.86	1.020	0.235	2.8740
1-003	99.99% Al	38.35	7.86	1.136	0.238	3.2123
1-004	99.99% Al	38.27	7.83	1.144	0.237	3.2561
1-005	99.99% Al	38.32	7.85	1.143	0.237	3.2660
1-006	99.99% Al	38.24	7.89	1.086	0.236	3.0786
6-201D	Alloy 6061	38.31	8.00	1.430	0.241	4.2467
6-202D	Alloy 6061	38.33	8.01	1.448	0.242	4.2770
6-203D	Alloy 6061	38.32	7.97	1.409	0.241	4.1811
6-204D	Alloy 6061	38.34	7.91	1.389	0.241	4.1548
6-205D	Alloy 6061	38.33	7.99	1.367	0.241	4.1055
6-206D	Alloy 6061	38.34	8.04	1.344	0.240	4.0641

Specimen	Material Type	Length, mm	Width, mm	Thickness, mm	Top Hole ID, mm	Bottom Hole ID, mm	Area, dm2	Initial Wt., g
1-201	99.99%Al	190.36	63.60	1.161	8.03	7.77	2.467	36.5657
1-202	99.99%Al	190.36	63.63	1.252	7.96	7.94	2.473	39.8147
1-203	99.99%Al	190.51	63.75	1.275	7.95	7.94	2.480	40.7251
1-204	99.99%Al	190.30	63.67	1.247	7.99	8.01	2.473	39.9754
1-205	99.99%Al	190.28	63.68	1.247	7.95	7.97	2.473	39.7972
1-206	99.99%Al	189.75	63.36	1.252	7.97	7.98	2.454	39.7625
6-201	Alloy 6061	190.33	63.38	1.507	8.08	8.05	2.476	48.4405
6-202	Alloy 6061	190.41	63.36	1.510	8.06	8.05	2.477	48.4161
6-203	Alloy 6061	190.39	63.34	1.507	8.04	7.98	2.476	48.3179
6-204	Alloy 6061	190.35	63.27	1.505	8.02	8.00	2.472	48.2349
6-205	Alloy 6061	190.41	63.39	1.495	8.01	8.01	2.477	48.0071
6-206	Alloy 6061	190.37	63.35	1.503	7.99	7.98	2.476	48.2260

TABLE B-11-2

Specimen Data, Test No. 2B

Test Type: Immersion

Test Environment: Simulated WIPP Brine A, CO_2 overpressure (10 atm)

Test Temperature: 30±5°C

Test Exposure: 13 months

Specimen	Material Type	Outer Diameter, mm	Hole ID, mm	Thickness, mm	Area, dm2	Initial Wt., g
1-007	99.99% Al	38.15	7.84	1.091	0.235	3.1032
1-008	99.99% Al	38.28	7.90	1.092	0.236	3.2015
1-009	99.99% Al	38.33	7.89	1.075	0.236	2.9747
1-010	99.99% Al	38.27	7.90	1.003	0.235	2.9173
1-011	99.99% Al	38.18	7.85	1.031	0.234	3.0333
1-012	99.99% Al	38.18	7.93	1.122	0.235	3.2259
6-207D	Alloy 6061	38.32	7.99	1.426	0.241	4.2544
6-208D	Alloy 6061	38.34	7.96	1.345	0.240	4.0582
6-209D	Alloy 6061	38.32	8.06	1.346	0.240	4.0485
6-210D	Alloy 6061	38.29	7.94	1.366	0.240	4.1203
6-211D	Alloy 6061	38.33	7.99	1.345	0.240	4.0414
6-212D	Alloy 6061	38.31	8.05	1.361	0.240	4.1389

Specimen	Material Type	Length, mm	Width, mm	Thickness, mm	Top Hole ID, mm	Bottom Hole ID, mm	Area, dm2	Initial Wt., g	Final Weight	Corrosion Rate MPY	Corrosion Rate Micron/Yr	Weight Loss g	Dummy
1-207	99.99%Al	190.55	63.70	1.248	7.93	8.00	2.477	39.8004		#REF!	#REF!	39.8004	24973.1032
1-208	99.99%Al	190.34	63.39	1.236	8.00	7.90	2.462	39.3304		#REF!	#REF!	39.3304	24820.2343
1-209	99.99%Al	190.27	63.70	1.238	7.94	7.95	2.473	39.5786		#REF!	#REF!	39.5786	24930.9972
1-210	99.99%Al	190.38	63.34	1.237	7.98	7.98	2.461	39.2889		#REF!	#REF!	39.2889	24807.0332
1-211	99.99%Al	190.60	63.22	1.242	7.97	7.95	2.459	39.2955		#REF!	#REF!	39.2955	24792.0390
1-212	99.99%Al	190.62	63.71	1.249	7.99	7.96	2.479	39.8300		#REF!	#REF!	39.8300	24986.6704
6-207	Alloy 6061	190.24	63.44	1.506	8.00	7.98	2.478	48.1945		#REF!	#REF!	48.1945	24977.3022
6-208	Alloy 6061	190.43	63.39	1.502	8.00	8.01	2.478	48.0059		#REF!	#REF!	48.0059	24980.6983
6-209	Alloy 6061	190.39	63.43	1.517	8.02	8.03	2.480	48.3655		#REF!	#REF!	48.3655	24999.4175
6-210	Alloy 6061	190.34	63.27	1.517	8.04	8.02	2.473	48.2693		#REF!	#REF!	48.2693	24931.5762
6-211	Alloy 6061	190.41	63.43	1.513	8.00	8.00	-0.020	48.2731					
6-212	Alloy 6061	190.40	63.37	1.504	8.04	8.04	-0.020	48.1301					

TABLE B-11-3

Specimen Data, Test No. 3B

Test Type: Immersion
Test Environment: Simulated WIPP Brine A, H2S overpressure (5 atm)
Test Temperature: 30±5°C
Test Exposure: 13 months

Specimen	Material Type	Outer Diameter, mm	Hole ID, mm	Thickness, mm	Area, dm2	Initial Wt., g
1-013	99.99% Al	38.31	7.96	1.075	0.236	3.2178
1-014	99.99% Al	38.27	8.00	1.061	0.235	3.0331
1-015	99.99% Al	38.29	7.93	1.009	0.235	2.9752
1-016	99.99% Al	38.27	7.88	1.136	0.237	3.2797
1-017	99.99% Al	38.25	7.96	1.111	0.236	3.2300
1-018	99.99% Al	38.29	7.90	1.086	0.236	3.1540
6-213D	Alloy 6061	38.35	7.98	1.349	0.241	4.1137
6-214D	Alloy 6061	38.34	7.99	1.282	0.239	3.9724
6-215D	Alloy 6061	38.36	8.04	1.382	0.241	4.1194
6-216D	Alloy 6061	38.37	8.04	1.394	0.241	4.2013
6-217D	Alloy 6061	38.31	8.03	1.392	0.241	4.1896
6-218D	Alloy 6061	38.33	8.05	1.358	0.240	4.1024

Specimen	Material Type	Length, mm	Width, mm	Thickness, mm	Top Hole ID, mm	Bottom Hole ID, mm	Area, dm2	Initial Wt., g
1-213	99.99%Al	190.36	63.66	1.213	7.94	7.89	2.472	38.5876
1-214	99.99%Al	190.79	63.43	1.260	7.95	8.01	2.471	40.2756
1-215	99.99%Al	190.01	63.15	1.263	7.95	7.97	2.450	39.9660
1-216	99.99%Al	190.62	63.85	1.267	7.95	8.01	2.485	40.7047
1-217	99.99%Al	190.23	63.41	1.255	7.93	7.92	2.463	40.0331
1-218	99.99%Al	190.42	63.46	1.246	7.97	7.99	2.466	39.5950
6-213	Alloy 6061	190.35	63.30	1.488	8.02	8.03	2.473	47.6890
6-214	Alloy 6061	190.25	63.17	1.510	7.87	7.89	2.468	48.1218
6-215	Alloy 6061	190.30	63.11	1.503	7.92	7.93	2.466	48.0210
6-216	Alloy 6061	190.31	63.34	1.502	7.92	7.92	2.475	48.1630
6-217	Alloy 6061	190.26	63.30	1.511	7.92	7.92	2.473	48.3244
6-218	Alloy 6061	190.29	63.21	1.518	7.92	7.92	2.470	48.4935

TABLE B-11-4

Specimen Data, Test No. 4B

Test Type: Immersion, with Fe contamination of the brine

Test Environment: Simulated WIPP Brine A, N2 overpressure (10 atm)

Test Temperature: 30±5°C

Test Exposure: 13 months

Specimen	Material Type	Outer Diameter, mm	Hole ID, mm	Thickness, mm	Area, dm2	Initial Wt., g
1-019	99.99% Al	38.16	7.96	1.127	0.235	3.2393
1-020	99.99% Al	38.09	8.06	1.071	0.233	3.0322
1-021	99.99% Al	38.14	7.91	1.155	0.235	3.3222
1-022	99.99% Al	38.22	8.16	1.145	0.236	3.2603
1-023	99.99% Al	38.28	7.89	1.131	0.237	3.2751
1-024	99.99% Al	38.30	8.00	1.050	0.236	2.9942
6-219D	Alloy 6061	38.31	8.02	1.358	0.240	4.1264
6-220D	Alloy 6061	38.29	8.06	1.359	0.240	4.1766
6-221D	Alloy 6061	38.33	7.93	1.396	0.241	4.1801
6-222D	Alloy 6061	38.32	8.04	1.381	0.240	4.1383
6-223D	Alloy 6061	38.30	8.03	1.341	0.240	4.1088
6-224D	Alloy 6061	38.31	7.93	1.378	0.241	4.1031

Specimen	Material Type	Length, mm	Width, mm	Thickness, mm	Top Hole ID, mm	Bottom Hole ID, mm	Area, dm2	Initial Wt., g	Final Wt., g	Corrosion Rate, mpy	Corrosion Rate, µm/yr	Weight Loss, g
1-219	99.99%Al	190.53	63.68	1.232	7.97	7.97	2.475	39.2955				
1-220	99.99%Al	190.51	63.74	1.251	7.96	8.00	2.479	39.8627				
1-221	99.99%Al	190.37	63.70	1.241	7.99	8.00	2.475	39.8281				
1-222	99.99%Al	190.52	63.67	1.272	8.00	7.97	2.477	40.8210				
1-223	99.99%Al	190.40	63.69	1.274	7.97	7.96	2.477	40.7374				
1-224	99.99%Al	190.45	63.71	1.235	7.97	7.96	2.476	39.3969				
6-219	Alloy 6061	190.28	63.22	1.503	7.92	7.92	2.470	48.1716				
6-220	Alloy 6061	190.31	63.31	1.506	7.88	7.90	2.474	48.0853				
6-221	Alloy 6061	190.33	63.26	1.515	7.93	7.90	2.473	48.4904				
6-222	Alloy 6061	190.34	63.28	1.513	7.92	7.93	2.473	48.2187				
6-223	Alloy 6061	190.38	63.29	1.516	7.92	7.88	2.475	48.3425				
6-224	Alloy 6061	190.33	63.28	1.513	7.93	7.91	2.473	48.3521				
4B-1	Low-C Steel, Lot J	189.96	63.45	0.682	8.72	8.70	2.425	61.6307	59.7896	0.34	8.6	1.8411
4B-2	Low-C Steel, Lot J	190.50	63.55	0.686	8.75	8.76	2.436	62.8733	60.9499	0.35	9.0	1.9234
4B-3	Low-C Steel, Lot J	190.10	63.50	0.689	8.75	8.71	2.429	62.3124	60.5707	0.32	8.2	1.7417
4B-4	Low-C Steel, Lot J	190.03	63.31	0.692	8.77	8.77	2.421	63.9032	62.6224	0.24	6.0	1.2808

TABLE B-11-5

Specimen Data, Test No. 5B

Test Type: Immersion, with Fe contamination of the brine
Test Environment: Simulated WIPP Brine A, CO2 overpressure (10 atm)
Test Temperature: 30±5°C
Test Exposure: 13 months

Specimen	Material Type	Outer Diameter, mm	Hole ID, mm	Thickness, mm	Area, dm2	Initial Wt., g
1-025	99.99% Al	38.31	7.86	0.995	0.235	2.8934
1-026	99.99% Al	38.24	7.88	1.126	0.236	3.3768
1-027	99.99% Al	38.09	7.92	1.127	0.234	3.3093
1-028	99.99% Al	38.08	7.92	0.977	0.232	2.8987
1-029	99.99% Al	38.00	7.79	1.022	0.232	3.0253
1-030	99.99% Al	38.24	7.89	1.151	0.236	3.4041
6-225D	Alloy 6061	38.38	7.99	1.323	0.241	4.1123
6-226D	Alloy 6061	38.37	7.86	1.391	0.242	4.1639
6-227D	Alloy 6061	38.41	8.00	1.291	0.240	4.0832
6-228D	Alloy 6061	38.33	7.96	1.350	0.240	4.0677
6-229D	Alloy 6061	38.32	8.03	1.347	0.240	4.0675
6-230D	Alloy 6061	38.30	8.02	1.365	0.240	4.0687

Specimen	Material Type	Length, mm	Width, mm	Thickness, mm	Top Hole ID, mm	Bottom Hole ID, mm	Area, dm2	Initial Wt., g	Final Wt., g	Corrosion Rate, mpy	Corrosion Rate, µm/yr	Weight Loss, g
1-225	99.99%Al	190.34	63.62	1.278	7.95	7.96	2.473	40.7449				
1-226	99.99%Al	190.47	63.68	1.253	7.95	7.95	2.476	39.9847				
1-227	99.99%Al	190.47	63.53	1.247	7.98	8.00	2.470	39.5457				
1-228	99.99%Al	190.28	63.16	1.240	7.96	7.96	2.453	39.4258				
1-229	99.99%Al	190.57	63.66	1.260	7.95	7.95	2.477	40.4703				
1-230	99.99%Al	190.60	63.59	1.265	7.96	7.97	2.475	40.3240				
6-225	Alloy 6061	190.17	63.28	1.500	7.96	7.95	2.470	47.8202				
6-226	Alloy 6061	190.30	63.27	1.516	7.90	7.92	2.473	48.1935				
6-227	Alloy 6061	190.28	63.26	1.514	7.90	7.91	2.472	48.2704				
6-228	Alloy 6061	190.34	63.35	1.509	7.91	7.92	2.476	48.3091				
6-229	Alloy 6061	190.27	63.36	1.512	7.94	7.92	2.476	48.2524				
6-230	Alloy 6061	190.26	63.32	1.516	7.92	7.91	2.474	48.2136				
5B-1	Low-C Steel, Lot J	190.31	64.49	0.691	8.75	8.68	2.470	65.3742	62.0017	0.61	16	3.3725
5B-2	Low-C Steel, Lot J	190.25	63.91	0.678	8.73	8.75	2.446	63.2545	60.3776	0.53	13	2.8769
5B-3	Low-C Steel, Lot J	190.25	63.67	0.688	8.78	8.74	2.437	63.7629	60.9643	0.51	13	2.7986
5B-4	Low-C Steel, Lot J	190.30	64.32	0.686	8.77	8.78	2.463	64.1755	60.7919	0.62	16	3.3836

TABLE B-11-6

Specimen Data, Test No. 6B

Test Type: Immersion, with Fe contamination of the brine
Test Environment: Simulated WIPP Brine A, H2S overpressure (5 atm)
Test Temperature: 30±5°C
Test Exposure: 13 months

Specimen	Material Type	Outer Diameter, mm	Hole ID, mm	Thickness, mm	Area, dm2	Initial Wt., g
1-031	99.99% Al	38.20	8.02	1.020	0.234	3.0490
1-032	99.99% Al	38.16	7.82	1.035	0.234	3.0484
1-033	99.99% Al	38.05	8.12	1.037	0.232	3.0889
1-034	99.99% Al	38.27	7.96	1.004	0.235	3.0109
1-035	99.99% Al	37.97	7.80	0.972	0.231	2.8789
1-036	99.99% Al	38.25	7.80	1.113	0.236	3.2670
6-231D	Alloy 6061	38.35	8.08	1.391	0.241	4.1300
6-232D	Alloy 6061	38.34	8.03	1.356	0.240	4.0701
6-233D	Alloy 6061	38.35	8.01	1.377	0.241	4.1072
6-234D	Alloy 6061	38.33	8.08	1.323	0.240	4.0466
6-235D	Alloy 6061	38.33	7.99	1.383	0.241	4.1263
6-236D	Alloy 6061	38.34	8.04	1.342	0.240	4.0745

Specimen	Material Type	Length, mm	Width, mm	Thickness, mm	Top Hole ID, mm	Bottom Hole ID, mm	Area, dm2	Initial Wt., g	Final Wt., g	Corrosion Rate, mpy	Corrosion Rate, µm/yr	Weight Loss, g
1-231	99.99%Al	190.68	63.69	1.250	7.94	7.97	2.479	40.4210				
1-232	99.99%Al	190.77	63.86	1.236	8.04	7.97	2.486	39.5340				
1-233	99.99%Al	190.62	63.62	1.245	7.96	8.00	2.475	39.9841				
1-234	99.99%Al	190.31	63.26	1.229	8.00	7.96	2.456	38.9747				
1-235	99.99%Al	190.41	63.69	1.266	7.95	7.98	2.476	40.1710				
1-236	99.99%Al	191.16	63.70	1.262	7.98	7.96	2.486	40.4370				
6-231	Alloy 6061	190.30	63.30	1.490	7.90	7.97	2.472	47.7713				
6-232	Alloy 6061	190.28	63.30	1.500	7.92	7.93	2.473	47.8912				
6-233	Alloy 6061	190.30	63.34	1.505	7.92	7.89	2.475	48.1043				
6-234	Alloy 6061	190.30	63.17	1.490	7.92	7.94	2.467	47.7506				
6-235	Alloy 6061	190.29	63.24	1.496	7.93	7.92	2.470	47.8839				
6-236	Alloy 6061	190.30	63.27	1.495	7.93	7.94	2.472	47.9197				
6B-1	Low-C Steel, Lot J	190.15	64.50	0.700	8.71	8.78	2.468	64.0074	63.8926	0.024	0.60	0.1148
6B-2	Low-C Steel, Lot J	190.67	64.18	0.691	8.76	8.75	2.462	65.0774	64.9670	0.023	0.58	0.1104
6B-3	Low-C Steel, Lot J	190.20	62.95	0.685	8.77	8.76	2.409	62.8579	62.6805	0.037	0.95	0.1774
6B-4	Low-C Steel, Lot J	190.25	64.10	0.689	8.78	8.75	2.454	64.8808	64.7475	0.028	0.70	0.1333

TABLE B-11-7
Specimen Data, Test No. 7B

Test Type: Vapor phase exposure
Test Environment: Simulated WIPP Brine A vapor + N2 (10 atm)
Test Temperature: 30±5°C
Test Exposure: 13 months

Specimen	Material Type	Outer Diameter, mm	Hole ID, mm	Thickness, mm	Area, dm2	Initial Wt., g
1-037	99.99% Al	38.17	7.91	1.062	0.234	3.1588
1-038	99.99% Al	37.78	7.91	1.053	0.229	3.0558
1-039	99.99% Al	38.20	7.82	1.055	0.235	3.1982
1-040	99.99% Al	38.27	8.03	1.095	0.236	3.2357
1-041	99.99% Al	38.20	7.93	1.096	0.235	3.2256
1-042	99.99% Al	38.04	8.03	1.159	0.234	3.3837
6-237D	Alloy 6061	38.36	8.07	1.352	0.241	4.1158
6-238D	Alloy 6061	38.33	8.02	1.376	0.241	4.1346
6-239D	Alloy 6061	38.34	8.04	1.350	0.240	4.1669
6-240D	Alloy 6061	38.36	8.00	1.351	0.241	4.1230
6-241D	Alloy 6061	38.31	8.04	1.386	0.240	4.1540
6-242D	Alloy 6061	38.39	8.02	1.304	0.240	4.0083

Specimen	Material Type	Length, mm	Width, mm	Thickness, mm	Top Hole ID, mm	Bottom Hole ID, mm	Area, dm2	Initial Wt., g
1-237	99.99%Al	190.51	63.41	1.260	7.97	8.00	2.466	39.9411
1-238	99.99%Al	190.33	63.61	1.247	7.97	7.97	2.471	39.9761
1-239	99.99%Al	190.49	63.84	1.261	8.02	7.99	2.483	40.6702
1-240	99.99%Al	190.45	63.69	1.265	7.99	7.97	2.477	40.2138
1-241	99.99%Al	190.47	63.60	1.257	7.95	7.96	2.473	40.2200
1-242	99.99%Al	190.65	63.65	1.244	7.96	7.95	2.477	39.9268
6-237	Alloy 6061	190.28	63.16	1.493	7.90	7.92	2.467	47.5386
6-238	Alloy 6061	190.26	63.20	1.513	7.91	7.91	2.469	48.3812
6-239	Alloy 6061	190.28	63.31	1.518	7.92	7.91	2.474	48.4311
6-240	Alloy 6061	190.33	63.34	1.525	7.91	7.92	2.476	48.5384
6-241	Alloy 6061	190.33	63.33	1.517	7.91	7.91	2.476	48.4810
6-242	Alloy 6061	190.33	63.33	1.514	7.93	7.94	2.475	48.4727

TABLE B-11-8
Specimen Data, Test No. 8B

Test Type: Vapor phase exposure
Test Environment: Simulated WIPP Brine A vapor +CO2 (10 atm)
Test Temperature: 30±5°C
Test Exposure: 13 months

Specimen	Material Type	Outer Diameter, mm	Hole ID, mm	Thickness, mm	Area, dm2	Initial Wt., g
1-043	99.99% Al	38.13	7.89	0.995	0.233	2.9669
1-044	99.99% Al	38.13	8.03	1.074	0.234	3.1067
1-045	99.99% Al	38.19	7.89	1.073	0.235	3.1943
1-046	99.99% Al	38.08	7.82	0.969	0.232	2.9388
1-047	99.99% Al	38.12	7.80	0.983	0.233	2.9314
1-048	99.99% Al	38.19	7.94	1.049	0.234	3.0870
6-243D	Alloy 6061	38.32	8.08	1.333	0.240	4.0680
6-244D	Alloy 6061	38.30	7.99	1.427	0.241	4.2350
6-245D	Alloy 6061	38.33	8.02	1.404	0.241	4.1664
6-246D	Alloy 6061	38.35	8.08	1.351	0.240	4.1326
6-247D	Alloy 6061	38.34	8.03	1.299	0.240	4.0354
6-248D	Alloy 6061	38.34	8.06	1.399	0.241	4.2238

Specimen	Material Type	Length, mm	Width, mm	Thickness, mm	Top Hole ID, mm	Bottom Hole ID, mm	Area, dm2	Initial Wt., g
1-243	99.99%Al	190.49	63.61	1.254	7.96	7.96	2.474	40.0667
1-244	99.99%Al	190.51	63.66	1.238	7.98	7.97	2.475	39.7234
1-245	99.99%Al	190.52	63.22	1.243	7.97	7.95	2.458	39.6685
1-246	99.99%Al	191.16	63.85	1.236	7.99	8.00	2.490	40.1407
1-247	99.99%Al	190.52	63.69	1.259	7.95	7.94	2.477	40.1177
1-248	99.99%Al	190.13	63.67	1.250	7.95	7.95	2.471	39.7866
6-243	Alloy 6061	190.23	63.28	1.507	7.93	7.92	2.472	48.4863
6-244	Alloy 6061	190.18	63.34	1.516	7.91	7.92	2.474	48.2613
6-245	Alloy 6061	190.29	63.28	1.527	7.94	7.94	2.474	48.4501
6-246	Alloy 6061	190.28	63.27	1.522	7.93	7.93	2.473	48.3887
6-247	Alloy 6061	190.28	63.20	1.512	7.93	7.93	2.470	47.9519
6-248	Alloy 6061	190.24	63.22	1.504	7.94	7.92	2.469	48.0471

TABLE B-11-9
Specimen Data, Test No. 9B

Test Type: Vapor phase exposure
Test Environment: Simulated WIPP Brine A vapor + H2S (5 atm)
Test Temperature: 30±5°C
Test Exposure: 13 months

Specimen	Material Type	Outer Diameter, mm	Hole ID, mm	Thickness, mm	Area, dm2	Initial Wt., g
1-049	99.99% Al	38.20	7.83	1.014	0.234	3.0713
1-050	99.99% Al	38.16	8.00	1.135	0.235	3.3136
1-051	99.99% Al	38.10	8.01	1.115	0.234	3.2823
1-052	99.99% Al	38.13	7.92	1.088	0.234	3.1793
1-053	99.99% Al	38.20	7.97	1.110	0.235	3.2571
1-054	99.99% Al	37.95	7.82	0.961	0.230	2.7499
6-249D	Alloy 6061	38.33	8.07	1.412	0.241	4.2321
6-250D	Alloy 6061	38.32	8.00	1.362	0.240	4.0930
6-251D	Alloy 6061	38.31	8.05	1.325	0.240	4.0482
6-252D	Alloy 6061	38.30	8.01	1.381	0.240	4.1415
6-253D	Alloy 6061	38.32	8.02	1.401	0.241	4.1314
6-254D	Alloy 6061	38.33	8.03	1.375	0.241	4.1322

Specimen	Material Type	Length, mm	Width, mm	Thickness, mm	Top Hole ID, mm	Bottom Hole ID, mm	Area, dm2	Initial Wt., g
1-249	99.99%Al	190.65	63.59	1.252	7.93	7.95	2.475	40.0539
1-250	99.99%Al	190.53	63.66	1.243	7.95	7.95	2.475	39.9383
1-251	99.99%Al	190.37	63.67	1.254	7.94	7.98	2.474	40.0093
1-252	99.99%Al	190.66	63.31	1.243	8.00	7.97	2.463	39.8360
1-253	99.99%Al	190.50	63.41	1.225	7.99	7.97	2.464	39.2710
1-254	99.99%Al	190.33	63.57	1.241	7.95	7.99	2.469	39.7999
6-249	Alloy 6061	190.29	63.29	1.506	7.92	7.89	2.473	48.0900
6-250	Alloy 6061	190.37	63.26	1.519	7.93	7.95	2.473	48.3939
6-251	Alloy 6061	190.31	63.13	1.514	7.94	7.91	2.467	48.2575
6-252	Alloy 6061	190.38	63.37	1.521	7.95	7.93	2.478	48.4967
6-253	Alloy 6061	190.32	63.38	1.521	7.93	7.93	2.478	48.5862
6-254	Alloy 6061	190.36	63.27	1.523	7.93	7.91	2.474	48.3707

TABLE B-11-10
Specimen Data, Test No. 10B

Test Type: Immersion
Test Environment: Simulated WIPP Brine A, N2 overpressure (10 atm)
Test Temperature: 30±5°C
Test Exposure: 24 months

Specimen	Material Type	Outer Diameter, mm	Hole ID, mm	Thickness, mm	Area, dm2	Initial Wt., g
1-055	99.99% Al	37.95	7.92	1.059	0.232	3.1231
1-056	99.99% Al	38.13	7.93	1.088	0.234	3.2160
1-057	99.99% Al	37.99	7.92	1.113	0.233	3.2130
1-058	99.99% Al	38.01	7.90	0.953	0.231	2.8195
1-059	99.99% Al	38.08	7.82	1.050	0.233	3.1782
1-060	99.99% Al	37.91	7.89	0.936	0.229	2.6772
6-255D	Alloy 6061	38.30	8.05	1.362	0.240	4.1548
6-256D	Alloy 6061	38.35	8.01	1.440	0.242	4.2704
6-257D	Alloy 6061	38.32	7.93	1.451	0.242	4.3278
6-258D	Alloy 6061	38.34	8.05	1.399	0.241	4.2003
6-259D	Alloy 6061	38.32	8.05	1.427	0.241	4.2761
6-260D	Alloy 6061	38.32	7.86	1.400	0.241	4.1992

Specimen	Material Type	Length, mm	Width, mm	Thickness, mm	Top Hole ID, mm	Bottom Hole ID, mm	Area, dm2	Initial Wt., g
1-255	99.99%Al	190.59	63.74	1.256	7.97	7.97	2.480	40.2687
1-256	99.99%Al	190.36	63.35	1.251	7.99	7.98	2.462	39.6495
1-257	99.99%Al	190.63	63.87	1.248	7.97	8.00	2.485	39.9391
1-258	99.99%Al	189.90	63.49	1.262	7.99	7.97	2.462	40.0350
1-259	99.99%Al	190.70	63.64	1.236	7.96	7.97	2.476	39.3253
1-260	99.99%Al	191.20	63.66	1.242	7.98	7.96	2.484	40.0699
6-255	Alloy 6061	190.27	63.22	1.517	7.93	7.95	2.470	48.3906
6-256	Alloy 6061	190.33	63.33	1.513	7.93	7.94	2.475	48.1070
6-257	Alloy 6061	190.36	63.32	1.509	7.94	7.93	2.475	48.3393
6-258	Alloy 6061	190.30	63.24	1.511	7.94	7.92	2.471	48.3041
6-259	Alloy 6061	190.30	63.25	1.498	7.95	7.92	2.471	47.7606
6-260	Alloy 6061	190.30	63.30	1.512	7.93	7.95	2.474	48.0220

TABLE B-11-11
Specimen Data, Test No. 11B

Test Type: Immersion
Test Environment: Simulated WIPP Brine A, CO2 overpressure (10 atm)
Test Temperature: 30±5°C
Test Exposure: 24 months

Specimen	Material Type	Outer Diameter, mm	Hole ID, mm	Thickness, mm	Area, dm2	Initial Wt., g
1-061	99.99% Al	37.96	7.86	0.926	0.230	2.7521
1-062	99.99% Al	38.00	7.90	1.156	0.234	3.3804
1-063	99.99% Al	38.11	7.86	0.990	0.233	2.9357
1-064	99.99% Al	38.04	7.93	0.985	0.232	3.0418
1-065	99.99% Al	38.01	7.90	1.106	0.233	3.3011
1-066	99.99% Al	38.12	8.05	0.934	0.232	2.7630
6-261D	Alloy 6061	38.31	7.89	1.445	0.242	4.3040
6-262D	Alloy 6061	38.37	7.98	1.473	0.243	4.3897
6-263D	Alloy 6061	38.31	8.03	1.448	0.241	4.3126
6-264D	Alloy 6061	38.29	7.92	1.455	0.241	4.3392
6-265D	Alloy 6061	38.33	8.06	1.421	0.241	4.2544
6-266D	Alloy 6061	38.33	8.01	1.454	0.242	4.3592

Specimen	Material Type	Length, mm	Width, mm	Thickness, mm	Top Hole ID, mm	Bottom Hole ID, mm	Area, dm2	Initial Wt., g
1-261	99.99%Al	190.63	63.80	1.259	7.98	8.00	2.483	40.4237
1-262	99.99%Al	190.93	63.68	1.254	7.96	7.96	2.482	40.2165
1-263	99.99%Al	191.33	63.66	1.259	7.97	7.95	2.487	40.5759
1-264	99.99%Al	190.49	63.29	1.218	7.98	7.98	2.459	38.8940
1-265	99.99%Al	190.20	63.60	1.259	7.97	7.98	2.470	40.2051
1-266	99.99%Al	190.28	63.65	1.265	8.00	7.96	2.473	40.2797
6-261	Alloy 6061	190.26	63.27	1.508	7.94	7.94	2.472	48.0363
6-262	Alloy 6061	190.20	63.27	1.504	7.92	7.94	2.471	47.7762
6-263	Alloy 6061	190.26	63.31	1.508	7.97	7.96	2.473	48.3746
6-264	Alloy 6061	190.34	63.37	1.518	7.92	7.92	2.477	48.5035
6-265	Alloy 6061	190.31	63.29	1.517	7.92	7.95	2.474	48.4314
6-266	Alloy 6061	190.33	63.35	1.526	7.94	7.94	2.477	48.5505

TABLE B-11-12

Specimen Data, Test No. 12B

Test Type: Immersion

Test Environment: Simulated WIPP Brine A, H2S overpressure (5 atm)

Test Temperature: 30±5°C

Test Exposure: 24 months

Specimen	Material Type	Outer Diameter, mm	Hole ID, mm	Thickness, mm	Area, dm2	Initial Wt., g
1-067	99.99% Al	38.05	8.12	1.108	0.233	3.2292
1-068	99.99% Al	37.99	8.09	0.922	0.230	2.7408
1-069	99.99% Al	38.02	7.87	1.031	0.232	3.0993
1-070	99.99% Al	38.06	7.86	0.968	0.232	2.8577
1-071	99.99% Al	38.17	7.89	1.029	0.234	3.0132
1-072	99.99% Al	38.03	7.96	1.058	0.232	3.2115
6-267D	Alloy 6061	38.37	8.06	1.486	0.243	4.3851
6-268D	Alloy 6061	38.33	7.98	1.473	0.242	4.2856
6-269D	Alloy 6061	38.42	8.05	1.441	0.243	4.2453
6-270D	Alloy 6061	38.33	8.03	1.430	0.241	4.2399
6-271D	Alloy 6061	38.31	8.02	1.426	0.241	4.2791
6-272D	Alloy 6061	38.28	7.82	1.418	0.241	4.2376

Specimen	Material Type	Length, mm	Width, mm	Thickness, mm	Top Hole ID, mm	Bottom Hole ID, mm	Area, dm2	Initial Wt., g
1-267	99.99%Al	190.11	63.61	1.275	7.98	8.02	2.470	40.3981
1-268	99.99%Al	190.24	63.72	1.265	7.98	7.97	2.475	40.4642
1-269	99.99%Al	190.14	63.66	1.261	7.95	7.98	2.471	40.0830
1-270	99.99%Al	190.28	63.70	1.251	7.96	7.99	2.474	39.7859
1-271	99.99%Al	190.36	63.41	1.245	7.96	7.99	2.464	39.1949
1-272	99.99%Al	190.44	63.72	1.257	7.99	7.99	2.477	40.1987
6-267	Alloy 6061	190.29	63.21	1.516	7.93	7.94	2.470	48.4382
6-268	Alloy 6061	190.32	63.30	1.521	7.95	7.93	2.474	48.5040
6-269	Alloy 6061	190.32	62.90	1.525	7.96	7.94	2.459	48.1297
6-270	Alloy 6061	190.36	63.15	1.518	8.01	8.01	2.469	48.3763
6-271	Alloy 6061	190.33	63.21	1.512	7.93	7.92	2.471	48.2867
6-272	Alloy 6061	190.38	63.21	1.511	7.95	7.92	2.471	48.3925

TABLE B-11-13

Specimen Data, Test No. 13B

Test Type: Immersion, with Fe contamination of the brine
Test Environment: Simulated WIPP Brine A, N2 overpressure (10 atm)
Test Temperature: 30±5°C
Test Exposure: 24 months

Specimen	Material Type	Outer Diameter, mm	Hole ID, mm	Thickness, mm	Area, dm2	Initial Wt., g
1-073	99.99% Al	38.14	7.91	1.027	0.233	2.9968
1-074	99.99% Al	38.24	7.93	1.144	0.236	3.3341
1-075	99.99% Al	38.13	7.79	1.123	0.235	3.3039
1-076	99.99% Al	37.83	7.94	1.075	0.230	3.0902
1-077	99.99% Al	38.03	7.94	1.152	0.234	3.3466
1-078	99.99% Al	38.07	7.93	1.164	0.234	3.3750
6-273D	Alloy 6061	38.34	7.98	1.442	0.242	4.2879
6-274D	Alloy 6061	38.37	7.94	1.427	0.242	4.2554
6-275D	Alloy 6061	38.32	7.99	1.490	0.242	4.3831
6-276D	Alloy 6061	38.34	7.97	1.482	0.242	4.3500
6-277D	Alloy 6061	38.31	8.03	1.481	0.242	4.3421
6-278D	Alloy 6061	38.37	8.05	1.428	0.242	4.2855

Specimen	Material Type	Length, mm	Width , mm	Thickness, mm	Top Hole ID, mm	Bottom Hole ID, mm	Area, dm2	Initial Wt., g	Final Wt., g	Corrosion Rate, mpy	Corrosion Rate, µm/yr	Weight Loss, g
1-273	99.99%Al	190.66	63.69	1.247	7.98	7.99	2.478	39.9262				
1-274	99.99%Al	190.01	63.67	1.262	7.97	7.96	2.470	40.0972				
1-275	99.99%Al	190.25	63.30	1.232	7.98	7.98	2.457	39.1179				
1-276	99.99%Al	189.83	63.47	1.241	7.97	7.98	2.459	39.4810				
1-277	99.99%Al	190.47	63.29	1.225	7.98	7.99	2.459	38.8048				
1-278	99.99%Al	190.36	63.61	1.273	7.95	7.98	2.473	40.7018				
6-273	Alloy 6061	190.31	63.17	1.514	7.95	7.95	2.469	48.5242				
6-274	Alloy 6061	190.36	62.59	1.517	7.94	7.95	2.447	47.9617				
6-275	Alloy 6061	190.32	63.24	1.509	7.93	7.94	2.471	48.2388				
6-276	Alloy 6061	190.37	63.28	1.514	7.94	7.96	2.474	48.1198				
6-277	Alloy 6061	190.36	63.19	1.517	7.94	7.96	2.470	48.1501				
6-278	Alloy 6061	190.30	63.32	1.508	7.95	7.90	2.474	48.1010				
13B-1	Low-C Steel, Lot J	190.31	63.92	0.703	8.76	8.76	2.448	64.7701	63.3106	0.14	3.7	1.4595
13B-2	Low-C Steel, Lot J	190.58	64.54	0.692	8.76	8.72	2.475	65.4726	63.7635	0.17	4.3	1.7091
13B-3	Low-C Steel, Lot J	190.19	63.78	0.688	8.72	8.77	2.441	63.3974	61.8764	0.15	3.8	1.5210
13B-4	Low-C Steel, Lot J	190.09	63.06	0.671	8.79	8.76	2.411	60.8953	59.4184	0.15	3.8	1.4769

TABLE B-11-14

Specimen Data, Test No. 14B

Test Type: Immersion, with Fe contamination of the brine
Test Environment: Simulated WIPP Brine A, CO2 overpressure (10 atm)
Test Temperature: 30±5°C
Test Exposure: 24 months

Specimen	Material Type	Outer Diameter, mm	Hole ID, mm	Thickness, mm	Area, dm2	Initial Wt., g
1-079	99.99% Al	38.09	7.82	1.111	0.234	3.1937
1-080	99.99% Al	38.09	7.96	1.159	0.235	3.3530
1-081	99.99% Al	38.10	7.92	1.142	0.235	3.3460
1-082	99.99% Al	38.11	7.91	1.150	0.235	3.3338
1-083	99.99% Al	38.04	7.92	1.141	0.234	3.3170
1-084	99.99% Al	38.10	8.13	1.133	0.234	3.3092
6-279D	Alloy 6061	38.33	8.06	1.454	0.242	4.3151
6-280D	Alloy 6061	38.33	8.09	1.449	0.242	4.2955
6-281D	Alloy 6061	38.33	7.99	1.456	0.242	4.3140
6-282D	Alloy 6061	38.31	8.03	1.439	0.241	4.2686
6-283D	Alloy 6061	38.32	8.06	1.432	0.241	4.2415
6-284D	Alloy 6061	38.34	8.04	1.456	0.242	4.3081

Specimen	Material Type	Length, mm	Width, mm	Thickness, mm	Top Hole ID, mm	Bottom Hole ID, mm	Area, dm2	Initial Wt., g	Final Wt., g	Corrosion Rate, mpy	Corrosion Rate, µm/yr	Weight Loss, g
1-279	99.99%Al	190.35	63.41	1.250	7.99	7.98	2.464	39.7751				
1-280	99.99%Al	190.47	63.33	1.211	7.96	7.99	2.460	38.4915				
1-281	99.99%Al	190.51	63.33	1.239	7.99	7.98	2.462	39.3864				
1-282	99.99%Al	190.39	63.59	1.257	7.94	7.95	2.472	40.3329				
1-283	99.99%Al	190.35	63.33	1.253	8.01	7.99	2.461	39.8458				
1-284	99.99%Al	190.70	63.67	1.249	7.97	8.01	2.478	40.1756				
6-279	Alloy 6061	190.26	63.33	1.514	7.91	7.92	2.474	48.1073				
6-280	Alloy 6061	190.21	63.35	1.519	7.91	7.93	2.475	48.2027				
6-281	Alloy 6061	190.27	63.29	1.506	7.94	7.93	2.473	48.2160				
6-282	Alloy 6061	190.28	63.20	1.514	7.95	7.95	2.470	48.2951				
6-283	Alloy 6061	190.33	63.20	1.510	7.92	7.95	2.470	48.3896				
6-284	Alloy 6061	190.32	63.31	1.510	7.94	7.93	2.474	48.3126				
14B-1	Low-C Steel, Lot J	190.57	63.87	0.693	8.77	8.74	2.449	64.2504	62.1451	0.21	5.4	2.1053
14B-2	Low-C Steel, Lot J	190.48	64.35	0.681	8.74	8.73	2.466	64.0848	62.0322	0.20	5.2	2.0526
14B-3	Low-C Steel, Lot J	190.41	64.28	0.680	8.75	8.77	2.462	63.4829	60.9159	0.26	6.5	2.5670
14B-4	Low-C Steel, Lot J	190.62	64.39	0.682	8.78	8.77	2.469	63.2412	60.8958	0.23	5.9	2.3454

TABLE B-11-15

Specimen Data, Test No. 15B

Test Type: Immersion, with Fe contamination of the brine
Test Environment: Simulated WIPP Brine A, H2S overpressure (5 atm)
Test Temperature: 30±5°C
Test Exposure: 24 months

Specimen	Material Type	Outer Diameter, mm	Hole ID, mm	Thickness, mm	Area, dm2	Initial Wt., g
1-085	99.99% Al	38.03	7.96	1.166	0.234	3.3833
1-086	99.99% Al	38.12	7.88	1.147	0.235	3.3368
1-087	99.99% Al	38.06	7.94	1.163	0.234	3.3651
1-088	99.99% Al	38.08	8.01	1.149	0.234	3.3570
1-089	99.99% Al	38.01	7.94	1.090	0.233	3.2488
1-090	99.99% Al	37.84	7.89	1.121	0.231	3.2348
6-285D	Alloy 6061	38.31	8.03	1.385	0.240	4.1871
6-286D	Alloy 6061	38.40	8.01	1.441	0.242	4.3164
6-287D	Alloy 6061	38.33	7.96	1.451	0.242	4.3312
6-288D	Alloy 6061	38.39	7.97	1.424	0.242	4.2332
6-289D	Alloy 6061	38.37	8.03	1.430	0.242	4.2799
6-290D	Alloy 6061	38.38	7.98	1.452	0.242	4.3071

Specimen	Material Type	Length, mm	Width, mm	Thickness, mm	Top Hole ID, mm	Bottom Hole ID, mm	Area, dm2	Initial Wt., g	Final Wt., g	Corrosion Rate, mpy	Corrosion Rate, µm/yr
1-285	99.99%Al	190.39	63.42	1.246	8.01	8.01	2.464	39.7158			
1-286	99.99%Al	190.40	63.89	1.264	7.99	8.01	2.483	40.5932			
1-287	99.99%Al	190.52	63.64	1.259	7.98	8.00	2.475	40.2146			
1-288	99.99%Al	190.99	63.49	1.244	7.97	7.97	2.475	39.6913			
1-289	99.99%Al	190.63	63.60	1.264	7.98	7.98	2.475	40.1521			
1-290	99.99%Al	190.39	63.69	1.259	7.99	7.97	2.475	40.1533			
6-285	Alloy 6061	190.25	63.30	1.517	7.94	7.94	2.473	48.5646			
6-286	Alloy 6061	190.27	63.29	1.512	7.94	7.94	2.473	48.4968			
6-287	Alloy 6061	190.26	63.29	1.514	7.92	7.94	2.473	48.5970			
6-288	Alloy 6061	190.35	63.27	1.529	7.94	7.94	2.474	48.7206			
6-289	Alloy 6061	190.29	63.14	1.514	7.95	7.93	2.467	48.5583			
6-290	Alloy 6061	190.33	63.34	1.517	7.92	7.91	2.476	48.6147			
15B-1	Low-C Steel, Lot J	190.30	62.81	0.675	8.73	8.76	2.404	61.4087	61.2788	0.013	0.34
15B-2	Low-C Steel, Lot J	190.21	64.28	0.703	8.75	8.76	2.461	65.2710	65.1139	0.016	0.40
15B-3	Low-C Steel, Lot J	190.79	63.62	0.693	8.74	8.73	2.443	64.6320	64.4035	0.023	0.59
15B-4	Low-C Steel, Lot J	190.78	64.23	0.700	8.77	8.77	2.466	65.4615	65.2620	0.020	0.51

TABLE B-11-16

Specimen Data, Test No. 16B

Test Type: Vapor phase exposure

Test Environment: Simulated WIPP Brine A vapor + N2 (10 atm)

Test Temperature: 30±5°C

Test Exposure: 24 months

Specimen	Material Type	Outer Diameter, mm	Hole ID, mm	Thickness, mm	Area, dm2	Initial Wt., g
1-091	99.99% Al	38.01	7.89	1.111	0.233	3.2100
1-092	99.99% Al	38.08	7.87	1.155	0.235	3.3751
1-093	99.99% Al	38.04	7.94	1.199	0.235	3.4793
1-094	99.99% Al	37.94	7.88	1.112	0.232	3.2707
1-095	99.99% Al	38.10	7.92	1.134	0.234	3.2199
1-096	99.99% Al	38.04	7.99	1.138	0.234	3.2175
6-291D	Alloy 6061	38.36	8.03	1.374	0.241	4.2311
6-292D	Alloy 6061	38.34	8.03	1.388	0.241	4.2069
6-293D	Alloy 6061	38.31	8.08	1.414	0.241	4.2396
6-294D	Alloy 6061	38.31	8.05	1.401	0.241	4.2164
6-295D	Alloy 6061	38.29	8.06	1.401	0.240	4.2490
6-296D	Alloy 6061	38.33	8.05	1.401	0.241	4.2178

Specimen	Material Type	Length, mm	Width, mm	Thickness, mm	Top Hole ID, mm	Bottom Hole ID, mm	Area, dm2	Initial Wt., g
1-291	99.99%Al	190.46	63.62	1.239	8.02	7.99	2.472	39.6809
1-292	99.99%Al	190.39	63.64	1.249	7.99	8.00	2.473	39.8249
1-293	99.99%Al	190.39	63.70	1.239	7.99	8.01	2.475	39.5840
1-294	99.99%Al	190.32	63.88	1.278	8.01	8.00	2.483	40.8600
1-295	99.99%Al	190.40	63.76	1.269	7.99	8.01	2.479	40.4974
1-296	99.99%Al	190.69	63.74	1.274	7.98	7.99	2.482	40.8422
6-291	Alloy 6061	190.21	63.37	1.512	7.95	7.92	2.475	48.4372
6-292	Alloy 6061	190.30	63.29	1.517	7.92	7.94	2.474	48.6265
6-293	Alloy 6061	190.26	63.27	1.507	7.94	7.95	2.472	48.4339
6-294	Alloy 6061	190.21	63.32	1.514	7.93	7.96	2.473	48.4364
6-295	Alloy 6061	190.29	63.21	1.515	7.94	7.93	2.470	48.3972
6-296	Alloy 6061	190.29	63.30	1.514	7.95	7.96	2.474	48.4300

TABLE B-11-17

Specimen Data, Test No. 17B

Test Type: Vapor phase exposure

Test Environment: Simulated WIPP Brine A vapor + CO2 (10 atm)

Test Temperature: 30±5°C

Test Exposure: 24 months

Specimen	Material Type	Outer Diameter, mm	Hole ID, mm	Thickness, mm	Area, dm2	Initial Wt., g
1-097	99.99% Al	38.06	7.89	1.116	0.234	3.2190
1-098	99.99% Al	37.96	7.91	1.125	0.233	3.2084
1-099	99.99% Al	38.00	7.89	1.120	0.233	3.2788
1-100	99.99% Al	38.01	7.90	1.063	0.232	3.1006
1-101	99.99% Al	38.08	8.05	1.093	0.233	3.1910
1-102	99.99% Al	37.91	7.87	1.109	0.232	3.2231
6-297D	Alloy 6061	38.31	8.04	1.447	0.241	4.3010
6-298D	Alloy 6061	38.32	8.04	1.395	0.241	4.2450
6-299D	Alloy 6061	38.33	8.04	1.396	0.241	4.2295
6-300D	Alloy 6061	38.33	8.09	1.475	0.242	4.4090
6-301D	Alloy 6061	38.33	8.03	1.476	0.242	4.3789
6-302D	Alloy 6061	38.27	8.04	1.448	0.241	4.2822

Specimen	Material Type	Length, mm	Width, mm	Thickness, mm	Top Hole ID, mm	Bottom Hole ID, mm	Area, dm2	Initial Wt., g
1-297	99.99%Al	190.75	63.71	1.279	8.00	8.00	2.482	40.8751
1-298	99.99%Al	190.50	63.79	1.277	7.99	7.99	2.482	40.7267
1-299	99.99%Al	190.71	63.78	1.275	7.99	7.98	2.484	40.9679
1-300	99.99%Al	190.40	63.76	1.285	8.01	8.00	2.480	41.1400
1-301	99.99%Al	190.31	63.65	1.250	8.01	8.00	2.472	40.1466
1-302	99.99%Al	190.75	63.75	1.268	8.00	7.99	2.483	40.8212
6-297	Alloy 6061	190.32	63.29	1.517	7.94	7.95	2.474	48.4855
6-298	Alloy 6061	190.31	63.21	1.509	7.94	7.97	2.470	48.4435
6-299	Alloy 6061	190.18	63.27	1.509	7.96	7.96	2.471	48.4057
6-300	Alloy 6061	190.26	63.29	1.525	7.95	7.96	2.473	48.6283
6-301	Alloy 6061	190.28	63.25	1.518	7.95	7.96	2.472	48.6375
6-302	Alloy 6061	190.30	63.28	1.517	7.94	7.96	2.473	48.6323

TABLE B-11-18

Specimen Data, Test No. 18B

Test Type: Vapor phase exposure

Test Environment: Simulated WIPP Brine A vapor + H2S (5 atm)

Test Temperature: 30±5°C

Test Exposure: 24 months

Specimen	Material Type	Outer Diameter, mm	Hole ID, mm	Thickness, mm	Area, dm2	Initial Wt., g
1-103	99.99% Al	38.00	7.87	1.132	0.233	3.3566
1-104	99.99% Al	38.07	7.79	1.165	0.235	3.4170
1-105	99.99% Al	38.02	7.74	1.104	0.233	3.2600
1-106	99.99% Al	38.08	7.93	1.191	0.235	3.4906
1-107	99.99% Al	37.88	7.91	1.157	0.232	3.3550
1-108	99.99% Al	37.93	7.79	1.155	0.233	3.3622
6-303D	Alloy 6061	38.40	8.03	1.416	0.242	4.2395
6-304D	Alloy 6061	38.31	8.00	1.424	0.241	4.2347
6-305D	Alloy 6061	38.35	8.01	1.389	0.241	4.1738
6-306D	Alloy 6061	38.40	8.02	1.373	0.241	4.1888
6-307D	Alloy 6061	38.33	8.05	1.353	0.240	4.1920
6-308D	Alloy 6061	38.34	8.04	1.439	0.242	4.3312

Specimen	Material Type	Length, mm	Width, mm	Thickness, mm	Top Hole ID, mm	Bottom Hole ID, mm	Area, dm2	Initial Wt., g
1-303	99.99%Al	190.56	63.78	1.262	7.97	7.99	2.481	40.4683
1-304	99.99%Al	190.48	63.80	1.265	7.99	7.99	2.481	40.3735
1-305	99.99%Al	190.76	63.55	1.245	7.99	8.01	2.474	39.6295
1-306	99.99%Al	190.26	63.76	1.253	8.01	8.00	2.476	40.0268
1-307	99.99%Al	190.52	63.86	1.264	8.00	7.99	2.484	40.3958
1-308	99.99%Al	190.56	63.83	1.265	7.99	7.99	2.483	40.5445
6-303	Alloy 6061	190.34	63.35	1.522	7.95	7.92	2.477	48.6840
6-304	Alloy 6061	190.32	63.36	1.517	7.94	7.93	2.476	48.6350
6-305	Alloy 6061	190.30	63.32	1.503	7.96	7.98	2.474	48.1777
6-306	Alloy 6061	190.12	63.05	1.502	7.96	7.99	2.461	47.9921
6-307	Alloy 6061	190.27	63.28	1.497	7.95	7.95	2.472	48.0312
6-308	Alloy 6061	190.27	63.26	1.511	7.95	7.96	2.472	48.2507

This page intentionally left blank.

APPENDIX C: ESTIMATION OF H_2 GENERATION RATES RESULTING FROM CORROSION OF Al-BASE MATERIALS IMMERSED IN BRINE A

APPENDIX C: ESTIMATION OF H_2 GENERATION RATES RESULTING FROM CORROSION OF Al-BASE MATERIALS IMMERSED IN BRINE A

APPROACH

The H_2 generation rate per unit area of specimen exposed to the brine environment was estimated through a knowledge of the gas pressure within the plenum, the volume of the plenum, the temperature of the gas, the total specimen area, and application of the ideal gas law. The gas generation kinetics were assumed to be linear with time. The basic equation used is given below:

$$n = \frac{PV}{2RTA} \text{ mol } H_2 \text{ produced/m}^2 \text{ Al-base material-yr} \qquad \text{(C-1)}$$

where P = pressure increase in 24 months, due to H_2 generation
V = volume of plenum (0.634 L)
R = gas constant (0.082 atm-L/K-mol)
T = absolute temperature, K
A = area of Al-base material specimens in test (0.33 m^2)
2 = factor to convert 24-month data to 12-month data

The determination of P is straightforward in the case of tests in which the overpressure gas is non-reactive and insoluble in the brine, i.e., tests with a N_2 gas overpressure. In these tests "P" is simply the difference between the initial pressure and final pressures in the system, and venting of the system is readily accounted for by simply summing the aliquots vented.

In the case of overpressure gases that are potentially directly reactive with the metal specimens, or significantly soluble in the brine phase, the determination of H_2 generation is not as straightforward, especially if venting of the container during test is required. If the overpressure gas reacts directly with the metal specimens, a pressure-differential approach to estimating H_2 present becomes difficult, because the "background" pressure of overpressure gas is decreasing at an unknown rate, making it impossible to determine the H_2 pressure accurately without frequent (system-perturbing) gas analysis.

Presence of a soluble (and unreactive) overpressure gas presents no difficulty in H_2 estimation if the container is never vented, as any pressure increase over the starting pressure can be directly attributable to H_2 from water decomposition. However, if the gas is soluble, a venting will release some of the gas from the plenum, leaving a disproportionate (nonequilibrium) amount dissolved in the brine. When the venting is concluded, gas will move from the brine into the plenum, causing a gas-phase pressure increase that will mimic H_2 generation. For this reason, corrections have to be made to the overall ΔP in such test containers that take such emissions into account. It can be readily seen that a "no venting" situation leads to a straightforward H_2 determination, because the total pressure increase can be ascribed to H_2; and that a large number of ventings also eliminates the soluble-gas accountability problem, because (a) the original *total* overpressure gas pressure (the virtual pressure of the total original charge) can be subtracted from the final gas pressure (including summation of ventings), to obtain an accurate assessment

of the H_2 generated, and (b) a large number of ventings is associated with such large H_2 generation rates that the original pressure of overpressure gas loses significance. A correction lying between the extremes described above is required in the case of an intermediate number (e.g., 1 to 10) of ventings.

Both CO_2 and H_2S are soluble to some extent in the brine, so corrections must be made for vented-vessel H_2 determinations, as outlined above. To correct for solubility effects, the following assumptions were made:

- The overpressure gas solubility is given by a Henry's law constant that is invariant with pressure, i.e., the fraction of the gas charge residing in the container plenum remains constant.
- In each venting operation, the pressure is reduced from 20 atm (300 psi) to 10 atm (150 psi).
- The ideal gas law holds throughout.
- The venting operation only removes a homogeneous aliquot of the plenum gas. No gas is removed from the brine phase during venting.
- The pressure in the plenum is directly proportional to the total amount of overpressure gas remaining in the system, and an equilibrium condition is arrived at shortly after each venting operation, i.e., a time period of a few hours.
- The Al-base material specimens do not react directly with the overpressure gas, but only with the water present in the brine phase.
- The plenum pressure is 10 atm prior to the initiation of the H_2-generation reaction for brine/CO_2 tests, and 5 atm for the brine/H_2S tests.

All of the foregoing assumptions are reasonable, and it is judged that errors introduced through the assumptions are relatively small compared with the errors that would result from not engaging in the gas-pressure correction procedure.

Only the 24-month tests are considered in the calculations of H_2 generation, and, as Equation C-1 implies, the rates are considered linear over the course of the 24-month tests.

RESULTS, BRINE/N_2 TESTS

Brine/N_2 Test 13B (Fe Present)

From Equation C-1,

$$n = 0.0386\ P$$

$$P = \frac{1245 \text{ psi} - 135 \text{ psi}}{14.7 \text{ psi/atm}} = 75.5 \text{ atm due to } H_2$$

$n = \underline{2.9 \text{ mol } H_2/m^2 \text{ Al-base material-yr}}$

Brine/N_2 Test 10B (No Fe Present)

$n = 0.0386\ P$

$$P = \frac{171 \text{ psi} - 144 \text{ psi}}{14.7 \text{ psi/atm}} = 2.52 \text{ atm due to } H_2$$

$n = \underline{0.097 \text{ mol } H_2/m^2 \text{ Al-base material-yr}}$

RESULTS, BRINE/CO_2 TESTS

General Approach

A determination must be made of the degree to which dissolved CO_2 mimics H_2 by repressurizing the container plenum after a venting has taken place. The original CO_2 charge is 10.5 L-atm at 30°C. The effect of CO_2 can be estimated in the following manner, assuming a temperature of 30°C throughout:

1st plenum inventory: All ΔP is H_2. Final P = 20 atm; 10 atm CO_2 and 10 atm H_2. After venting, 5 atm CO_2 and 5 atm H_2 remain. 1st venting eliminates 5 atm CO_2, or $5 \times 0.634 = 3.2$ L-atm. There is no effect of CO_2 repressuration at this time.

2nd plenum inventory: CO_2 can recharge to a pressure of $\left[10 \times \frac{10.5 - 3.2}{10.5}\right]$ atm, or 7.0 atm. ΔP due to CO_2 = 7.0 atm - 5.0 atm, or 2.0 atm. This is equivalent to 29 psi, which must be subtracted from total P in order to obtain P_{H_2}. 2nd venting eliminates

$\frac{7.0}{2} \times 0.634$ L-atm CO_2, or 2.2 L-atm CO_2.

3rd plenum inventory: CO_2 can recharge to a pressure of $\left[10 \times \frac{10.5 - 3.2 - 2.2}{10.5}\right]$ atm, or 4.9 atm. ΔP due to CO_2 = 4.9 atm - 3.5 atm = 1.4 atm, or 21 psi, which must be subtracted from total P in order to obtain P_{H_2}. The 3rd venting eliminates

$\frac{4.9}{2} \times 0.634$ L-atm CO_2, or 1.6 L-atm CO_2.

Similar calculations were made for the 4th plenum inventory (13 psi due to CO_2) and 5th plenum inventory (9 psi due to CO_2). Additional inventories are arbitrarily assigned 5 psi CO_2. However,

regardless of the number of ventings, the virtual pressure of the initial charge in a 0.634 L plenum (244 psi) cannot be surpassed.

In summary, the procedure used for correcting the container pressure for CO_2 involves the following steps:

1. Determine overall ΔP in test. Initial (zero) pressure begins at the beginning of the test, when the pressure gauge reads 10 atm, and ends at the final pressure reading. Pressure differentials due to ventings are summed.

2. For each venting, subtract the pressure of CO_2 recharging the plenum masquerading as H_2. These values were calculated in the foregoing computations.

3. Calculate the rate of H_2 formation by means of Equation C-1 and the corrected pressure.

Brine/CO_2 Test 14B (Fe Present)

$$\Delta P = \frac{1893 \text{ psi} - 148 \text{ psi}}{14.7 \text{ psi/atm}} = 119 \text{ atm in 24 months}$$

Correction due to ventings (12 container ventings performed):

First five ventings	= (0 psi + 29 psi + 21 psi + 13 psi + 9 psi)	= 72 psi
Next seven ventings	= 7 × 5 psi	= 35 psi
		107 psi

[Check: initial charge (150 psi) + 107 psi = 257 psi. This exceeds virtual pressure of initial charge (244 psi). Therefore, a correction of 244 - 150, or 94 psi, will be made to the pressure differential rather than the 107 psi calculated.]

$$\text{corrected } \Delta P = 119 \text{ atm} - \frac{94 \text{ psi}}{14.7 \frac{\text{psi}}{\text{atm}}}$$

$$\text{corrected } \Delta P = 113 \text{ atm}$$

$$n = 0.0386 \, P$$

$$n = \underline{4.4 \text{ mol } H_2/m^2 \text{ Al-base material-yr}}$$

Brine/CO_2 Test 11B (No Fe Present)

$$\Delta P = \frac{516 \text{ psi} - 143 \text{ psi}}{14.7 \frac{\text{psi}}{\text{atm}}} = 25.4 \text{ atm in 24 months}$$

Correction due to ventings:

Two ventings: 0 psi + 29 psi = 29 psi

$$\text{corrected } \Delta P = 25.4 \text{ atm} - \frac{29 \text{ psi}}{14.7 \frac{\text{psi}}{\text{atm}}}$$

corrected ΔP = 23.4 atm

n = 0.0386 P

n = 0.90 mol H_2/m^2 Al-base material-yr

RESULTS, BRINE/H_2S TESTS

General Approach

The basic approach taken is the same as that previously presented for the CO_2/brine studies, except that the starting pressure of H_2S in the gas phase is 5 atm, and the virtual pressure of the overall gas charge (11.2 L-atm) in the 0.634 L plenum is 260 psi at 30°C.

1st plenum inventory: All ΔP is H_2. Final P = 20 atm; 5 atm H_2S and 15 atm H_2. After venting, 2.5 atm H_2S and 7.5 atm H_2 remain. 1st venting eliminates 2.5 atm × 0.634 L = 1.6 L-atm of H_2S. There is no impact of H_2S on H_2 estimation at this point.

2nd plenum inventory: H_2S can recharge to a pressure of $\left[5 \times \frac{11.2 - 1.6}{11.2}\right]$ atm, or 4.3 atm. ΔP due to H_2S is 4.3 atm - 2.5 atm = 1.8 atm, or 26 psi due to H_2S. 2nd venting eliminates 4.3/2 × 0.634 = 1.4 L-atm of H_2S.

3rd plenum inventory: H_2S can recharge to a pressure of $\left[5 \times \frac{11.2 - 1.6 - 1.4}{11.2}\right]$ atm, or 3.7 atm. ΔP due to H_2S is 3.7 atm - 2.2 atm = 1.5 atm, or 22 psi due to H_2S. 3rd venting eliminates 3.7/2 × 0.634 = 1.2 L-atm of H_2S.

Similar calculations were made for the 4th plenum inventory (19 psi due to H_2S) and the 5th plenum inventory (16 psi due to H_2S). Succeeding inventories are arbitrarily assigned 10 psi H_2S, until the virtual pressure of the initial charge (260 psi) is attained.

Brine/H_2S Test 15B (Fe Present)

$$\Delta P = \frac{1076 \text{ psi} - 71 \text{ psi}}{14.7 \frac{\text{psi}}{\text{atm}}} = 68.4 \text{ atm}$$

Corrections due to ventings (5 container ventings total):
0 psi + 26 psi + 22 psi + 19 psi + 16 psi = 83 psi

$$\text{corrected } \Delta P = 68.4 \text{ atm} - \frac{83 \text{ psi}}{14.7 \frac{\text{psi}}{\text{atm}}}$$

corrected ΔP = 62.8 psi
n = 0.0386 P
n = 2.4 mol H_2/m^2 Al-base material-yr

Brine/H_2S Test 12B (No Fe Present)

$$\Delta P = \frac{594 \text{ psi} - 69 \text{ psi}}{14.7 \frac{\text{psi}}{\text{atm}}} = 35.7 \text{ atm}$$

Corrections due to ventings (2 container ventings total):
0 psi + 26 psi = 26 psi

$$\text{corrected } \Delta P = 35.7 \text{ atm} - \frac{26 \text{ psi}}{14.7 \frac{\text{psi}}{\text{atm}}}$$

corrected ΔP = 33.9 psi
n = 0.0386 P
n = 1.3 mol H_2/m^2 Al-base material-yr

This page intentionally left blank.

WIPP
UC721 - DISTRIBUTION LIST
SAND96-2538

Federal Agencies

US Department of Energy (4)
Office of Civilian Radioactive Waste Mgmt.
Attn: Deputy Director, RW-2
Acting Director, RW-10
Office of Human Resources & Admin.
Director, RW-30
Office of Program Mgmt. & Integ.
Director, RW-40
Office of Waste Accept., Stor., & Tran.
Forrestal Building
Washington, DC 20585

Attn: Project Director
Yucca Mountain Site Characterization Office
Director, RW-3
Office of Quality Assurance
P. O. Box 98608
Las Vegas, NV 89193-8608

US Department of Energy
Albuquerque Operations Office
Attn: National Atomic Museum Library
P.O. Box 5400
Albuquerque, NM 87185-5400

US Department of Energy
Research & Waste Management Division
Attn: Director
P.O. Box E
Oak Ridge, TN 37831

US Department of Energy (5)
Carlsbad Area Office
Attn: G. Dials
D. Galbraith
M. McFadden
R. Lark
J. A. Mewhinney
P.O. Box 3090
Carlsbad, NM 88221-3090

US Department of Energy
Office of Environmental Restoration and
Waste Management
Attn: J. Lytle, EM-30
Forrestal Building
Washington, DC 20585-0002

US Department of Energy (3)
Office of Environmental Restoration and
Waste Management
Attn: M. Frei, EM-34, Trevion II
Washington, DC 20585-0002

US Department of Energy
Office of Environmental Restoration and
Waste Management
Attn: S. Schneider, EM-342, Trevion II
Washington, DC 20585-0002

US Department of Energy (2)
Office of Environment, Safety & Health
Attn: C. Borgstrom, EH-25
R. Pelletier, EH-231
Washington, DC 20585

US Department of Energy (2)
Idaho Operations Office
Fuel Processing & Waste Mgmt. Division
785 DOE Place
Idaho Falls, ID 83402

US Environmental Protection Agency (2)
Radiation Protection Programs
Attn: M. Oge
ANR-460
Washington, DC 20460

Boards

Defense Nuclear Facilities Safety Board
Attn: D. Winters
625 Indiana Ave. NW, Suite 700
Washington, DC 20004

Nuclear Waste Technical Review Board (2)
Attn: Chairman
S. J. S. Parry
1100 Wilson Blvd., Suite 910
Arlington, VA 22209-2297

State Agencies

Attorney General of New Mexico
P.O. Drawer 1508
Santa Fe, NM 87504-1508

Environmental Evaluation Group (3)
Attn: Library
7007 Wyoming NE
Suite F-2
Albuquerque, NM 87109

NM Energy, Minerals, and Natural
Resources Department
Attn: Library
2040 S. Pacheco
Santa Fe, NM 87505

NM Environment Department (3)
Secretary of the Environment
Attn: Mark Weidler
1190 St. Francis Drive
Santa Fe, NM 87503-0968

NM Bureau of Mines & Mineral Resources
Socorro, NM 87801

NM Environment Department
WIPP Project Site
Attn: P. McCasland
P.O. Box 3090
Carlsbad, NM 88221

Laboratories/Corporations

Battelle Pacific Northwest Laboratories (2)
Attn: S. Pitman
M. Telander
Battelle Blvd.
Richland, WA 99352

INTERA, Inc.
Attn: G. A. Freeze
1650 University Blvd. NE, Suite 300
Albuquerque, NM 87102

INTERA, Inc.
Attn: J. F. Pickens
6850 Austin Center Blvd., Suite 300
Austin, TX 78731

Brookhaven National Laboratory (2)
Attn: A. J. Francis
J. B. Gillow
Dept. of Applied Sciences
Upton, NY 11973

INTERA, Inc.
Attn: W. Stensrud
P.O. Box 2123
Carlsbad, NM 88221

Los Alamos National Laboratory
Attn: B. Erdal, INC-12
P.O. Box 1663
Los Alamos, NM 87544

RE/SPEC, Inc
Attn: Angus Robb
4775 Indian School NE, Suite 300
Albuquerque, NM 87110-3927

RE/SPEC, Inc
Attn: J. L. Ratigan
P.O. Box 725
Rapid City, SD 57709

Tech Reps, Inc. (3)
Attn: J. Chapman (1)
Loretta Robledo (2)
5000 Marble NE, Suite 222
Albuquerque, NM 87110

Westinghouse Electric Corporation (5)
Attn: Library
J. Epstein
J. Lee
B. A. Howard
R. Kehrman
P.O. Box 2078
Carlsbad, NM 88221

S. Cohen & Associates
Attn: Bill Thurber
1355 Beverly Road
McLean, VA 22101

**National Academy of Sciences,
WIPP Panel**

Howard Adler
Oxyrase, Incorporated
7327 Oak Ridge Highway
Knoxville, TN 37931

Bob Andrews
Board of Radioactive Waste Management
GF456
2101 Constitution Ave.
Washington, DC 20418

Rodney C. Ewing
Department of Geology
University of New Mexico
Albuquerque, NM 87131

Charles Fairhurst
Department of Civil and Mineral Engineering
University of Minnesota
500 Pillsbury Dr. SE
Minneapolis, MN 55455-0220

B. John Garrick
PLG Incorporated
4590 MacArthur Blvd., Suite 400
Newport Beach, CA 92660-2027

Leonard F. Konikow
US Geological Survey
431 National Center
Reston, VA 22092

Carl A. Anderson, Director
Board of Radioactive Waste Management
National Research Council
HA 456
2101 Constitution Ave. NW
Washington, DC 20418

Christopher G. Whipple
ICF Kaiser Engineers
1800 Harrison St., 7th Floor
Oakland, CA 94612-3430

John O. Blomeke
720 Clubhouse Way
Knoxville, TN 37909

Sue B. Clark
University of Georgia
Savannah River Ecology Lab
P.O. Drawer E
Aiken, SC 29802

Konrad B. Krauskopf
Department of Geology
Stanford University
Stanford, CA 94305-2115

Della Roy
Pennsylvania State University
217 Materials Research Lab
Hastings Road
University Park, PA 16802

David A. Waite
CH_2 M Hill
P.O. Box 91500
Bellevue, WA 98009-2050

Thomas A. Zordon
Zordan Associates, Inc.
3807 Edinburg Drive
Murrysville, PA 15668

Universities

University of New Mexico
Geology Department
Attn: Library
141 Northrop Hall
Albuquerque, NM 87131

University of Washington
College of Ocean & Fishery Sciences
Attn: G. R. Heath
583 Henderson Hall, HN-15
Seattle, WA 98195

Libraries

Thomas Brannigan Library
Attn: D. Dresp
106 W. Hadley St.
Las Cruces, NM 88001

Government Publications Department
Zimmerman Library
University of New Mexico
Albuquerque, NM 87131

New Mexico Junior College
Pannell Library
Attn: R. Hill
Lovington Highway
Hobbs, NM 88240

New Mexico State Library
Attn: N. McCallan
325 Don Gaspar
Santa Fe, NM 87503

New Mexico Tech
Martin Speere Memorial Library
Campus Street
Socorro, NM 87810

WIPP Public Reading Room
Carlsbad Public Library
101 S. Halagueno St.
Carlsbad, NM 88220

Foreign Addresses

Atomic Energy of Canada, Ltd.
Whiteshell Laboratories
Attn: B. Goodwin
Pinawa, Manitoba, CANADA R0E 1L0

Francois Chenevier (2)
ANDRA
Route de Panorama Robert Schumann
B. P. 38
92266 Fontenay-aux-Roses, Cedex
FRANCE

Claude Sombret
Centre d'Etudes Nucleaires de la Vallee Rhone
CEN/VALRHO
S.D.H.A. B.P. 171
30205 Bagnols-Sur-Ceze, FRANCE

Commissariat a L'Energie Atomique
Attn: D. Alexandre
Centre d'Etudes de Cadarache
13108 Saint Paul Lez Durance Cedex
FRANCE

Bundesanstalt fur Geowissenschaften und Rohstoffe
Attn: M. Langer
Postfach 510 153
D-30631 Hannover, GERMANY

Bundesministerium fur Forschung und Technologie
Postfach 200 706
5300 Bonn 2, GERMANY

Institut fur Tieflagerung
Attn: K. Kuhn
Theodor-Heuss-Strasse 4
D-3300 Braunschweig, GERMANY

Gesellschaft fur Anlagen und Reaktorsicherheit (GRS)
Attn: B. Baltes
Schwertnergasse 1
D-50667 Cologne, GERMANY

Shingo Tashiro
Japan Atomic Energy Research Institute
Tokai-Mura, Ibaraki-Ken, 319-11
JAPAN

Netherlands Energy Research Foundation ECN
Attn: J. Prij
3 Westerduinweg
P.O. Box 1
1755 ZG Petten
THE NETHERLANDS

Svensk Karnbransleforsorjning AB
Attn: F. Karlsson
Project KBS (Karnbranslesakerhet)
Box 5864
S-102 48 Stockholm
SWEDEN

Nationale Genossenschaft fur die Lagerung Radioaktiver Abfalle (2)
Attn: S. Vomvoris
P. Zuidema
Hardstrasse 73
CH-5430 Wettingen
SWITZERLAND

AEA Technology
Attn: J. H. Rees
D5W/29 Culham Laboratory
Abington, Oxfordshire OX14 3DB
UNITED KINGDOM

AEA Technology
Attn: W. R. Rodwell
044/A31 Winfrith Technical Centre
Dorchester, Dorset DT2 8DH
UNITED KINGDOM

AEA Technology
Attn: J. E. Tinson
B4244 Harwell Laboratory
Didcot, Oxfordshire OX11 ORA
UNITED KINGDOM

Other

R. E. Westerman (25)
1804 Marshall
Richland, WA 99352

Internal

MS	Org.	
1324	6115	P. B. Davies
1320	6831	E. J. Nowak
1322	6121	J. R. Tillerson
1328	6849	D. R. Anderson
1328	6848	H. N. Jow
1335	6801	M. Chu
1341	6832	J. T. Holmes
1395	6800	L. Shephard
1395	6821	M. Marietta
1395	6841	V. H. Slaboszewicz
1341	6832	L. Brush (25)
1341	6832	A. C. Peterson (2)
1341	6832	Y. Wang (5)
1341	6832	L. J. Storz
1320	6832	H. W. Papenguth
0706	6113	M..A. Molecke (2)
1330	6811	K. Hart (2)
1330	4415	NWM Library (20)
9018	8940-2	Central Technical Files
0899	4414	Technical Library (5)
0619	12630	Review and Approval Desk (2), For DOE/OSTI